④

AD-A206 219

STUDIES OF PHASE-CONJUGATE OPTICAL DEVICE CONCEPTS

FINAL REPORT FOR THE PERIOD
April 1, 1985 through June 30, 1988

Prepared for

I.C. McMichael and P.A. Yeh

DTIC
ELECTE
MAR 2 7 1989
S D
H

MARCH 1989

Rockwell International
Science Center

REPORT DOCUMENTATION PAGE	FORM APPROVED OMB No. 0704-0188

1a. REPORT SECURITY CLASSIFICATION **UNCLASSIFIED**	1b. RESTRICTIVE MARKINGS

2a. SECURITY CLASSIFICATION AUTHORITY	3. DISTRIBUTION/AVAILABILITY OF REPORT
2b. CLASSIFICATION/DOWNGRADING SCHEDULE	**Approved for public release; distribution is unlimited**

4. PERFORMING ORGANIZATION REPORT NUMBER(S) **SC5424.FR**	5. MONITORING ORGANIZATION REPORT NUMBER(S)

6a. NAME OF PERFORMING ORGANIZATION **ROCKWELL INTERNATIONAL** Science Center	6b. OFFICE SYMBOL (If Applicable)	7a. NAME OF MONITORING ORGANIZATION

6c. ADDRESS (City, State, and ZIP Code) **1049 Camino Dos Rios** **Thousand Oaks, CA 91360**	7b. ADDRESS (City, State and ZIP Code)

8a. NAME OF FUNDING/SPONSORING ORGANIZATION **Physics Division, Code 1112** **Office of Naval Research**	8b. OFFICE SYMBOL (If Applicable)	9. PROCUREMENT INSTRUMENT IDENTIFICATION NUMBER **CONTRACT NO. N00014-85-C-0219**

8c. ADDRESS (City, State and ZIP Code) **800 North Quincy Street** **Arlington, Virginia 22217-5000**	10. SOURCE OF FUNDING NOS

PROGRAM ELEMENT NO	PROJECT NO.	TASK NO.	WORK UNIT ACCESSION NO

11. TITLE (Include Security Classification)

STUDIES OF PHASE CONJUGATE OPTICAL DEVICE CONCEPTS

12. PERSONAL AUTHOR(S)

McMichael, I.C. and Yeh, P.A.

13a. TYPE OF REPORT **Final Report**	13b. TIME COVERED FROM **04/01/85** TO **06/30/88**	14. DATE OF REPORT (Year, Month, Day) **1989, MARCH**	15. PAGE COUNT **175**

16. SUPPLEMENTARY NOTATION

17. COSATI CODES			18. SUBJECT TERMS (Continue on reverse if necessary and identify by block number)
FIELD	GROUP	SUB-GROUP	

19. ABSTRACT (Continue on reverse if necessary and identify by block number)

20. DISTRIBUTION/AVAILABILITY OF ABSTRACT UNCLASSIFIED/UNLIMITED ☒ SAME AS RPT ☐ DTIC USERS ☐	21. ABSTRACT SECURITY CLASSIFICATION **UNCLASSIFIED**

22a. NAME OF RESPONSIBLE INDIVIDUAL **Dr. Herschel Pilloff**	22b. TELEPHONE NUMBER (Include Area Code)	22c. OFFICE SYMBOL

DD FORM 1473, JUN 86   Previous editions are obsolete.

TABLE OF CONTENTS

GALLIUM ARSENIDE

TABLE OF CONTENTS

LIST OF FIGURES

1.0 SUMMARY

1.1 Contract Description

This contract focused on the physics of phase-conjugate gyroscopy and the development of the phase-conjugate fiber-optic gyro. The efforts studied a unique approach in which phase conjugation was used to correct for modal scrambling in fiber-optic gyros without the need for polarization-preserving fibers and couplers. This involved both theoretical and experimental studies of photorefractive phenomena and novel phase conjugators, especially mutually pumped and self-pumped conjugators.

1.2 Scientific Problem

Phase-conjugate gyroscopy is a new area promising significant advances in state-of-the-art inertial navigation. Under this contract we demonstrated the first phase-conjugate fiber-optic gyros (PCFOG's) and their ability to use low cost multimode fiber components. As a direct result of the contract efforts, the development of the PCFOG is now at the stage where its sources of noise and drift can be isolated, and its competitiveness with conventional fiber optic gyros can be tested. To come to this stage in development, several scientific and technical issues had to be resolved. For example, to correct for the modal scrambling of multimode fibers, the theory and practice of polarization preserving conjugators that worked at milliwatt power levels had to be developed and tested. Another issue was the mutual coherence requirement for two beams interacting with a self-pumped conjugator that at first restricted the PCFOG from using the most desireable form of biasing (fast phase modulation). This issue was resolved only recently when a new class of phase conjugators (mutually pumped conjugators) was developed that have the ability to operate with mutually incoherent beams. Almost as quickly as the first mutually pumped conjugators were discovered, this contract demonstrated the first PCFOG to use one. In addition to, and in the process of developing the PCFOG, this contract investigated several new photorefractive phenomena.

1.3 Progress Summary

There were many areas of significant progress achieved under this contract that are directly related to the development of the phase-conjugate fiber-optic gyro. These include:

- First measurement of the Sagnac phase shift in a phase-conjugate fiber-optic gyro.

- First demonstrations of rotation sensing with multimode fiber gyros using both self-pumped and mutually pumped conjugators.

- First measurements of the properties of a mutually pumped phase-conjugate ring interferometer including,

    - measurements of the outputs indicating a Sagnac nature

    - no measurable nonreciprocal effects introduced by the conjugator

    - dependance on spatial intensity profiles

    - output power vs crystal position for the bird wing conjugator indicating hysteresis

    - conjugate reflectivities vs beam ratios indicating gain in reflection

    - measurement of a nonreciprocal phase shift (Faraday effect)

    - correction of modal scrambling in fibers by both polarization preserving and nonpolarization preserving phase-conjugation with the bird wing conjugator

    - demonstration of image subtraction.

- First measurement of a nonreciprocal phase shift (Faraday effect) in a double phase-conjugate interferometer.

- Development of self-pumped and externally-pumped polarization-preserving phase-conjugate mirrors that operate at milliwatt power levels.

- First demonstration and theoretical modelling of the correction of polarization and modal scrambling in multi-mode fibers by polarization-preserving phase conjugation.

- First measurements of the phase of phase-conjugate reflections, and the phase shifts of photorefractive gratings.

In addition to the progress mentioned above, we have also carried out other interesting scientific research and have achieved many significant results. These include,

- Development of models for mutually pumped phase conjugation.

- Theory of two-beam coupling in cubic photorefractive materials indicating the possibility of cross-polarization coupling.

- Analysis of nondegenerate two-wave mixing in ruby.

- First demonstration of gain and oscillation with the bird-wing mutually pumped conjugator.

- Theory of frequency shifts in photorefractive resonators

- Resonator model of self-pumped phase conjugation

- Theory of photorefractive conical diffraction, and

- Theory and experimental design of image addition and subtraction in a phase-conjugate Michelson interferometer.

Details of this progress are presented in Section 2.0, and in the publications included in this report as Appendices.

1.4   Special Significance of Results

Three of the areas of progress noted in the previous section are of special significance in that they are not restricted in their use to the phase-conjugate fiber optic gyro. (1) The polarization-preserving phase-conjugate mirror opens a whole new area of *interferometry with multi-mode fibers*. The significance of this work was recently acknowledged when it appeared as a news item in the "Recent Research" section of Optics News (August 1987, page 39). (2) Measurements of the phase of the phase-conjugate reflection can be used to determine the phase shift (with respect to the intensity pattern) and the type of gratings (index, absorption, gain, or mixture) involved in degenerate four wave mixing in nonlinear media. Proper selection of nonlinear media will allow the construction of phase-conjugate interferometers that "self-quadrature" for high sensitivity and linear response. The phase shift of phase conjugators also plays an important role in the frequency shift of double phase-conjugate resonators. (3) Our studies on cross-polarization two-beam coupling resulted in the invention of a new filter/amplifier concept that represents a significant advance in the state-of-the-art. The filter/amplifier is wavelength and bandwidth tunable, with potential for extremely narrow bandwidth, it has a wide field-of-view (many degrees), and is simpler than schemes using four-wave mixing.

1.5   Publications and Presentations

Publications

*   "Coupled-Mode Theory of Hologram Sharing in Mutually Pumped Phase Conjugators," Pochi Yeh, to appear in Appl. Opt. (1989).

*   "Photorefractive Two-Beam Coupling in Cubic Crystals. II. General Case ($\phi \neq \pi/2$)," Pochi Yeh, J. Opt. Soc. Am. B 5, 1811 (1988).

*   "Model for Mutually Pumped Phase-Conjugation," Pochi Yeh, Tallis Y. Chang, and M. D. Ewbank, J. Opt. Soc. Am. B 5, 1743 (1988).

*   "Cross-Polarization Photorefractive Two-Beam Coupling in Gallium Arsenide," Tallis Y. Chang, Arthur E. Chiou, and Pochi Yeh, J. Opt. Soc. Am. B 5, 1724 (1988).

* "Nondegenerate Two-Wave Mixing in Ruby," Ian McMichael, Pochi Yeh, and Paul Beckwith, Opt. Lett. 13, 500 (1988).

"Externally Pumped Polarization-Preserving Phase Conjugator," Ian McMichael, J. Opt. Soc. Am. B 5, 863 (1988).

"Phase-Conjugate Multimode Fiber Gyro," Ian McMichael, Paul Beckwith, and Pochi Yeh, Opt. Lett. 12, 1023 (1987).

"Image Distortion in Multimode Fibers and Restoration by Polarization-Preserving Phase Conjugation," Paul Beckwith, Ian McMichael, and Pochi Yeh, Opt. Lett. 12, 510 (1987).

"Correction of Polarization and Modal Scrambling in Multimode Fibers by Phase-Conjugation," Ian McMichael, Pochi Yeh, and Paul Beckwith, Opt. Lett. 12, 507 (1987).

"Phase Shifts of Photorefractive Gratings and Phase Conjugate Waves," Ian McMichael and Pochi Yeh, Opt. Lett. 12, 48 (1987).

"Self-Pumped Phase-Conjugate Fiber-Optic Gyro," Ian McMichael and Pochi Yeh, Opt. Lett. 11, 686 (1986).

* "Photorefractive Conical Diffraction in BaTiO3," M. D. Ewbank, Pochi Yeh and J. Feinberg, Opt. Comm. 59, 423 (1986).

"Polarization-Preserving Phase Conjugator," Ian McMichael, Pochi Yeh and Monte Khoshnevisan, Opt. Lett. 11, 525 (1986).

"Absolute Phase Shift of Phase Conjugators," Ian McMichael, Pochi Yeh and Monte Khoshnevisan, Proc. Soc. Photo-Opt. Instrum. Eng. 613, 32 (1986).

* "Parallel Image Subtraction Using a Phase-Conjugate Michelson Interferometer," A. E. T. Chiou and Pochi Yeh, Opt. Lett. 11, 306 (1986).

"Phase-Conjugate Fiber Optic Gyro," Pochi Yeh, Ian McMichael and Monte Khoshnevisan, Applied Optics, 25, 1029 (1986).

* "Frequency Shift of Self-Pumped Phase Conjugator," M. D. Ewbank and Pochi Yeh, Proc. Soc. Photo-Opt. Instrum. Eng. 613, 59 (1986).

* "Theory of Unidirectional Photorefractive Ring Oscillators," Pochi Yeh, J. Opt. Soc. Am. B2, 1924 (1985).

* "Frequency Shift and Cavity Length in Photorefractive Resonators," M. D. Ewbank and Pochi Yeh, Opt. Lett. 10, 496 (1985).

Presentations

"Multimode Fiber Gyro Using a Mutually Pumped Conjugator," Ian McMichael, Paul Beckwith, and Pochi Yeh, presented at the Annual Meeting of the Optical Society of America, Santa Clara, CA, October 31 - November 4, 1988.

* "Recent Advances in Photorefractive Nonlinear Optics," Pochi Yeh, invited paper presented at the Laser Materials and Laser Spectroscopy Meeting, Shanghai, China, July 25 (1988).

* "Two-Wave Mixing in Nonlinear Media," M. Khoshnevisan, A. Chiou, T. Chang, M. Ewbank, I. McMichael, and P. Yeh, presented at the International Conference on Nonlinear Optical Phenomena, Ashford Castle, Ireland, May 2-6, 1988.

"Phase-Conjugate Ring Interferometer," Ian McMichael, M. D. Ewbank, and Pochi Yeh, presented at the Conference on Lasers and Electro-Optics, Anaheim, CA, April 25 - 29, 1988.

"Phase-Conjugate Multimode Fiber Gyro," Ian McMichael, Paul Beckwith, and Pochi Yeh, presented at the topical meeting on Photorefractive Materials, Effects, and Devices, Los Angeles, CA, August 12-14, 1987.

"Correction of Polarization and Modal Scrambling in Multimode Fibers by Phase Conjugation, " Ian McMichael, Pochi Yeh, and Paul Beckwith, presented at the Conference on Lasers and Electro-Optics, Baltimore, Maryland, April 27 - May 1, 1987.

"Double Phase-Conjugate Fiber-Optic Gyro," Ian McMichael and Pochi Yeh, presented at the Annual Meeting of the Optical Society of America, Seattle, WA, October 19-24, 1986; summary published in J. Opt. Soc. Am. A 3, 63 (1986).

"Measurements of the Phase of Phase-Conjugate Reflections," Ian McMichael, Pochi Yeh and Monte Khoshnevisan, Paper FDD4, presented at the International Conference on Quantum Electronics, San Francisco, CA, June 9-13, 1986; summary published in J. Opt. Soc. Am. B 3, 214 (1986).

"Phase-Conjugate Interferometry and Applications," Quantum Electronics Seminar, University of Southern California, March 5, 1986.

"Absolute Phase Shift of Phase Conjugators," Ian McMichael, Pochi Yeh and Monte Khoshnevisan, presented at O-E LASE'86, Los Angeles, CA, January 19-24, 1986.

"Phase-Conjugate Fiber Optic Gyro," Pochi Yeh, Ian McMichael and Monte Khoshnevisan, presented at the Annual Meeting of the Optical Society of America, Washington, D.C., October 14-18, 1985; summary published in Opt. Soc. Am. A 2, P67 (1985).

"Scalar Phase Conjugation Using a Barium Titanate Crystal," Ian McMichael and Monte Khoshnevisan, presented at the Conference on Lasers and Electro-Optics, Baltimore, Maryland, May 20-24, 1985.

* Works only partially supported by this contract.

2.0 PROGRESS

2.1   Phase-Conjugate Fiber-Optic Gyros

Since its first demonstration under this contract, the phase-conjugate fiber-optic gyro (PCFOG) has made steady progress.   This progress is summarized below and is described in detail in the publications that are included in this report as appendices.

Our first objective was to demonstrate that the PCFOG is sensitive to the nonreciprocal phase shift produced by the Sagnac effect and can be used to sense rotation. A proof of concept experiment was set up for this objective using an externally-pumped crystal of barium titanate as the phase conjugator.   This experiment, reported in Ref. 1 (Appendix 4.16), provided the first demonstration of rotation sensing with a PCFOG.

In the proof of concept demonstration of the PCFOG mentioned above, the length of the fiber-optic coil, and therefore the sensitivity of the gyro, was limited by the coherence length of the laser.   To solve this problem we set up a PCFOG consisting of a Michelson interferometer in which the light beams from two arms travel as clockwise and counterclokwise beams respectively, in the same fiber optic coil and reflect from the same self-pumped phase-conjugator.   We reported the demonstration of rotation sensing with this PCFOG in Ref. 2 (Appendix 4.11).

Since phase conjugation can correct for modal scrambling, a PCFOG can use multimode fibers.   However, complete correction of modal scrambling requires a polarization-preserving conjugator and the corresponding experimental setup of a PCFOG is complicated.   To solve this problem we set up a PCFOG using a multimode fiber coil, a nonpolarization-preserving conjugator, and a spatial filter to discriminate against the portion of the light reflected by the conjugator that does not correct for modal scrambling.   This experiment, reported in Ref. 3 (Appendix 4.7), provided the first demonstration of rotation sensing with a PCFOG using multimode fiber.

The demonstrations of PCFOG's described above used a quarter-wave retarder for biasing. This biasing technique is known to be a source of noise and drift. The preferred biasing technique in interferometric fiber-optic gyros is to use a fast (faster than the rountrip time in the fiber coil) phase modulation at one end of the fiber coil. In our first demonstrations of PCFOG's it was not possible to use this technique due to the requirement of mutual coherence between the two beams entering the photorefractive phase conjugator.

However, the recently discovered mutually pumped phase conjugators (MPPC's)[4-6] provided a solution to this problem. (For information on MPPC's see Section 2.5.1). The MPPC's have the unique ability to generate the conjugates of two beams that are mutually incoherent. To test this concept we set up the PCFOG shown in Fig. 1 using the bird-wing MPPC. Light from a laser was coupled onto a rotating table by a single mode polarization-preserving fiber SMPPF. The light exiting from tthe fiber was split into two components by the polarizing beamsplitter PBS. One component traveled in a multimode fiber MMF, and both components were eventually became the pumping beams for the bird-wing MPPC in a crystal of BaTiO3. Although the coherence length of the laser was much shorter than the path length difference between for the components entering the $BaTiO_3$ crystal, the MPPC was able to generate the conjugates of the two components.
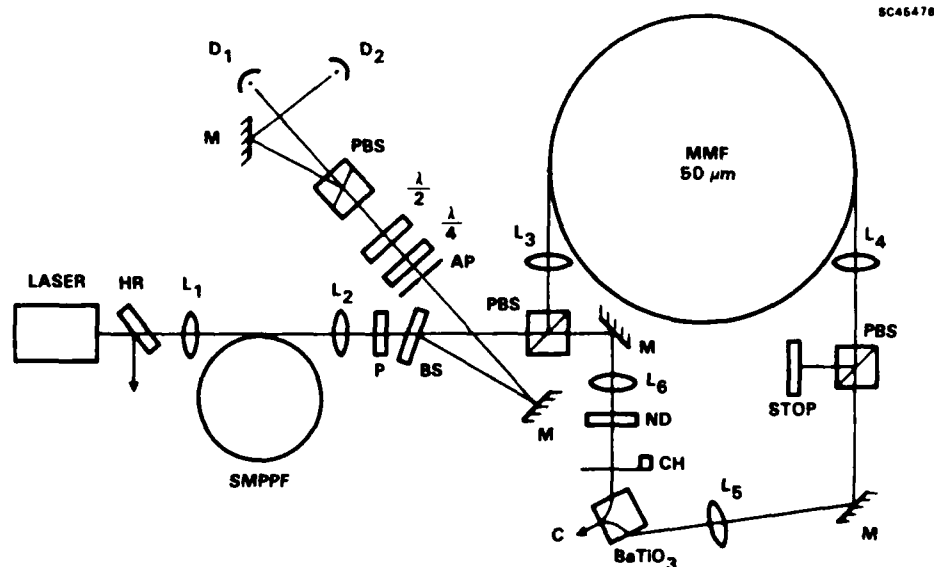
Fig. 1 Multimode fiber gyro using a mutually pumped phase conjugator.

Figure 2 shows representative gyro signals obtained from detectors D1 and D2. For the upper trace, the gyro was first stationary, then it was rotated clockwise, stopped, and then rotated counterclockwise for several cycles with an amplitude of approximately 6°/s. The experimentally measured phase shift was in good agreement with the predicted phase shift. The background noise level with the gyro stationary is shown in the lower trace

SC45475
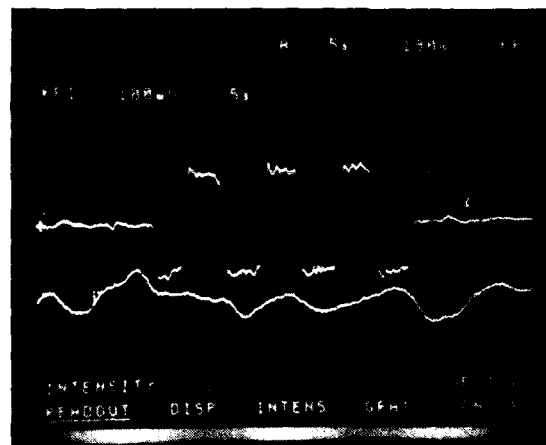
Fig. 2

Gyro signals.

(vertical scale is 10 times more sensitive). We are not certain of the noise source, but we have preliminary data indicating that it is due to the Shupe effect.[7]   Efforts are now underway to minimize the Shupe effect in our PCFOG by quadrature winding and thermal isolation of the fiber coil. The results of our studies of the PCFOG using a MPPC were presented at the 1988 Annual Meeting of the Optical Society of America.[8]   The summary and viewgraphs from that presentation are included in this report as Appendix 4.20.

2.2   Phase-Conjugate Ring Interferometer

The PCFOG is essentilly a ring interferometer utilizing a long fiber-optic coil to increase the accumulated Sagnac phase shift. Before setting up the PCFOG with the MPPC as described in the previous section, we first investigated the simpler phase-conjugate ring interferometer (PCRI) shown in Fig. 3. Incident light was split by beamsplitter BS into two beams that entered a bird-wing MPPC. Light incident on one side of the bird-wing MPPC exits from the opposite side. In this sense, the MPPC acts like a reflector and, consequently, the PCRI acts like a Sagnac interferometer. For a Sagnac interferometer, with no nonreciprocal phase-shifts present, the percentage of power at the subtractive output is given by,

$$(1 - 4RT) \times 100\% \tag{1}$$

where R and T are the intensity reflection and transmission coefficients of the beamsplitter. For our beamsplitter with T = 2/3, R = 1/3, Eq. (1) gives 11.1%. We found, after taking extreme care to insure good overlap of the two beams in the MPPC, that 11.7% of the total

Fig. 3

Phase-conjugate ring interferometer.
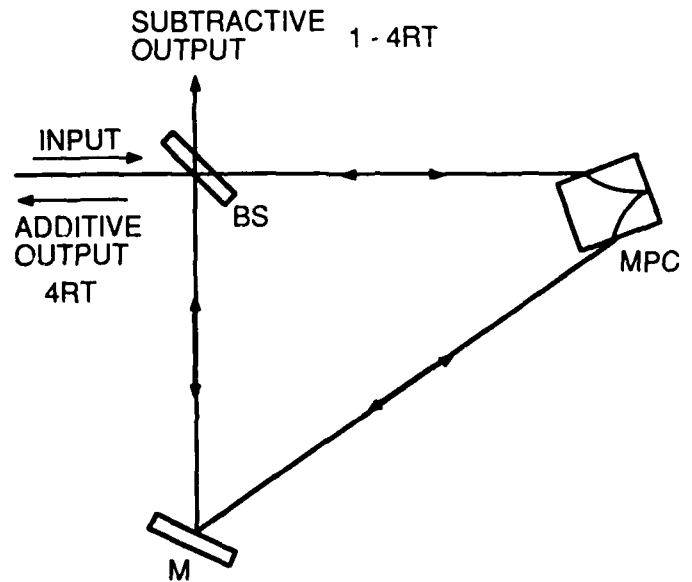
power exits from the subtractive output port of the PCRI; thus verifying its Sagnac nature. This contrasts what occurs when the MPPC is replaced by a self-pumped conjugator where less than 1% exits from the subtractive output.[9]

SUBTRACTIVE OUTPUT   1 - 4RT

INPUT

ADDITIVE OUTPUT 4RT

BS

MPC

M

     Unlike the Sagnac interferometer, the PCRI has a wide field-of-view and can be used to perform image inversion, addition and subtraction. We demonstrated this by placing transparencies in the arms of the PCRI. Figure 4(a) shows the image inversion obtained for an image of five horizontal bars, and Fig. 4(b) shows the subtraction of five horizontal bars and one vertical bar.

SC44760

IMAGE INVERSION

IMAGE

IMAGE SUBTRACTION

IMAGE #1   IMAGE #2
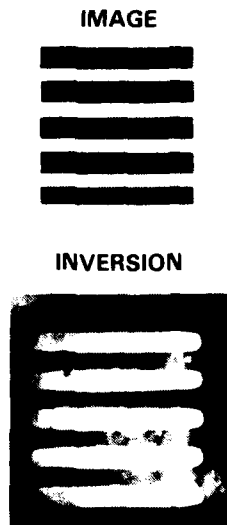
INVERSION
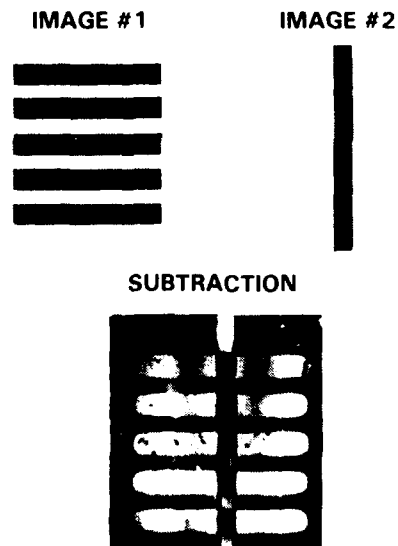
SUBTRACTION

Fig. 4   Image inversion and subtraction with the phase-conjugate ring interferometer.

A second PCRI was set up as shown in Fig. 5. Incident light is split into two linear polarization components by polarizing beamsplitter PBS, one component is rotated by 90° by the half-wave retarder λ/2, and both components are incident on a bird-wing MPPC.
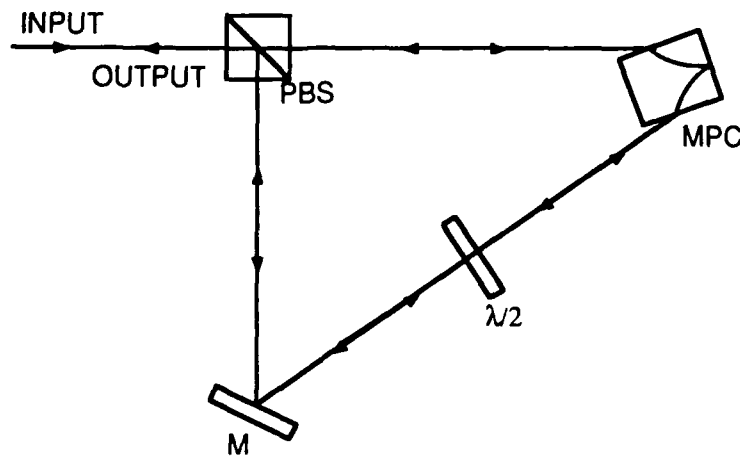
Fig. 5 Another phase-conjugate ring interferometer.

Figure 6 shows the reflected output power (squares) and polarization angle θ_R (crosses) as a function of the polarization angle of the incident beam θ_I. Due to the half-wave retarder in the PCRI, the x (y) component of the input becomes the y (x) component of the output. This is represented by the solid line, $\theta_R = 90° - \theta_I$, that fits well to the crosses. One should note that although the optical setup of this PCRI looks much like the polarization-preserving phase-conjugator described in the following section, it does not pre-serve polarization (ie. the reflected and incident polarization angles are not equal). For θ_I > 80°, corresponding to intensity ratios >32 for the beams incident or the MPPC, the MPPC stopped working.

To demonstrate that the PCRI could be used to measure nonreciprocal phase shifts, we placed a Faraday modulator in the PCRI as shown in Fig. 7. For a voltage of ±0.4 V applied to the modulator, we measured a change in the output polarization corresponding to a nonreciprocal phase shift of 20 mrad. This is exactly what one would predict based on the polarization rotation (10 mrad) produced by the Faraday modulator for the same voltage.

BEAM RATIO
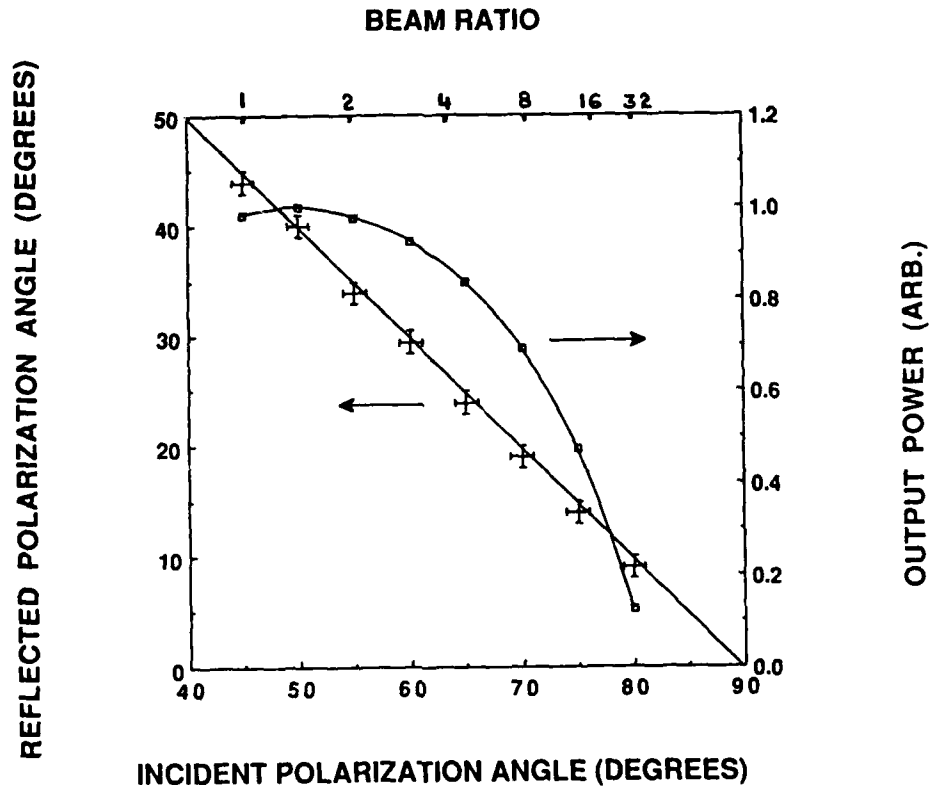
Fig. 6   Reflected polarization angle and output power vs input polarization
angle in the PCRI.
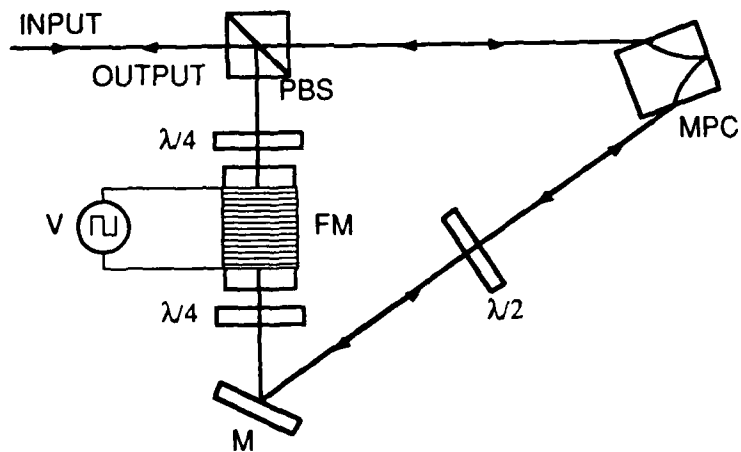
Fig. 7 Setup to demonstrate sensing of nonreciprocal phase shifts in the PCRI.

We also studied the correction of modal scrambling in multimode fibers using the MPPC in the experimental setup shown in Fig. 8. Incident light was first split into two beam by beamsplitter BS. One beam was incident on one side of the MPPC and the other beam was input into a multi-mode fiber. Due to modal scrambling, the emerging light from the fiber is randomly distributed among the spatial and polarization modes of the output. This output was split into its polarization components by polarizing beamsplitter PBS, one component was rotated by 90°, and both were then incident on the other side of the MPPC. The combination of components PBS, $\lambda/2$, and MPPC act as a polarization-preserving conjugator, so that when the reflected waves from the MPPC recombine at the PBS they formed a true time reversed wave. When this wave propagates back through the multimode fiber it will have the same polarization as the beam that was incident on the fiber. To test this we sent linearly polarized light into the fiber with a polarization at 45° to the plane of the figure, and with a major to minor axis ratio of 10^4 (ie. nearly linearly polarized). The measured output polarization was at (45±1)°, with a major to minor axis ratio of 10^2; indicating that this arrangement corrected for the modal scrambling of the fiber to within 1%. We also looked at the case when one of the two polarization components from PBS was blocked (nonpolarization-preserving case). In this case, measured output polarization was again (45±1)°, but the major to minor axis ratio decreased to 10^1; indicating that this arrangement does not do as good a job of correcting for the modal scrambling of the fiber as the previous case.
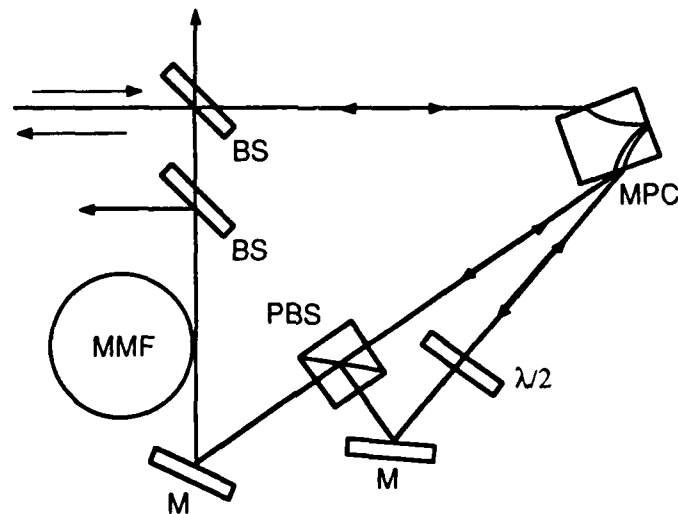
Fig. 8   Setup to demonstrate correction of modal scrambling in fibers by a polarization preserving, mutually pumped phase conjugator.

The results of our investigations of phase-conjugate ring interferometers were presented at the 1988 International Quantum Electronics Conference.[10] The summary and viewgraphs from that presentation are included in this report as Appendix 4.22.

2.3 Polarization-Preserving Phase-Conjugators

As noted in the previous section, complete correction of modal scrambling re-quires a polarization-preserving conjugator (PPPC). With this motivation we developed the first PPPC that operates at milliwatt power levels. The PPPC works by decomposing an in-cident light beam into its two polarization components, rotating one with a half-wave re-tarder, and reflecting both from the same conjugator. When the reflected components re-combine they form a conjugate wave that has the same polarization as the inciden' beam. Our report of this development is contained in Ref. 11 (Appendix 4.13) and Ref. 12 (Appen-dix 4.6).

2.4 Correction of Modal Scrambling in Multimode Fibers by Phase-Conjugation

We investigated both theoretically and experimentally the correction of modal scrambling in multimode fibers by phase conjugation and reported our results in Ref. 13 (Appendix 4.9) and Ref. 14 (Appendix 4.8). A summary of our results is presented here. When polarized light is incident on one end of a long multimode fiber, the light exiting from the other end is randomly distributed among the spatial and polarization modes. Recovery of the spatial and polarization modes of the incident light takes place only when the conjugator at the fiber output preserves polarization on reflection. However, if the fiber supports a large number of spatial modes and one uses spatial filtering to look at only the light returning in the same spatial mode as the incident light, then one will see nearly complete polarization recovery, even when only one polarization component is conjugated at the output of the fiber. This is a result of the fact that light returning down the fiber that is orthogonal in polarization to the inpuut is randomly distributed among all of the spatial modes.

2.5 Phase Shifts of Photorefractive Gratings and Phase-Conjugate Waves

The phase of the phase-conjugate reflection determines the operating point of phase-conjugate interferometers such as the PCFOG. With the proper choice of nonlinear

media, these interferometers can be biased at the operating point of highest sensitivity and linear response (quadrature). With this motivation we studied the phase shifts of photorefractive gratings and phase-conjugate waves. Our results are presented in Ref. 15 (Appendix 4.10) and Ref. 16 (Appendix 4.14), and summarized here.

In four-wave mixing, the phase of the phase-conjugate wave contains the phase of the pumping and probe waves, and a phase shift determined by the nonlinear medium. This second term, the phase shift of the phase conjugator ϕ_0, is a function of the type of grating (refractive index, absorption, or gain) and the phase shift of this grating ϕ_g with respect to the light interference pattern. For kerr media (index grating, $\phi_g = 0°$) $\phi_0 \sim 90°$, and for photorefractive media (index grating, $\phi_g \sim \pm90°$) $\phi_0 \sim 0°$ or $180°$.

Measurements show that the two-wave mixing gain in barium titanate is an asymmetric function of frequency detuning, indicating that ϕ_g is not exactly $90°$, as is often assumed. The value of ϕ_g obtained from the two-wave mixing measurements compares well with that obtained from four-wave mixing measurements of ϕ_0.

2.6 Photorefractive Phenomena

2.6.1 Theory and Model of Mutually Pumped Phase Conjugation

Many phase-conjugate mirrors have been reported in the literature. One way to classify these conjugators is by their method of pumping, and the corresponding number of main beams incident on the nonlinear medium. There are at present at least three classes in this classification scheme; (1) externally pumped phase conjugators (three beams incident), (2) self-pumped phase conjugators (one beam incident), and (3) mutually pumped phase conjugators (two beams incident). Figure 9 illustrates the class known as mutually pumped phase conjugators (MPPC's). Two beams, A1 and A3, are incident on a nonlinear material, and their conjugates, A3 and A4 respectively, are generated. Although MPPC's were predicted several years ago, their demonstration is very recent.[4-6] Presently, a lot of attention is being focussed on MPPC's for a number of reasons. Perhaps the most important reason is the ability of the MPPC to operate with mutually incoherent beams, and the resulting implications for applications such as the phasse-conjugate fiber-optic gyro, phase-conjugate communications. In this section we summarize progress in the areas of theory and modelling of MPPC's that was made under this contract.
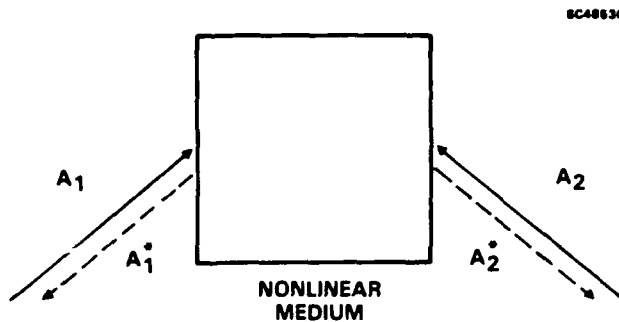
Fig. 9

Mutually pumped phase conjugator.

We have developed a theory that explains the operation of MPPC's.[17] The details of this theory are presented in the preprint of our paper which is attached as Appendix 4.1, and a summary of this theory is presented here. To obtain an understanding of MPPC's, first consider what happens when only one beam, A_1, is incident on a photorefractive crystal as shown in Fig. 10(a). Light scattered in the crystal forms gratings with the incident beam and is amplified by two-beam coupling. This results in a broad fan of light, A_3, that exits from the crystal. When a second beam, A_2, is turned on, an interesting thing happens. Initially, the two beams will fan into each other as shown in Fig. 10(b). Each of the two fanning beams A_3 and A_4 can be decomposed into two components, a component that is the conjugate of A_1 and A_2, respectively, and a component that is orthogonal to the conjugate, or nonconjugate. Using coupled mode theory, we have shown that the exponential gain coefficient for the conjugate component is twice that of the nonconjugate component. (This factor of two is reminisent of that which explains the phase-conjugate nature of stimulated Brilloin scattering.) Although the initial fanning indicates that the total power carried by the nonconjugate components dominates in the beginning, the higher gain for the conjugate component eventually causes nearly all of the power carried by the fanning beams A_3 and A_4 to collapse into the conjugate waves A_1^* and A_2^*, respectively as shown in Fig. 10(c) In the end, the incident beams share a single grating or hologram which diffracts A_1 to produce the conjugate of A_2, and diffracts A_3 to produce the conjugate of A_1. Therefore, this model of MPPC's is often referred to as "hologram sharing."

We have also studied a new resonator model for MPPC's illustrated in Fig. 11. Crystal C1 and its pumping beam A_1 are oriented such that two-beam coupling is the source of gain for the counterclockwise oscillation B_1 in the ring resonator formed by mirrors M1-M3. Similarly, C2 and A_2 provide gain for the clockwise oscillation B_2. Readout by B_2 of
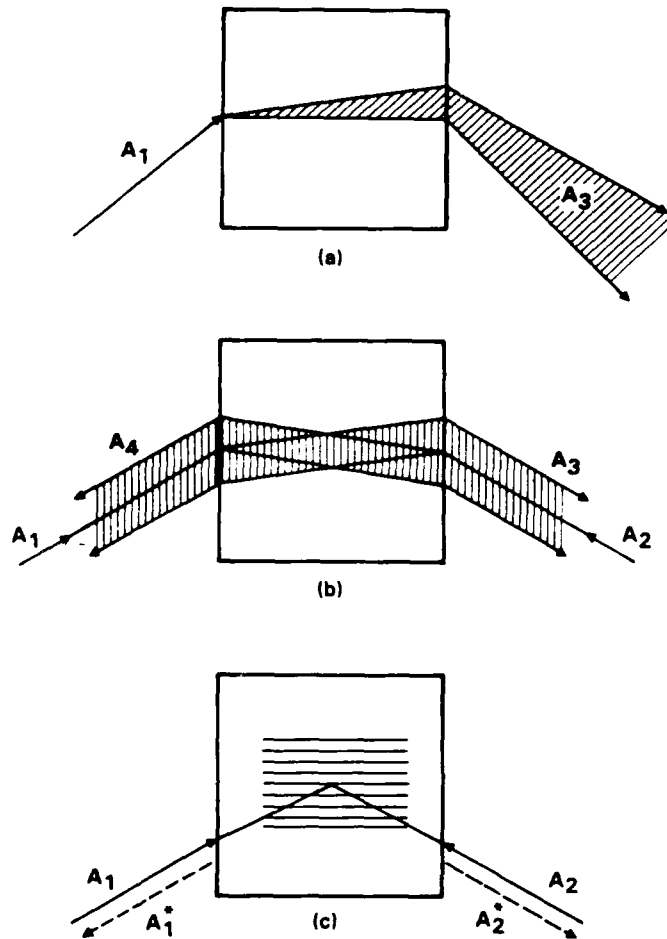
Fig. 10

Hologram sharing model of
mutually pumped phase con-
jugation.
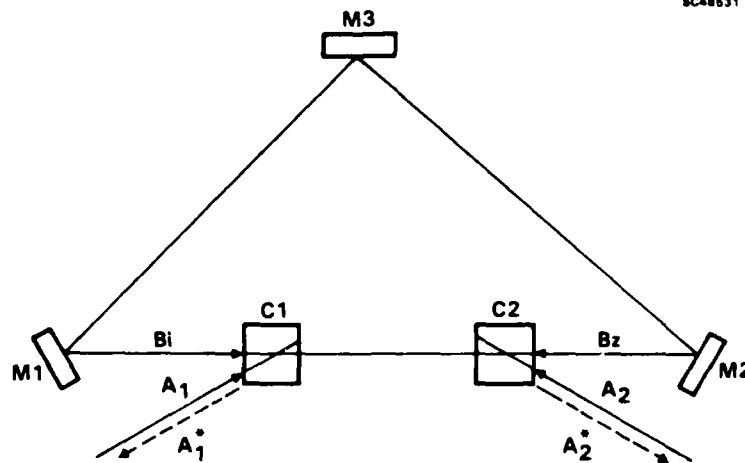
Fig. 11 Resonator model of mutually pumped phase conjugation.

the grating written by A_1 and B_1 produces the conjugate A_1^* by four-wave mixing, provided that $B_2 = B_1^*$. Similarly, readout by B_1 of the grating written by A_2 and B_2 produces the conjugate A_2^*. The condition $B_2 = B_1^*$ will be satisfied whenever the counterpropagating oscillations occupy the same spatial modes. For example, this can be accomplished by placing an aperature in the cavity to restrict both of the counterpropagating oscillations to the lowest order mode. We have demonstrated and studied a resonator MPPC using two separate crystals of $BaTiO_3$.[18] The resonator model and experiments are described in detail in Appendix 4.3.

2.6.2 Cross-Polarization Coupling in Cubic Photorefractive Crystals

Two-beam coupling usually refers to a process in which two beams of the same polarization exchange energy in a photorefractive crystal. We have developed a theory and performed experiments demonstrating the possibility of cross-polarization two-beam coupling in which two beams of same polarization can interact to generate a beam of orthogonal polarization in cubic photorefractive crystals. This is a result of the fact that the photorefractive gratings are in general birefringent due to the tensor nature of the electro-optic effect. In general, cross polarization coupling is not possible in non-cubic crystals, since the optical anisotropy of these crystals will not allow for phase matching except along certain special directions. The unique property of cross polarization coupling - that the presence of a pump beam can transform the polarization of the probe - has potential applications in optical-image and -signal processing (e.g., spatial light modulators and narrow band filters). Details of the theory and experiments on cross-polarization coupling are presented in Refs. 19, 20 (Appendix 4.2) and Ref. 21 (Appendix 4.4).

2.6.3 Artificial Photorefractive Effect in Ruby

In two-wave mixing, the interference of two light waves results in a spatial modulation of the optical susceptibility of some medium. The two waves then interact through this grating, and net energy transfer between the two waves takes place when the grating is shifted in phase with respect to the interference pattern. Energy transfer is observed in photorefractive media, where a phase shift of approximately 90° results from the grating formation process.[22] In other media where the grating is usually in phase with the interference pattern, it is possible to produce a phase shift between the grating and the interference pattern, and to observe energy transfer, by moving the grating at a rate

comparable to the response time of the medium. This can be accomplished in several ways: by nondegenerate two-wave mixing (NDTWM or "artificial photorefractive effect") in which a frequency shift between the interacting waves results in a moving interference pattern, by moving the medium itself,[23] or by using the Lorentz force to move the free-carrier grating in a semiconducting medium.[24] NDTWM takes place in such stimulated scattering processes as Rayleigh line, Brillouin, Rayleigh wing, and Raman scattering. In these processes, the corresponding nonlinearity is increased by the resonant Q, $Q = f/\Delta f$ (for backward SBS in CS2, $Q \sim 100$). However, since the corresponding nonlinearities (Kerr effect where a change of polarizability of individual molecules is due to field-induced deformation and reorientation, and electrostriction and absorptive thermal nonlinearities) are very small to begin with, the power densities required to observe these effects are still very large (~ 10 MW/cm^2). It is therefore surprising that NDTWM in saturable resonant media has not been investigated extensively, since the corresponding nonlinearities can be many orders of magnitude higher and the power densities required can be many orders of magnitude lower. To our knowledge in the past there were only two reports of such investigations; oone using sodium vapour[25] and another using a fluorescein-doped glass.[26] Our studies involved NDTWM in ruby.[27] We have shown that our results are in agreement with the theory of NDTWM[28] when it is generalized to take into account a complex nonlinear index, we have demonstrated two-wave mixing gain exceeding the absorption and reflection losses, indicating that NDTWM can be used for optical amplification, and we have pointed out that these experiments provide a simple and accurate method for determining the complex nonlinear index, response time, and saturation intensity. The details of our studies on NDTWM in ruby are presented in Appendix 4.5.

2.6.4   Photorefractive Conical Diffraction

A linearly polarized beam incident on a photorefractive crystal can cause a cone of light to emerge with polarization orthogonal to that of the incident beam. The cone angle is determined by the phase-matching condition for the incident and cone beams. Measurement of the cone angle as a function of the incident angle provides a simple and accurate method for determining the dispersion of the birefringence in photorefractive crystals. Details of our theoretical and experimental investigations into the phenomena of conical diffraction are presented in Ref. 29 which is included in this report as Appendix 4.12.

2.6.5   Frequency Shifts in Photorefractive Oscillators and Conjugators

Photorefractive oscillators exhibit a frequency difference between the oscillating and pump beams on the order of one Hertz, and they oscillate over a large range of cavity detuning despite their narrow gain bandwith. We have developed a theory showing that nondegenerate two-wave mixing results in a phase shift that compensates for the cavity detuning; thus explaining the previously mentioned properties of photorefractive oscillators.   The details of our theory and its experimental verification are presented in Ref. 30 (Appendix 4.18) and Ref. 31 (Appendix 4.19).

The reflection from most photorefractive, self-pumped phase conjugators differs in frequency from the incident beam by approximately one Hertz. We have developed a theory and carried out supporting experiments to explain such frequency shifts. In our model, oscillating beams build up in a resonant cavity formed by external mirrors or crystal faces, and these beams provide the pump waves for four-wave mixing. The frequency shifts of the oscillating beams and reflected beam are proportional to the cavity length detuning as noted above. Details of our theory and experiments are presented in Ref. 32 which is included in this report as Appendix 4.17.

3.0 REFERENCES

1. P. Yeh, I. McMichael and M. Khoshnevisan, Appl. Opt. 25, 1029 (1986).

2. I. McMichael and P. Yeh, Opt. Lett. 11, 686 (1986).

3. I. McMichael, P. Beckwith, and P. Yeh, Opt. Lett. 12, 1023 (1987).

4. R.W. Eason and A.M.C. Smout, Opt. Lett. 12, 51 (1987); A.M.C. Smout and R.W. Eason, Opt. Lett. 12, 498 (1987).

5. S. Weiss, S. Sternklar and B. Fischer, Opt. Lett. 12, 114 (1987); S. Sternklar, S. Weiss, M. Segev and B. Fischer, Opt. Lett. 11, 528 (1986).

6. M.D. Ewbank, Opt. Lett. 13, 47 (1988).

7. D. Shupe, Appl. Opt. 19, 654 (1980).

8. I. McMichael, P. Beckwith, and P. Yeh, "Multimode Fiber Gyro Using a Mutually Pumped Conjugator," OSA Annual Meeting, 1988 Technical Digest Series, Vol. 11 (Optical Society of America, Washington, DC, 1988), p. 180.

9. M.D. Ewbank, P. Yeh, M. Khoshnevisan, and J. Feinberg, Opt. Lett. 10, 282 (1985).

10. Ian McMichael, M. D. Ewbank, and Pochi Yeh, "Phase-Conjugate Ring Interferometer," in Conference on Lasers and Electro-Optics Technical Digest Series 1988, (Optical Society of America, Washington, DC, 1988), paper TUQ2, p. 134.

11. I. McMichael, P. Yeh and M. Khoshnevisan, Opt. Lett. 11, 525 (1986).

12. I. McMichael, J. Opt. Soc. Am. B 5, 863 (1987).

13. I. McMichael, P. Yeh, and P. Beckwith, Opt. Lett. 12, 507 (1987).

14. P. Beckwith, I. McMichael, and P. Yeh, Opt. Lett. 12, 510 (1987).

15. I. McMichael and P. Yeh, Opt. Lett. 12, 48 (1987).

16. I. McMichael, P. Yeh and M. Khoshnevisan, Proc. Soc. Photo-Opt. Instrum. Eng. 613, 32 (1986).

17. Pochi Yeh, "Coupled-Mode Theory of Hologram Sharing in Mutually Pumped Phase Conjugators," submitted to Opt. Lett., May 24 (1988).

18. P. Yeh, T. Y. Chang, and M. Ewbank, J. Opt. Soc. Am. B 5, 1743 (1988).

19. P. Yeh, J. Opt. Soc. Am. B 4, 1382 (1987).

20. P. Yeh, J. Opt. Soc. Am. B 5, 1811 (1988).

21. T. Chang, A. Chiou, and P. Yeh, J. Opt. Soc. Am. B, 5, 1724 (1988).

22. D. Staebler and J. Amodei, J. Appl. Phys. 43, 1042 (1972).

23. Y. Anan'ev, Sov. J. Quant. Electron. 4, 929 (1975).

24. V. Vinetskii, N. Kukhtarev, S. Odulov, and M. Soskin, Sov. Phys. Tech. Phys. 22, 729 (1977).

25. G. Grynberg, E. Le Bihan, and M. Pinard, J. Physique 47, 1321 (1986).

26. M. Kramer, W. Tompkin, and R. Boyd, Phys. Rev. A 34, 2026 (1986).

27. I. McMichael and P. Yeh, Opt. Lett. 13, 500 (1988).

28. P. Yeh, J. Opt. Soc. Am. B 3, 747 (1986).

29. M. Ewbank, P. Yeh and J. Feinberg, Opt. Comm. 59, 423 (1986).

30. P. Yeh, J. Opt. Soc. Am. B 2, 1924 (1985).

31. M. Ewbank and P. Yeh, Opt. Lett. 10, 496 (1985).

32. M. Ewbank and P. Yeh, Proc. Soc. Photo-Opt. Instrum. Eng. 613, 59 (1986).

4.0 APPENDICES

APPENDIX 4.1

COUPLED-MODE THEORY OF HOLOGRAM SHARING IN MUTUALLY PUMPED PHASE CONJUGATORS

COUPLED-MODE THEORY OF HOLOGRAM SHARING

IN MUTUALLY PUMPED PHASE CONJUGATORS

Pochi Yeh

Rockwell International Science Center

Thousand Oaks, CA 91360

Abstract

A coupled-mode theory is developed for photorefractive hologram sharing in mutually pumped phase conjugators. The theory shows that the spatial gain coefficients for the mutually conjugated beams are twice as large as those of other scattered beams.

Mutually pumped phase conjugators (MPPCs) are nonlinear optical devices in which two incident laser beams can mutually pump each other and produce phase-conjugated beams inside photorefractive crystals. Such phase conjugators operating in the degenerate regime were first studied theoretically[1] in terms of self-oscillations in a four-wave mixing process. Recently, these mutually pumped phase conjugators were demonstrated experimentally using two incoherent laser beams in barium titanate crystals.[2-4] These MPPCs with mutually incoherent beams can be explained by the hologram-sharing model[5] or the resonator model.[6]

The hologram-sharing model proposed earlier,[5] provides a very good explanation of the phenomenon of mutually pumped phase conjugation in photorefractive crystals. The model is based on the fact that cross washout of index gratings generally occurs except when two sets of beams share the common hologram. Although the model gives a very clear picture of the physical mechanisms involved in MPPC, no quantitative results are given to describe the growth of the phase-conjugated waves. In this paper, the author presents a coupled-mode analysis for the hologram-sharing model of the mutually pumped phase conjugators.

Referring to Fig. 1, let us consider the interaction of two sets of beams in a photorefractive medium. Beam 1 and beam 2 are mutually coherent; beam 3 and beam 4 are also mutually coherent. But beam 2 and beam 3 (or 2 and 4) are mutually incoherent. The electric field can be written as

$$E = \sum_{j=1}^{4} A_j \, e^{i(\omega_j t - \vec{k}_j \cdot \vec{r})} \tag{1}$$

where A_1, A_2, A_3, A_4 are the complex amplitude of the four waves, ω_1, ω_2, ω_3, ω_4 are the angular frequencies, and $\vec{k}_1$, $\vec{k}_2$, $\vec{k}_3$, $\vec{k}_4$ are the wavevectors. The frequencies of the beam satisfy the following condition:

$$\omega_1 = \omega_2 \neq \omega_3 = \omega_4 \tag{2}$$

This condition indicates that beams 1 and 2 are mutually coherent, beams 3 and 4 are also mutually coherent. In addition, these two sets of beams are mutually incoherent. Inside the photorefractive medium, these four beams intersect and form volume holograms. We assume that beams 1 and 2 enter the medium at the face $z = 0$, and beams 3 and 4 enter the medium from the back face $z = L$. If we assume that the frequencies are very different such that $(\omega_3 - \omega_1)\tau \gg 1$ (where τ is the photorefractive grating decay time), the fundamental component of the index grating can be written

$$\Delta n = \frac{1}{2} n_1 e^{i\phi} \frac{A_1^* A_2 e^{-i\vec{K}_{21} \cdot \vec{r}} + A_3^* A_4 e^{-i\vec{K}_{43} \cdot \vec{r}}}{I_0} + c.c. \tag{3}$$

where I_0 is proportional to the total intensity and is given by

$$I_0 = |A_1|^2 + |A_2|^2 + |A_3|^2 + |A_4|^2 \tag{4}$$

and $\vec{K}_{21}$ and $\vec{K}_{43}$ are the grating wavevectors

$$\vec{K}_{21} = \vec{k}_2 - \vec{k}_1 , \qquad \vec{K}_{43} = \vec{k}_4 - \vec{k}_3 \tag{5}$$

and c.c. denotes the complex conjugate term. We note that there are only two contributions to the index grating since beams 1 and 2 are incoherent with respect to beams 3 and 4. If $\vec{K}_{21}$ is distinct from $\vec{K}_{43}$, then the coupled mode equations can be written

$$\frac{d}{dz} A_1 = -\frac{1}{2} \gamma_{21} |A_2|^2 A_1 / I_o$$

$$\frac{d}{dz} A_2 = \frac{1}{2} \gamma_{21} |A_1|^2 A_2 / I_o$$

$$\frac{d}{dz} A_3 = -\frac{1}{2} \gamma_{43} |A_4|^2 A_3 / I_o \qquad (6)$$

$$\frac{d}{dz} A_4 = \frac{1}{2} \gamma_{43} |A_3|^2 A_4 / I_o$$

where γ_{21} and γ_{43} are coupling constants. In deriving the coupled-mode equations, we assume that the photorefractive medium operates by diffusion only so that $\phi = \pi/2$. In addition, we neglect the material absorption. We notice that there are two sets of two-beam coupled-mode equations in Eq. (6). In other words, the two sets of beams undergo two-beam coupling independent of each other, except the denominator I_o which accounts for the cross washout of the gratings due to the presence of the other set of beams. The cross washout is a result of two gratings sharing the same volume of photorefractive medium.

When $\vec{k}_4 = -\vec{k}_1$ and $\vec{k}_2 = -\vec{k}_3$, the wavevectors of the two gratings are identical, i.e.,

$$\vec{K}_{21} = \vec{K}_{43} \qquad (7)$$

the coupled-mode equations can be written

$$\frac{d}{dz} A_1 = -\frac{1}{2} \gamma \left[A_2^* A_1 + A_4^* A_3 \right] A_2/I_0$$

$$\frac{d}{dz} A_2 = \frac{1}{2} \gamma \left[A_1^* A_2 + A_3^* A_4 \right] A_1/I_0$$

$$\frac{d}{dz} A_3 = -\frac{1}{2} \gamma \left[A_4^* A_3 + A_2^* A_1 \right] A_4/I_0 \tag{8}$$

$$\frac{d}{dz} A_4 = \frac{1}{2} \gamma \left[A_3^* A_4 + A_1^* A_2 \right] A_3/I_0$$

where $\gamma = \gamma_{21} = \gamma_{43}$ is the coupling constant. We notice that there are two terms on the right side of each equation in (8). Each term represents Bragg scattering from one grating. Since these two gratings have the same wavevector, they contribute equally to the Bragg scattering. If in addition,

$$A_4 = \rho A_1^* \tag{9}$$

$$A_2 = \rho A_3^*$$

where ρ is an arbitrary constant, then the two terms in the square brackets in Eq. (8) are identical, and the coupled equations become

$$\frac{d}{dz} A_1 = -\gamma \, |A_2|^2 A_1/I_o$$

$$\frac{d}{dz} A_2 = \gamma \, |A_1|^2 A_2/I_o$$

(10)

$$\frac{d}{dz} A_3 = -\gamma \, |A_4|^2 A_3/I_o$$

$$\frac{d}{dz} A_4 = \gamma \, |A_3|^2 A_4/I_o$$

Let us assume that beams 2 and 4 are the ones that get amplified due to two-beam coupling (i.e., $\gamma > 0$). We now examine the spatial growth of beams 2 and 4. The exponential growth constant for these two beams in Eqs. (10) is twice as large as that of the same beams in Eqs. (6) as a result of the hologram sharing. This factor of 2 is reminiscent of the theoretical proof of the phase-conjugated nature of SBS.[7-8] It was shown that the gain coefficient for the conjugated wave in SBS is twice that of any other scattered wave.[9] In photorefractive media such as $BaTiO_3$ or SBN, the exponential gain coefficient can be as large as $40 \, cm^{-1}$.[10] Thus in a sample of 1 cm, the ratio between the gain of mutually phase conjugated beams and that of the randomly scattered beams can be as large as a factor of exp (20). This enormous factor indicates that the mutually phase conjugate beams are the dominant ones in terms of spatial growth and that the conjugated beams can be generated from the noise.

In photorefractive crystals such as $BaTiO_3$ or SBN, mutually pumped phase conjugation starts from scattering of the two incident beams (beams 1 and 3) (see Fig. I(b)). These scattered waves are represented by A_2 amd A_4 in Eq. (1). As a result of photorefractive coupling, these scattered waves will be amplified in the medium.

Initially these scattered waves A_2 and A_4 may have arbitrary wavefronts. These scattered waves may be decomposed into two parts

$$A_2(0) = \rho A_3^*(0) + A_2'(0)$$
$$A_4(L) = \rho A_1^*(L) + A_4'(L)$$
(11)

where $A_2'(0)$ and $A_4'(L)$ represent the portions which are orthogonal to the conjugate waves. As indicated earlier, these nonconjugated parts have smaller gain coefficients compared to the conjugated parts. Although these nonconjugated parts may be significant in the beginning, the conjugated parts dominate at the end due to the exponential growth. Thus in high gain media such as $BaTiO_3$ and SBN, the mutually phase conjugated beams are often many orders of magnitude higher than other scattered beams.

In conclusion, a coupled-mode theory is developed for the hologram-sharing model of mutually pumped phase conjugation (MPPC). The theory predicts that the amplification coefficient for the mutually phase conjugated beams is twice that of other scattered beams, and provides a quantitative basis for the hologram sharing model.

References:

1.   M. Cronin-Golomb, B. Fischer, J.O. White and A. Yariv, IEEE J. Quantum Electron. QE-20, 12 (1984).

2.   S. Weiss, S. Sternklar and B. Fischer, Opt. Lett., 12, 114 (1987).

3.   M.D. Ewbank, Topical meeting on photorefractive materials, effects, and devices technical digest Vol. 17 (Optical Society of America, Washington DC, 1987), pp. 179-182.

4.   R.W. Eason and A.M.C. Smout, Opt. Lett., 12, 51 (1987); A.M.C. Smout and R.W. Eason, Opt. Lett., 12, 114 (1987).

5.   M.D. Ewbank, Opt. Lett., 13, 47 (1988).

6.   P. Yeh, T.Y. Chang, and M.D. Ewbank, to appear in J. Opt. Soc. Am. B (August 1988).

7.   B. Ya. Zel'dovich, V.I. Popovichev, V.V. Ragul'skii, and F.S. Faizullov, ZhETF Pis. Red. 15, 160 (1972).

8.   R.W. Hellworth, J. Opt. Soc. Am., 68, 1050 (1978).

9.   B. Ya. Zel'dovich, N.F. Pilipetskii, and V.V. Shkunov, Optical Phase Conjugation, p. 135-167 (Academic Press, 1983).

10.   F. Laeri, T. Tschudi, J. Albers, Opt. Comm., 47 387 (1983).

(a)

(b)
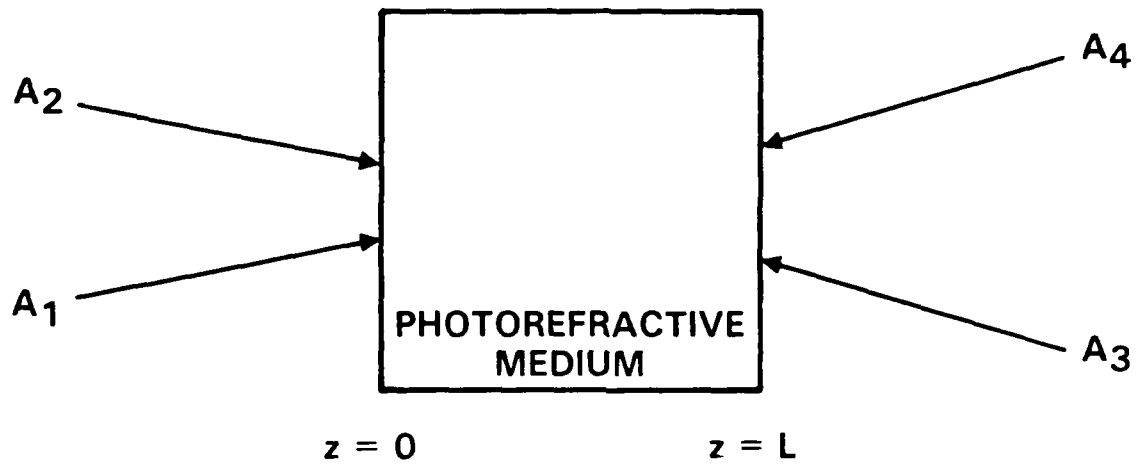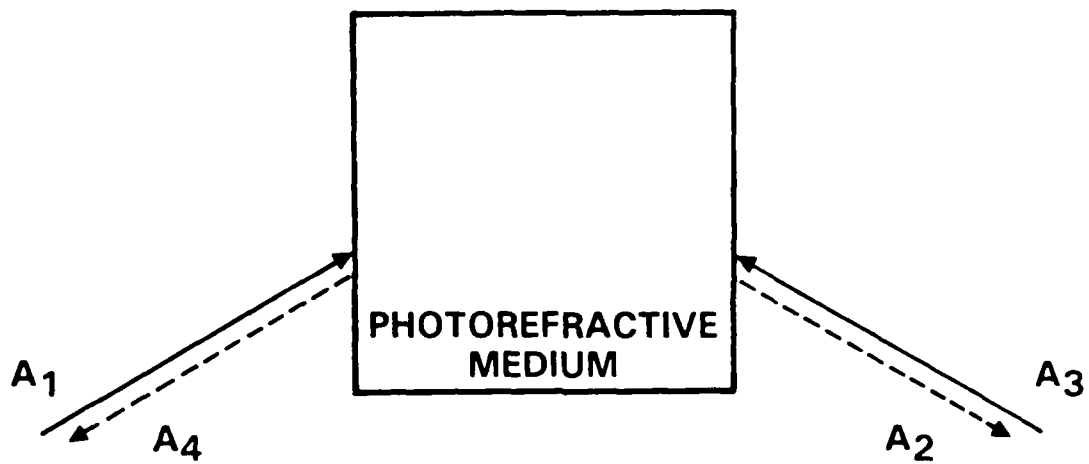
APPENDIX 4.2

PHOTOREFRACTIVE TWO-BEAM COUPLING IN CUBIC CRYSTALS

II. GENERAL CASE ($\phi \int \pi/2$)

Photorefractive two-beam coupling in cubic crystals. II. General case ($\phi \neq \pi/2$)

Pochi Yeh

Rockwell International Science Center, P.O. Box 1085, Thousand Oaks, California 91360

Photorefractive two-beam coupling in cubic crystals in which the spatial phase shift between the index grating and the intensity pattern is not $\pi/2$ is considered. Exact solutions for codirectional cross-polarization two-wave mixing are obtained. The results are useful for the case of nondegenerate two-wave mixing when the spatial phase shift is not $\pi/2$.

A nonlinear model of photorefractive two-wave mixing in cubic crystals was recently developed.[1] In the model each beam consisted of two orthogonally polarized components that were designated s and p components. Coupled-mode equations for the four-wave amplitudes were derived. The theory shows that cross-polarization two-wave mixing is possible in cubic crystals with a zinc-blende structure (point group symmetry $\overline{4}3m$). At the same time, several experimental investigations were carried out to study such cross-polarization couplings in GaAs crystals.[2-5]

In the previous work a $\pi/2$ spatial phase shift between the index grating and the intensity pattern was assumed. This phase shift corresponds to the case of pure diffusion (i.e., no externally applied static electric field). Exact solutions of the coupled-mode equations were obtained for the case of codirectional coupling. Approximate solutions for both the codirectional and the contradirectional coupling were also obtained.

In this paper we will derive exact solutions for the general case of codirectional cross coupling when the spatial phase shift is not $\pi/2$. This corresponds to situations when the two beams are different in frequency or when an external electric field is applied. Deviation from $\phi = \pi/2$ has been observed with oxide materials such as BaTiO$_3$ and Sr$_{0.6}$Ba$_{0.4}$Nb$_2$O$_6$.[6] The exact solutions are formally identical to those of the case $\phi = \pi/2$, except for a complex phase factor in the argument of a transcendental function.

Following the notation used in Ref. 1 and referring to Fig. 1, we can write the coupled-mode equations as

$$\frac{d}{dz} A_s = \frac{i}{2\beta_1} e^{i\phi}[\Gamma_{ss}B_s + \Gamma_{sp}B_p](A_sB_s{}^* + A_pB_p{}^* \cos\theta)/I_0,$$

$$\frac{d}{dz} B_s = \frac{i}{2\beta_2} e^{-i\phi}[\Gamma_{ss}A_s + \Gamma_{sp}A_p](A_s{}^*B_s + A_p{}^*B_p \cos\theta)/I_0,$$

$$\frac{d}{dz} A_p = \frac{i}{2\beta_1} e^{i\phi}[\Gamma_{ps}B_s + \Gamma_{pp}B_p](A_sB_s{}^* + A_pB_p{}^* \cos\theta)/I_0,$$

$$\frac{d}{dz} B_p = \frac{i}{2\beta_2} e^{-i\phi}[\Gamma_{ps}A_s + \Gamma_{pp}A_p](A_s{}^*B_s + A_p{}^*B_p \cos\theta)/I_0,$$

(1)

where A_s, A_p, B_s, and B_p are the wave amplitudes, β_1 and β_2 are the z components of the wave vector, θ is the angle between the two beams inside the crystal, ϕ is the spatial phase shift between the grating and the intensity pattern, and I_0 is given by

$$I_0 = A_s{}^*A_s + A_p{}^*A_p + B_s{}^*B_s + B_p{}^*B_p.$$

(2)

The coupling matrix Γ is given by

$$\Gamma = \omega^2\mu\epsilon_0\epsilon_1,$$

(3)

with

$$\epsilon_1 = n^4 r_{41}\begin{bmatrix} 0 & E_z & E_y \\ E_z & 0 & E_x \\ E_y & E_x & 0 \end{bmatrix}.$$

(4)

where $r_{41} = r_{231} = r_{312} = r_{123}$ and $E_x, E_y,$ and E_z are the three components of the amplitude of the space-charge field.
Also,

$$\Gamma_{ij} = \langle i|\Gamma|j\rangle, \qquad i, j = \hat{s}, \hat{p}_1, \hat{p}_2.$$

(5)

where $\hat{s}$, $\hat{p}_1$, and $\hat{p}_2$ are unit vectors along the direction of polarization.

As indicated by the subscripts, Γ_{ij} are the coupling constants between the ith and jth polarized waves. Thus Γ_{ss} and $\Gamma_{p_1p_2}$ are the parallel coupling constants, and Γ_{sp} and Γ_{sp_2} are the cross-coupling constants.

For the case of pure codirectional cross coupling, as described in Ref. 1,

$$\Gamma_{ss} = \Gamma_{p_1p_2} = 0,$$

(6)

$$\Gamma_{sp} = \Gamma_{p_1s} = \Gamma_{sp_2} = \Gamma_{p_2s} = (2\pi/\lambda)^2 n^4 r_{41}E^{sc} \cos(\theta/2),$$

(7)

where E^{sc} is the amplitude of the space charge field and we assume that the beams enter the crystal symmetrically such that

$$\beta_1 = \beta_2 = (2\pi/\lambda)n \cos(\theta/2).$$

(8)

The coupled-mode equations (1) become
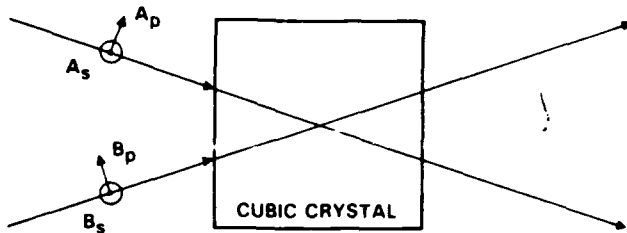
Fig. 1. Schematic drawing of two-beam coupling in photorefractive cubic crystals.

$$\frac{d}{dz} A_s = ie\gamma B_p (A_s B_s{}^* + A_p B_p{}^* \cos\theta)/I_0,$$

$$\frac{d}{dz} B_s = ie^*\gamma A_p (A_s{}^* B_s + A_p{}^* B_p \cos\theta)/I_0,$$

$$\frac{d}{dz} A_p = ie\gamma B_s (A_s B_s{}^* + A_p B_p{}^* \cos\theta)/I_0,$$

$$\frac{d}{dz} B_p = ie^*\gamma A_s (A_s{}^* B_s + A_p{}^* B_p \cos\theta)/I_0, \qquad (9)$$

where

$$e = e^{i\phi} \qquad (10)$$

and γ is a real coupling constant given by

$$\gamma = \tfrac{1}{2} (2\pi/\lambda) n^3 r_{41} E^{sc}. \qquad (11)$$

We notice that Eqs. (9) reduce to the previous case[1] if we put $\phi = \pi/2$. The constants of integration are still given by

$$A_s A_s{}^* + B_p B_p{}^* = c_1, \qquad (12)$$

$$A_p A_p{}^* + B_s B_s{}^* = c_2, \qquad (13)$$

$$A_s A_p{}^* + B_s{}^* B_p = c_3, \qquad (14)$$

$$A_s B_s - A_p B_p = c_4 \qquad (15)$$

regardless of the phase factor $\exp(i\phi)$.

When a change of variable is used that is similar to that used in Refs. 1, 7, and 8, the coupled equations can be written as

$$\frac{d}{dz} g = ie^*\gamma (g^2 c_2 \cos\theta + g\sigma^* - c_1), \qquad (16)$$

$$\frac{d}{dz} f = -ie\gamma (f^2 c_1 \cos\theta + f\sigma - c_2), \qquad (17)$$

where

$$f = A_p/A_s, \qquad g = B_p/B_s, \qquad (18)$$

$$\sigma = c_3 - c_3{}^* \cos\theta. \qquad (19)$$

We notice that the only difference is the additional phase factors ie^* and $-ie$, as compared with the special case ($\phi = \pi/2$) in Ref. 1.

Equations (16) and (17) can now be integrated, and the results are

$$f = A_p/A_s = [-\sigma + q \tanh(ieq\gamma z/2 + C)]/(2c_1 \cos\theta), \qquad (20)$$

$$g = B_p/B_s = [-\sigma^* + q^* \tanh(ie^* q^* \gamma z/2 + C')]/(2c_2 \cos\theta), \qquad (21)$$

with

$$q^2 = 4c_1 c_2 + \sigma^2. \qquad (22)$$

where C and C' are constants of integration that are determined by the boundary condition at $z = 0$.

When f and g are known, the intensity of all four waves is given by

$$|A_p|^2 = \frac{|f|^2 c_1 - |fg|^2 c_2}{1 - |fg|^2},$$

$$|B_p|^2 = \frac{|g|^2 c_2 - |fg|^2 c_1}{1 - |fg|^2},$$

$$|A_s|^2 = \frac{|A_p|^2}{|f|^2} = \frac{c_1 - |g|^2 c_2}{1 - |fg|^2},$$

$$|B_s|^2 = \frac{|B_p|^2}{|g|^2} = \frac{c_2 - |f|^2 c_1}{1 - |fg|^2}. \qquad (23)$$

If we put $\phi = \pi/2$, the solutions of Eqs. (20) and (21) reduce to my earlier results reported in Ref. 1. Although the solutions for the general case ($\phi \neq \pi/2$) look almost formally identical to those of the special case ($\phi = \pi/2$), they are actually quite different. The hyperbolic tangent of a complex argument has a range between $(-1, 1)$ and $(-\infty, \infty)$, depending on whether the argument is real or pure imaginary. Thus the value of spatial phase shift will affect the behavior of energy transfer between the waves.

For the special case of particular interest in which the cubic crystal is sandwiched between a pair of cross polarizers, the boundary conditions are

$$A_p(0) = B_p(0) = 0. \qquad (24)$$

Using Eqs. (14) and (18)–(21), we have $f(0) = g(0) = 0$, $c_3 = 0$, and $\sigma = 0$, and the solutions become

$$f = \frac{q \tanh(ieq\gamma z/2)}{2c_1 \cos\theta},$$

$$g = \frac{q \tanh(ie^* q\gamma z/2)}{2c_2 \cos\theta}, \qquad (25)$$

where $q = 2(c_1 c_2)^{1/2}$.

Consider the special case of $\phi = 0$. The solutions of Eqs. (25) become

$$f = \frac{iq \tan(q\gamma z/2)}{2c_1 \cos\theta},$$

$$g = \frac{iq \tan(q\gamma z/2)}{2c_2 \cos\theta}. \qquad (26)$$

When $\theta = 0$ and when we use Eqs. (23), the intensity of the four waves becomes

$$|A_s|^2 = c_1 \cos^2(q\gamma z/2),$$

$$|A_p|^2 = c_2 \sin^2(q\gamma z/2),$$

$$|B_s|^2 = c_2 \cos^2(q\gamma z/2),$$

$$|B_p|^2 = c_1 \sin^2(q\gamma z/2). \qquad (27)$$

where $c_1 = |A_s(0)|^2$, $c_2 = |B_s(0)|^2$. Notice that the intensities of these waves are periodic functions of z. This is distinctly different from the case when $\phi = \pi/2$. The case of $\phi = 0$ corresponds to a pure local response of the material. Although the energy is exchanged back and forth between A_s and B_p as well as between A_p and B_s, there is no nonreciprocal energy transfer. In other words, there is no unique direction of energy flow as compared with the case when $\phi \neq 0$. For cases with $0 < |\phi| < \pi$, nonreciprocal energy transfer is possible according to our solutions [Eqs. (20) and (21)], with maximum energy transfer at $\phi = \pm\pi/2$.

For the case of weak coupling ($\gamma L \ll 1$) or little pump depletion, we may assume that the pump-beam amplitudes (A_s, A_p) remain virtually unchanged throughout the interaction. Under these conditions, the coupled equations become

$$\frac{d}{dz} B_s = ie^*(\gamma a B_p + \gamma b B_s),$$

$$\frac{d}{dz} B_p = ie^*(\gamma c B_p + \gamma d B_s), \qquad (28)$$

where a, b, c, and d are dimensionless constants and are given by

$$a = |A_p|^2 \cos\theta/I_0,$$
$$b = A_p A_s^*/I_0,$$
$$c = A_s A_p^* \cos\theta/I_0,$$
$$d = |A_s|^2/I_0. \qquad (29)$$

We note that the magnitude of all four of these constants is less than unity.

An approximate solution to Eqs. (28) when $\gamma z \ll 1$ can be written as

$$B_s(z) = B_s(0) + B_s(0) \frac{A_p A_s^*}{I_0} ie^*\gamma z,$$

$$B_p(z) = B_s(0) \frac{|A_s|^2}{I_0} ie^*\gamma z. \qquad (30)$$

We notice that the amplitude of B_s may increase or decrease depending on the polarization state of the pump beam A and the phase shift ϕ, whereas the amplitude B_p is an increasing function of γz.

In conclusion, we have investigated the photorefractive coupling of two polarized beams in cubic crystals with a spatial phase shift $\phi \neq \pi/2$. An exact solution for the case of codirectional cross coupling is established. The results for $\phi = 0$, which are distinctly different from those of $\phi = \pi/2$, indicate that there is no nonreciprocal energy transfer.

ACKNOWLEDGMENTS

REFERENCES

1. P. Yeh, "Photorefractive two-beam coupling in cubic crystals," J. Opt. Soc. Am. B **4**, 1382 (1987).
2. T. Y. Chang, A. E. T. Chiou, and P. Yeh, "Photorefractive two-beam coupling with polarization flip in gallium arsenide," in *Digest of Topical Meeting on Photorefractive Materials, Effects, and Devices* (Optical Society of America, Washington, D.C., 1987), pp. 55–58.
3. P. Yeh and Li-Jen Cheng, "Cross polarization two-beam coupling photorefractive GaAs crystals," in *Digest of Topical Meeting on Photorefractive Materials, Effects, and Devices* (Optical Society of America, Washington, D.C., 1987), pp. 59–61.
4. Li-Jen Cheng and P. Yeh, "Cross-polarization beam coupling in photorefractive GaAs crystals," Opt. Lett. **13**, 50 (1988).
5. A. E. T. Chiou, T. Y. Chang, and P. Yeh, "Cross-polarization photorefractive two-beam coupling in GaAS," J. Opt. Soc. Am. B (to be published).
6. I. McMichael and P. Yeh, "Phase shifts of photorefractive gratings and phase-conjugate waves," Opt. Lett. **12**, 48 (1987).
7. B. Fischer, J. O. White, M. Cronin-Golomb, and A. Yariv, "Nonlinear vectorial two-beam coupling and forward four-wave mixing in photorefractive materials," Opt. Lett. **11**, 239 (1986).
8. M. Cronin-Golomb, J. O. White, B. Fischer, and A. Yariv, "Exact solution of a nonlinear model of four-wave mixing and phase conjugation," Opt. Lett. **7**, 313 (1982).

APPENDIX 4.3

MODEL FOR MUTUALLY PUMPED PHASE-CONJUGATION

Model for mutually pumped phase conjugation

Pochi Yeh, Tallis Y. Chang, and M. D. Ewbank

Rockwell International Science Center, P.O. Box 1085, Thousand Oaks, California 91360

A model is proposed and demonstrated for mutually pumped phase conjugation when two mutually incoherent laser beams pump each other, producing a pair of phase-conjugate beams through a cross-readout process. The model considers the buildup of two independent counterpropagating oscillations in a ring resonator containing two-beam-coupling gain media. The experimental demonstration of the model using two photorefractive BaTiO$_3$ crystals in a ring cavity gave simultaneous phase-conjugate images with good fidelity and no image cross talk. As expected, the counterpropagating oscillations were slightly detuned in frequency (~1 Hz) from the corresponding pumping beams with frequency shifts related to the ring-cavity length. Frequency shifts were also observed in the phase-conjugate beams, with their magnitudes dictated by energy conservation for nondegenerate four-wave mixing.

1. INTRODUCTION

Recently several papers reported[1-3] on a new type of phase conjugation in photorefractive BaTiO$_3$ in which two mutually incoherent laser beams pump each other to generate the respective phase-conjugate reflections. These new phase conjugators, which were implemented in slightly different configurations within BaTiO$_3$, exhibited basically the same properties. Their common characteristics include the following:

1. One beam by itself does not generate a phase-conjugate reflection.
2. Two incident beams can be mutually incoherent (e.g., from two different lasers).
3. The phase conjugate of one beam originates from the other beam (i.e., a cross-readout process).

We refer to these phase conjugators collectively as mutually pumped phase conjugators (MPPC's) because of their common property of mutual pumping. Diagrams for the demonstrated MPPC's[1-3] are shown in Fig. 1. One MPPC, known as the double phase-conjugate mirror,[1] was first studied theoretically[4] and explained in terms of self-oscillations in a four-wave mixing process. An alternative explanation for MPPC's was recently given in terms of hologram sharing.[3] All the demonstrated MPPC's[1-3] rely on the photorefractive stimulated scattering phenomenon known as beam fanning.[5-7] The major distinguishing feature is, as illustrated in Fig. 1, the number of internal reflections from the sides of the BaTiO$_3$ crystal[3]: two for the mutually incoherent beam coupler,[2] one for the bird-wing phase conjugator,[3] and none for the double phase-conjugate mirror.[1]

In this paper we propose and demonstrate a new model for mutually pumped phase conjugation. The model offers a mechanism for the phase conjugation of two mutually incoherent laser beams interacting in a photorefractive crystal and possibly explains what occurs in the previously demonstrated MPPC's.[1-3] The proposed model consists of two mutually incoherent laser beams pumping two separate two-beam coupling media, such as photorefractive BaTiO$_3$ crys-

tals, inside a ring cavity. The resulting two counterpropagating ring oscillations, which are mutually incoherent, are then used to explain the common characteristics of MPPC's, including the mutual pumping, the absence of image cross talk, and the exchange of temporal information. In addition, the model predicts a slight frequency shift of a conjugate beam from its corresponding pump, which originates from the cavity-length detuning. The experimental verification of the model is given in Section 3. Because the photorefractive grating formation and readout processes are clearly differentiated in the two crystals, this model provides an easy understanding for mutually pumped phase conjugation. Finally, we speculate that the type of resonator given in our model can exist within a single BaTiO$_3$ crystal.

2. MUTUALLY PUMPED PHASE CONJUGATOR MODEL

Referring to Fig. 2, we consider a ring resonator containing a pair of two-beam coupling gain media, e.g., photorefractive BaTiO$_3$ crystals, inserted into the cavity. Each crystal is pumped by a laser beam to produce a unidirectional ring oscillation from the two-beam-coupling gain, resulting in two counterpropagating ring oscillations. This arrangement closely follows the geometry for a unidirectional oscillator (a ring resonator with a single photorefractive crystal pumped by one laser beam), which was previously studied and demonstrated.[8,9] In Fig. 2 the two crystals are oriented in such a way that BaTiO$_3$ #1 will provide two-wave mixing gain for a counterclockwise unidirectional oscillation when it is pumped by laser beam 1 (P_1), and BaTiO$_3$ #2 will provide two-wave mixing gain for a clockwise unidirectional oscillation when it is pumped by laser beam 2 (P_2). If the gains are large enough to overcome the cavity losses, as is the case for BaTiO$_3$ with proper crystal orientation and beam polarization, then oscillations will occur.

Let ω_1 and ω_2 be the frequencies of the two pumping laser beams with the amplitudes P_1 and P_2, respectively. When the cavity oscillations occur, the frequencies of the oscillations can be slightly detuned[8,9] from those of the pumping

(a)   **(b)**   **(c)**

Fig. 1.   Drawings of the previously demonstrated[1-3] MPPC's.   In MPPC's, two mutually incoherent laser beams, E_1 and E_2, pump each other to generate a pair of phase-conjugate reflections, $E_1{}^*$ and $E_2{}^*$, by cross readout of photorefractive holograms.   Here, E_1, E_2, $E_1{}^*$, and $E_2{}^*$ are short notations for $E_1(\mathbf{r})\exp(i\mathbf{k}_1 \cdot \mathbf{r} - i\omega_1 t)$, $E_2(\mathbf{r})\exp(i\mathbf{k}_2 \cdot \mathbf{r} - i\omega_2 t)$, $E_1{}^*(\mathbf{r})\exp(-i\mathbf{k}_1 \cdot \mathbf{r} - i\omega_2 t)$, and $E_2{}^*(\mathbf{r})\exp(-i\mathbf{k}_2 \cdot \mathbf{r} - i\omega_1 t)$, respectively; note the temporal-frequency cross talk.   The three demonstrated MPPC's are (a) the double phase-conjugate mirror,[1] (b) the mutually incoherent beam coupler,[2] and (c) the bird-wing phase conjugator.[3]

beams and are designated $\omega_1 + \delta_1$ and $\omega_2 + \delta_2$. According to the theory developed in Ref. 8, the frequency detunings are given by

$$\delta_i = -\frac{2(\Delta\Gamma_i + 2m_i\pi)}{\tau_i A}, \qquad i = 1, 2. \tag{1}$$

with

$$\Delta\Gamma_i = 2N_i\pi - \int_L k_i ds, \qquad i = 1, 2, \tag{2}$$

where $\Delta\Gamma_i$ is the cavity detuning for the cavity modes at frequency ω_i and is defined between $-\pi$ and π; m_i and N_i are integers; τ_i is the photorefractive response time of the ith crystal; A is the total cavity loss given by $-\ln(RT_sT_p)$, with R the product of the reflectivities of the cavity reflectors, T, the transmission through the BaTiO$_3$ crystals accounting for the absorption, surface reflections, and scattering losses (including beam fanning), and T_p the effective transmission through the pinhole aperture (usually placed to confine the oscillations to the fundamental spatial mode[9]). The path integral in Eq. (2) is performed over one round trip inside the ring cavity, where $k_i = n_i\omega_i/c$, L is the cavity length, n_i is the refractive index at ω_i, and c is the speed of light in vacuum. The magnitudes of δ_1 and δ_2 are small (typically of the order of a few hertz). There is a threshold condition for oscillation given by[8] (assuming $m = 0$, the lowest-order oscillation)

$$|\delta_i| \le \frac{(\gamma_i l_i/A - 1)^{1/2}}{\tau_i}, \qquad i = 1, 2, \tag{3}$$

where γ_i is the degenerate two-beam-coupling gain coefficient for the crystal i, and l_i is the coupling interaction length inside the ith crystal. When inequality (3) is satisfied, the gain overcomes the losses and permits the oscillations to build up, as mentioned above.

We now examine the cross readout of the holograms inside the photorefractive crystals. Within each crystal, a volume hologram is formed by the pumping beam and the corresponding unidirectional oscillation beam. For example, a hologram (moving with a velocity proportional to δ_1) is formed by the pump beam $P_1(\omega_1)$ and the counterclockwise oscillation beam, with the amplitude $R_1(\omega_1 + \delta_1)$, inside the BaTiO$_3$ #1 crystal. The amplitude of the index grating is

proportional to $R_1 P_1{}^*$. When the clockwise oscillation, with the amplitude $R_2(\omega_2 + \delta_2)$, intersects the hologram inside BaTiO$_3$ #1, it is Bragg diffracted in the direction counterpropagating to P_1 with the frequency $\omega_2 + \delta_1 + \delta_2$, provided that ω_1 and ω_2 are close enough to maintain the Bragg condition. We denote the amplitude of the signal generated from BaTiO$_3$ #1 as $S_1(\omega_2 + \delta_1 + \delta_2)$. (Note that $\omega_1 - \omega_2$ can be

Fig. 2.   Diagram of the proposed model of a MPPC. The model is based on the buildup of two counterpropagating oscillations in a ring cavity and a subsequent cross-readout process. The ring oscillations with amplitudes (frequencies) $R_1(\omega_1 + \delta_1)$ and $R_2(\omega_2 + \delta_2)$ are generated independently from a pair of two-beam-coupling gain media (photorefractive BaTiO$_3$ crystals #1 and #2) that are pumped by two mutually incoherent incident beams with amplitudes $P_1(\omega_1)$ and $P_2(\omega_2)$. The clockwise oscillation beam R_2 can read out the hologram in BaTiO$_3$ #1 (depicted as dashed lines), and if these ring oscillations constitute a spatially phase-conjugate pair, i.e., $R_1 = R_2{}^*$, then the phase conjugate of pump beam 1 will be generated $[P_1{}^*(\omega_2 + \delta_1 + \delta_2)]$. Similarly, the counterclockwise oscillation beam R_1 can generate the phase conjugate of pump beam 2 $[P_2{}^*(\omega_1 + \delta_1 + \delta_2)]$. The frequencies of the pump beams, ω_1 and ω_2, must be nearly equal in order to satisfy the Bragg condition in the holographic readout process. As indicated, both oscillation beams are frequency shifted to satisfy the round-trip phase condition for the cavity. Also, the phase-conjugate beams are frequency shifted according to energy conservation of the nondegenerate four-wave mixing process.

tens of gigahertz, and the Bragg phase-matching condition will still be well satisfied.) A similar situation occurs in BaTiO$_3$ #2, with $R_1(\omega_1 + \delta_1)$ reading out the hologram in BaTiO$_3$ #2 to produce a second signal beam $S_2(\omega_1 + \delta_1 + \delta_2)$ counterpropagating with respect to P$_2$. According to the holographic interpretation of four-wave mixing,[10] the relationships between the pumps and the oscillations are given by

$$S_1(\omega_2 + \delta_1 + \delta_2) \propto R_1(\omega_1 + \delta_1)P_1{}^*(\omega_1)R_2(\omega_2 + \delta_2),$$
$$S_2(\omega_1 + \delta_1 + \delta_2) \propto R_2(\omega_2 + \delta_2)P_2{}^*(\omega_2)R_1(\omega_1 + \delta_1). \quad (4)$$

Here, it is important to note that the signal beams S_1 and S_- can be spatial phase conjugates of the incident beams P_1 and P_2, respectively, *if the two ring oscillations are phase conjugates of each other.* That is, if $R_1 = R_2{}^*$, then $S_1 \propto P_1{}^*$ and $S_2 \propto P_2{}^*$. Because the oscillation beam path is defined by the resonator cavity, the two modes of oscillation are exactly counterpropagating. In addition, the two counterpropagating oscillations in a stable cavity are exactly a phase-conjugate pair, provided that they oscillate at the same transverse mode. The cavity can easily be forced to oscillate in the fundamental transverse mode by placing a pinhole in the beam path, as was done in our experiments. The important consequence of the two ring oscillations' being a phase-conjugate pair in our model is that it results in the absence of image cross talk. On the other hand, if the ring oscillations did not form a phase-conjugate pair but instead consisted of orthogonal transverse modes, then an image cross talk could occur by transfer of the dark regions in the nonuniform intensity distributions on the ring oscillations to the signal beams during the readout processes.

The temporal characteristics of MPPC's[1-3] are different from that of phase conjugation using a single pump beam, such as self-pumped phase conjugation[11-13] or stimulated photorefractive backscattering.[14] Although the spatial wave fronts are reconstructed, the frequencies of the phase-conjugated beams from MPPC's are exchanged and modified. The phase conjugate of pump beam 1 has a frequency of $\omega_2 + \Delta$, and the phase conjugate of pump beam 2 has a frequency of $\omega_1 + \Delta$, where $\Delta = \delta_1 + \delta_2$. In other words, the phase conjugate of beam 1 originates from beam 2, and vice versa; the temporal characteristic of one pump beam is transferred to the phase conjugate of the other pump beam. The situation is similar to that of four-wave mixing when the grating written by two mutually coherent beams is read out by a third (reading) beam that is mutually incoherent with respect to the writing beams.

The counterpropagating ring oscillations illustrated in Fig. 2 and described above can occur within a single BaTiO$_3$ crystal. By virtue of total internal reflections at the surfaces, the crystal can act as an optical cavity that is capable of supporting many modes. These types of internal oscillation were suggested[9,12,13] to explain the frequency shift in a self-pumped phase conjugator.[11] For the MPPC, one may consider that each incident beam initiates a unidirectional ring oscillation within the crystal, in accordance with the model given above. When both beams are present, counterpropagating oscillations occur, which lead to mutually pumped phase conjugation.

3. MUTUALLY PUMPED PHASE CONJUGATOR EXPERIMENTS AND RESULTS

A. Phase-Conjugate Images

The experimental arrangement used to check the phase-conjugate imaging properties of the proposed model is shown in Fig. 3. The 514.5-nm output of an Ar$^+$ laser was first passed through a Faraday cell to isolate the laser from phase-conjugate feedback as well as from any other reflections. The polarization of the output was oriented to excite extraordinary waves in the BaTiO$_3$ crystals. A beam splitter BS$_1$ separated the output into two beams, which were expanded, then transmitted through image transparencies T$_1$ (spoke pattern) and T$_2$ (U.S. Air Force resolution chart), and finally focused into the BaTiO$_3$ crystals #1 and #2, respectively. When we used BS$_2$, a portion of the incident laser beam was reserved for precisely aligning the ring cavity and was normally blocked by a shutter. The ring cavity consisted of a stationary 100% reflecting mirror, a 100% reflecting mirror mounted on a piezoelectric translator, PZT #2, and a 95% reflector, BS$_3$; all these reflectors were flat. The ring cavity was aligned by monitoring the interference on a silicon photodetector, D, as a function of cavity length controlled by PZT #2. When the mirrors of the cavity were properly adjusted, the cavity finesse (F) without the two BaTiO$_3$ crystals was observed to be fairly high $(F \approx 40)$. However, when the crystals were inserted and the cavity was realigned, the finesse was significantly reduced, to $F \approx 2$, as one would expect from the losses due to crystal-surface re-
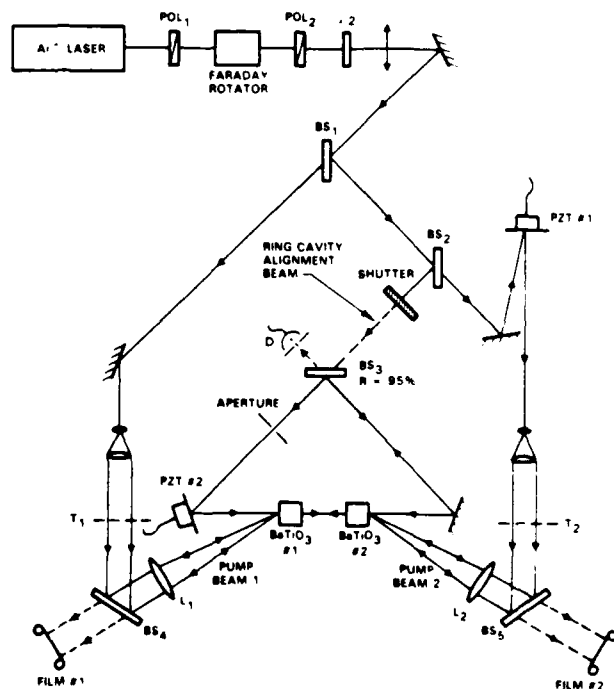
Fig. 3. Experimental arrangement for phase-conjugate imaging with the MPPC shown in Fig. 2, where image-bearing beams pump the photorefractive crystals. The phase-conjugate beams were projected onto the film planes without using any imaging optics. POL$_1$, POL$_2$, polarizers; $\lambda/2$, half-wave retardation plate; BS$_1$–BS$_5$, beam splitters; D, silicon detector; T$_1$, T$_2$, image transparencies; L$_1$, L$_2$, lenses; PZT #1, PZT #2, piezoelectric translators.

flections and absorption. Despite the poor cavity finesse, ring oscillations occurred in our experiments because the two-beam coupling gain of the crystals could still overcome the cavity losses. The ring oscillations built up and were sustained even with the placement of a pinhole (~200-μm diameter) inside the cavity to confine the oscillations to the fundamental spatial mode.

The two incident pumping beams in the MPPC were made mutually incoherent so that competing photorefractive gratings did not form. This mutual incoherence was achieved with the previously demonstrated MPPC's[1-3] either by simply removing the étalon from the Ar$^+$ laser and making the optical path lengths between the laser and the photorefractive crystal for the two incident beams differ by more than the Ar$^+$ laser coherence length (~3 cm) or by using two different lasers. In our experiment, shown in Fig. 3, removing the étalon will not work because each incident beam must be coherent with its respective unidirectional ring oscillation, with the implication that a coherence length greater than the ring-cavity length is required.

One way to obtain mutually incoherent pump beams P_1 and P_2 while at the same time maintaining a coherence length greater than the ring-cavity length is to use two independent Ar$^+$ lasers, both with étalons installed, operating on the same laser line. However, our solution for the dual requirement was to use a single Ar$^+$ laser and frequency shift one of the pumping beams with respect to the other, thereby mimicking mutual incoherence by taking advantage of the slow photorefractive response time. The coherence length of our Ar$^+$ laser, with an étalon installed, was approximately 10 m, making both the clockwise and counterclockwise cavity oscillations coherent with their corresponding pump beams P_2 and P_1, respectively, since the ring-cavity length was approximately 50 cm. One of the pump beams was Doppler frequency shifted by approximately 1 kHz by using a moving mirror mounted on PZT #1. Introducing the 1-kHz frequency shift does not make the beams mutually incoherent in the usual sense, but it does simulate mutual incoherence within the BaTiO$_3$ crystals because of the slow (in the 1-Hz range) photorefractive response time. That is,
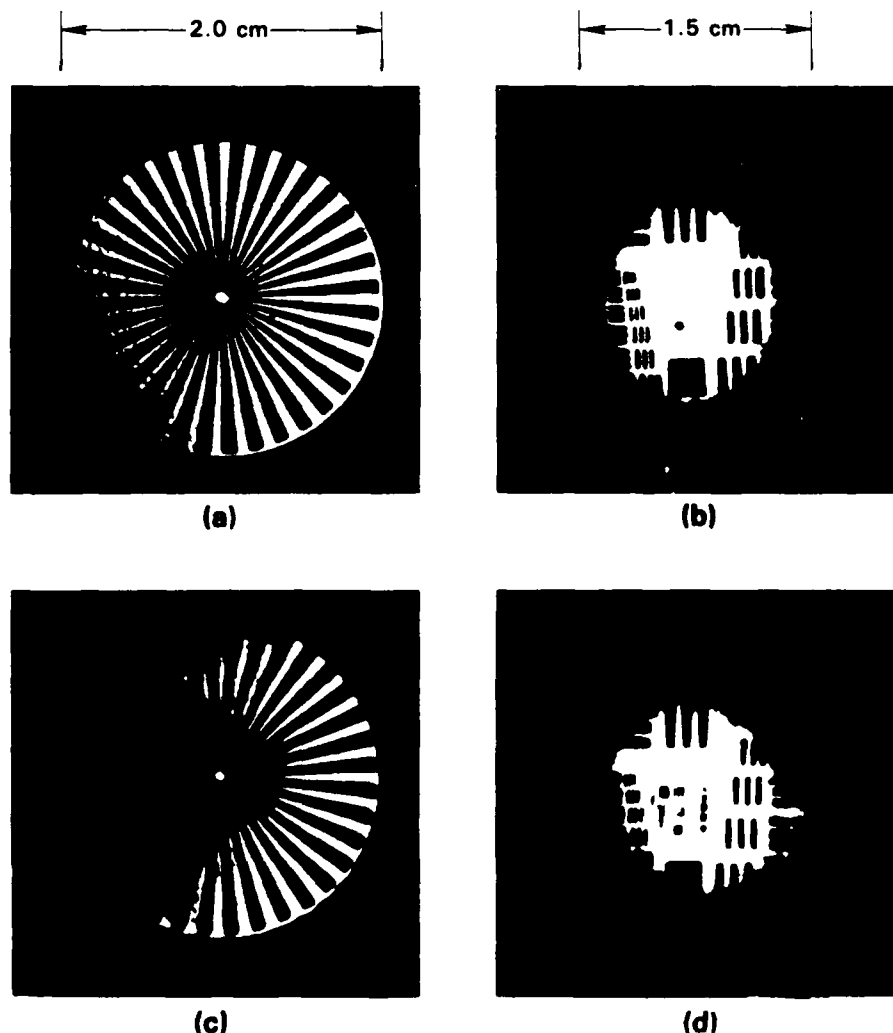
Fig. 4.   Photographs of the incident and phase-conjugate images produced by the setup in Fig. 3: (a) incident pump beam 1 (spoke chart), (b) incident pump beam 2 (U.S. Air Force resolution chart), (c) phase conjugate of pump beam 1, and (d) phase conjugate of pump beam 2. As predicted by the model, no image cross talk was visible in the two images. The fidelity of the phase-conjugate beams was good; the smallest bar resolvable in (d) corresponds to approximately 6-line/mm resolution.
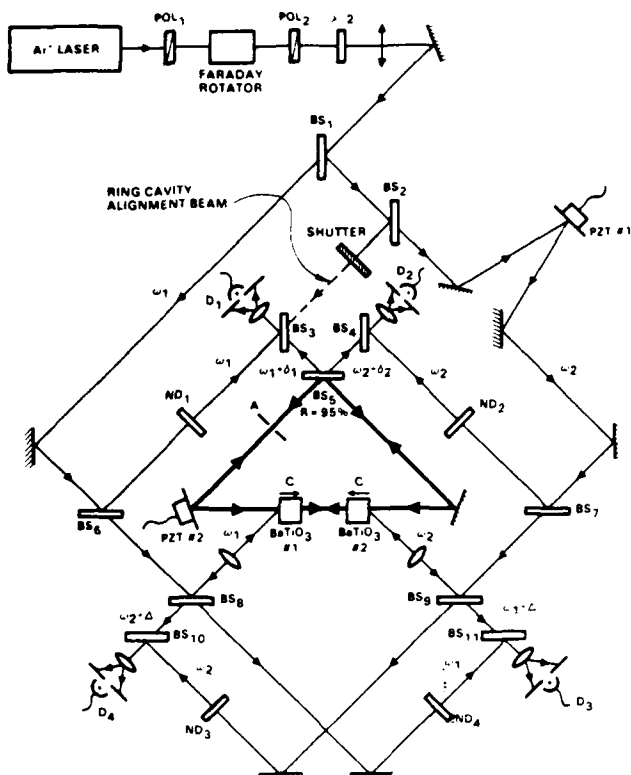
Fig. 5. Experimental arrangement used to examine the frequency shifts generated by the MPPC shown in Fig. 2. Four interferometers were constructed to monitor simultaneously the beat frequencies in the two counterpropagating ring oscillations and the two phase-conjugate signals relative to the appropriate reference beams: POL_1, POL_2, polarizers; $\lambda/2$, half-wave retardation plate: BS_1–BS_{11}, beam splitters; D_1–D_4, silicon detectors; ND_1–ND_4, neutral-density filters; PZT #1, PZT #2, piezoelectric translators.

struction through phase aberrators, the quality of the reconstructed images was not so good as expected. We speculate that part of the problem arises from the way in which the pump and oscillation beams intersect in the crystals. The model assumes that there is complete overlap between each pump beam and the corresponding unidirectional ring oscillation. However, if the diameters of the pump beams are large compared with the beam diameter of the fundamental cavity mode inside the crystals, then each holographic read-out beam will not contain all the spatial information from the corresponding incident pump beam. This seems to be the case when the aberrations are used, because the beams cannot be focused so tightly. We believe, however, that this may not be a problem in a crystal resonator with internal reflection (as in Refs. 11–13). There, the crystal is free to choose all the proper modes and interaction volume required to produce high-fidelity phase-conjugate beams.

B. Frequency Shifts

The proposed resonator model also predicts the existence of frequency shifts in the phase-conjugate beams, as we have
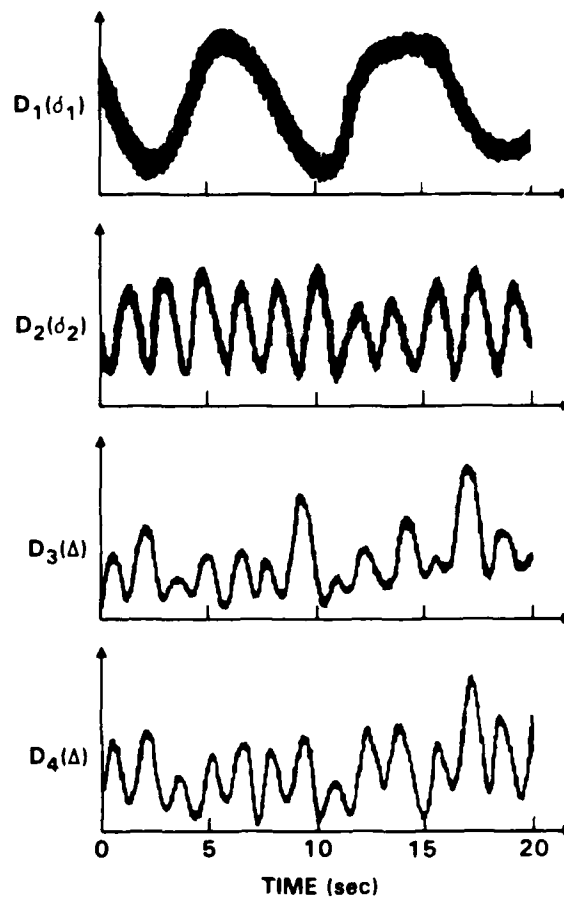
Fig. 6. Beat frequencies of the ring-oscillation beams and phase-conjugate beams produced by the setup in Fig. 5. The detectors D_1 and D_2 are used to measure the frequency shifts δ_1 and δ_2, respectively. D_3 and D_4 are used to measure the frequency shifts in the phase conjugates of beam 2 and beam 1 respectively. According to the theory, both D_1 and D_2 should have measured the same frequency shift Δ as observed. In the 20-sec time period D_1 and D_2 captured 2.5 and 11 fringes respectively, while both D_3 and D_4 captured 13.5 fringes indicating that $\Delta = \ldots$

no photorefractive gratings would form directly from the rapidly moving interference patterns generated by light from both pumping beams.

The phase-conjugate images were recorded on photographic films #1 and #2. The distance between film #1 and BS_4 was identical to the distance between T_1 and BS_4 (and similarly for film #2) so that the phase-conjugate beam would be imaged at the film. No additional optics were used to image the phase-conjugate beams onto the film planes. The resulting images are shown in Fig. 4. Compared with the input images shown in Figs. 4(a) and 4(b), the phase-conjugate images have good fidelity, as evidenced in Figs. 4(c) and 4(d). In addition, there is no indication of any image cross talk: no horizontal or vertical bars are superimposed upon the phase-conjugate image of the spoke pattern, for example. The phase conjugate of beam 1 clearly originated from beam 2; when beam 2 was blocked, the phase conjugate of beam 1 disappeared instantly. Additionally, as expected, when beam 2 was blocked, the phase conjugate of beam 2 decayed with the characteristic photorefractive grating decay time as the hologram in crystal 2 was being erased. Similar behavior was observed in phase-conjugate beams 1 and 2 when beam 1 was blocked.

We have attempted to place phase aberrators in the beams to see the quality of image reconstruction. Although we have succeeded in generating phase-conjugate image recon

checked experimentally by using the arrangement in Fig. 5. The setup is similar to that of Fig. 3 but without image transparencies in the pump beams. Instead, four interferometers were constructed to monitor the relative frequencies of four beams simultaneously: the two phase-conjugate beams and the two counterpropagating cavity oscillations. The detectors D_1 and D_2 monitored the two counterpropagating unidirectional oscillations that interfered with the corresponding pump beams, thereby measuring the detuning frequencies δ_1 and δ_2. The detectors D_3 and D_4 monitored the frequency shift Δ in the phase conjugates of beams 2 and 1, respectively. From conservation-of-energy considerations for the nearly degenerate four-wave mixing occurring in $BaTiO_3$ #1 and in $BaTiO_3$ #2, as illustrated in Fig. 2, both D_3 and D_4 should measure the same Δ.

Typical results from the frequency-detuning experiments are shown in Fig. 6. From the output of D_1 and D_2, δ_1 and δ_2 were measured to be ~0.13 Hz (2.5 fringes per 20 sec) and ~0.55 Hz (11 fringes per 20 sec), respectively. D_3 and D_4 both gave nearly the same Δ of ~0.68 Hz (13.5 fringes per 20 sec), which agrees with the theory, $\Delta = \delta_1 + \delta_2$. The frequency shift Δ can be positive, negative, or zero, depending on the cavity-length detuning, as controlled by PZT #2. The signs of the frequency shifts were checked by simultaneously noting the direction of fringe movement in each of the four interference patterns produced by the four interferometers. The signs of δ_1, δ_2, and Δ were all the same for a given ring cavity length, and they were reversed in a controllable way by changing the cavity length. The phase-conjugate signals had some long-term fluctuations, of the order of seconds, as evidenced from the signal in D_3 and D_4 in Fig. 6. We attribute this mainly to variations in cavity length from air currents.

4. DISCUSSION

The observed frequency detunings of the two counterpropagating ring oscillations were consistent with the predicted values given by Eqs. (1) and (2). For the lowest-order oscillation (i.e., $m = 0$), the frequency-detuning difference $\delta_2 - \delta_1$ is given by

$$\delta_2 - \delta_1 = \frac{2\Delta\Gamma}{A}\left(\frac{1}{\tau_2} - \frac{1}{\tau_1}\right). \tag{5}$$

where the cavity detunings are assumed to be equal ($\Delta\Gamma = \Delta\Gamma_1 = \Delta\Gamma_2$) by neglecting any nonreciprocal change in the optical paths of the two counterpropagating ring oscillations. The measured frequency-detuning difference $\delta_2 - \delta_1$ of 0.42 Hz is consistent with the observed photorefractive time constants of $\tau_1 = 0.10$ sec and $\tau_2 = 0.025$ sec at the intensities used in our experiments (typically ~1 W/cm^2). The time constant τ_2 that is shorter by a factor of 4 can easily be accounted for by the differences in the crystal parameters and orientations.

In our experiments the intensities of the output signals S_1 and S_2 became unstable when the two pump beams were coherent. We speculate that the instability arose from the competition among various index gratings formed by the mutually coherent beams. This type of instability has been observed experimentally in other MPPC's.[2,3]

Our model for MPPC's should not be restricted to photorefractive crystals only. The coupling gain is also possible in Kerr media if nondegenerate two-beam coupling is used.[15,16]
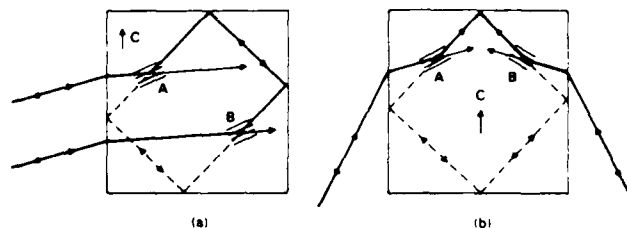

Fig. 7. Possible internal oscillations producing MPPC in (a) the mutually incoherent beam combiner[2] and (b) the bird-wing phase conjugator.[3] Owing to the preferential direction in two-beam coupling at the two interaction regions (or photorefractive gratings), A and B, the solid-line portion of the counterpropagating internal oscillation is more intense than the dashed-line portion.

That is, by moving the grating at a rate comparable with the inverse of the response time of the medium, one can achieve the phase shift between the intensity pattern and the resulting index grating, which is necessary for energy coupling. A unidirectional ring oscillator using sodium vapor as the gain medium was already demonstrated.[17] Therefore it is conceivable that two such Kerr media can be used to construct this type of MPPC.

Finally, further investigations are needed to verify whether the proposed model accurately describes the previously demonstrated MPPC's.[1-3] Although one of the previously reported MPPC's appears to exhibit oscillations internal to the crystal,[3] it has not shown the frequency shifts predicted by our model. Possibilities of these internal oscillations for two of the demonstrated MPPC's are shown in Fig. 7. Further experiments are suggested. For example, one can blacken[12] the crystal surfaces of a $BaTiO_3$ MPPC to eliminate the internal oscillations because mutually pumped phase conjugation supposedly disappears when the ring oscillations cease, according to our model. These types of verification will be included in a future report.

5. CONCLUSION

We have presented a new model of mutually pumped phase conjugation for producing phase conjugates of two mutually incoherent incident beams. The model considers the buildup of two independent counterpropagating oscillations, which form a phase-conjugate pair, in a ring cavity containing two-beam-coupling gain media, such as photorefractive crystals. Cross readouts of the holograms in the gain media by the two oscillation beams generate the two corresponding phase-conjugate beams. The model predicts that there will be no cross talk of spatial information between the two incident images and that the frequencies of the phase-conjugate beams will be governed by the cavity-length detuning. We have verified these predictions experimentally by using a ring cavity with two $BaTiO_3$ crystals, pumped by two mutually incoherent beams from an Ar^+ laser. The phase-conjugate images showed good fidelity and no image cross talk, whereas the observed frequency detunings were controlled by varying the cavity length and were constrained by the conditions for nondegenerate four-wave mixing.

REFERENCES

1. S. Weiss, S. Sternklar, and B. Fischer. "Double phase-conjugate mirror: analysis, demonstration, and applications." Opt. Lett. **12**, 114 (1987); S. Weiss, S. Sternklar, M. Segev, and B. Fischer, "Mach–Zender interferometer with multimode fibers using the double phase-conjugate mirror," Appl. Opt. **25**, 4518 (1986); S. Weiss, S. Sternklar, and B. Fischer, "Optical information processing with the double phase-conjugate mirror," Opt. Eng. **26**, 423 (1987).

2. R. W. Eason and A. M. C. Smout. "Bistability and noncommutative behavior of multiple-beam self-pulsing and self-pumping in BaTiO₃," Opt. Lett. **12**, 51 (1987); A. M. C. Smout and R. W. Eason. "Analysis of mutually incoherent beam coupling in BaTiO₃," Opt. Lett. **12**, 498 (1987).

3. M. D. Ewbank, "Mechanism for photorefractive phase conjugation using incoherent beams," Opt. Lett. **13**, 47 (1988); "Incoherent beams sharing photorefractive holograms." in *Digest of Topical Meeting on Photorefractive Materials, Effects, and Devices* (Optical Society of America, Washington, D.C., 1987), p. 179.

4. M. Cronin-Golomb, B. Fischer, J. O. White, and A. Yariv, "Theory and applications of four-wave mixing in photorefractive media." IEEE J. Quantum Electron. **QE-20**, 12 (1984).

5. J. Feinberg, "Asymmetric self-defocusing of an optical beam from the photorefractive effect." J. Opt. Soc. Am. **72**, 46 (1982).

6. V. V. Obukhovskii and A. V. Stoyanov. "Photoinduced light scattering in crystals with a nonlocal response." Sov. J. Quantum Electron. **15**, 367 (1985).

7. G. C. Valley. "Competition between forward- and backward-simulated photorefractive scattering in BaTiO₃." J. Opt. Soc. Am. B **4**, 14 (1987); errata. J. Opt. Soc. Am. B **4**, 934 (1987).

8. P. Yeh, "Theory of unidirectional photorefractive ring oscillators," J. Opt. Soc. Am. B **2**, 1924 (1985).

9. M. D. Ewbank and P. Yeh. "Frequency shift and cavity length in photorefractive resonators." Opt. Lett. **10**, 496 (1985).

10. For example, see D. M. Pepper and A. Yariv, "Optical phase conjugation using three-wave and four-wave mixing via elastic photon scattering in transparent media." in *Optical Phase Conjugation*, R. A. Fisher, ed. (Academic, Orlando, Fla., 1983), pp. 52–53.

11. J. Feinberg, "Self-pumped, continuous-wave phase conjugator using internal reflection." Opt. Lett. **7**, 486 (1982).

12. M. D. Ewbank and P. Yeh, "Frequency shifts of self-pumped phase conjugators," in *Nonlinear Optics and Applications*. P. Yeh, ed., Proc. Soc. Photo-Opt. Instrum. Eng. **613**, 59 (1986).

13. M. C. Gower, "Mechanisms for self-pumped phase-conjugate emission from BaTiO₃ crystals." in *Digest of Conference on Lasers and Electro-Optics* (Optical Society of America, Washington, D.C., 1987), p. 196.

14. T. Y. Chang and R. W. Hellwarth. "Optical phase conjugation by backscattering in barium titanate." Opt. Lett. **10**, 408 (1985).

15. V. L. Vinetskii, N. V. Kukhtarev, S. G. Odulov, and M. S. Soskin, "Dynamic self-diffraction of coherent light beams." Sov. Phys. Usp. **22**, 742 (1979).

16. P. Yeh, "Exact solution of a nonlinear model of two-wave mixing in Kerr media." J. Opt. Soc. Am. B **3**, 747 (1986).

17. G. Grynberg, E. Le Bihan, and M. Pinard. "Two-wave mixing in sodium vapor," J. Phys. **47**, 1321 (1986).

APPENDIX 4.4

CROSS-POLARIZATION PHOTOREFRACTIVE TWO-BEAM COUPLING
IN GALLIUM ARSENIDE

Cross-polarization photorefractive two-beam coupling in gallium arsenide

Tallis Y. Chang, Arthur E. Chiou, and Pochi Yeh

Rockwell International Science Center. 1049 Camino dos Rios, Thousand Oaks. California 91360

Experimental investigations are presented of cross- olarization two-beam coupling in a photorefractive GaAs crystal. in which two mutually coherent laser beams with the same polarization state (e.g., s waves) interact to generate and couple energy into an orthogonally polarized beam (p wave). We demonstrate cross-polarization coupling of 1.06-μm YAG laser beams (both cw and pulsed) in a semi-insulating single crystal of GaAs and show that the coupling coefficient is ~0.4 cm^{-1}. The experimental data are shown to be in good agreement with the theoretical results for the weak-coupling regime: the theoretical results are calculated from a set of coupled equations describing generalized two-beam coupling in cubic photorefractive crystals. The photorefractive response time of our crystal is also determined using nondegenerate cross-polarization two-beam coupling and is shown to be approximately 0.5 msec at the total intensity of 1 W/cm^2.

1. INTRODUCTION

Two-beam coupling in photorefractive crystals. in which two mutually coherent beams interact to transfer energy from one beam to the other. has been studied extensively.[1-3] Its potential applications to many areas of advanced optics include image amplification,[4,5] vibration analysis,[6] laser-beam processing,[7,8] and novelty filtering.[9] Most of the demonstrated applications utilize oxide materials such as barium titanate (BaTiO$_3$). bismuth silicon oxide (BSO), and strontium barium niobate (SBN) because of their large two-beam coupling coefficients. However. semiconductor photorefractive materials such as GaAs,[10-12] InP,[11-13] and CdTe (Ref. 14) in general have faster response times than the oxides.[15]

Two-beam coupling in photorefractive crystals can take two different forms, depending on the polarization states of the coupled waves.[16] The first form is the usual two-beam coupling, which we shall call parallel-polarization coupling. in which two laser beams (a probe and a pump) of the same polarization state interact to transfer energy from the pump to the probe, while preserving the polarization state of both beams. In fact. it is the parallel-polarization coupling that has been analyzed in Refs. 1-3 and demonstrated in Refs. 4–14.

In the second form, cross-polarization two-beam coupling. two laser beams of the same polarization state (s waves. e.g.) can interact in a photorefractive crystal to generate a wave in an orthogonal polarization state (p wave) and transfer energy into it. The fact that the polarization state of the probe can change under the influence of the pump in two-beam coupling was recognized and applied to modulate the intensity of the probe beam in BSO (Ref. 17) and GaAs.[18] However, the energy-transfer aspect of cross-polarization coupling was not fully realized until the theory, based on nonlinear coupled equations. was formulated.[16] Since then we have presented[19-21] some comparisons of experimental results with the calculations made from the coupled-wave theory. Cross-polarization coupling arises from the birefringent nature of the induced index grating inside photorefrac-

tive crystals. What is required is the phase-velocity matching of the two orthogonally polarized beams, which is not generally possible in BaTiO$_3$ and SBN because of the optical anisotropies, except along certain special directions. In cubic crystals such as GaAs. InP, and CdTe the electro-optic tensor element r_{41} ($=r_{52} = r_{63}$) can provide cross-polarization coupling for a wide range of beam geometries. The unique property of cross-polarization coupling—that the information of the probe can be transferred from one polarization state into the orthogonal state by the presence of the pump—has potential applications in optical-image and -signal processing (e.g., spatial light modulators).[21,22]

In this paper we present the results of experimental investigations of cross-polarization two-beam coupling in a photorefractive GaAs crystal. We report the successful demonstration of cross-polarization coupling using both cw and pulsed 1.06-μm Nd:YAG laser beams. We use a codirectional two-beam-coupling geometry with the grating wave vector parallel to the ⟨110⟩ direction. which is different from that of a recent report.[20] The polarization of the probe, after its interaction with the pump. is analyzed as a function of the initial polarization state of the pump, and its dependence is shown to agree well with predictions based on the nonlinear coupled-wave theory.[16] Also reported is a measurement of the photorefractive response time using nondegenerate cross-polarization two-beam coupling. In Section 2 the theory of the cross-polarization coupling is reviewed briefly. There, we modify the theory slightly to include the effects of bulk optical absorption. The experiments mentioned above and their results are described in Section 3.

2. THEORY

Cross-polarization two-beam coupling. which is significantly different from the conventional two-beam (parallel) coupling. must be analyzed with a generalized formulation.[16] The conventional coupling. as given in Refs. 1-3, cannot predict the cross-polarization coupling and must be extended. Consider a two-beam coupling geometry. as shown in
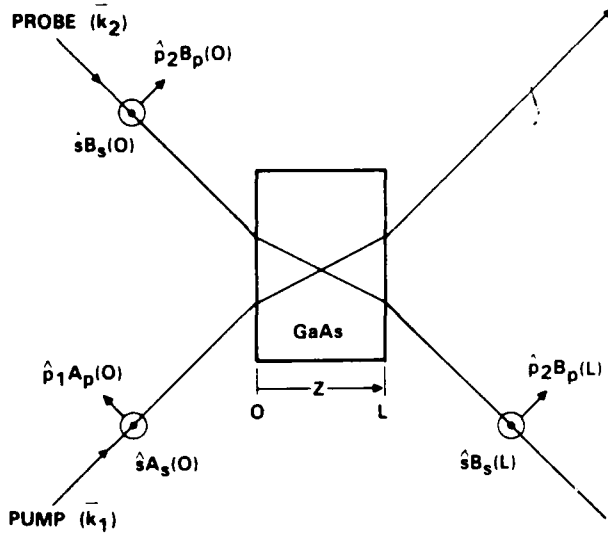
Fig. 1. The crystal and beam geometries of cross-polarization two-beam coupling used in this work.

Fig. 1, ignoring the crystal orientation for the moment. Assume that all the waves have the same frequency, ω, and that the crystal does not exhibit optical activity. The polarization of each beam (a pump and a probe) consists of a linear combination of the two orthogonal polarization states, s and p states in our analysis, where the s and the p polarizations are defined to be perpendicular and parallel to the plane of the beams, respectively. The coupled-mode equations for the four waves with their amplitudes A_s, A_p, B_s, and B_p are then given by[16]

$$\frac{dA_s}{dz} = \frac{i}{2\beta_1}\frac{e^{i\phi}}{I_0}(\Gamma_{ss}B_s + \Gamma_{sp}B_p)(A_sB_s^*$$
$$+ A_pB_p^*\cos\theta) - \frac{|\beta_1|}{2\beta_1}\alpha A_s,$$

$$\frac{dB_s}{dz} = \frac{i}{2\beta_2}\frac{e^{-i\phi}}{I_0}(\Gamma_{ss}A_s + \Gamma_{sp}A_p)(A_s^*B_s$$
$$+ A_p^*B_p\cos\theta) - \frac{|\beta_2|}{2\beta_2}\alpha B_s,$$

$$\frac{dA_p}{dz} = \frac{i}{2\beta_1}\frac{e^{i\phi}}{I_0}(\Gamma_{ps}B_s + \Gamma_{pp}B_p)(A_sB_s^*$$
$$+ A_pB_p^*\cos\theta) - \frac{|\beta_1|}{2\beta_1}\alpha A_p,$$

$$\frac{dB_p}{dz} = \frac{i}{2\beta_2}\frac{e^{-i\phi}}{I_0}(\Gamma_{ps}A_s + \Gamma_{pp}A_p)(A_s^*B_s$$
$$+ A_p^*B_p\cos\theta) - \frac{|\beta_2|}{2\beta_2}\alpha B_p, \qquad (1)$$

with

$$\Gamma = \omega^2\mu\epsilon_0 n^4(\mathbf{R}\cdot\mathbf{E}^{sc}) \qquad (2)$$

and

$$\Gamma_{ij} = (i|\Gamma|j), \quad \text{where } i,j = s, p, p.$$

where β_1 and β_2 (either positive or negative) are the z components of the wave vectors $\mathbf{k}_1$ and $\mathbf{k}_2$, respectively, ϕ is the spatial phase shift between the intensity fringe pattern and the index grating, I_0 is the total intensity of the input beams $(=A_s^*A_s + A_p^*A_p + B_s^*B_s + B_p^*B_p)$, θ is the angle between the beams inside the crystal, α is the bulk optical absorption coefficient, μ is the permeability of the crystal, ϵ_0 is the permittivity of the vacuum, n is the refractive index of the crystal, $\mathbf{R}$ is the electro-optic tensor (third rank), and $\mathbf{E}^{sc}$ is the space-charge electric field. The polarization vectors $\mathbf{p}_1$ and $\mathbf{p}_2$ indicate the p-polarization states of the pump and probe beams, respectively. Γ is the coupling tensor (second rank) that permits both parallel- and cross-polarization couplings. As denoted by the subscripts in Γ_{ij}, Γ_{ss} and $\Gamma_{p_1p_2}$ are the parallel-polarization coupling coefficients, and Γ_{sp_1} and Γ_{sp_2} are the cross-polarization coupling coefficients. For a cubic crystal with point-group symmetry $\bar{4}3m$, Γ is given by[16,23]

$$\Gamma = \omega^2\mu\epsilon_0 n^4 r_{41}\begin{pmatrix} 0 & E_z & E_y \\ E_z & 0 & E_x \\ E_y & E_x & 0 \end{pmatrix}, \qquad (3)$$

where r_{41} $(=r_{231} = r_{312} = r_{123})$ is the electro-optic coefficient and E_x, E_y, and E_z are the three amplitude components of the space-charge field.

There are many possible configurations for parallel- and cross-polarization couplings, as shown in Fig. 2. The left-hand column of Fig. 2 [i.e., Figs. 2(a), 2(c), and 2(e)] shows some geometries for codirectional two-beam coupling (beams entering the same side of a crystal face), and the right-hand column [Figs. 2(b), 2(d), and 2(f)] shows some geometries for contradirectional two-beam coupling (beams entering from the opposite sides of the crystal). For the geometries in Figs. 2(a) and 2(b), the electro-optic tensor is such that no parallel-polarization coupling is permitted for any polarization state of the incident beams, but cross-polarization coupling is permitted. The geometries in Figs. 2(c) and 2(d) permit parallel-polarization coupling but not cross-polarization coupling. Finally, in Figs. 2(e) and 2(f) no coupling (parallel or cross polarization) is permitted for any polarization state of the incident beams.

The configuration of interest for this work is that of Fig. 2(a), the codirectional cross-polarization coupling in which no parallel-polarization coupling is permitted. In this geometry, because the grating wave vector is parallel to the (110) direction, it can be simply shown by using Eq. (3) that $\Gamma_{ss} = \Gamma_{pp} = 0$ and $\Gamma_{sp} \neq 0$. The coupled equations given in Eqs. (1) can then be simplified as

$$\frac{dA_s}{dz} = -\frac{\gamma}{I_0}B_p(A_sB_s^* + A_pB_p^*\cos\theta) - \frac{1}{2}\alpha A_s,$$

$$\frac{dB_s}{dz} = \frac{\gamma}{I_0}A_p(A_s^*B_s + A_p^*B_p\cos\theta) - \frac{1}{2}\alpha B_s,$$

$$\frac{dA_p}{dz} = -\frac{\gamma}{I_0}B_s(A_sB_s^* + A_pB_p^*\cos\theta) - \frac{1}{2}\alpha A_p,$$

$$\frac{dB_p}{dz} = \frac{\gamma}{I_0}A_s(A_s^*B_s + A_p^*B_p\cos\theta) - \frac{1}{2}\alpha B_p, \qquad (4)$$
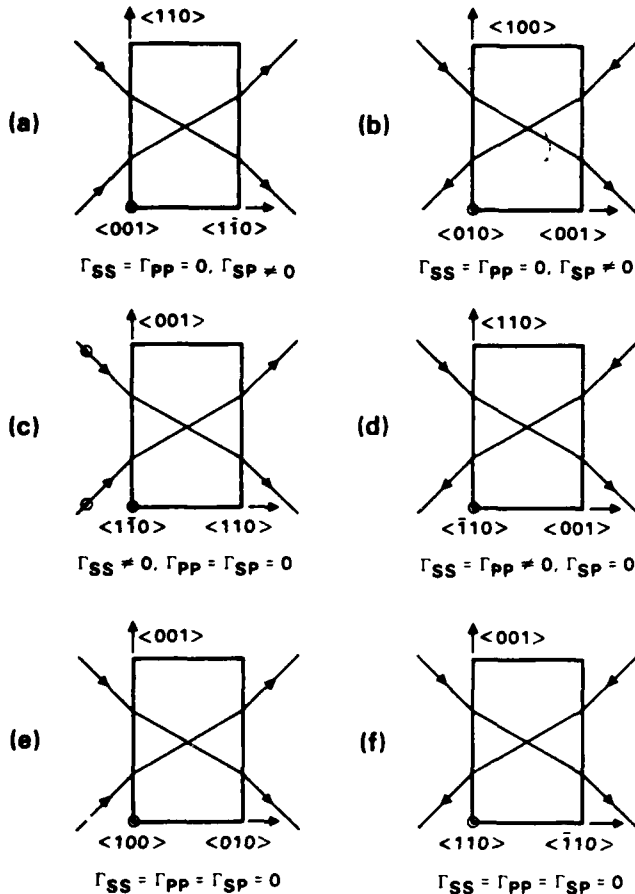
with

Fig. 2. Various crystal and beam geometries for two-beam coupling in a crystal with $\bar{4}3m$ point-group symmetry. (a), (c), and (e) Show the variations of codirectional two-beam coupling. (b), (d), and (f) Show the variations of contradirectional two-beam coupling. In (a) and (b) cross-polarization coupling is permitted but not parallel-polarization coupling for any polarization; in (c) and (d) parallel-polarization coupling is permitted but not cross-polarization coupling; in (e) and (f) no two-beam coupling is permitted. The two beams are assumed to enter the crystal symmetrically in these figures.

$$\gamma = \frac{\pi}{\lambda} n^3 r_{41} E^{sc}, \tag{5}$$

where λ is the vacuum wavelength of the beam. In deriving Eqs. (4) we assume the phase shift between the light-intensity modulation and the index grating to be optimal, $\varphi = \pi/2$. Note that the coupling constant γ is real and is the same for both parallel- and cross-polarization couplings. There are two contributions to the holographic index grating in Eqs. (4), the $A_s B_s^*$ (or $A_s^* B_s$) and $A_p B_p^*$ (or $A_p^* B_p$) terms. The relative phase of these two contributions is important because it determines whether the two terms enhance or destroy the index grating. Thus the energy exchange among the four waves critically depends on the input polarization states.

The exact solutions for all four waves in Eqs. (4) can be derived as demonstrated in Ref. 16. However, in our experiments the coupling coefficient γ was only approximately 0.4 cm^{-1}, giving $\gamma L \cong 0.2$, where L (=0.5 cm) is the interaction length. One can therefore apply a weak-coupling approximation, $\gamma L \ll 1$, which assumes no pump-beam depletion.

Thus, using the initial conditions $A_s(0) \neq 0$, $A_p(0) \neq 0$, $B_s(0) \neq 0$, and $B_p(0) = 0$, we can derive the following approximate solutions for the probe-beam intensities:

$$|B_s(z)|^2 = |B_s(0)|^2 \left| 1 + \frac{A_p A_s^*}{I_0} \gamma z \right|^2 e^{-\alpha z},$$

$$|B_p(z)|^2 = |B_s(0)|^2 \frac{|A_s|^4}{I_0^2} (\gamma z)^2 e^{-\alpha z}. \tag{6}$$

Note that the intensity of the s component of the probe beam, $|B_s(z)|^2$, may increase or decrease from its initial value depending on the polarization state of the pump beam. In addition, the intensity of the p component of the probe beam, $|B_p(z)|^2$, is nonzero except at $z = 0$. This means that although there is no p component in the probe beam initially, the p component will be created, and energy will be coupled into it from the s component of the pump beam as it passes through the crystal, thus producing cross-polarization two-beam coupling.

3. EXPERIMENTS AND RESULTS

The experimental configuration for demonstrating cross-polarization two-beam coupling is illustrated schematically in Fig. 3. The 1.06-μm output of a cw Nd:YAG laser was roughly collimated by a lens (L$_0$) and split into two beams, the pump and the probe, by a beam splitter (BS) with 90% reflectivity. These two beams were focused by 50-cm focal length lenses L$_1$ and L$_2$, polarized by calcite polarizers P$_1$ and P$_2$, and intersected in a semi-insulating (undoped) GaAs crystal. The beam diameter of both beams was approximately 1 mm just before entering the crystal. The intensities of the pump and the probe beams were approximately 1 W/cm^2 and 10 mW/cm^2, respectively, and the angle between the beams was 90° outside the crystal. A neutral-density filter ND was used in the probe beam to achieve the desired intensity ratio between the pump and the probe beams. The half-wave plate $\lambda/2$ was used in the pump beam to control the initial mixture of the s and p components. Also, a chopper CH was used to modulate the pump beam at approximately 100 Hz. Finally, the probe beam transmitted through the crystal was analyzed by a polarizing beam splitter PBS, and the p and s components were simulta-
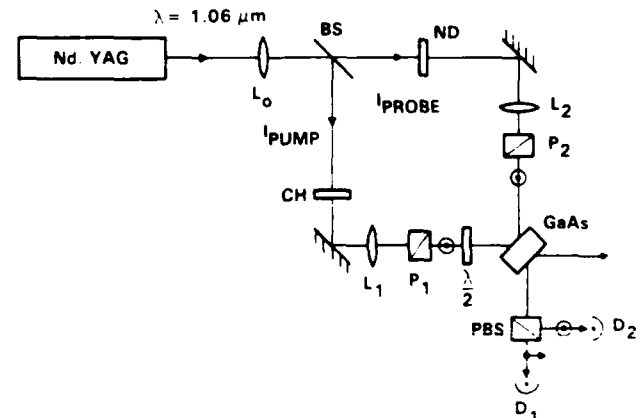

Fig. 3. The experimental arrangement used to demonstrate cross-polarization two-beam coupling.
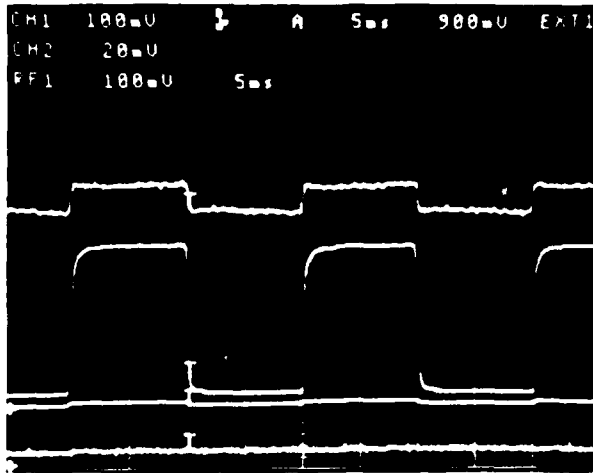
Fig. 4. Typical oscilloscope traces of the signals from D_1 and D_2 (see Fig. 3), demonstrating cross-polarization two-beam coupling: top trace, s-polarization component of the transmitted probe beam, $|B_s(L)|^2$, with the pump beam on; second trace from the top, p-polarization component of the transmitted probe beam, $|B_p(L)|^2$, with the pump beam on; third trace, the zero level of $|B_p(L)|^2$ with the probe off; bottom trace, the zero level of $|B_s(L)|^2$. The triggering cursor (labeled +) indicates when the chopper turned off the pump beam.

neously monitored by photodetectors D_1 and D_2, respectively. The crystal orientation used in our experiment is shown in Fig. 1, as discussed in Section 2.

Typical oscilloscope traces of the signal, as detected by D_1 and D_2, for initially s polarized pump and probe beams are shown in Fig. 4. In this example cross-polarization coupling is demonstrated explicitly; the probe beam gains energy in the p-polarization component, although the probe and the pump beams were initially purely s polarized. The signals were averaged in a digital storage oscilloscope in order to average out the laser-intensity fluctuation, which was approximately 10% in our cw-laser output. The top two traces of Fig. 4 represent the s- and p-polarization components of the transmitted probe-beam intensity $|B_s(L)|^2$ and $|B_p(L)|^2$. The modulation in the signal is from the pump being chopped, showing the cross-polarization coupling gain when the pump is on. The triggering cursor (labeled +) indicates when the pump is turned off. (Note that the scales in the top two traces are different.) The lower two traces represent the corresponding background-noise levels obtained by blocking the probe beam [$|B_s(0)|^2 = |B_p(0)|^2 = 0$], thus monitoring the pump beam that is scattering spuriously into the detectors. Another source of the background noise, which is not indicated in the oscillograph, is the leakage through the polarizers. With the crystal removed and the pump turned off, the extinction of the probe between P_2 and PBS (what D_1 sees) was measured to be approximately 10^{-6}, which is what one expects from good-quality calcite polarizers. However, with the GaAs crystal inserted, the extinction dropped to $\sim 10^{-5}$, probably because of the birefringence induced by imperfections within the crystal. This small leakage is not important for the s-polarization component of the transmitted probe beam but becomes important for the p-polarization component, especially when the cross-polarization coupling gain is small. However, in our experiments the leakage was insignificant because it was less than 1% of

the light intensity coupled into the p-polarization component. In any case, what is significant about the traces in Fig. 4 is that they clearly indicate the presence of cross-polarization two-beam coupling: with no p-polarization component initially, the probe beam gains energy in the p-polarization component. In this particular example the s-polarization component also gains energy. However, it can lose energy according to Eqs. (6), and, indeed, this is exactly what we observed for certain initial pump-beam polarizations, as shall be shown below.

The experiment described above was repeated using 70-μsec and 20-nsec (Q-switched) Nd:YAG pulses at 1.06 μm. The experimental arrangement was identical to that of Fig. 3, except that L_1, L_2, and the chopper were removed. The results of the 70-μsec-pulse experiment, with both the pump and probe beams initially s polarized, are shown in Fig. 5. In these scope traces only the p-polarization component of the transmitted probe beam is shown. The top trace shows $|B_p(L)|^2$ with the pump on; the middle trace shows $|B_p(L)|^2$ with the pump off, indicating the amount of the probe-beam leakage through the polarizers; the bottom trace shows the pump beam scattering into D_1 when the probe was blocked. Again, these traces clearly indicate the presence of cross-polarization two-beam coupling. The cross-polarization coupling in the pulsed regime was accomplished within a single pulse; no pulse averaging was used. The results of the 20-nsec experiments were similar to those of the 70-μsec experiments and are not repeated here.

To compare our experimental data with the theoretical calculations from Eqs. (6) we have repeated the cw experiments described above for various initial pump-beam polarizations. Equations (6) can be further simplified using the approximation that the pump intensity is much stronger than the probe intensity, a condition satisfied in our experiments. The solutions for the transmitted probe beam can then be written as

$$|B_s(L)|^2 \approx |B_s(0)|^2[1 + \gamma L \sin(2\psi)]e^{-\alpha L},$$

$$|B_p(L)|^2 \approx |B_s(0)|^2[(\gamma L)^2 \cos^4 \psi]e^{-\alpha L}, \qquad (7)$$
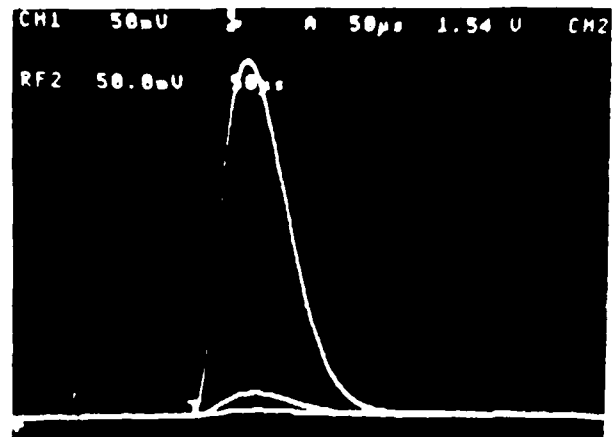
Fig. 5. Typical oscilloscope traces of the cross-polarization coupling signal (from D_1) for 70-μsec pulses at 1.06 μm: top trace, $|B_p(L)|^2$ with the pump on; middle trace, $|B_p(L)|^2$ with the pump off; bottom trace, with the pump on and the probe off to measure the spurious pump scattering into the detector.

where the polarization of the pump beam is linear and forms an angle ψ with the s-polarization direction. We can see from Fig. 1 that ψ is 0° (or 180°) for a purely s wave and 90° for a purely p wave. In our experiment various pump-beam (linear) polarizations were achieved by rotating the half-wave plate (Fig. 3), while both $|B_s(L)|^2$ and $|B_p(L)|^2$ were monitored simultaneously. The experimental results and the comparison with the theory are shown in Fig. 6. To emphasize the ac component of the signal, we have plotted in Fig. 6 the normalized quantities defined as

$$\text{Normalized } |B_s(L)|^2 = \frac{1}{\gamma L}\left[\frac{|B_s(L)|^2}{|B_s(0)|^2 e^{-\alpha L}} - 1\right] = \sin(2\psi),$$

$$\text{Normalized } |B_p(L)|^2 = \frac{|B_p(L)|^2}{(\gamma L)^2|B_s(0)|^2 e^{-\alpha L}} = \cos^4\psi. \qquad (8)$$

The solid curves are the theoretical fit to the experimental data points. In general there is good agreement between the experimental points and the calculated values, indicating that the theory, as well as the approximations used in deriving expressions (7), is valid. The slight asymmetry in the experimental points is attributed to the nonuniformity of the half-wave plate, which would affect the initial pump-beam polarization state. Similar cross-polarization two-beam coupling results were recently reported[20] for a contra-directional cross-polarization coupling geometry using an xyz-cut GaAs crystal, as shown in Fig. 2(b).

The coupling coefficient can be calculated from Fig. 6 and expressions (7). We can solve for the coupling γL by taking the ratio of the measured value of $|B_s(L)|^2$ and $|B_p(L)|^2$ at $\psi = 0$. Using the measured interaction length L of 0.5 cm, we have calculated the cross-polarization coupling coefficient γ to be approximately 0.4 cm^{-1}. This value is consistent with the gain coefficient measured[24] for parallel-polarization cou-

Fig. 7. The cross-polarization coupling coefficient versus the frequency detuning of the probe beam in nondegenerate photorefractive two-beam coupling. From the degradation of the coupling efficiency the photorefractive response time τ can be calculated. In this experiment τ is measured to be ~0.5 msec at 1 W/cm^2 and ~0.2 msec at 10 W/cm^2. The solid and dashed curves are the theoretical fits to the experimental data for 1 and 10 W/cm^2, respectively.

pling in the same sample. According to the theory the gain coefficients for both parallel- and cross-polarization coupling should be the same.

The photorefractive response time of our GaAs crystal was measured using nondegenerate cross-polarization coupling. Here, the frequency of the probe beam was shifted relative to the pump beam, and the degradation in the cross-polarization coupling efficiency was monitored. To frequency shift the probe beam, a pair of acousto-optic (AO) cells, each with an approximate 5-MHz bandwidth centered at 80 MHz, was cascaded so that a frequency upshift from the first cell could be nearly compensated for by a frequency downshift from the second cell. Using this arrangement and varying the relative driving frequency of the two AO cells, we have achieved a frequency detuning ranging from approximately 100 Hz to 10 MHz (with approximately 100-Hz resolution), which is the range needed for the measurement of the photorefractive response time in GaAs. The experimental arrangement for these response-time measurements was essentially identical to that of Fig. 3, except for the introduction of the AO cell assembly into the probe beam, as described above. The incident pump and probe beams were purely s polarized throughout this experiment. The measured p component of the transmitted probe beam, arising from the cross-polarization coupling, is shown as a function of the frequency detuning in Fig. 7. The experimental points were fitted according to the theory of nondegenerate two-wave mixing (for the grating that is exactly $\pi/2$ out of phase with respect to the intensity modulation) with the coupling coefficient given by[4]

PUMP-BEAM POLARIZATION ANGLE ψ (DEGREES)

Fig. 6. (a) Normalized $|B_s(L)|^2$ versus the initial pump-beam polarization state; (b) normalized $|B_p(L)|^2$ versus the initial pump-beam polarization state. ψ is the angle between the pump-beam polarization (linear) and the s-polarization direction. The probe is initially purely s polarized. The solid curves show the predictions from the nonlinear coupled wave theory described in the text and the filled squares are the experimental points. The normalization used in the figure, as defined in Eqs. (8), is to accentuate the ac component of the signal.

$$\gamma(\Delta f) = \frac{\gamma_0}{1 + (2\pi\Delta f\tau)^2}. \qquad (9)$$

where γ_0 is the coupling coefficient for degenerate two-beam coupling, Δf is the frequency detuning, and τ is the response time of the medium. In Fig. 7 the experimental points, the filled circles and filled triangles, which indicate the total intensities of 1 and 10 W/cm^2, respectively, correspond rea-

sonably well to the theoretical curves. The response time calculated from these curves is $\tau = 0.5$ msec for 1 W/cm^2 and $\tau = 0.2$ msec for 10 W/cm^2. The slight asymmetry in the experimental points indicates that the phase between the grating and the intensity modulation is not exactly $\pi/2$.[25]

Our sample exhibited relatively high dark conductivity ($\sim 10^{-7}$ Ω^{-1} cm^{-1}). The effect of high dark conductivity is manifested in Fig. 7 as the intensity-dependent coupling coefficient γ_0. The saturation intensity at which the light-induced process completely dominates the dark-conduction process was near 10 W/cm^2, which is much higher (10^2–10^3 times) than what has been reported.[13] However, this is not surprising because great differences exist among various GaAs samples, owing to the different stoichiometry involved in growing each sample. The effect of dark conductivity is also evident in the measured time constant τ. The fact that τ is not reduced by 10 times when the total intensity I is increased by a factor of 10 indicates the presence of a strong dark-conduction process; nonlinear mechanisms can also contribute to the observed deviation from the linear relationship between $1/\tau$ and I.[26]

4. CONCLUSIONS

We have demonstrated cross-polarization two-beam coupling in a semi-insulating GaAs crystal by using both cw and pulsed Nd:YAG laser beams at 1.06 μm. The cross-polarization coupling coefficient was measured to be approximately 0.4 cm^{-1}, which agrees well with the previously measured value obtained using parallel-polarization coupling. An analysis of the polarizations of the transmitted probe beam for various initial pump-beam polarizations showed that the experimental points closely followed the calculated functional form. This indicates that the theory is valid, as are the approximations. Using nondegenerate cross-polarization two-beam coupling, we measured the photorefractive response time to be approximately 0.5 msec for 1-W/cm^2 intensities. This agrees well with the response time measured using parallel-polarization coupling in the same crystal. Although the demonstrated coupling efficiency ($\gamma \cong 0.4$ cm^{-1}) was not high compared with the bulk optical absorption ($\alpha \cong 1.8$ cm^{-1}), the unique property of cross-polarization two-beam coupling may find applications in such areas as optical image and signal processing, especially with the anticipated improvements in photorefractive materials.

ACKNOWLEDGMENTS

REFERENCES

1. D. L. Staebler and J. J. Amodei, "Coupled wave analysis of holographic storage in LiNbO," J. Appl. Phys. 34, 1042 (1972).

2. V. L. Vinetskii, N. V. Kukhtarev, S. G. Odulov, and M. S. Soskin, "Dynamic self-diffraction of coherent light beams," Sov. Phys. USP. 22, 742 (1979).

3. N. V. Kukhtarev, V. B. Markov, S. G. Odulov, M. S. Soskin, and V. L. Vinetskii, "Holographic storage in electro-optic crystals. Beam coupling and light amplification," Ferroelectrics 22, 961 (1979).

4. J. P. Huignard and A. Marrakchi, "Coherent signal beam amplification in two-wave mixing experiments with photorefractive BSO crystals," Opt. Commun. 38, 249 (1981).

5. Y. Fainman, E. Klancnik, and S. H Lee, "Optimal coherent image amplification by two-wave coupling in photorefractive BaTiO$_3$," Opt. Eng. 25, 228 (1986).

6. J. P. Huignard and A. Marrakchi, "Two-wave mixing and energy transfer in BSO crystals: amplification and vibration analysis," Opt. Lett. 6, 622 (1981).

7. A. E. Chiou and P. Yeh, "Beam cleanup using photorefractive two-wave mixing," Opt. Lett. 10, 621 (1985).

8. A. E. Chiou and P. Yeh, "Laser-beam cleanup using photorefractive two-wave mixing and optical phase conjugation," Opt. Lett. 11, 461 (1986).

9. M. Cronin-Golomb, A. M. Biernacki, C. Lin, and H. Kong, "Photorefractive time differentiation of coherent optical images," Opt. Lett. 12, 1029 (1987).

10. M. B. Klein, "Beam coupling in undoped GaAs at 1.06 μm using the photorefractive effect," Opt. Lett. 9, 350 (1984).

11. A. M. Glass, A. M. Johnson, D. H. Olsen, W. Simpson, and A. A. Ballman, "Four-wave mixing in semi-insulating InP and GaAs using the photorefractive effect," Appl. Phys. Lett. 44, 948 (1984).

12. G. Albanese, J. Kumar, and W. H. Steier, "Investigation of the photorefractive behavior of chrome-doped GaAs by using two-beam coupling," Opt. Lett. 11, 650 (1986).

13. S. McCahon, M. B. Klein, and G. C. Valley, "Photorefractive properties of iron-doped InP at 1.06 μm," in *Digest of Topical Meeting on Photorefractive Materials, Effects, and Devices* (Optical Society of America, Washington, D.C., 1987), p. 46.

14. R. B. Bylsma, P. M. Bridenbaugh, D. H. Olson, and A. M. Glass, "Photorefractive properties of doped cadmium telluride," Appl. Phys. Lett. 51, 889 (1987).

15. See, for example, P. Yeh, "Fundamental limit of the speed of photorefractive effect and its impact on device applications and material research," Appl. Opt. 26, 602 (1987), and references therein.

16. P. Yeh, "Photorefractive two-beam coupling in cubic crystals," J. Opt. Soc. Am. B 4, 1382 (1987).

17. J. P. Herriau, J. P. Huignard, A. G. Apostolidis, and S. Mallick, "Polarization properties in two wave mixing with moving grating in photorefractive BSO crystals. Application to dynamic interferometry," Opt. Commun. 56, 141 (1985).

18. A. Partovi, E. M. Garmire, and L. J. Cheng, "Enhanced beam coupling modulation using the polarization properties of photorefractive GaAs," Appl. Phys. Lett. 51, 299 (1987).

19. T. Y. Chang, A. E. Chiou, and P. Yeh, "Photorefractive two-beam coupling with polarization-flip in gallium arsenide," in *Digest of Topical Meeting on Photorefractive Materials, Effects, and Devices* (Optical Society of America, Washington, D.C., 1987), p. 55.

20. L. J. Cheng and P. Yeh, "Cross-polarization beam coupling in photorefractive GaAs crystals," Opt. Lett. 13, 50 (1988).

21. L. J. Cheng, G. Gheen, T. H. Chao, H. K. Liu, A. Partovi, J. Katz, and E. M. Garmire, "Spatial light modulation by beam coupling in GaAs crystals," Opt. Lett. 12, 705 (1987).

22. L. J. Cheng, G. Gheen, M. E. Rau, and F. C. Wang, "Image transfer in photorefractive GaAs," J. Appl. Phys. 62, 3991 (1987).

23. See, for example, A. Yariv and P. Yeh, *Optical Waves in Crystals* (Wiley, New York, 1984), Chap. 7.

24. A. E. Chiou, "Nondegenerate two-wave mixing in GaAs at 1.06 μm," J. Opt. Soc. Am. B 4(13), P84 (1987).

25. I. McMichael and P. Yeh, "Phase shifts of photorefractive gratings and phase-conjugate waves," Opt. Lett. 11, 48 (1987).

26. S. Ducharme and J. Feinberg, "Speed of the photorefractive effect in a BaTiO single crystal," J. Appl. Phys. 56, 839 (1984).

APPENDIX 4.5

NONDEGENERATE TWO-WAVE MIXING IN RUBY

C9943DA/jbs

Nondegenerate two-wave mixing in ruby

Ian McMichael, Pochi Yeh, and Paul Beckwith

Rockwell International Science Center, 1049 Camino Dos Rios, Thousand Oaks, California 91360

We demonstrate energy exchange by nondegenerate two-wave mixing in ruby. Our results are in agreement with the theory of nondegenerate two-wave mixing when the theory is generalized to take into account a complex nonlinear index. Two-wave mixing gain exceeding the absorption and reflection losses is demonstrated, and we show that these experiments provide a simple and accurate method for determining the complex nonlinear index, response time, and saturation intensity of the medium.

In two-wave mixing (see Fig. 1) the interference of two light waves results in a spatial modulation of the optical susceptibility of some medium. The two waves then interact through this grating, and a net energy transfer between the two waves takes place when the grating is shifted in phase with respect to the interference pattern. Energy transfer is observed in photorefractive media, where a phase shift of approximately 90° results from the grating formation process.[1] In other media, where the grating is usually in phase with the interference pattern, it is possible to produce a phase shift between the grating and the interference pattern, and to observe energy transfer, by moving the grating at a rate comparable with the response time of the medium. This can be accomplished in one of several ways: by nondegenerate two-wave mixing (NDTWM) in which a frequency shift between the interacting waves results in a moving interference pattern, by moving the medium itself,[2] or by using the Lorentz force to move the free-carrier grating in a semiconducting medium.[3] NDTWM takes place in such stimulated scattering processes as Rayleigh line, Brillouin, Rayleigh wing, and Raman scattering. In these processes the corresponding nonlinearity is increased by the resonant Q, $Q = f/\Delta f$ (for backward stimulated Brillouin scattering in CS_2, $Q \sim 100$). However, since the corresponding nonlinearities (Kerr effect, in which a change of polarizability of individual molecules is due to field-induced deformation and reorientation, and electrostriction and absorptive thermal nonlinearities) are small to begin with, the power densities required for these effects to be observed are still very large (~ 10 MW/cm^2). It is therefore surprising that NDTWM in saturable resonant media has not been investigated extensively, since the corresponding nonlinearities can be many orders of magnitude higher and the power densities required can be many orders of magnitude lower. To our knowledge there are only two other reports of such investigations, one using sodium vapor[4] and another using a fluorescein-doped glass.[5] In this Letter we present the details of our work on NDTWM in ruby.[6] We show that our results are in agreement with the theory of NDTWM[7] when it is generalized to take into account a complex nonlinear index, we demonstrate two-wave mixing gain exceed-

ing the absorption and reflection losses, indicating that NDTWM can be used for optical amplification, and we point out that these experiments provide a simple and accurate method for determining the complex nonlinear index, response time, and saturation intensity.

For a light wave of intensity I much less than the saturation intensity I_s in ruby, the refractive index is given by[8]

$$n = n_0 + n_2 I, \qquad (1)$$

where n_0 is the linear refractive index and the nonlinear index n_2 is complex to account for changes in the absorption as well as the refractive index:

$$n_2 = n_2' - i n_2''. \qquad (2)$$

The problem of NDTWM in media with a refractive index described by Eq. (1) is solved in Ref. 7. For a pump of intensity I_1 interacting with a much weaker probe wave of intensity I_2,

$$I_2(L) = I_2(0) \exp\left(\gamma \frac{\delta - r}{1 + \delta^2} - \alpha \right) L. \qquad (3)$$
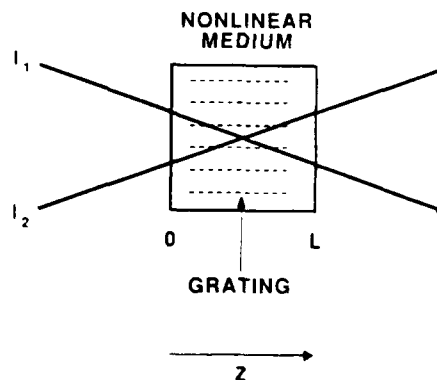

NONLINEAR MEDIUM

Fig. 1. Schematic of two-wave mixing. Two beams interfere in a nonlinear medium and modulate the optical susceptibility to produce a grating. When the frequency shift between the two beams is of the order of the response time of the medium, the modulation of the optical susceptibility is shifted spatially with respect to the interference pattern, and one beam gains energy from the other.
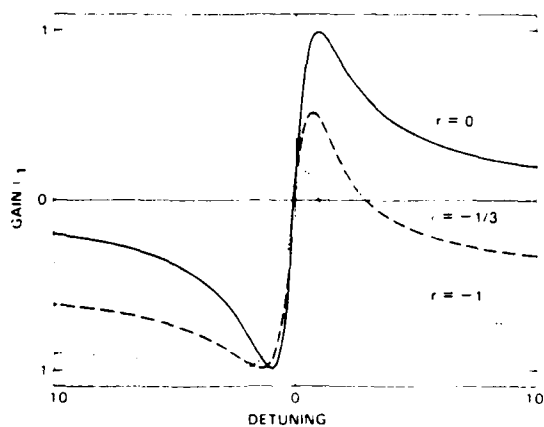
Fig. 2. Calculations of the nondegenerate two-wave mixing gain as a function of the frequency detuning between the two waves for various ratios r of the imaginary to real parts of the nonlinear index n_2.

where the coupling coefficient γ is given by

$$\gamma = \frac{2\pi}{\lambda \cos(\theta/2)} \left(\frac{1 - e^{-\alpha L}}{\alpha L}\right) n_2' I_1. \qquad (4)$$

The detuning δ is the product of the frequency difference between the two waves and the response time of the medium [$\delta = (\omega_1 - \omega_2)\tau$], $r = n_2''/n_2'$, λ is the wavelength of the pump and probe waves, θ is the angle between the pump and probe waves, α is the absorption coefficient, and L is the length of the medium.

Figure 2 shows plots of the two-wave mixing gain parameter Γ_1 defined by

$$\Gamma_1 \equiv \ln \frac{I_2(L, \delta)}{I_2(L, 0)} = \gamma L \frac{\delta + r\delta^2}{1 + \delta^2}. \qquad (5)$$

for $r = 0, -1/3$, and -1. The values of Γ_1 are normalized to their minimum values. For $r = 0$, Γ_1 is an antisymmetric function of the detuning δ, so that $r \neq 0$ can be recognized by a departure from antisymmetry.

Our experimental setup is shown in Fig. 3. Light from an argon laser is focused by lens L (focal length, 0.8 m) into a ruby crystal. Most of the light (approximately 99%) is reflected by beam splitter BS to provide the pump wave for NDTWM; the remaining 1% of the light provides the probe wave. The power in the pump wave is 0.5 W, the spot size is approximately 0.3 mm, the interaction length is 1 cm, and the angle between the pump and probe waves is 0.5°. The frequency of the probe is shifted by reflecting it from a mirror mounted to a piezoelectric transducer (PZT). An aperture (A) blocks the transmitted pump wave, and the transmitted probe wave is measured by a detector and displayed on an oscilloscope. Figure 4 shows a photograph from the oscilloscope. The lower straight trace, a, was recorded with the pump blocked, and the upper straight trace, b, representing $I_2(L, 0)$, was recorded with the pump on but with no frequency shift. The fact that trace b is higher than trace a represents the saturation of the absorption by the pump wave. With a triangular voltage wave (trace c)

applied to the PZT, a square-wave signal (trace d) results for the transmitted probe. In the left half of the photograph the voltage applied to the PZT is decreasing, the probe is upshifted with respect to the pump (negative δ), and energy flows from the probe wave into the pump wave as indicated by the fact that trace d drops below trace b to a level $I_2(L, \delta^-)$. In the right half of the photograph the voltage applied to the PZT is increasing, the probe is downshifted with respect to the pump, and energy flows from the pump wave into the probe wave as indicated by the fact that trace d rises above trace b to a level $I_2(L, \delta^+)$.

By varying the period of the the triangular voltage wave driving the PZT and measuring $I_2(L, 0)$, $I_2(L, \delta^-)$, and $I_2(L, \delta^+)$, one can obtain the two-wave mixing gain parameter $\Gamma_1(\delta)$ defined by Eq. (5). Figure 5 shows fits of $\Gamma_1(\delta)$ to measurements made at 488 and 580 nm (using a dye laser). At both wavelengths, $\Gamma_1(\delta)$ is approximately antisymmetric, indicating that the contribution due to the refractive-index grating dominates over that due to the absorption. At 488 nm, Eq. (5) with $r = 0$ provides a good fit to the data (solid line in Fig. 5). The fit gives a value for the excited-state lifetime $\tau = 3.4$ msec and for the nonlinear index $n_2 = n_2' = 10^{-5}$ cm²/W. (If one is careful in measuring the
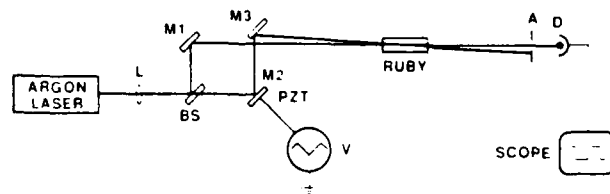

Fig. 3. Experimental setup for nondegenerate two-wave mixing in ruby. Light from a laser is split into two beams (pump and probe) that interfere in a ruby crystal. The probe beam is frequency shifted by a mirror (M2) mounted to a PZT and measured by detector D. A voltage source applies a triangular wave to the PZT.
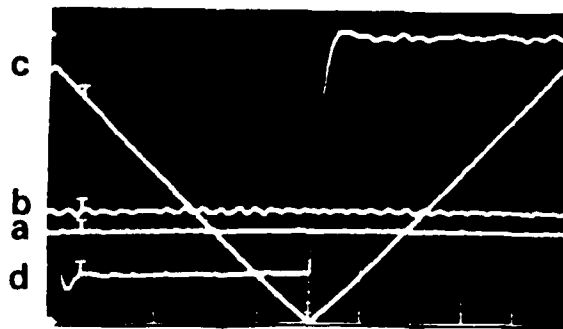

Fig. 4. Photograph from oscilloscope (see Fig. 3) showing two-wave mixing attenuation and gain. Traces a and b show the transmitted probe power as measured by detector D with the pump beam blocked and unblocked, respectively, but no frequency shift. Trace c shows the voltage applied to the PZT to produce a frequency shift, and trace d shows the corresponding attenuation and gain for the probe. Zero is indicated by the cross in the lower left, one horizontal division corresponds to 20 msec, and the vertical axis gives relative intensity.
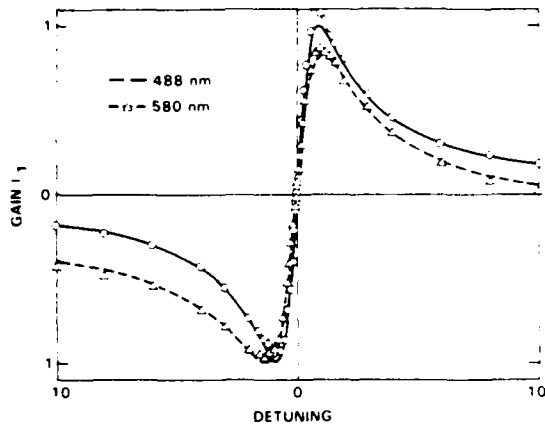
Fig. 5. Measurements of the nondegenerate two-wave mixing gain in ruby as a function of frequency detuning between the two waves for various wavelengths. At 488 nm the gain is antisymmetric, indicating an index grating, while at 580 nm there is a departure from antisymmetry, indicating a mixed grating (index and absorption).
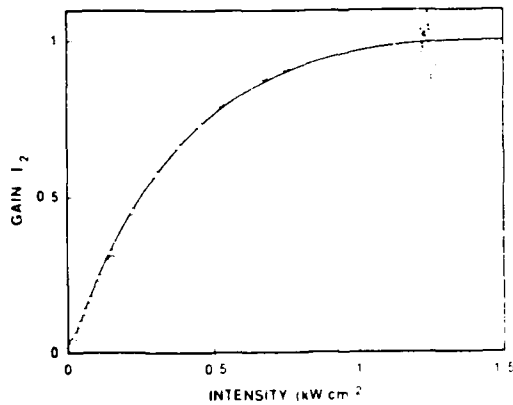

Fig. 6. Measurements of the nondegenerate two-wave mixing gain in ruby as a function of the intensity of the pump wave at 515 nm.

spot size and taking into account the intensity profile, one can obtain an accurate determination of n_2 by using this technique.) These values are in good agreement with those obtained in Ref. 8. At 580 nm. $\Gamma_1(\delta)$ departs slightly from antisymmetry [e.g.. $\Gamma_1(\delta = +1)$ $\neq \Gamma_1(\delta = -1)$] and the fit of Eq. (5) to the data (dashed line in Fig. 5) gives $r = -0.1$. indicating that saturated absorption is contributing to the nonlinear

index. At 606 nm we have observed a positive value of r. indicating that the absorption of the excited state is greater than that of the ground state at this wavelength.

When the pump intensity I_1 exceeds the saturation intensity I_s, the nonlinear index. and therefore the gain, is reduced by a factor $1/(1 + I_1/I_s)^2$. To study the effect of saturation. we measured the two-wave mixing gain parameter $\Gamma_2(I_1)$,

$$\Gamma_2 \equiv \ln \frac{I_2(L, \delta = +1)}{I_2(L, \delta = -1)} = \gamma L \frac{I_1}{(1 + I_1/I_s)^2}. \quad (6)$$

at 515 nm. Figure 6 shows a fit of Eq. (6) to the measurements of Γ_2, where Γ_2 is normalized to its maximum value. The fit gives a value of $I_s = 1.5$ kW cm², in good agreement with previously calculated values.[8]

In conclusion, we have demonstrated energy exchange by NDTWM in ruby and have shown that our results are in good agreement with theory. By operating at 488 nm with a pump intensity of the order of the saturation intensity we have observed a net two-wave mixing gain (exceeding the absorption and reflection losses) of 50%. indicating that it should be possible to construct oscillators. (It should be noted. however. that such gain is accompanied by strong self-focusing.) These experiments provide a simple and accurate method for determining the complex nonlinear index. response time. and saturation intensity of resonant saturable media.

References

1. D. Staebler and J. Amodei. J. Appl. Phys. **43**, 1042 (1972).
2. Y. Anan'ev. Sov. J. Quantum Electron. **4**, 929 (1975).
3. V. Vinetskii. N. Kukhtarev. S. Odulov. and M. Soskin. Sov. Phys. Tech. Phys. **22**, 729 (1977).
4. G. Grynberg. E. Le Bihan. and M. Pinard. J. Phys. (Paris) **47**, 1321 (1986); D. Grandclément. G. Grynberg. and M. Pinard. Phys. Rev. Lett. **59**, 40 (1987); M. Gruneisen. K. MacDonald. and R. Boyd. J. Opt. Soc. Am. B **5**, 123 (1988).
5. M. Kramer. W. Tompkin. and R. Boyd. Phys. Rev. A **34**, 2026 (1986).
6. I. McMichael and P. Yeh. J. Opt. Soc. Am. B **4** (13), P32 (1987).
7. P. Yeh. J. Opt. Soc. Am. B **3**, 747 (1986).
8. T. Catunda. J. Andreeta. and J. Castro. Appl. Opt. **25**, 2391 (1986).

\

APPENDIX 4.6

EXTERNALLY PUMPED POLARIZATON-PRESERVING
PHASE CONJUGATOR

Externally pumped polarization-preserving phase conjugator

Ian McMichael

Rockwell International Science Center, 1049 Camino Dos Rios, Thousand Oaks, California 91360

We demonstrate an externally pumped phase conjugator that preserves polarization on reflection and does not exhibit the frequency shift present in self-pumped phase conjugators. Our results show that for linearly polarized incident light the phase-conjugate reflection reproduces the angle of polarization to within the experimental error of 1%. For circularly polarized incident light, our results show that the helicity of polarization is preserved on reflection.

The distortion resulting from the propagation of a light wave through an aberrating medium can be corrected by generating a time-reversed wave with a phase conjugator that propagates back through the aberrating medium. However, most phase conjugators reflect only one polarization state, and therefore they do not produce time-reversed waves when the incident light is of arbitrary polarization. As a result, most phase conjugators do not correct for the changes in polarization induced by optically anisotropic media. Only a phase conjugator for which the conjugate reflection has the same polarization as the incident wave can produce true time-reversed waves that correct for both the wave-front distortions and the changes in polarization induced by optically anisotropic wave-front distorting media.[1]

Phase conjugation was demonstrated first by stimulated Brillouin scattering (SBS) in methane.[2] It was realized that polarization is not preserved in SBS.[3] In fact, circularly polarized light changes handedness in SBS, as it does when reflected from a normal mirror. Polarization-preserving phase conjugation was first proposed and demonstrated by Basov and co-workers using a scheme in which an incident beam is converted into two linearly polarized beams before entering the SBS cell.[4] During this time, phase conjugation by four-wave mixing was proposed[5] and demonstrated in CS_2.[6] In 1979 Zeldovich and Shkunov proposed two additional schemes for polarization-preserving phase conjugation by four-wave mixing in isotropic media.[7] The first scheme, utilizing counterrotating circularly polarized pump waves, was first demonstrated by Martin *et al.* in CS_2.[8] The second scheme, utilizing a geometry in which the probe beam propagates perpendicular to the pump waves, was first demonstrated by Blashchuk *et al.*, again in CS_2.[9] Polarization-preserving phase conjugation was also obtained by four-wave mixing in a two-photon absorber.[10] In addition to the pioneering works mentioned above, which deal with the specific problem of polarization-preserving phase conjugation, there are more recent works dealing with the general polarization properties of phase conjugators.[11]

We reported[12] recently on the demonstration of a polarization-preserving phase conjugator (PPPC) using the Ba-

sov scheme[4] with a self-pumped crystal of barium titanate ($BaTiO_3$) as the conjugator. However, the self-pumped conjugator produces a reflection that is shifted in frequency with respect to the incident wave.[13] This shift may not be tolerable in interferometric applications. In this Communication we report on the demonstration of a PPPC using the Basov scheme with an externally pumped conjugator that does not have this frequency shift. Experimental results are presented showing that the externally pumped PPPC reproduces the polarization of the incident wave.

Our experimental setup is shown in Fig. 1. We use an argon-ion laser operating in multilongitudinal mode at 514.5 nm. The arrangement of optical components BS2, M1, M2, M3, $BaTiO_3$, PBS, and $\lambda/2$ (shown as a solid line) forms a PPPC for light incident from the left on the polarizing beam splitter PBS. The remaining optical components are used to test the PPPC. External pumping waves for four-wave mixing in the crystal of $BaTiO_3$ are provided by the reflection from mirrors M1 (power, ~4 mW) and M2 (power, ~1 mW). The polarization components transmitted and reflected by the PBS are probe waves (total power, ~0.5 mW). Optical path lengths are adjusted to ensure that the pump and probe waves are coherent at the crystal. The half-wave retarder $\lambda/2$ (shown as a solid line) rotates the polarization of one probe so that all waves entering the $BaTiO_3$ crystal are extraordinary. The conjugate reflections of the probe waves recombine at the PBS to form a phase-conjugate wave that has the same polarization as the incident wave. However, this result occurs only when the phase-conjugate reflectivity is the same for both probe waves. For this reason, we made the angle between the probe waves small. After initial alignment we found that the reflectivities of the probe waves were not equal. To solve this problem, the alignment of the probe wave having the highest reflectivity was adjusted to obtain equal reflectivities. We should be able to avoid this procedure if we use an angle of incidence for the probe waves at which reflectivity is maximum and changes little with angle. To test the PPPC, either a half-wave retarder $\lambda/2$ or a quarter-wave retarder $\lambda/4$ (shown as a dashed line) is inserted into the experimental setup and used to alter the
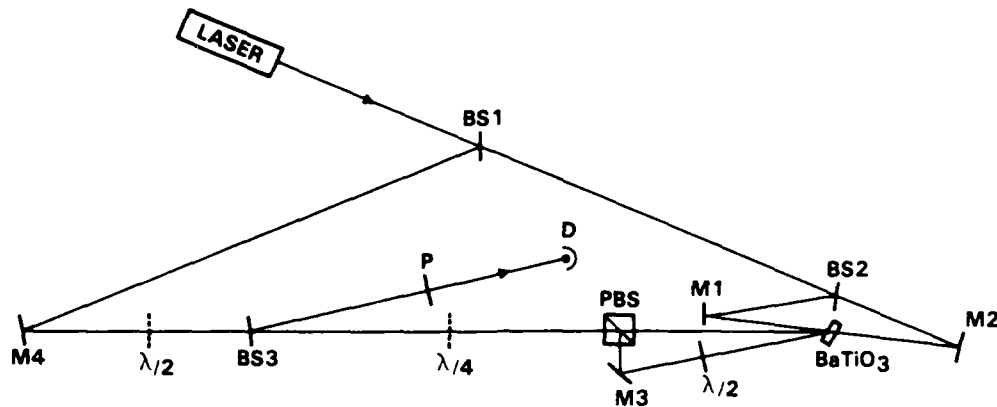
Fig. 1. Experimental setup used to test the externally pumped PPPC.
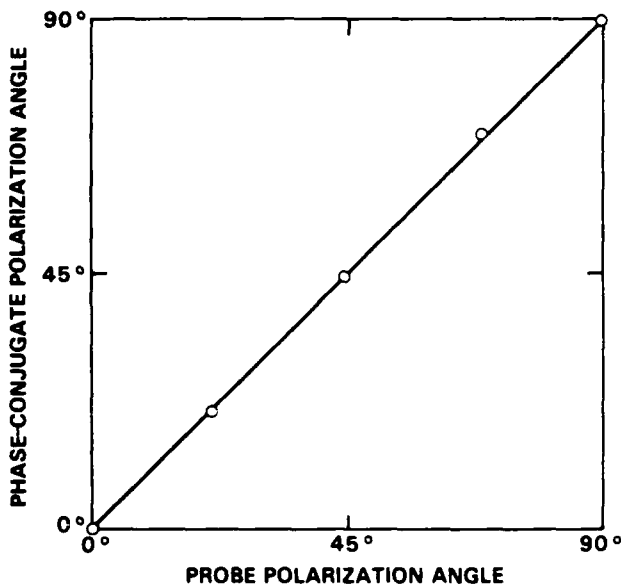
Fig. 2. Measured angle of polarization for the reflection from the PPPC versus the angle of polarization for the incident wave. Zero degrees corresponds to polarization in the plane of Fig. 1.

measurements indicates that our externally pumped PPPC preserves the angle of polarization to within 1%. The measured power ratio of the minor polarization axis to the major axis never exceeded 5%.

To demonstrate that the externally pumped PPPC reproduces the helicity of polarization on reflection, a quarter-wave retarder $\lambda/4$ (shown as a dashed line in Fig. 1) is placed between BS3 and PBS and is oriented such that light incident upon the PPPC is converted from linearly polarized light (in the x direction) to circularly polarized light. Figure 3 shows the measured polarization ellipses for the reflections from a normal mirror and from the externally pumped PPPC. Light reflected from a normal mirror changes helicity, and, after passing back through the quarter-wave retarder, the reflected light has a polarization orthogonal to that of the incident light. This principle is the one by which quarter-wave isolation works. On the other hand. light reflected by the PPPC has the same helicity as the incident

polarization state of light incident on the PPPC. The conjugate reflection from the PPPC is sampled by beam splitter BS3 and analyzed by the combination of polarizer P and detector D. Because BS3 is an uncoated pellicle beam splitter used near normal incidence (the angle of incidence is exaggerated in the figure; the actual angle of incidence is 2°), the reflection coefficients for s and p polarizations are nearly equal (to within 0.2%), and the polarization measured by P and D is nearly the same as that of the conjugate reflection.

In our first test, we rotate the polarization of the light incident upon the PPPC to various angles using the half-wave plate $\lambda/2$ (shown as a dashed line) and measure the corresponding angles of polarizations for the phase-conjugate reflection. Our measurements are shown in Fig. 2 as open circles; the diameters correspond to their uncertainty. The phase-conjugate reflection from a PPPC should have the same angle of polarization as the incident wave, as indicated by the solid line in Fig. 2. The excellent fit of the

**POLARIZATION AFTER DOUBLE PASS THROUGH QUARTER-WAVE RETARDER**

Fig. 3. Reproduction of the helicity of polarized light by the externally pumped PPPC. I_x and I_y are the intensities measured along the x and y axes. respectively. The x axis corresponds to polarization in the plane of Fig. 1.

light and returns to its original polarization state after pass-
ing back through the quarter-wave retarder.

The electro-optic coefficients in $BaTiO_3$ are such that the
diffraction efficiency of the photorefractive gratings is much
greater for extraordinary waves than for ordinary waves. To
take advantage of this feature, all waves entering the crystal
in our experiments had extraordinary polarization. For the
most part, changing the polarization states of the pumping
waves will reduce the reflectivity of the PPPC without af-
fecting the polarization-preserving properties. As long as
the extraordinary components of the two pumping waves are
conjugates of each other, the polarization-preserving prop-
erties will not be affected by pump waves having random
polarization over their wave fronts. However, if the pump-
ing waves are not conjugates of each other, the fidelity of the
PPPC will be affected in the same manner as would any
conjugator. Although we have not verified this experimen-
tally, we expect that our PPPC will produce a true time-
reversed replica of a probe wave having random polarization
over its wave front.

We have demonstrated an externally pumped polariza-
tion-preserving phase conjugator. The experimental results
show good reproduction of the polarization of the incident
wave, although the reproduction is not so good as that ob-
tained previously with a self-pumped PPPC.[12] We believe
this is due to the problem of balancing the conjugate reflec-
tivities for the two probe waves and can be solved as noted in
the text. The advantage of this scheme over the previous
one is the absence of any frequency shift in the phase-conju-
gate return.

REFERENCES

1. P. Yeh, Opt. Commun. 51, 195–197 (1984).
2. B. Zeldovich, V. Popovichev, V. Ragulskii, and F. Faizullov, JETP Lett. 15, 109 (1972).
3. B. Zeldovich and V. Shkunov, Sov. Phys. JETP 48, 214 (1978); V. Blashchuk, B. Zeldovich, V. Krasheninnikov, N. Melnikov, N. Pilipetski, V. Ragulskii, and V. Shkunov, Sov. Phys. Dokl. 23, 588 (1978); V. Blashchuk, V. Krasheninnikov, N. Melnikov, N. Pilipetsky, V. Ragusky, V. Shkunov, and B. Zeldovich, Opt. Commun. 27, 137 (1978).
4. N. Basov, V. Efimkov, I. Zubarev, A. Kotov, S. Mikhailov, and M. Smirnov, JETP Lett. 28, 197 (1978).
5. R. W. Hellwarth, J. Opt. Soc. Am. 67, 1 (1977).
6. D. Bloom and G. Bjorklund, Appl. Phys. Lett. 31, 592 (1977); S. Jensen and R. Hellwarth, Appl. Phys. Lett. 32, 166 (1978).
7. B. Zeldovich and V. Shkunov, Sov. J. Quantum Electron. 9, 379 (1979).
8. G. Martin, L. Lam, and R. Hellwarth, Opt. Lett. 5, 185 (1980).
9. V. Blashchuk, B. Zeldovich, A. Mamev, N. Pilipetski, and V. Shkunov, Sov. J. Quantum Electron. 10, 356 (1980).
10. L. Chase, M. Claude, D. Hulin, and A. Mysyrowicz, Phys. Rev. A 28, 3696 (1983).
11. G. Grynberg, Opt. Commun. 48, 432 (1984); M. Ducloy and D. Bloch, Phys. Rev. A 30, 3107 (1984).
12. I. McMichael, M. Khoshnevisan, and P. Yeh, Opt. Lett. 11, 525 (1986).
13. W. Whitten and J. Ramsey, Opt. Lett. 9, 44 (1984); J. Feinberg and G. Bacher, Opt. Lett. 9, 420 (1984).

APPENDIX 4.7

PHASE-CONJUGATE MULTIMODE FIBER GYRO

Phase-conjugate multimode fiber gyro

Ian McMichael, Paul Beckwith, and Pochi Yeh

Rockwell International Science Center, 1049 Camino Dos Rios, Thousand Oaks, California

Phase conjugation is used to correct the detrimental effects of modal scrambling in a passive optical gyro that uses multimode fiber. A proof-of-principle demonstration of rotation sensing is presented.

Modal scrambling is a major source of noise and signal fading in fiber-optic gyros.[1] Therefore the most sensitive fiber-optic gyros use single-mode polarization-preserving fiber and couplers.[2] Phase conjugation can be used to correct modal scrambling[3–5] and can also be incorporated into the construction of fiber-optic gyros.[6–9] In this Letter we describe and demonstrate the combination of these two possibilities: a passive phase-conjugate fiber-optic gyro using multimode fiber. To our knowledge, this is the first demonstration of rotation sensing with a phase-conjugate multimode fiber gyro. Multimode fiber gyros have been made without phase-conjugate mirrors, but in that case the fringe visibility is reduced by the number of fiber modes.[10–12]

Figure 1 shows a schematic of a phase-conjugate fiber-optic gyro. Light from a laser is split by beam splitter BS and passed into two fibers, F1 and F2 by means of mirror M. F1 and F2 are coiled such that the incident light travels counterclockwise (CCW) in F1 and clockwise (CW) in F2. Light waves traversing the fibers experience reciprocal phase shifts due to propagation and environmental effects and nonreciprocal phase shifts due to the Sagnac effect. The phase-conjugate mirror PCM produces time-reversed waves that correct the reciprocal phase shifts when they propagate back through the fibers but do not correct the nonreciprocal phase shifts. The phase difference ϕ between the recombining waves at detector D is given by[9]

$$\phi = 4\pi(R_1 L_1 + R_2 L_2)\Omega/\lambda c,$$

where R_1, R_2 and L_1, L_2 are the radii and lengths, respectively, of fiber coils F1 and F2, Ω is the rotation rate, λ is the wavelength, and c is the speed of light. Since the phase difference ϕ is proportional to the rotation rate Ω, the output of detector D can be used to sense rotation.

Figure 2 shows the experimental setup of the phase-conjugate multimode fiber gyro. Instead of using two separate fibers to carry CW and CCW traveling waves as shown in Fig. 1, we use polarization states to distinguish the CW and CCW waves in our experimental setup. The laser is an argon-ion laser operating multi-longitudinal mode at 515 nm. The highly reflective beam splitter BS isolates the laser from retroreflections. The single-mode polarization-preserving fiber

F1 couples light from the laser to the remaining part of the apparatus that is mounted on a rotating table. Lenses L1 and L2 (20× microscope objectives), respectively, focus light into F1 and collimate the output. The output end of F1 is oriented such that the polarization of light emerging from the fiber is at an angle of 45° to the plane of the figure. This light (power ~10 mW) is then focused by lens L3 (focal length f = 10 cm) into the multimode fiber coil. The component polarized in the plane of the page is transmitted by the polarizing beam splitter PBS1 and travels as a CCW wave in the fiber coil, whereas the component polarized perpendicular to the page travels as a CW wave. The fiber coil consists of approximately 20 m of graded-index multimode fiber (core diameter 50 μm, numerical aperture 0.2, attenuation 30 dB/km) coiled in a square of 0.57-m sides. Because of modal scrambling in the fiber, when the counterpropagating waves (CW and CCW) exit from the coil, their energy will be randomly distributed among the spatial and polarization modes at the fiber output. Therefore one half of the light from each wave will exit the port of PBS1 that returns toward the laser. The other one half of the light is collected by lens L4 (f = 10 cm), and one half of that (one quarter of the total) passes through polarizer P oriented at 45° to the page, in order to produce
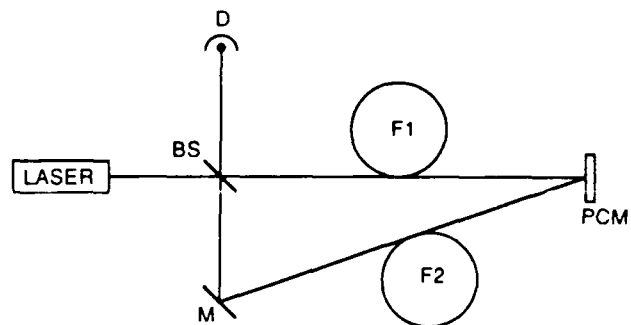

Fig. 1. Schematic of a passive phase-conjugate fiber-optic gyro. Light split by beam splitter BS is passed into fibers F1 and F2 by means of the mirror M, where it experiences phase shifts due to thermal, mechanical, and rotational effects. The phase-conjugate mirror PCM produces time-reversed waves that correct the reciprocal phase shifts but not the nonreciprocal phase shifts produced by rotation. Rotation can be sensed by measuring the interference between the recombining waves at detector D.
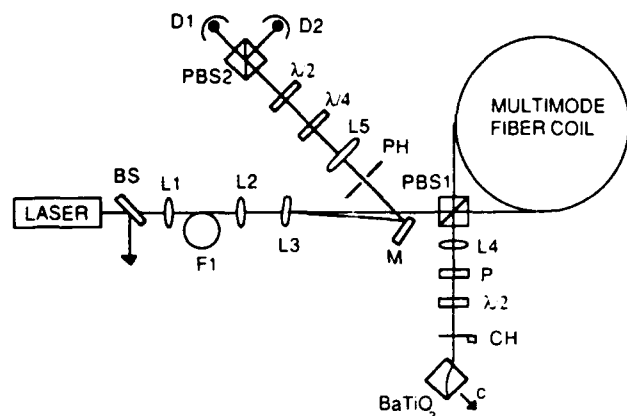
Fig. 2.   Experimental setup of the passive phase-conjugate multimode fiber gyro. Laser light is incident upon polarizing beam splitter PBS1 with polarization at 45° to the plane of the page. The components reflected and transmitted by PBS1 travel CW and CCW, respectively, in the multimode fiber coil. Part of the light exiting from both ends of the fiber passes through PBS1, lens L4, polarizer P, half-wave retarder $\lambda/2$, and chopper CH and is incident upon a phase conjugator $BaTiO_3$. Part of the reflected light retraverses the fiber in both directions, recombines at PBS1, and travels back to the laser. This light is sampled by the reflection from one surface of L3 and is passed through the pinhole PH to reject light that is not phase conjugate. The quarter-wave retarder $\lambda/4$ biases the gyro for maximum sensitivity, and the half-wave retarder $\lambda/2$ is oriented such that the interferences at detectors D1 and D2 contain equal components from the original CW and CCW waves. The signals from the detectors go to a differential amplifier, a lock-in amplifier, and an oscilloscope.

linearly polarized light with equal contributions from the CW and CCW waves. The polarization of the light exiting from P is rotated back into the plane of the page by a half-wave retarder $\lambda/2$. The light is then chopped at 200 Hz by chopper CH and is incident upon a barium titanate crystal $BaTiO_3$ with extraordinary polarization so that efficient self-pumped phase conjugation[13] occurs. The power incident upon the crystal is ~1 mW, and the phase-conjugate reflectivity is ~20%.

The phase-conjugated light will retraverse the fiber in both directions, recombine at PBS1, and travel back toward the laser. This light is sampled by the reflection from the uncoated plano surface of L3 (plano surface of L3 faces L2) and is also focused by L3 through pinhole PH (diameter $d = 150 \mu m$). The pinhole acts as a spatial filter to pass the phase-conjugated light and to block returning light that is not phase conjugate.[4,5] Although the filter may not be essential to the measurement of the gyro signal, it greatly enhances the signal-to-background-noise ratio. Lens L5 ($f = 5$ cm) collimates the light passing through the pinhole. The quarter-wave retarder $\lambda/4$ produces a 90° phase shift between the CW and CCW waves and biases the gyro at the point of maximum sensitivity. The half-wave retarder is oriented such that the interferences of the light passing through PBS2 and measured by detectors D1 and D2 contain equal components from the original CW and CCW

waves. The power incident upon each detector is ~1 μW. The signals from these detectors go to a differential amplifier, a lock-in amplifier referenced to the chopper frequency, and a digital oscilloscope.

Figure 3 shows representative signals from the oscilloscope. For the upper photograph the gyro was first stationary; then it was rotated clockwise, stopped, and then rotated counterclockwise for several cycles with an amplitude of approximately 6°/sec. Each vertical division corresponds to a 0.10-rad phase shift, and each horizontal division corresponds to 5 sec. The time required for the gyro rotation signal to reach steady state after each rotational acceleration has ended is a result of the response time of the $BaTiO_3$ phase conjugator (seconds at milliwatt power levels) and the time constant set on the lock-in amplifier (1 sec). The experimentally measured phase shift is in good agreement with the predicted phase shift of 0.09 rad. Various rotational amplitudes and periods were examined. In all cases, the signal decayed only after the rotation had stopped. The background-noise level with the gyro stationary is shown in the lower photograph (the vertical scale is five times more sensitive). Short-term noise corresponds to a sensitivity that is an order of magnitude larger than that required to measure the rotation rate of the Earth. At present, we do not know

GYRO ROTATION SIGNAL
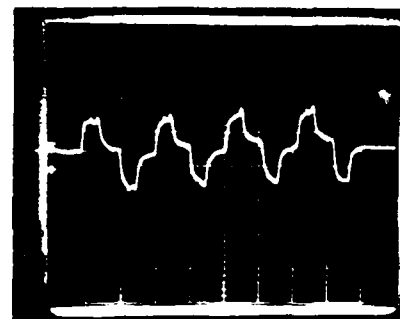
BACKGROUND NOISE LEVEL (VERTICAL SCALE ÷ 5)
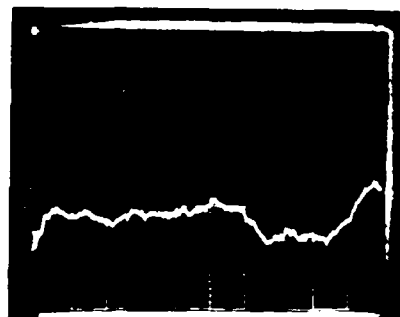
Fig. 3.   Measurement of the Sagnac phase shift in the phase-conjugate multimode fiber gyro. The upper photograph is taken from the oscilloscope mentioned in the caption of Fig. 2. Each vertical division corresponds to a 0.10-rad phase shift, and each horizontal division corresponds to 5 sec. First the gyro was stationary; then it was rotated CW, stopped, and then rotated CCW for several cycles with an amplitude of approximately 6°/sec. The measured phase shift is in good agreement with the predicted phase shift of 0.09 rad. The lower photograph shows the background-noise level (gyro stationary) on a scale five times more sensitive than in the upper photograph.

the source of the short-term noise. Also apparent in the photograph is drift on a longer time scale, which is thought to be due to changes in the phase-conjugate reflectivity of the self-pumped conjugator.

It should be noted that most of the original optical energy entering the fiber coil does not reach the detectors in our simple experimental configuration. As noted above, one half of the light is lost when the CW and CCW waves pass through PBS1 on their way to the phase conjugator. Another one half is lost when the waves go through polarizer P. For the reflected light, only one half of the original CCW wave will reenter the fiber as a CW wave, and of this light, only one half (one quarter of the original energy in the CCW wave) is the phase conjugate of the original CCW wave. The other one half of this light returns scrambled among the various spatial and polarization modes of the fiber.[5] Combining these factors and assuming unit phase-conjugate reflectivity and lossless optics, we find that only one sixteenth of the original energy returns to lens L3 in the original spatial and polarization mode, of which 4% is reflected and directed toward the detectors. Most of the light arriving at the pinhole PH is not phase conjugate. Fortunately, this light is distributed over the full numerical aperture of the fiber, and most of it is rejected by the pinhole.[4,5] The portion of this non-phase-conjugate light that passes through the pinhole acts as a source of noise. The losses resulting in the factor of one sixteenth mentioned above arise from two sources and can be eliminated by using a different optical configuration as noted below. The first source of loss is due to the configuration required to use a single multimode fiber coil. In this configuration, light consisting of many modes having random polarization must pass through a polarizing beam splitter (PBS1 in Fig. 2) twice: once when it leaves the fiber on its way toward the conjugator and once when it returns to the fiber from the conjugator. This results in a loss of $1/2 \times 1/2 = 1/4$. This loss can be avoided by using the configuration

having two fibers shown in Fig. 1. The second source of loss is the non-polarization-preserving phase conjugator formed by optical elements P, $\lambda/2$, and $BaTiO_3$. This results in an additional loss of 1/4,[5] which can be avoided by using a polarization-preserving phase conjugator.[3]

In conclusion, we have described and demonstrated, for the first time to our knowledge, rotation sensing with a phase-conjugate fiber-optic gyro using multimode fiber.

References

1. R. Ulrich, Opt. Lett. **5**, 173 (1980).
2. W. Burns, R. Moeller, C. Villarruel, and M. Abebe, Opt. Lett. **8**, 540 (1983).
3. I. McMichael, M. Khoshnevisan, and P. Yeh, Opt. Lett. **11**, 525 (1986).
4. K. Kyuma, A. Yariv, and S. Kwong, Appl. Phys. Lett. **49**, 617 (1986).
5. I. McMichael, P. Yeh, and P. Beckwith, Opt. Lett. **12**, 507 (1987).
6. C. J. Bordé, in *Experimental Gravitation and Measurement Theory*, P. Meystre and M. O. Scully, eds. (Plenum, New York, 1983), p. 269.
7. B. Fischer and S. Sternklar, Appl. Phys. Lett. **47**, 1 (1985).
8. P. Yeh, I. McMichael, and M. Khoshnevisan, Appl. Opt. **25**, 1029 (1986).
9. I. McMichael and P. Yeh, Opt. Lett. **11**, 686 (1986).
10. G. Pavlath and H. Shaw, in *Fiber-Optic Rotation Sensors*, S. Ezekial and H. Arditty, eds. (Springer-Verlag, Berlin, 1982), pp. 111–114.
11. S. V. Bessonova, A. A. Boradkin, A. G. Dobrolyubova, E. V. Polyakov, V. P. Sanantsev, A. T. Semenov, and V. A. Simakov, Sov. J. Quantum Electron. **13**, 1403 (1983).
12. R. Fredricks and D. Johnson, Proc. Soc. Photo-Opt. Instrum. Eng. **838** (to be published).
13. J. Feinberg, Opt. Lett. **7**, 486 (1982).

APPENDIX 4.8

IMAGE DISTORTION IN MULTIMODE FIBERS AND RESTORATION BY
POLARIZATION-PRESERVING PHASE CONJUGATION

Image distortion in multimode fibers and restoration by polarization-preserving phase conjugation

Paul H. Beckwith, Ian McMichael, and Pochi Yeh

Rockwell International Science Center. 1049 Camino Dos Rios, Thousand Oaks, California 91360

Image restoration after a double pass through a multimode fiber using a polarization-preserving phase conjugator is demonstrated. Results indicate that the resolution of the restored image is limited by the number of guided modes and that the contrast is restored only when the phase conjugator preserves polarization on reflection.

It is well known that image information, encoded as a spatial intensity pattern, is rapidly scrambled because of mode coupling as it propagates in a multimode fiber. The image information will be completely scrambled (energy leaving the fiber is randomly distributed among all the spatial modes as well as the polarization modes) when the beam diffraction is large enough to result in many reflections off the fiber core walls (i.e., $\lambda L/d^2 \gg 1$; L is the fiber length, d is the fiber diameter, and λ is the wavelength).[1] The concept of using phase conjugation to restore the original image is not new.[2-4] An image is sent through a multimode fiber, and the scrambled output is reflected from a phase conjugator. After traversing a second identical fiber or retraversing the same fiber, the output image is proportional to the input image. In principle, the first case involving two identical fibers can be used to transmit images through fibers. However, in practice it is unlikely that the mode coupling of two fibers will be identical, and to the best of our knowledge such a case has never been demonstrated. The latter case of image restoration involving a double pass through a single fiber has been demonstrated by using phase conjugators that do not preserve polarization.[5,6] In a recent paper[1] we demonstrated that in multimode-fiber systems the recovery of the original spatial and polarization modes takes place only when the phase conjugator preserves polarization on reflection.[7] In this Letter we report on image restoration after a double pass through a multimode fiber using a polarization-preserving phase conjugator. We present results indicating that the spatial resolution of the restored image is limited by the number of guided spatial modes and is therefore independent of whether the phase conjugator preserves polarization. However, we also present results indicating that the contrast of the original image is restored only when the phase conjugator preserves polarization on reflection.

In order to study image restoration after a double pass through a multimode fiber using phase conjugation, we set up the experiment shown in Fig. 1. Linearly polarized light from an argon-ion laser operating in a single longitudinal mode on the 514.5-nm transition is expanded by lens L_1 (focal length $f = -2$ cm)
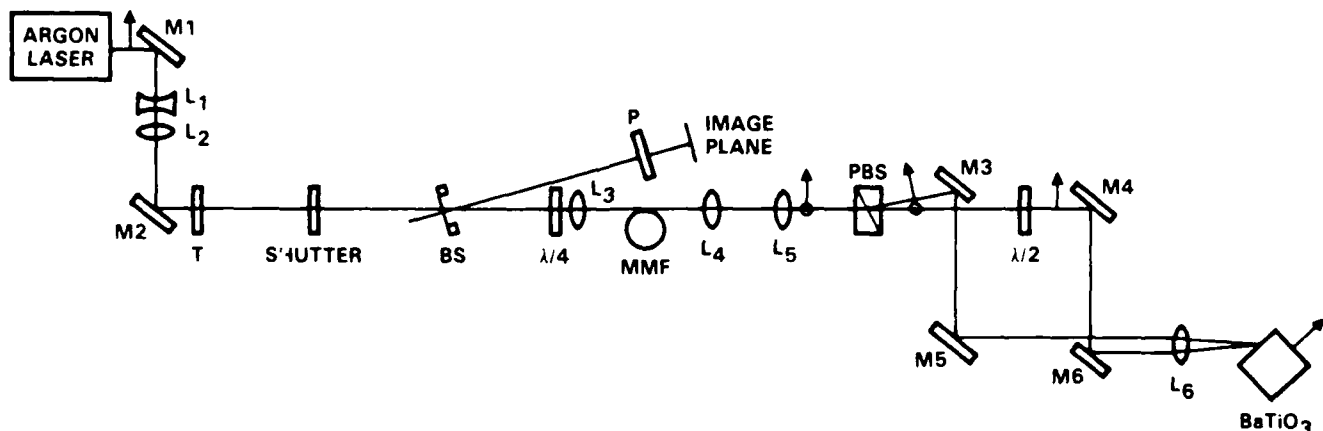

Fig. 1. Experimental setup used to demonstrate image restoration after a double pass through a multimode fiber by polarization-preserving phase conjugation. The image impressed upon the expanded argon-ion laser beam by transparency T is focused into a multimode fiber (MMF). Light leaving the MMF is reflected from the PPPC formed by the optical elements PBS. M_3-M_6, $\lambda/2$, and the BaTiO$_3$ crystal. The effect of conjugating only one polarization component can be observed by blocking one of the output beams from the polarizing beam splitter PBS. After propagating back through the fiber, the restored image is sampled by beam splitter BS, analyzed by polarizer P, and photographed at the image plane.

RESOLUTION CHART   **GRAY-SCALE GRID**

INPUT IMAGE
PATTERN

SINGLE-PASS
FIBER OUTPUT

POLARIZATION
PRESERVING
PHASE-CONJUGATE
MIRROR

DOUBLE-PASS
FIBER OUTPUT

PHASE-CONJUGATE
MIRROR
(NONPOLARIZATION
PRESERVING)
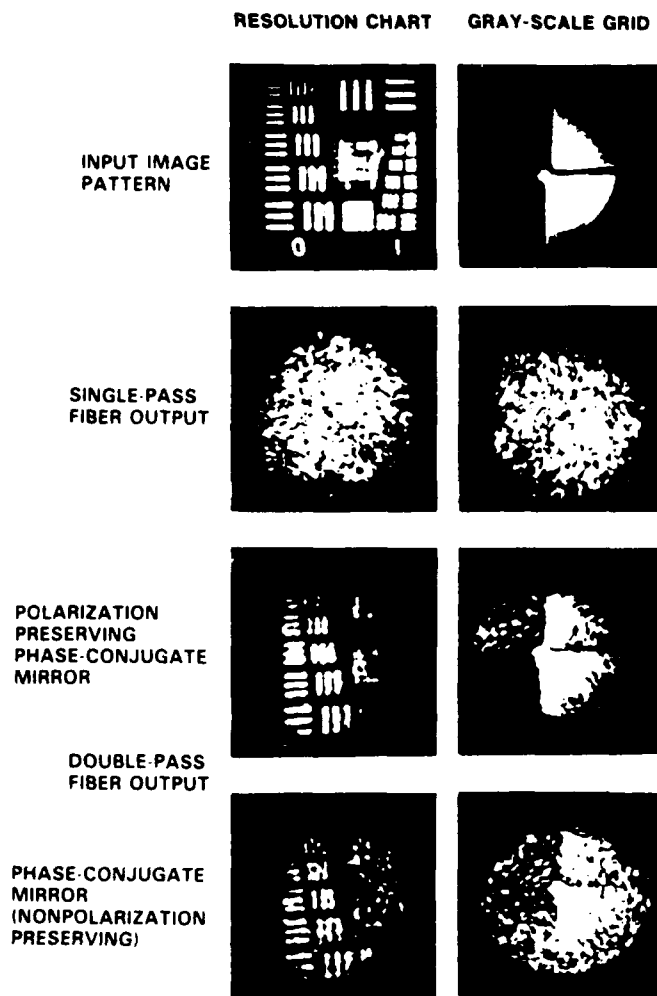
Fig. 2. Photographs demonstrating image restoration after a double pass through a multimode fiber by polarization-preserving phase conjugation. The first row of photos shows the input image patterns (a resolution chart and a gray-scale grid) impressed upon the laser beam, and the second row of photos shows the scrambled single-pass fiber output. The third and fourth rows show photographs, taken at the image plane in Fig. 1, of the image reconstructed by phase conjugation after a double pass through the multimode fiber. For the third row, the PPPC is at the fiber end, and for the fourth row, one of the outputs from the polarizing beam splitter in Fig. 1 is blocked to illustrate the effect of conjugating only one of the polarization components (NPPPC). Although the resolution is comparable for the two cases, the contrast is severely degraded in the case of the NPPPC.

and collimated by lens L_2 ($f = 15$ cm). After an image is impressed upon the expanded beam by transparency T, it is focused into a step-index multimode fiber MMF (core diameter $d = 100$ μm, numerical aperture N.A. = 0.3, length $L = 100$ m) by lens L_3 ($f = 5$ cm, $D = 4$ cm). The quarter-wave retarder $\lambda/4$ is used in conjunction with the polarizer P to eliminate the reflection from the air–fiber interface at the fiber input end. The light leaving the fiber is collimated by a 10× microscope objective L_4, then split into its polarization

components by the polarizing beam splitter PBS; one of the polarization components is rotated 90° by the half-wave retarder $\lambda/2$, and both components are focused into a crystal of barium titanate (BaTiO$_3$) by lens L_5 ($f = 0.5$ m) and lens L_6 ($f = 5$ cm) such that self-pumped phase conjugation takes place. Power levels incident upon the crystal are of the order of 1 mW, with half of the power in each of the two components. The arrangement of optical components PBS, mirrors M_3–M_6, $\lambda/2$, L_5, L_6, and the BaTiO$_3$ crystal, forms a polarization-preserving phase conjugator PPPC. When the phase-conjugate reflections of the two components recombine at the PBS, they form a phase-conjugate wave that has the same polarization as the incident wave. The effect on the image quality of conjugating only one of the polarization components (nonpolarization-preserving phase conjugation, NPPPC) can be observed by blocking the other component. After retraversing the fiber, the restored image is sampled by the beam splitter BS and photographed at the image plane. With the NPPPC, only one half of the returning light reconstructs the image; the other half is randomly distributed among all the spatial and polarization modes.[1] The restored image is improved by filtering out one half of the light that does not reconstruct the image (one quarter of the returning light) using P oriented to pass light having the polarization of the image. In order to obtain high phase-conjugate reflectivities ($R \sim 40\%$) from the BaTiO$_3$ crystal, it was necessary to encase the 100-m fiber in a Styrofoam container. This reduces thermal fluctuations on time scales shorter than the response time of the BaTiO$_3$ crystal (which tend to reduce the phase-conjugate signal by washing out the index gratings in the crystal).

Figure 2 shows photographs of two images sent into the fiber: a standard U.S. Air Force resolution target in the first column and a gray-scale grid in the second column. The gray-scale grid consists of neutral-density filters having a transmission (starting in the lower left-hand corner and proceeding clockwise) of 1, 10, 50, and 100%. The first row of photos shows the input images. The second row shows the single-pass output from the end of the fiber. The uniformity of the output interference speckle patterns indicates severe image scrambling by the fiber. The graininess of the patterns is indicative of the number of modes supported by the fiber. The last two rows show the double-pass fiber output as sampled by the BS, filtered by P, and recorded at the image plane (see Fig. 1). The third row of photos shows the image restoration with the PPPC; and the fourth row, with the NPPPC (one component in the PPPC blocked). Exposure time is adjusted so that equal energy falls upon the film in each case (PPPC and NPPPC). As expected, the photos of the resolution target show that there is little difference in resolution for the two cases. The measured resolution is somewhere in the range from 1.59 lines/mm (Group 0, Element 5) to 1.78 lines/mm (Group 0, Element 6) and agrees well with the resolution calculated from the number of guided modes in the fiber and the imaging optics, ~1.62 lines/mm.

DOUBLE-PASS FIBER OUTPUT

| INPUT IMAGE PATTERN | POLARIZATION PRESERVING PHASE-CONJUGATE MIRROR | PHASE-CONJUGATE MIRROR (NONPOLARIZATION PRESERVING) |
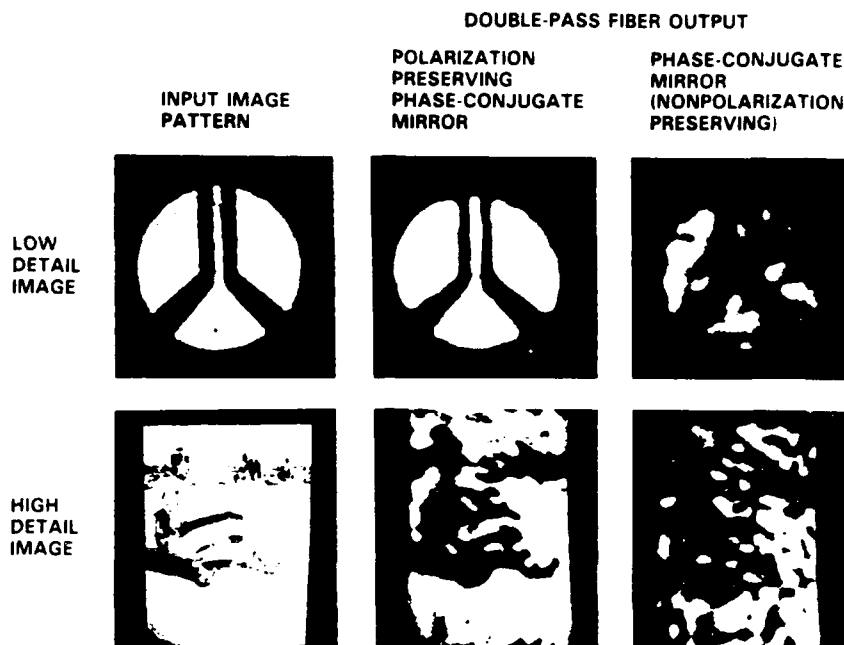
Fig. 3. Photographs demonstrating image restoration after a double pass through a multimode fiber by polarization-preserving phase conjugation for a low-detail image and for a high-detail image. The input image and the image reconstructed by phase conjugation after a double pass through the multimode fiber are photographed for both PPPC's and NPPPC's. Degradation of image contrast is so severe for the image reconstructed by the NPPPC that the picture of the high-detail image is barely discernible.

However, the photos of the gray-scale grid show clearly that the restoration of image contrast is much better in the PPPC case than in the NPPPC case (in the NPPPC case, the light areas are darker, and vice versa).

Figure 3 shows photographs of the double-pass fiber output for low-detail and high-detail images. The first column shows the image patterns focused into the fiber, and the second and third columns show the double-pass output for the PPPC and the NPPPC cases, respectively. As in Fig. 2, although the resolution is comparable in the two cases, the contrast is greater in the PPPC case. The difference in contrast is best seen with the high-detail image, where the picture is barely discernible in the NPPPC case.

We also examined the effect of using unpolarized light to illuminate the image transmitted through the fiber. Unpolarized light was obtained by passing the polarized output of the laser through a 7-m-long, 100-μm-diameter step-index multimode fiber before expanding the beam and passing it through the transparency T in Fig. 1. In this case, it was not possible either to improve the restoration with the NPPPC by using the polarizer or to eliminate the reflection from the air–fiber interface at the fiber input by using the $\lambda/4$ retarder. Results similar to the above but with a greater reduction in contrast were obtained for the NPPPC case.

In conclusion, we have presented experimental results demonstrating that high-contrast image restoration after a double pass through a multimode fiber requires the use of polarization-preserving phase conjugation. When only one polarization leaving the fiber is phase conjugated, only one half of the returning light reconstructs the image[1]; the other half is randomly distributed among all the spatial and polarization modes, thereby severely degrading the contrast of the reconstructed image.

References

1. I. McMichael, P. Yeh, and P. Beckwith, Opt. Lett. 12, 507 (1987).
2. A. Yariv, Appl. Phys. Lett. 28, 88 (1976).
3. A. Yariv, J. Opt. Soc. Am. 66, 301 (1976).
4. A. Gover, C. P. Lee, and A. Yariv, J. Opt. Soc. Am. 66, 306 (1976).
5. G. J. Dunning and R. C. Lind, Opt. Lett. 7, 558 (1982).
6. B. Fischer and S. Sternklar, Appl. Phys. Lett. 46, 113 (1985).
7. I. McMichael, M. Khoshenevisan, and P. Yeh, Opt. Lett. 11, 525 (1986).

APPENDIX 4.9

CORRECTION OF POLARIZATION AND MODAL SCRAMBLING IN MULTIMODE
FIBERS BY PHASE CONJUGATION

Correction of polarization and modal scrambling in multimode fibers by phase conjugation

Ian McMichael, Pochi Yeh, and Paul Beckwith

Rockwell International Science Center, 1049 Camino dos Rios, Thousand Oaks, California 91360

When polarized light is incident upon a long multimode fiber, the emerging light is randomly distributed among the spatial and polarization modes. We present experimental and theoretical results demonstrating that recovery of the spatial and polarization modes of the incident light takes place only when a phase conjugator at the fiber output preserves polarization on reflection.

When polarized light is incident upon a long multimode fiber, the emerging light is randomly distributed among the spatial and polarization modes because of modal scrambling. We previously reported preliminary results on the correction of modal scrambling by phase conjugation.[1,2] In this Letter we present recent results of experimental and theoretical investigations into the correction of modal scrambling for the cases when both polarization components are conjugated at the fiber output (polarization-preserving phase conjugator,[2,3] PPPC) and when only one polarization component is conjugated (nonpolarization-preserving phase conjugator, NPPPC). We find that recovery of the original spatial and polarization modes takes place only when the reflection from the phase conjugator preserves the polarization of the incident light. However, if the fiber supports a large number of spatial modes and one uses spatial filtering to look only at the light returning in the same spatial mode as the incident light, then one will see nearly complete polarization recovery, even when only one polarization component is conjugated at the output of the fiber.[4,5] This is because light returning down the fiber that is orthogonal in polarization to the input is randomly distributed among all spatial modes.

A PPPC produces a time-reversed wave that can correct for modal scrambling.[1,2] We now consider the result of conjugating only one polarization component. The specific case of a linearly polarized incident wave is analyzed graphically in Fig. 1. In what follows we analyze the case of an incident wave of arbitrary polarization. Consider a multimode fiber that supports N modes with wave functions

$$\mathbf{E}_n(x, y)\exp(-i\beta_n z), \qquad n = 1, 2, \ldots, N, \qquad (1)$$

where β_n is the propagation constant and n is the mode number. An incident electric field $\mathbf{E}_I$ can be expressed as a sum over the N modes at the input ($z = 0$):

$$\mathbf{E}_I = \sum_n A_n \mathbf{E}_n. \qquad (2)$$

where A_n's are the mode amplitudes. The output ($z = L$) field $\mathbf{E}_{II}$ can be written as

$$\mathbf{E}_{II} = (E_{IIx}, E_{IIy}), \qquad (3)$$

where E_{IIx} and E_{IIy} are the x and y components. If modal scrambling is complete, then the energy is distributed equally among the x and y polarizations:

$$\int |E_{IIx}|^2 dxdy = \int |E_{IIy}|^2 dxdy. \qquad (4)$$

Let this field be incident upon a phase conjugator that has unit reflectivity and a polarizer along the x axis in front of it. The reflected field $\mathbf{E}_{III}$ is given by

$$\mathbf{E}_{III} = (E_{IIx}{}^*, 0). \qquad (5)$$

This field can be written as the sum of two components: a component $\mathbf{E}_{II}{}^*$ that is the phase conjugate of the light emerging from the fiber at $z = L$ and a component $\mathbf{E}_{II}{}^*{}_\perp$ that is orthogonal to the conjugate in the sense that $\int \mathbf{E}_{II} \cdot \mathbf{E}_{II}{}^*{}_\perp dxdy = 0$,

$$\mathbf{E}_{III} = a\mathbf{E}_{II}{}^* + b\mathbf{E}_{II}{}^*{}_\perp, \qquad (6)$$

where a and b are constants. Scalar multiplying both sides of Eq. (6) by $\mathbf{E}_{II}$, integrating over x and y, and using Eqs. (4) and (6), we obtain the results $a = \frac{1}{2}$, $b = \frac{1}{2}$, and $\mathbf{E}_{II\perp} = (E_{IIx}, -E_{IIy})$. With these results, $\mathbf{E}_{III}$ becomes

$$\mathbf{E}_{III} = \frac{1}{2}\mathbf{E}_{II}{}^* + \frac{1}{2}\mathbf{E}_{II}{}^*{}_\perp. \qquad (7)$$

This field propagates back through the fiber. If the fiber is linear and lossless, then the conjugate component $\frac{1}{2}\mathbf{E}_{II}{}^*$ generates $\frac{1}{2}\mathbf{E}_I{}^*$ by time reversal and the orthogonal component $\frac{1}{2}\mathbf{E}_{II}{}^*{}_\perp$ generates $\frac{1}{2}\mathbf{E}_I{}^*{}_\perp$, where $\mathbf{E}_I{}^*{}_\perp$ is orthogonal to $\mathbf{E}_I{}^*$ in the sense that $\int \mathbf{E}_I \cdot \mathbf{E}_I{}^*{}_\perp dxdy = 0$; note that $\mathbf{E}_I{}^*{}_\perp \neq (E_{Ix}, -E_{Iy})$. Since we assume complete modal scrambling, the energy in $\mathbf{E}_I{}^*{}_\perp$ is distributed equally among the x and y polarizations. The returning field at the fiber input becomes

$$\mathbf{E}_{IV} = \frac{1}{2}\mathbf{E}_I{}^* + \frac{1}{2}\mathbf{E}_I{}^*{}_\perp. \qquad (8)$$

Note that when only one polarization component is

perform spatial filtering of the returning phase-conjugate signal by closing it to the size of the input beam. The quarter-wave retarder $\lambda/4$ can be used in conjunction with the polarizer to eliminate the reflection from the air–fiber interface at the fiber input. Light emerging from the fiber is collimated by a $10\times$ microscope objective L2, focused by lens L3 ($f = 0.5$ m), and
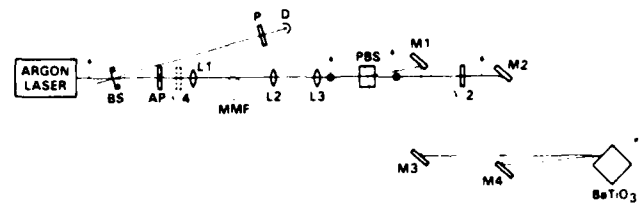

Fig. 2. Experimental setup. Light emerging from the multimode fiber MMF is reflected from the PPPC formed by the optical elements PBS, M1–M4, $\lambda/2$, and the $BaTiO_3$ crystal. The effect of conjugating only one polarization component can be observed by blocking one of the outputs from the polarizing beam splitter PBS. After propagating back through the fiber, the light is sampled by beam splitter BS, analyzed by the polarizer P, and measured by detector D or photographed.

Fig. 1. Illustration of what happens when light propagates in a multimode fiber (MMF) and only one polarization component is conjugated at its output. The top section shows a sketch of the optics, and (a)–(c) show the evolution of the polarization of the light as it propagates. The field $E_I = \hat{x}$ enters the MMF at $z = 0$. (a) Because of modal scrambling, the output field E_{II} is equally distributed among the x and y polarizations and the change in polarization is represented by rotation of E_I to E_{II}. (b) The x component of E_{II} passes through the polarizer and reflects from the phase-conjugate mirror PCM to produce $E_{III} = E_{IIx}^*\hat{x}$. This field has a phase-conjugate component, $\frac{1}{2}E_{II}^*$, and an orthogonal component, $\frac{1}{2}E_{II}^*{}_{\perp}$. (c) When the conjugate component propagates back to $z = 0$ it generates $\frac{1}{2}E_I^*$ by time reversal (depicted as rotation of $\frac{1}{2}E_{II}^*$ to $\frac{1}{2}E_I^*$), and the orthogonal component generates $\frac{1}{2}E_I^*{}_{\perp}$, where $E_I^*{}_{\perp}$ is orthogonal to E_I^*. Because of modal scrambling, $E_I^*{}_{\perp}$ is distributed equally among the x and y polarizations. Note that only one fourth of the energy is recovered in the reconstruction of the input field. The other one fourth is randomly distributed among the spatial and polarization modes. One half of the energy is lost at the polarizer.

conjugated at the output of the fiber only one quarter of the energy ($|\frac{1}{2}E_I^*|^2$) is recovered in the reconstruction of the input field. The other one quarter of the energy ($|\frac{1}{2}E_I^*{}_{\perp}|^2$) is randomly distributed among the spatial and polarization modes. Therefore (1/4 + 1/2 × 1/4) = 3/8 of the original energy returns with the polarization of the input and (1/2 × 1/4) = 1/8 returns orthogonal to it. One half of the original energy is lost at the polarizer.

Our experimental setup is shown in Fig. 2. Light from a single-mode argon-ion laser is focused into a step-index multimode fiber (core diameter $d = 100$ μm, numerical aperture 0.3, attenuation 30 dB/km, length 20 m) by lens L1 (focal length $f = 5$ cm, diameter $D = 4$ cm). The aperture AP can be used to

Fig. 3. Photographs of the returning light as seen at the position of detector D in Fig. 2. ‖ corresponds to the polarization of the light incident upon the fiber. The first set of photos was taken with the phase-conjugate mirror blocked, the second set of photos with the PPPC at the fiber end, and the third set of photos with the NPPPC (one of the outputs from the polarizing beam splitter in Fig. 2 is blocked). For the PPPC all the light returns as the phase conjugate (bright spot in the photo of ‖ polarization). However, for the NPPPC only one half of the returning light is the phase conjugate; the other half is randomly distributed among the spatial and polarization modes.

Table 1.   Measured and Predicted Power Ratios for Phase-Conjugation with Multimode Fibers[a]

Aperture	$P_\perp/P$ [b]		P_{NPPPC}/P_{PPPC}
	PPPC	NPPPC	
Open	$(4.4 \pm 1.3) \times 10^{-3}$ [0]	0.32 ± 0.02 [1/3]	0.42 ± 0.09 [1/2]
Reduced[c]	$(1.0 \pm 0.4) \times 10^{-3}$ [0]	$(1.4 \pm 0.3) \times 10^{-2}$ [≪1]	0.22 ± 0.03 [1/4]

[a] See Fig. 2; predicted values are in square brackets.

[b] $P_\perp/P$ is the ratio of the power in the polarization orthogonal to the input to that parallel to the input as measured by the detector (see Fig. 2): PPPC corresponds to the situation shown in Fig. 2: NPPPC corresponds to blocking one of the outputs from the polarizing beam splitter in Fig. 2.

[c] Aperture size reduced to the input beam size (~4 mm).

reflected from the PPPC[2] formed by the polarizing beam splitter (PBS), mirrors M1–M4, half-wave retarder $\lambda/2$, and the barium titanate crystal $BaTiO_3$. The effect of conjugating only one polarization component can be observed by blocking one of the outputs from the PBS. After propagating back through the fiber, the light is sampled by a beam splitter, analyzed by a polarizer, and measured by a detector or photographed.

Figure 3 shows photographs of equal exposure of the returning light as seen at the position of the detector with the aperture open. ∥ corresponds to the polarization of the light incident upon the fiber. For the first column, a $\lambda/4$ retarder is used to avoid the reflection from the air–fiber interface at the fiber input. The first row of photos was taken with the phase conjugator blocked. The grainy circular patterns observed in both polarizations are from the light reflected at the air–fiber interface at the fiber output. The fact that the circular patterns are uniform and equal in intensity indicates complete modal scrambling. The second row of photos was taken with the PPPC at the fiber end. A strong phase-conjugate return can be seen in the center of the photo of the ∥ polarization, and there is little change in the intensity of the grainy circular patterns (in fact, we observed that the backscattering from the output end of the fiber with polarization orthogonal to the input reduces by 5–10% owing to phase conjugation[6]), indicating that all the light returns as the phase conjugate. The third row of photos was taken with a NPPPC (one component in the PPPC blocked) at the fiber end. The conjugate return is weaker than that for the PPPC, and the intensity of the grainy circular pattern has increased over that produced by the fiber end reflection, indicating that some of the returning light is not the phase conjugate of the input.

Table 1 lists measured and predicted power ratios. As before, ∥ corresponds to the polarization of the light incident upon the fiber. For the PPPC, the measured ratio $P_\perp/P$ is small, indicating nearly complete correction of polarization scrambling. The ratio decreases when the aperture is closed down to the size of the input beam to provide spatial filtering of the returning phase-conjugate signal. For the NPPPC, with the aperture open, the measured ratio is 0.32 ± 0.02, in agreement with our theory [(1/8)/(3/8) = 1/3]. This indicates that when only one polarization is conjugated at the output of the fiber, one third of the returning light is orthogonal in polarization to the

input. When the aperture is closed, the measured ratio decreases to $(1.4 \pm 0.3) \times 10^{-2}$. This indicates that the returning light with polarization orthogonal to the input is spatially orthogonal to the input. With the aperture open, when we block the central phase-conjugate return with a mask in front of the detector to look only at the grainy circular pattern, the measured power ratio is 1.0 ± 0.1, indicating equal power distribution in the two polarizations. We also compared the total power in the returning light for a PPPC with that for a NPPPC. With the aperture open, the measured ratio P_{NPPPC}/P_{PPPC} is 0.42 ± 0.09, reflecting the fact that one half of the light from the fiber output is blocked in the NPPPC. With the aperture closed, the measured ratio is 0.22 ± 0.03, indicating that with the NPPPC only one fourth of the light incident upon the fiber returns as the phase conjugate.

In conclusion, we have presented theoretical and experimental results demonstrating that correction of modal scrambling by multimode fibers requires a PPPC. The technique described in Ref. 4 (using a modal filter followed by a multimode fiber, a polarizer, and a non-polarization-preserving phase conjugator) can be used to correct for polarization scrambling when the wave to be conjugated contains much less spatial information than the maximum that can be supported by the fiber and when a reduction of the phase-conjugate signal by a factor of 4 and an increase in noise is tolerable.

References

1. I. McMichael and M. Khoshnevisan. in *Digest of the Conference on Lasers and Electro-Optics* (Optical Society of America. Washington. D.C.. 1985), paper THN1. p. 220.

2. I. McMichael. M. Khoshnevisan. and P. Yeh. Opt. Lett. 11, 525 (1986).

3. P. Yeh. Opt. Commun. 51, 195 (1984).

4. K. Kyuma. A. Yariv. and S. Kwong. Appl. Phys. Lett. 49, 617 (1986).

5. A. Yariv. Y. Tomita. and K. Kyuma. Opt. Lett. 11, 809 (1986).

6. P. D. Drummond and A. T. Friberg. J. Appl. Phys. 54, 5618 (1983).

APPENDIX 4.10

PHASE SHIFTS OF PHOTOREFRACTIVE GRATINGS AND
PHASE CONJUGATE WAVES

C9943DA/jbs

Phase shifts of photorefractive gratings and phase-conjugate waves

Ian McMichael and Pochi Yeh

Rockwell International Science Center, 1049 Camino Dos Rios, Thousand Oaks, California 91360

We present measurements of the two-wave mixing gain as a function of frequency detuning in photorefractive crystals. In many cases, this function is asymmetric, indicating that the phase shift of the photorefractive index grating with respect to the light interference pattern is not exactly 90°, as is often assumed. In four-wave mixing, the phase of the phase-conjugate wave contains the phase of the pumping and probe waves and a phase shift determined by the interaction taking place in the nonlinear medium. This second term, the phase shift of the phase conjugator, is a function of the type of grating and the phase shift of this grating. The phase shift of the grating obtained from the two-wave mixing measurements compares well with that obtained from four-wave mixing measurements of the phase of the phase conjugator.

In two-wave mixing (TWM) in photorefractive media,[1-3] carriers are generated in the bright regions of the interference pattern formed by the two waves, and they are eventually trapped in the darker regions. The redistribution of charge results in a spatial modulation of the electric field, and the refractive index (electro-optic effect) with the frequency of the interference pattern, but shifted in phase by 90°. This nonlocal response leads to energy exchange between the two waves. The exchange is optimized when the phase shift of the refractive-index grating is exactly 90°. However, fields in the media,[4] such as the bulk photovoltaic field,[5] can determine a preferential direction for the migration of charges, and this can result in a phase shift for the grating that is different from 90°. To optimize the TWM gain, this field-induced phase shift can be compensated for by frequency shifting one of the two waves to create a grating moving at a rate comparable with the response time of the medium.[6] In the first part of this Letter, we present measurements of the TWM gain as a function of frequency detuning between the two waves for the photorefractive crystals barium titanate (BaTiO₃) and strontium barium niobate (SBN). This function is asymmetric for BaTiO₃, indicating that the phase shift of the grating is not exactly 90°. The degree of asymmetry and therefore the phase shift of the grating depend on the angle between the grating vector and the crystal axis, the pump intensity, and the particular crystal.

In four-wave mixing (FWM), the phase of the phase-conjugate wave contains the phase of the pumping and probe waves and a phase shift due to the interaction taking place in the nonlinear medium. We refer to this second term as the phase shift of the phase conjugator.[7,8] It is a function of the type of grating (refractive index, absorption, or gain) and the phase shift of the grating. In the second part of this Letter, we derive an expression describing this dependence, present measurements of the phase shift of the phase conjugator, and compare these measurements with the phase shift of the grating obtained from the TWM measurements.

The TWM gain Γ is related to the frequency detuning between the two waves by the proportionality[6]

$$\Gamma \propto \sin (\phi_g + \tan^{-1} \delta)/\sqrt{1 + \delta^2}, \qquad (1)$$

where ϕ_g is the phase shift of the grating and the detuning δ is the product of the frequency difference between the two waves and the response time of the medium. If $\phi_g \neq 90°$ then Γ is an asymmetric function of the detuning.

Figure 1 shows measurements of $\Gamma(\delta)/\Gamma(0)$ for a crystal of SBN ($Sr_{0.6}Ba_{0.4}NbO_3$) and two crystals of BaTiO₃. The measurement technique described in Ref. 9 is used to obtain Γ. The figure shows data for a representative sample of SBN, but measurements were taken for four different samples including a cerium-doped sample. In all cases Γ was symmetric, indicating that the phase shift of the grating is almost
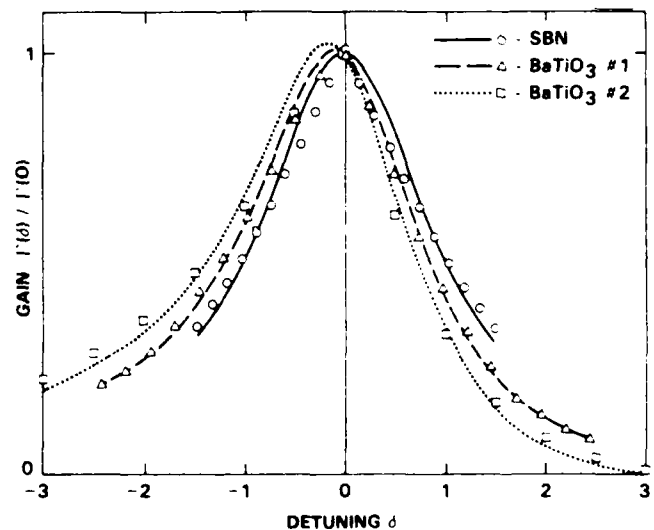

Fig. 1. Measurements of the TWM gain $\Gamma(\delta)/\Gamma(0)$ as a function of frequency detuning δ for SBN and BaTiO₃. For BaTiO₃, Γ is asymmetric, indicating that the phase shift of the grating is not 90°.
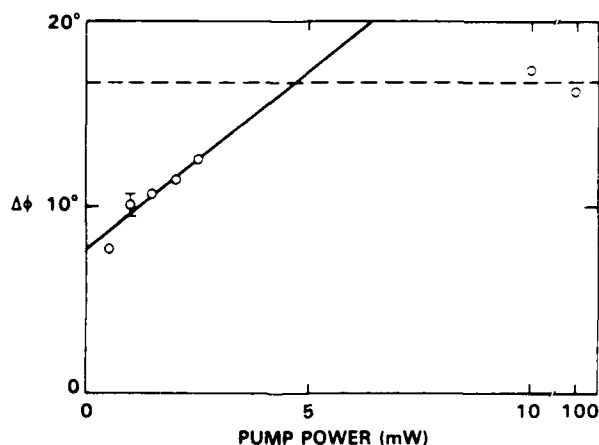
Fig. 2. Measured difference between the phase shift of the grating ϕ_g and 90° ($\Delta\phi = \phi_g - 90°$) as a function of the TWM pump power for BaTiO$_3$ #1. The lines are to aid the viewer: they are not theoretical fits.

exactly 90° in SBN. The fit of Eq. (4) to the data, indicated by the solid line, gives $\phi_g = 91°$. For BaTiO$_3$, Γ is clearly asymmetric. The fits give $\phi_g = 100°$ and $\phi_g = 109°$ for crystals #1 and #2, respectively, and $\phi_g = 106°$ for a third crystal (not shown in the figure). Other investigators, using the same method, did not notice the asymmetry in their data.[10] For this figure, the angle between the beams was 8°, the crystals were oriented with their c axes parallel to the grating vector such that there was TWM gain for the probe, the bisector to the beams was normal to the entrance face, and the pump and probe waves had extraordinary polarization and powers of 1 (514.5 nm) and 0.01 mW, respectively, in spot diameters of 0.4 mm.

Figure 2 shows the measured difference between ϕ_g and 90° ($\Delta\phi = \phi_g - 90°$) as a function of the pump power for BaTiO$_3$ #1. All other parameters are identical to those for Fig. 1. The results shown are expected from the theory of the bulk photovoltaic effect. Using a different technique, other investigators obtained $\Delta\phi = (0 \pm 10)°$ for a single sample of BaTiO$_3$ with a total incident intensity of 0.5 W/cm^2.[11] From Fig. 2 we find that for BaTiO$_3$ #1 with the same incident intensity, $\Delta\phi = (9 \pm 0.5)°$ is within the experimental error of the value reported in Ref. 11. For SBN, Γ was very symmetric even at pump powers of 10 mW.

Figure 3 shows $\Delta\phi$ as a function of the angle θ between the crystal axis and the perpendicular to the bisector of the two waves. The features shown are indicative of a field oriented along the crystal axis. For such a field, the component along the grating vector determines the phase shift $\Delta\phi$.[2,3] For $\theta = 0°$, the grating vector is parallel to the crystal axis, and this results in the largest $\Delta\phi$.

We can calculate the field in the crystal E_0 from the measured phase shift of the grating at $\theta = 0°$ by using the equation[4,11]

$$\phi_g = \tan^{-1}[(E_D/E_0) + (E_D^2/E_0 E_N) + (E_0/E_N)], \quad (2)$$

where $E_D \approx 1.6/\Lambda$ kV/cm and $E_N \approx 2.8\,N_T\,\Lambda/\epsilon$ are the diffusion and maximum space-charge fields, Λ is the grating spacing in micrometers, N_T is the trap density

of majority carriers in units of 10^{14}/cm^3, and ϵ is the dielectric constant. For a trap density of 10^{16}/cm^3 we obtain $E_0 \approx 200$ V/cm.

Now we consider the phase shifts of phase conjugators. To obtain an expression for the functional dependence of the phase of phase-conjugate waves, we consider the simplest case of FWM, in which the transmission grating dominates, the coupling is weak, and the probe wave is much weaker than the pump waves. Let the notation for the four fields (n = 1, 2, 3, 4) be

$$\mathbf{E}_n = A_n \exp[i(\mathbf{k}_n \cdot \mathbf{r} - \omega t + \phi_n)\mathbf{e}_n], \quad (3)$$

where A_1 and A_2 are the amplitudes of the counterpropagating pump waves, A_4 is the amplitude of the probe wave propagating in the $+z$ direction, and A_3 is the amplitude of the phase-conjugate wave. The intensity of the interference pattern formed by the writing pump ($\mathbf{E}_1$) and the probe wave is given by

$$I = A_1^2 + A_4^2 + A_1 A_4 (\mathbf{e}_1 \cdot \mathbf{e}_4)$$
$$\times (\exp\{i[(\mathbf{k}_1 - \mathbf{k}_4) \cdot \mathbf{r} + (\phi_1 - \phi_4)]\} + c.c.). \quad (4)$$

The intensity pattern results in a spatial modulation of the propagation constant k given by

$$k = k_0 + \Delta k \,(\exp\{i[(\mathbf{k}_1 - \mathbf{k}_4) \cdot \mathbf{r}$$
$$+ (\phi_1 - \phi_4) + \phi_\sigma]\} + c.c.). \quad (5)$$

The diffraction of $\mathbf{E}_2$ off this grating forms the phase-conjugate wave $\mathbf{E}_3$. The phase of the phase-conjugate wave ϕ_3 is obtained from the solution to the scalar-wave equation

$$\phi_3 = \phi_1 + \phi_2 - \phi_4 + \phi_0, \quad (6)$$

where ϕ_0 is phase shift of the phase conjugator:

$$\phi_0 = \pi/2 + \phi_{\Delta k} + \phi_\sigma, \quad (7)$$

and $\phi_{\Delta k}$ is the phase of the complex quantity Δk. ϕ_0 depends on the type of grating (refractive index, absorption, gain, or mixture) and the phase shift of the
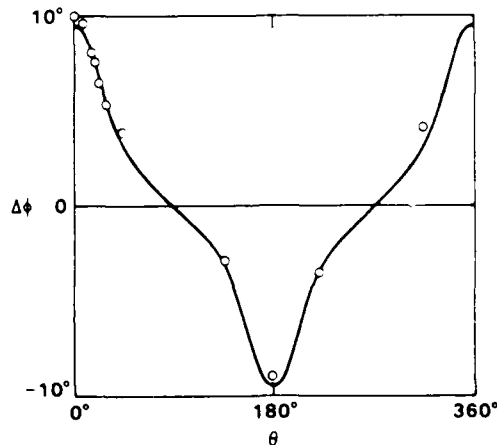
Fig. 3. Measured difference between the phase shift of the grating ϕ_g and 90° ($\Delta\phi = \phi_g - 90°$) as a function of the angle θ between the perpendicular to the bisector to the two waves and the crystal axis for BaTiO$_3$ #1. The dependence of $\Delta\phi$ on θ indicates the existence of a field oriented along the crystal axis. The line is to aid the viewer; it is not a theoretical fit.

grating. For a transparent medium (refractive-index grating, Δk real, $\phi_k = 0°$ or $180°$) with a local response ($\phi_L = 0°$), $\phi_0 = 90°$ for $\phi_{\Delta l} = 0°$ or $\phi_0 = -90°$ for $\phi_{\Delta l} = 180°$. For saturable absorbers (Δk negative imaginary, $\phi_{\Delta l} = -90°$) $\phi_0 = 0°$, and for saturable amplifiers (Δk positive imaginary, $\phi_{\Delta l} = +90°$), $\phi_0 = 180°$. If one makes the assumption that $\phi_L = 90°$, then for photorefractive media (refractive-index grating, Δk real, $\phi_{\Delta l} = 0°$ or $180°$), $\phi_0 = 0°$ for $\phi_{\Delta l} = 180°$ or $\phi_0 = 180°$ for $\phi_{\Delta k} = 0°$.

ϕ_0 can be measured with the interferometer shown in Fig. 4. The light transmitted by the beam splitter, BS, and the light reflected from the self-pumped crystal of BaTiO$_3$ provide the pump waves for FWM in the crystal XTL. The light reflected by the beam splitter provides the probe wave. The conjugate wave and the reflection from the self-pumper interfere at the detector D. Using Stokes's relation, $tr^* = -t^*r'$, where t, r, and r' are the amplitude transmission and internal and external reflection coefficients of the beam splitter, respectively, one can show that the intensity measured at detector D is given by

$$I_1 + I_- - 2\sqrt{I_1 I_-}\cos\phi_0. \tag{8}$$

where I_1 and I_- are the intensities of the interfering waves at the detector. To obtain an accurate determination of ϕ_0, we apply a phase modulation to mirror M2 with amplitude ϕ_m and frequency ν by using a piezoelectric transducer. The phase modulation is fast, so that it is not compensated for by phase conjugation, and small, so that it does not wash out the grating. ϕ_0 can then be obtained from the relation

$$\phi_0 \approx \tan^{-1}(R\phi_m/4). \tag{9}$$

where R is the ratio of the power measured by detector D at the frequency ν to that at 2ν.

Two improvements were made to our interferometer since our first report. At first, we did not use the self-pumper but used a mirror instead. In initial experiments our results were sensitive to the alignment of this mirror. We also apply a fast phase modulation to mirror M1 to avoid the grating that would otherwise be written by this pump and the probe.

Table 1 lists measurements of ϕ_0 taken for various
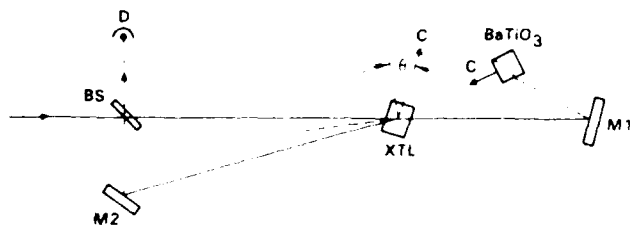
Fig. 4. Interferometer used to measure the phase shift of the phase conjugator. The light transmitted by the beam splitter, BS, and the light reflected from the self-pumped crystal of BaTiO$_3$ provide the pump waves for FWM in the crystal XTL. The light reflected by the beam splitter provides the probe wave. The conjugate wave and the reflection from the self-pumper interfere at the detector D with a relative phase shift ϕ_0, the phase shift of the phase conjugator.

Table 1. Phase of Phase Conjugators

Material	θ (deg)	ϕ_0 (deg)	$\Delta\phi$ (deg)
BaTiO (1 mW)	0	(10 ± 3)	10
	23	(8 ± 1)	6
	45	(4 ± 1)	4
	180	(169 ± 4)	-9
BaTiO (10 mW)	0	(19 ± 5)	16
SBN	0	(1 ± 1)	1

pump powers and angles θ defined in Fig. 4. ϕ_0 is close to $0°$ or $180°$ as predicted. The reason that the measured values for BaTiO$_3$ are not exactly $0°$ or $180°$ is that the refractive-index grating is not shifted by exactly $90°$. Values of $\Delta\phi$ obtained from the TWM measurements are given in the right-hand column. As Eq. (7) indicates, they should be equal to or differ by $180°$ from the values of ϕ_0. A comparison of the right-hand columns indicates that the results of the TWM and FWM measurements are in good agreement.

In conclusion, our measurements show that the TWM gain in barium titanate is an asymmetric function of frequency detuning, indicating that the phase shift of the grating is not exactly $90°$ as is often assumed. We have shown that, for FWM, the phase of the phase-conjugate wave contains the phases of the pumping and probe waves and is a function of the type of grating and the phase shift of the grating with respect to the light interference pattern. This phase determines the operating point of some phase-conjugate interferometers. If this phase can be controlled, such interferometers can be biased at the operating point of highest sensitivity and linear response. Calculations of the phase shift of the refractive-index grating from measurements of the phase of the phase conjugator agree with the phase shift of the grating obtained from the TWM gain measurements.

References

1. D. Staebler and J. Amodei. J. Appl. Phys. 43, 1042 (1972).
2. V. Vinetskii, N. Kukhtarev, S. Odolov, and M. Soskin. Sov. Phys. Usp. 22, 742 (1979).
3. N. Kukhtarev, V. Markov, S. Odolov, M. Soskin, and V. Vinetskii. Ferroelectrics 22, 961 (1979).
4. M. Gower. Opt. Lett. 11, 458 (1986).
5. A. Glass, D. von der Linde, and T. Negran. Appl. Phys. Lett. 25, 233 (1974).
6. J. P. Hugnard and A. Marrakchi. Opt. Commun. 38, 249 (1981).
7. J. McMichael, P. Yeh, and M. Khoshnevisan. Proc. Soc. Photo-Opt. Instrum. Eng. 613, 32 (1986).
8. S. Kwong, A. Yariv, M. Cronin-Golomb, and B. Fischer. J. Opt. Soc. Am. A 3, 157 (1986).
9. M. Klein and G. Valley. J. Appl. Phys. 57, 4901 (1985).
10. K. MacDonald and J. Feinberg. Phys. Rev. Lett. 55, 821 (1985).
11. J. Feinberg, D. Heiman, A. Tanguay, and R. Hellwarth. J. Appl. Phys. 51, 1297 (1980).

APPENDIX 4.11

SELF-PUMPED PHASE-CONJUGATE FIBER-OPTIC GYRO

C9943DA/jbs

Self-pumped phase-conjugate fiber-optic gyro

Ian McMichael and Pochi Yeh

Rockwell International Science Center, 1049 Camino Dos Rios, Thousand Oaks, California 91360

We describe a new type of phase-conjugate fiber-optic gyro that uses self-pumped phase conjugation. The self-pumped configuration is simpler than externally pumped configurations and permits the use of sensing fibers longer than the coherence length of the laser. A proof-of-principle demonstration of rotation sensing with the device is presented.

Several types of phase-conjugate gyro are described in the literature,[1-4] and we recently reported on the first demonstration to our knowledge of rotation sensing with a phase conjugate gyro.[5] The passive phase-conjugate fiber-optic gyros described in Refs. 3 and 5 are Michelson interferometers in which the arms contain fiber-optic coils that are terminated by externally pumped phase-conjugate mirrors. Since the phase-conjugate mirrors produce time-reversed waves, all reciprocal phase changes in the optical paths are compensated for and do not effect the output of the interferometer. However, since the phase shift produced by the Sagnac effect is nonreciprocal, the output of the interferometer is sensitive to rotation and can be used as a gyro.

Standard fiber-optic gyros[6] are Sagnac interferometers that are inherently insensitive to reciprocal phase changes and sensitive to nonreciprocal phase changes. This is true only when their operation is restricted to a single polarization mode,[7] and the best fiber-optic gyros use polarization-preserving fibers and couplers.[8] However, if the phase-conjugate mirrors in the phase-conjugate fiber-optic gyro preserve polarization,[9] then nonpolarization-preserving single-mode fibers, and even multimode fibers, can be used in the gyro.

In the externally pumped configurations described in Ref. 3 and 5, the fiber-optic coils can be no longer than the coherence length of the laser. This limits the sensitivity of the device. It is true that longer coils can be used if a polarization-preserving fiber of equal length is used to carry the pumping waves to the phase-conjugate mirrors. However, this defeats the above-mentioned advantage in that the phase-conjugate gyro can use inexpensive multimode fibers and couplers. In this Letter we describe and demonstrate a self-pumped configuration of the phase-conjugate fiber-optic gyro that is not only simpler than the externally pumped configurations but also allows for the use of fiber-optic coils that are longer than the coherence length of the laser.

Figure 1 shows a schematic of a self-pumped phase-conjugate fiber-optic gyro. Light from a laser is split by beam splitter BS into two fibers, F1 and F2. Fibers F1 and F2 are coiled such that light travels clockwise in F1 and counterclockwise in F2. Light waves tra-

versing fibers F1 and F2 experience reciprocal phase shifts

$$\phi_{r_1} = \int k_1 dl_1, \quad \phi_{r_2} = \int k_2 dl_2, \quad (1)$$

respectively, where dl_1 and dl_2 are elements of length along F1 and F2, and $k_{1,2} = 2\pi n_{1,2}/\lambda$. In addition, the nonreciprocal phase shifts

$$\phi_{nr_1} = +2\pi R_1 L_1 \Omega/\lambda c, \quad \phi_{nr_2} = -2\pi R_2 L_2 \Omega/\lambda c \quad (2)$$

are due to the Sagnac effect, where $R_{1,2}$ and $L_{1,2}$ are the radii and lengths of the fiber loops, respectively, and Ω is the rotation rate. The net phase shifts are then $\phi_{r_1} + \phi_{nr_1}$ and $\phi_{r_2} + \phi_{nr_2}$. On reflection of the light from the phase-conjugate mirror, the phase shifts become $-\phi_{r_1} - \phi_{nr_1}$ and $-\phi_{r_2} - \phi_{nr_2}$, where we have dropped the phase shift of the phase conjugator[10,11] since it is common to both waves and we are interested only in the phase difference. It should be noted that the phase shift of the phase conjugator is common to both waves
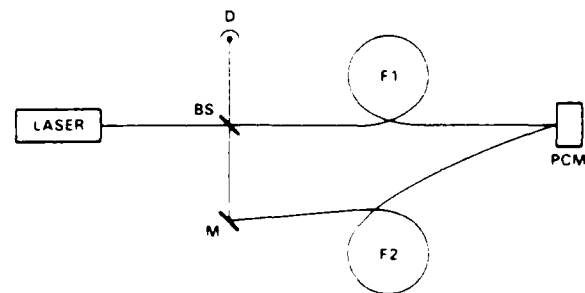

Fig. 1. Schematic of a self-pumped phase-conjugate fiber-optic gyro. Light from a laser is split by beam splitter BS into two fibers F1 and F2 that are coiled such that light travels clockwise in F1 and counterclockwise in F2. Light traversing the fibers experiences phase shifts due to thermal, mechanical, and rotational effects. The self-pumped phase-conjugate mirror PCM produces time-reversed waves that compensate for the reciprocal phase changes produced by thermal and mechanical effects but do not compensate for the nonreciprocal phase shift produced by rotation (Sagnac effect). Therefore rotation can be sensed by measuring the interference between the recombining waves at detector D.

only when both waves are reflected from the same phase-conjugate mirror or when the phase-conjugate mirrors are coupled.[12] In the case of self-pumped phase conjugation in barium titanate, the two incident waves interact by coherently pumping the oscillation of a resonator formed by internal reflections in the crystal.[13] The counterpropagating waves in the resonator provide the pumping waves for degenerate four-wave mixing (DFWM) with the incident waves. Because of the resonance condition, the DFWM pumping waves may be frequency shifted[14,15] with respect to the incident waves, resulting in a frequency shift or time-varying phase shift for the phase-conjugate reflections. But again, since the two incident waves see the same pumping waves, this phase shift is common to both and does not affect the operation of this device since it is sensitive only to the phase difference. The phase shifts for the return trip in the fiber are given by $\phi_{r_1} - \phi_{nr_1}$ and $\phi_{r_2} - \phi_{nr_2}$; note that the sign of the reciprocal contribution is the same as before, whereas the nonreciprocal contribution has opposite sign. In the round trip, the reciprocal contributions cancel, and net phase shifts are given by $-2\phi_{nr_1}$ and $-2\phi_{nr_2}$. The phase difference measured by the interference at detector D,

$$\phi = -2(\phi_{nr_2} - \phi_{nr_1}) = 4\pi(R_1 L_1 + R_2 L_2)\Omega/\lambda c, \quad (3)$$

is proportional to the rotation rate Ω and can be used to sense rotation.

This configuration has several advantages over our previously reported configuration.[5] Here, we can use self-pumped phase conjugation, with the obvious advantage of not having to provide external pump waves that are coherent and form a phase-conjugate pair. In the externally pumped configuration, the pump beam(s) involved in writing the index grating must be coherent with the probe wave to within the response time of the phase conjugator, and the two counterpropagating pump beams must be phase conjugates of each other to produce high-fidelity phase-conjugate reflection. In initial experiments in which an entire externally pumped phase-conjugate gyro was mounted on a rotating table, because of the slow time response of phase conjugation in the barium titanate crystal used, vibrations of the mounts providing the external pumping washed out the gratings involved in the phase conjugation and precluded the measurement of rotation. As an additional advantage of the self-pumped configuration, the sensing fibers F1 and F2 can be made longer (thereby increasing the sensitivity) than the coherence length of the laser, provided that they are equal in length to within the coherence length.

Figure 2 shows the experimental setup of the self-pumped phase-conjugate fiber-optic gyro. Instead of using two separate fibers as shown in Fig. 1, we use the two polarization modes of a single polarization-preserving fiber coil. All experiments are done with the argon laser running multilongitudinal mode at 515 nm. The highly reflective beam splitter BS1 isolates the laser from retroreflections. The polarization-preserving fiber F1 couples light from the laser to the remaining part of the apparatus that is mounted on a
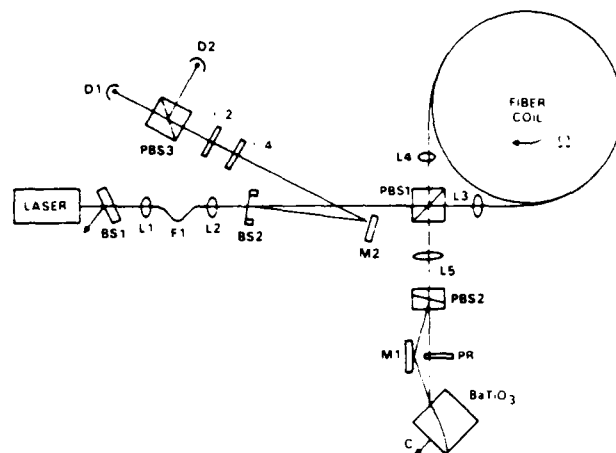

Fig. 2. Experimental setup of the self-pumped phase-conjugate fiber-optic gyro. Instead of the two fibers shown in Fig. 1, the experimental setup shown here uses the two polarization modes of the polarization-preserving fiber-optic coil. Light from the laser is incident upon polarizing beam splitter PBS1 with its polarization at 45° to the plane of the page. The components reflected and transmitted by PBS1 travel clockwise and counterclockwise, respectively, in the fiber coil. The two beams recombine at PBS1 and are then split at PBS2. One of the beams has its polarization rotated by PR, and both beams are incident upon a barium titanate crystal such that self-pumped phase conjugation occurs. The reflected waves retraverse the fiber in an opposite sense, recombine at PBS1, and travel back toward the laser with a phase difference ϕ, which is proportional to the rotation rate. These waves are sampled by the beam splitter BS2, and an additional phase delay of $\pi/2$ rad is impressed on them when they propagate through the quarter-wave retarder $\lambda/4$. The half-wave retarder is oriented such that the intensities of the interferences measured by detectors D1 and D2 are proportional to $\sin \phi$ and $-\sin \phi$, respectively.

rotating table. The output end of F1 is oriented such that the polarization of light emerging from the fiber is at 45° to the plane of the figure. The component polarized in the plane of the page is transmitted by the polarizing beam splitter PBS1 and travels counterclockwise in the fiber coil, whereas the component polarized perpendicular to the page travels clockwise in the fiber coil. The fiber coil is made of approximately 9 m of polarization-preserving fiber coiled in a square of 0.57-m sides and is oriented such that the polarizations of the clockwise and counterclockwise waves are preserved. When the two waves leave the coil they are separated by a Rochon polarizer PBS2. The polarization of the light that travels straight through PBS2 is rotated by the polarization rotator PR such that its polarization becomes identical to that of the light deflected by PBS2. Both beams are incident as extraordinary waves on a barium titanate crystal such that self-pumped phase conjugation occurs.[16] The reflected waves retraverse the fiber in an opposite sense, recombine at PBS1, and travel back toward the laser with a phase difference $\phi = 8\pi R L \Omega/\lambda c$. These waves are sampled by the uncoated pellicle beam splitter BS2, and an additional phase delay of $\pi/2$ rad is impressed on them when they propagate through the
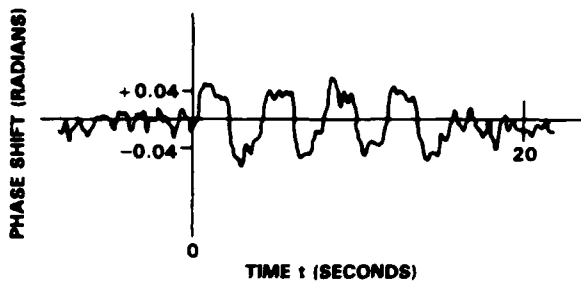
Fig. 3. Measurement of the Sagnac phase shift in the self-pumped phase-conjugate fiber-optic gyro. This figure shows a chart recording of the output of a differential amplifier connected to detectors D1 and D2 in the experimental setup of a self-pumped phase-conjugate fiber-optic gyro shown in Fig. 2. For $t < 0$, the gyro was stationary. At $t = 0$, the gyro was rotated first clockwise, then counterclockwise in a square-wave fashion for four cycles with an amplitude of approximately $6°/sec$. The experimentally measured phase shift is in good agreement with the predicted phase shift of 0.04 rad.

quarter-wave retarder $\lambda/4$. The half-wave retarder is oriented such that the intensities of the interferences measured by detectors D1 and D2 are proportional to $\sin \phi$ and $-\sin \phi$, respectively. The signals from these detectors go to a differential amplifier and a chart recorder.

Figure 3 shows the signal from the chart recorder. For $t < 0$, the gyro was stationary. At $t = 0$, the gyro was rotated first clockwise, then counterclockwise in a square-wave fashion for four cycles with an amplitude of approximately $6°/sec$. The experimentally measured phase shift is in good agreement with the predicted phase shift of 0.04 rad. The fast rotation rate is necessary for the signal to overcome the noise that is evident in the phase shift recorded during the time $t < 0$. Although we are not certain of the major noise source, we believe that it is rapid reciprocal phase shifts that are not corrected owing to the finite response time of the phase conjugator.

Although this experiment does not demonstrate the correction of polarization scrambling in multimode fibers, it does demonstrate the measurement of the Sagnac phase shift, Eq. (3). To demonstrate a self-pumped phase-conjugate fiber-optic gyro using multimode fibers, one must use two multimode fibers terminated by the same self-pumped polarization-preserving phase-conjugate mirror. Simply replacing the polarization-preserving fiber in Fig. 2 with a multimode fiber does not work, since the polarization of light after traveling down the fiber is scrambled, and when the light reaches PBS1 part of it will go to the detectors without being reflected from the phase-conjugate mirror. In addition to the added complication

of using two fibers and the associated complexity of terminating them on the same self-pumped polarization-preserving phase-conjugate mirror (four beams going into one crystal), it is necessary to ensure that the light waves from the two fibers are coherent to within the response time of the phase conjugator (the change in phase shifts for the two waves due to environmental effects on the fibers must be slower than the response time of the phase conjugator). The second of the above-mentioned effects can be reduced by wrapping the two fibers together so that they see nearly the same environment.

In conclusion, we have described a new type of phase-conjugate fiber-optic gyro in which self-pumped phase conjugation can be employed to permit the use of sensing fibers that are longer than the coherence length of the laser source. In other, externally pumped, configurations, it is possible to use fibers longer than the coherence length of the laser by using a fiber to carry the pumping waves. This, however, complicates the setup and defeats some of the advantages of using phase conjugation. We have constructed a self-pumped phase-conjugate fiber-optic gyro and demonstrated rotation sensing.

References

1. J.-C. Diels and I. C. McMichael. Opt. Lett. **6**, 219 (1981).
2. P. Yeh. J. Tracy. and M. Khoshnevisan. Proc. Soc. Photo-Opt. Instrum. Eng. **412**, 240 (1983).
3. C. J. Bordé, in *Experimental Gravitation and Measurement Theory*, P. Meystre and M. O. Scully. eds. (Plenum, New York, 1983), p. 269.
4. B. Fischer and S. Sternklar. Appl. Phys. Lett. **47**, 1 (1985).
5. P. Yeh. I. McMichael. and M. Khoshnevisan. Appl. Opt. **25**, 1029 (1986).
6. R. Bergh. H. Lefevre and H. Shaw. IEEE J. Lightwave Technol. **LT-2**, 91 (1984).
7. R. Ulrich. Opt. Lett. **5**, 173 (1980).
8. W. Burns. R. Moeller. C. Villarruel. and M. Abebe. Opt. Lett. **8**, 540 (1983).
9. I. McMichael. M. Khoshnevisan, and P. Yeh. Opt. Lett. **11**, 525 (1986).
10. I. McMichael. P. Yeh, and M. Khoshnevisan. Proc. Soc. Photo-Opt. Instrum. Eng. **613**, 32 (1986).
11. S. Kwong, A. Yariv, M. Cronin-Golomb. and B. Fischer. J. Opt. Soc. Am. A **3**, 157 (1986).
12. M. Ewbank. P. Yeh. M. Khoshnevisan. and J. Feinberg. Opt. Lett. **10**, 282 (1985).
13. M. Ewbank and P. Yeh. Proc. Soc. Photo-Opt. Instrum. Eng **613**, 59 (1986).
14. P. Yeh. J. Opt. Soc. Am. B **2**, 1924 (1985).
15. M. Ewbank and P. Yeh. Opt. Lett. **10**, 496 (1985).
16. J. Feinberg. Opt. Lett. **7**, 486 (1982).

APPENDIX 4.12

PHOTOREFRACTIVE CONICAL DIFFRACTION IN BaTiO$_3$

PHOTOREFRACTIVE CONICAL DIFFRACTION IN BaTiO₃

M.D. EWBANK, Pochi YEH

Rockwell International Science Center, Thousand Oaks, CA 91360, USA

and

Jack FEINBERG

Department of Physics, University of Southern California, Los Angeles, CA 90089-0484, USA

A laser beam incident on BaTiO₃ can cause a cone of light to exit the crystal. If the incident beam is polarized as an extraordinary ray, the cone of light is formed by ordinary rays. The cone angle is fixed by a phase-matching condition for the incident and cone beams. Measurement of this cone angle as a function of the incident angle is a simple and sensitive method for determining the birefringence of a BaTiO₃ crystal over the entire range of wavelengths where the sample is photorefractive.

A single beam of coherent light incident on a BaTiO₃ crystal can cause a cone of light to emerge from the far face of the crystal. This cone has a polarization orthogonal to that of the incident ray and appears when the incident beam is an extraordinary ray in the crystal. There have been previous accounts of rings, fans, and other forms of photoinduced light scattering in photorefractive crystals, which have been attributed to a variety of physical mechanisms [1–9]. Recently, similar light cones in BaTiO₃ have been reported and shown to be due to stimulated two-wave mixing via the photorefractive effect [10]. Here, we account for the phase-matching condition in BaTiO₃ for anisotropic Bragg scattering [11] by using a simple geometrical construction to predict the angular position of the light in the exit plane. We also show that precise measurements of the cone angle can be used to determine the dispersion of the birefringence, $\Delta n = n_e - n_o$, of a BaTiO₃ sample.

Fig. 1 shows the experimental setup, with a laser beam incident on one of the a-faces of a BaTiO₃ crystal. The incident beam makes an angle θ in air with the face normal and is polarized to be an extraordinary ray, with its electric-field vector in the plane of inci-
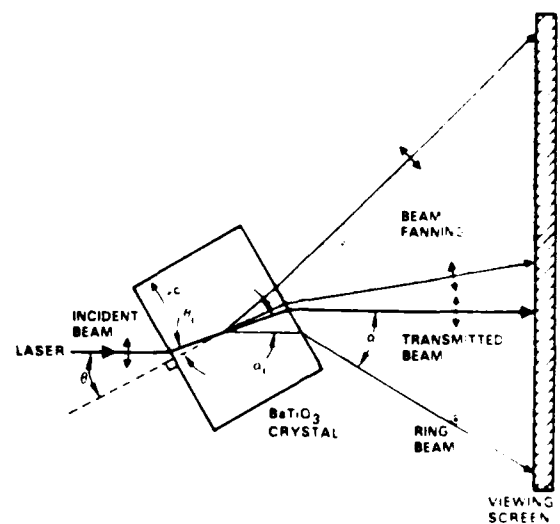

Fig. 1. A laser beam with extraordinary polarization incident on a photorefractive BaTiO₃ crystal causes fanned beams and a ring beam to appear. The fanned beams are polarized extraordinary and the ring beam is ordinary, as indicated.

dence defined by the beam direction and the c-axis of the crystal. A broad fan [12] of extraordinary light is observed on the +c-axis side of the transmitted beam, as shown in fig. 2a. Simultaneously, a single ring of light with ordinary polarization appears on the negative c-axis side of the transmitted beam (see the multiple exposure photograph in fig. 2b). For an incident beam intensity of ~1 W/cm^2 the fan and the ring appear within a few seconds. As shown in fig. 2b, the shape of the ring varies with the angle of incidence. The ring is visible for both positive and negative angles of incidence θ (with positive θ defined in fig. 1), although for negative angles the ring intensity is diminished because self-pumped phase conjugation [13] depletes the incident beam intensity.

The rings observed in fig. 2b for BaTiO$_3$ result from anisotropic Bragg scattering [11] of the incident beam off photorefractive gratings formed during beam fanning [10]. The incident beam, with wavevector K_i, scatters from defects or impurities into a broad fan having a range of wavevectors K_f. These scattered beams interfere with the incident beam and create photorefractive index gratings with wavevectors K given by

$$K = K_f - K_i. \tag{1}$$

The incident beam then Bragg-scatters off these gratings and either reinforces or depletes the fanning beams by two-wave mixing [14] depending on the sign of the projection of K onto the positive c-axis direction. The collection of all amplified scattered beams is a broad fan of light directed towards the positive c-axis side of the crystal.

The photorefractive grating wavevectors K formed during beam fanning can also deflect the incident beam into a cone of light. As illustrated in fig. 3a, some of these photorefractive gratings will have wavevectors of exactly the right length and direction $-K$ to deflect the extraordinary incident wavevector K_i into an ordinary ring beam K_r

$$K_r = K_i - K. \tag{2}$$

Eliminating K from eqs. (1) and (2) gives the phase-matching condition

$$K_r = 2K_i - K_f. \tag{3}$$

Eq. (3) selects a cone of wavevectors K_r as can be seen in the following simple geometric interpretation.

EXTRAORDINARY POLARIZATION   ORDINARY POLARIZATION

TRANSMITTED BEAM

HORIZONTAL DISPLACEMENT (ARB

VERTICAL DISPLACEMENT (ARB)

Fig. 3. Phase matching for anisotropic Bragg scattering in photorefractive $BaTiO_3$. (a) Ordinary and extraordinary normal wave surfaces in the plane of incidence. Photorefractive gratings deflect the incident wavevector K_i into a range of fanned wavevectors K_f. One particular grating, with wavevector $-K$, also deflects the incident wavevector K_1 and generates the ring beam with wavevector K_r. Because the polarization of the incident and fanned beams is extraordinary and the ring beam is ordinary, only the one wavevector $-K$ in the plane of incidence will permit the ring beam to be phase-matched. (b) A graphical solution in the plane of incidence to the phase-matching condition. $K_r = 2K_1 - K_f$. The ring wavevector K_r is determined by the intersection of a circle (representing all possible ordinary ring beams) and an ellipse (representing the extraordinary fanned beams) whose centers are separated by $2K_1$. (c) Extending the geometric construction of fig. 3b to three dimensions. the intersection of the two normal surfaces defines a cone of wavevectors (note that the K_r is shown coming out of the $x-z$ plane, which produces the diffraction ring observed in fig. 2b

The locus of all possible K_r (ordinary ring beams) is a sphere of radius $2\pi n_o$ λ. The locus of all possible K_f (extraordinary fanned beams) is an ellipsoid of revolution with semi-minor and semi-major axes of lengths $2\pi n_e/\lambda$ and $2\pi n_o/\lambda$, respectively. Displace the center of the ellipsoid from the center of the sphere by an amount $2K_i$. Then the intersection of the ellipsoid and the sphere selects a cone of phase-matched wavevectors K_r. Fig. 3b shows this geometric construction in the $x-z$ plane. while fig. 3c extends it to three dimensions. As can be seen in fig. 3c. the intersection of the two normal surfaces is a ring centered around the direction of the incident beam. For materials with small birefringence. this ring is approximately a circle inside the crystal.

The intensity and the polarization of the cone of light is determined by the electro-optic tensor of the crystal. BaTiO$_3$ has point group symmetry 4mm. and its largest electro-optic coefficient is $r_{42} = r_{51} = 1640$ pm/V [15]. A photorefractive space-charge electric field $E_{sc} = (E_x. E_y. E_z)$ formed during beam fanning will. through the r_{42} coefficient. cause a change in the susceptibility tensor $\Delta\chi$ given by [16]

$$\Delta\chi = \begin{pmatrix} 0 & 0 & ar_{42}E_x \\ 0 & 0 & ar_{42}E_y \\ ar_{42}E_x & ar_{42}E_y & 0 \end{pmatrix}. \quad (4)$$

where $a \equiv -\epsilon_a\epsilon_c/4\pi$ with ϵ_a and ϵ_c being the static dielectric constants along the a- and c-axes. respectively. The $\Delta\chi_{13} = \Delta\chi_{31}$ components in eq. (4) produce beam fanning by coupling the incident extraordinary beam. whose polarization vector is in the $x-z$ plane. into the extraordinary fanned beams. which also have $x-z$ polarization. The $\Delta\chi_{23} = \Delta\chi_{32}$ components produce anisotropic scattering of the incident extraordinary beam into the ring beam. which has ordinary (y) polarization. Anisotropic scattering of a beam into the $x-z$ plane itself cannot occur because if the grating K lies entirely in the $x-z$ plane then $E_y = 0$. and the intensity of the anisotropically scattering beam is zero [10]. This is evident in fig. 2b. where the observed intensity of the conical diffraction vanishes along the plane of incidence.

The angular position and shape of the diffraction cone depend on the angle of incidence. as observed in fig. 2b. Referring to fig. 3b. for a given incident beam

angle θ_i inside the crystal. the diffraction angle α_i inside the crystal in the plane of incidence can he obtained from

$$n_0^2 v^2 + n_e^2 w^2 = n_0^2 n_e^2. \quad (5)$$

where

$$v \equiv 2n_1 \cos\theta_i - n_0 \cos(\theta_i + \alpha_i), \quad (6)$$

and

$$w \equiv 2n_1 \sin\theta_i - n_0 \sin(\theta_i + \alpha_i). \quad (7)$$

with $n_1(\theta) = n_0 n_e/(n_e^2 \sin^2\theta_i + n_0^2 \cos^2\theta_i)^{1/2}$. the effective extraordinary refractive index at an incident angle θ_i.

For normal incidence ($\theta = \theta_i = 0$). the internal diffraction angle α_i in the plane containing the incident beam and the c-axis is given by

$$\cos\alpha_i = 2n_e/(n_0 + n_e). \quad (8a)$$

and for scattering in the plane containing the incident beam but normal to the c-axis is given by

$$\cos\alpha_i = (3n_e^2 + n_0^2)/(4n_e n_0). \quad (8b)$$

For small birefringence. eq. 8(a) is valid for any incident angle θ_i if n_e is replaced by the effective index $n_1(\theta_i)$. defined after eq. (7) above.

Closed-form expressions for the diffraction angle α of the ring beam outside the crystal can be obtained using Snell's law. For normal incidence. assuming a fractional birefringence much less than unity ($(n_0 - n_e)$ $n_0 \approx 0.025$ in BaTiO$_3$) and using small angle approximations. the external scattering angle α becomes

$$\alpha \sim [n_0(n_0 - n_e)]^{1/2} \quad (9)$$

in both planes associated with eqs. (8a) and (8b). that is. the external diffraction ring is nearly circular at $\theta = 0$. As a function of the incident angle θ outside of the crystal. the external diffraction angle α in the plane of incidence can be obtained from a quadratic solution to eqs. (5)-(7) for small internal angles and Snell's law. Out of the plane of incidence. the external angle of diffraction can be determined numerically.

Fig. 2c shows the calculated shape of the diffraction rings external to the crystal using the values [17] $n_0 = 2.521$ and $n_e - n_c = -0.072$. Excellent agreement between theory and experiment is seen by comparing figs. 2b and c. As the angle of incidence θ increases. portions of the diffraction ring eventually un-

dergo total internal reflection at the crystal's exit face, and the rings become open-ended teardrop shapes. as shown in figs. 2b and c.

At large scattering angles, where the diffracted ring approaches total internal reflection ($\theta + \alpha \sim 90°$ in the plane of incidence), the precise direction of the scattered light is a sensitive function of the birefringence $n_e - n_o$ in the crystal. Consequently, a measurement of α versus θ provides a simple method to determine the birefringence in a photorefractive BaTiO$_3$ sample. This method is independent of crystal length. unlike traditional methods of determining birefringence where a phase retardation between orthogonal polarizations is directly measured. Fig. 4 shows the dependence of α on θ for one BaTiO$_3$ sample at a number of visible wavelengths (from HeNc. Ar$^+$ and R6G-dye laser sources). Since the intensity of the ring approaches zero in the $x-z$ plane (see eq. (4)), the data were taken by projecting the path of the ring into this plane. Uncertainty in the precise orientation of the crystal's c-axis with respect to the fabricated faces is a possible source of error. However, we found that rotating the crystal by $180°$ about the y-axis gave the same measured values for the scattering angle (although now in the opposite direction). as long as care was taken to locate the angle $\theta = 0°$ by retroreflecting the incident beam off the *back a*-face of the crystal.
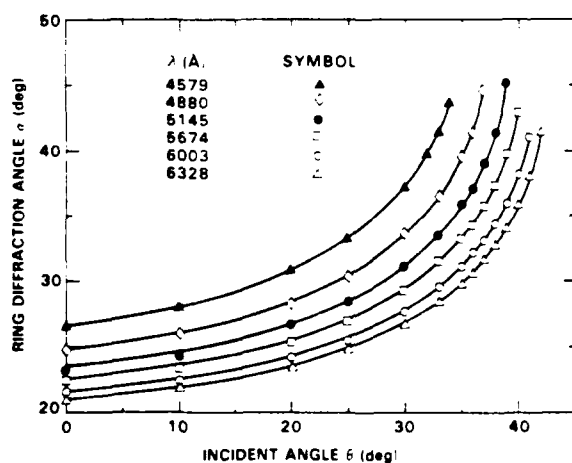

Fig. 4. Measured external ring diffraction angle α versus incident angle θ as a function of wavelength for one photorefractive BaTiO$_3$ crystal. The solid curves are nonlinear least squares fits to eq. (5) (as described in the text) and provide the values for the birefringence listed in table 1.

By performing a nonlinear least squares fit to the data in fig. 4 using the closed-form solution to eq. (5) and by assuming a value for n_o [17], the birefringence $n_e - n_o$ at each wavelength has been obtained with an estimated accuracy of $\sim 1.5\%$. The results of this fitting procedure are given in table 1 and closely agree with the values previously reported in the literature [17]. (Note: the Sellmeier coefficients for BaTiO$_3$ reported in ref. [17] are better than those in ref. [18] for calculating the birefringence.) A measurement of the room-temperature birefringence in six different BaTiO$_3$ samples [19] at $\lambda = 4880$ Å gave the same value with a standard deviation of 1.4 $\times 10^{-3}$, even though these crystals exhibit different photorefractive behavior.

Multiple conical diffraction rings are observed in photorefractive BaTiO$_3$ in two different situations. First, if more than one beam is incident on a crystal. extra diffraction rings appear. For example. in two-wave mixing with two incident beams. each beam produces its own ring via the phase-matching process described in fig. 3. In addition. two other diffraction rings are also present. Both of these extra rings are due to anisotropic Bragg diffraction of either incident beam off the photorefractive gratings generated via beam fanning of the other incident beam. Secondly. a transient diffraction ring is visible when the incident angle of a single beam is abruptly changed. The photorefractive gratings stored in the crystal from beam fanning for the previous angle of incidence can anisotropically Bragg-scatter the new incident beam

Table 1
Birefringence $\Delta n = n_e - n_o$ of BaTiO$_3$ at various visible laser wavelengths.

λ (A)	Calculated [a] n_o	Calculated [a] Δn	This work [b] Δn
4579	2.560	−0.0791	−0.0777
4880	2.521	−0.0718	−0.0693
5145	2.494	−0.0668	−0.0634
5674	2.452	−0.0594	−0.0597
6003	2.432	−0.0564	−0.0554
6328	2.416	−0.0534	−0.0529

[a] From the Sellmeier equations given in ref. [17].
[b] From a nonlinear least squares fit to the θ versus α data shown in fig. 4 assuming the reported value for n_o listed above.

into a transient ring. However, as the new fanned light and corresponding diffraction ring at the new angle of incidence become more intense, the previous photorefractive gratings are erased and the transient ring disappears.

In conclusion, we have observed and explained the appearance of conical diffraction rings, both transient and steady state, caused by anisotropic Bragg scattering off self-induced photorefractive gratings in $BaTiO_3$. Since these gratings are birefringent, the polarization of the rings is orthogonal to the extraordinary polarization of the incident beam. A precise measurement of the diffraction angle of the rings provides an accurate value for the birefringence of the $BaTiO_3$ crystal.

References

[1] W. Phillips, J.J. Amodei and D.L. Staebler, RCA Rev. 33 (1972) 94.

[2] J.M. Morgan and I.P. Kaminow, Appl. Optics 12 (1973) 1964.

[3] M.R.B. Forhsaw, Appl. Optics 13 (1974) 2.

[4] R. Magnusson and T.K. Gaylord, Appl. Optics 13 (1974) 1545.

[5] S.I. Ragnarsson, Appl. Optics 17 (1978) 116.

[6] I.R. Dorosh, Yu.S. Kuzminov, N.M. Polozkov, A.M Prokhorov, V.V. Osiko, N.V. Tkachenko, V.V. Voronov and D.Kh. Nurligareev, Phys. Stat. Sol. (a) 65 (1981) 513.

[7] E.M. Avakyan, K.G. Belabaev and S.G. Odoulov, Sov. Phys. Sol. St. 25 (1983) 1887.

[8] R. Grousson, S. Mallick and S. Odoulov, Optics Comm. 51 (1984) 342.

[9] S. Odoulov, K. Belabaev and I. Kiseleva, Optics Lett. 10 (1985) 31.

[10] D.A. Temple and C. Warde, J. Opt. Soc. Am. B3 (1986) 337.

[11] N.V. Kukhtarev, E. Kratzig, H.C. Kulich and R.A. Rupp, Appl. Phys. B35 (1984) 17.

[12] J. Feinberg, J. Opt. Soc. Am. 72 (1982) 46.

[13] J. Feinberg, Optics Lett. 7 (1982) 486.

[14] See, for example, D. Rak, I. Ledoux and J.P. Huignard, Optics Comm. 49 (1984) 302, and references cited therein.

[15] A.R. Johnston and J.M. Weingart, J. Opt. Soc. Am. 55 (1965) 828.

[16] See, for example, A. Yariv and P. Yeh, Optical waves in crystals (John Wiley and Sons, New York, 1984) p. 228.

[17] R.J. Pressley, ed., Handbook of lasers (Chemical Rubber Company, Cleveland, 1971) p. 509.

[18] S.H. Wemple, M. DiDomenico, Jr., and I. Camlibel, J. Phys. Chem. Sol. 29 (1968) 1797.

[19] All samples purchased from Sanders Associates, Nashua, NH 03061.

APPENDIX 4.13

POLARIZATION-PRESERVING PHASE CONJUGATOR

Polarization-preserving phase conjugator

Ian McMichael, Monte Khoshnevisan, and Pochi Yeh

Rockwell International Science Center, Thousand Oaks, California 91360

Using a single self-pumped crystal of barium titanate, we demonstrate a method for producing the phase conjugate of an incident wave having arbitrary polarization. Our experimental results show that the phase-conjugate wave produced by this method reproduces both the ellipticity and the helicity of the polarization of the incident wave.

Most demonstrations of the correction of wave-front distortions by phase conjugation use linearly polarized light and optically isotropic wave-front-distorting media. In some cases, however, one may also wish to correct for the changes in polarization induced by optically anisotropic media. For example, one may wish to correct for the polarization scrambling due to environmentally dependent birefringence that is a source of noise and signal fading in fiber-optic gyros.[1] Self-pumped phase conjugation is efficient in barium titanate[2] but only for extraordinary light since it utilizes the large electro-optic coefficients r_{42} and r_{51}. In this Letter we demonstrate a scheme for using a single self-pumped crystal of barium titanate to produce the phase conjugate of a wave having arbitrary polarization.

In general, the reflectivity of a phase-conjugate mirror is described by a 2×2 tensor that determines the amplitude, phase, and polarization state of the reflected light. Only when this tensor reduces to a scalar can a phase-conjugate mirror correct for both the wave-front distortions and the changes in polarization induced by optically anisotropic wave-front-distorting media.[3] We call a phase-conjugate mirror for which the reflectivity tensor reduces to a scalar a polarization-preserving phase conjugator (PPPC). To show that a PPPC can correct for the change in polarization state introduced by optically anisotropic media, consider the situation of a plane wave with polarization state described by a vector amplitude A:

$$A = \begin{bmatrix} A_x \\ A_y \end{bmatrix} \qquad (1)$$

that is incident upon an optically anisotropic medium, followed by a phase-conjugate mirror. After the wave passes through the anisotropic medium, the amplitude becomes

$$A' = TA, \qquad T = \begin{bmatrix} t_{xx} & t_{xy} \\ t_{yx} & t_{yy} \end{bmatrix}, \qquad (2)$$

where T is a Jones matrix[4] that describes transmission through the anisotropic medium and where $t_{xx}, t_{xy}, t_{yx},$ and t_{yy} are the tensor elements. After the wave is reflected from the phase-conjugate mirror, its amplitude becomes

$$A'' = R(TA)^*, \qquad R = \begin{bmatrix} r_{xx} & r_{xy} \\ r_{yx} & r_{yy} \end{bmatrix}, \qquad (3)$$

where R is a tensor that describes reflection from the phase-conjugate mirror and where $r_{xx}, r_{xy}, r_{yx},$ and r_{yy} are the tensor elements. After the returning wave passes back through the anisotropic medium, its amplitude is given by

$$TRT^*A^*. \qquad (4)$$

Since in general this is not proportional to the phase conjugate of the amplitude of the incident wave, the returning wave does not have the same polarization as the incident wave. However, if the reflectivity tensor reduces to a scalar r, then the amplitude of the reflected wave becomes

$$rTT^*A^* \quad \text{for } R = \begin{bmatrix} r & 0 \\ 0 & r \end{bmatrix} = r. \qquad (5)$$

For optically anisotropic media, such as birefringent or optically active media, the Jones matrix has the property $TT^* = 1$. In this case, the amplitude of the reflected wave becomes

$$rA^* \quad \text{for } R = r, \quad TT^* = 1. \qquad (6)$$

Since this is proportional to the phase conjugate of the incident wave, the polarization of the reflected wave is identical to that of the incident wave. Thus we have shown that a PPPC can correct for the change in polarization state introduced by optically anisotropic media. The PPPC cannot correct for the changes in polarization introduced by nonreciprocal phenomena such as the Faraday effect, where $TT^* \neq 1$.

Several methods have been proposed for polarization-preserving phase conjugation.[3,5,6] PPPC's can be made by using media that have a tensor reflectivity, by decomposing the incident wave into two components having orthogonal polarizations, phase conjugating these components, and recombining the conjugates.[5] The result is a PPPC only if the components recombine with the correct amplitude and phase. This is ensured if the losses and the amplitudes and phases of the complex phase-conjugate reflectivities are the same for both components. A schematic of our PPPC that uses this method is shown in Fig. 1. To understand how it works, consider an incident wave having a
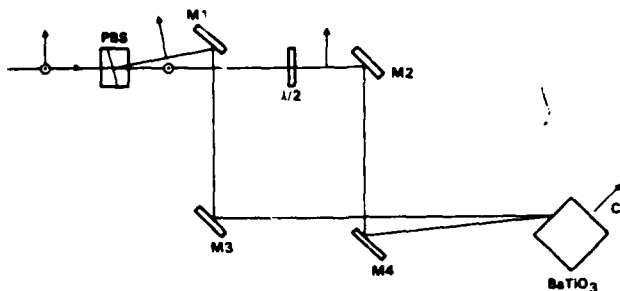
Fig. 1. PPPC. Light incident upon the polarizing beam splitter PBS is decomposed into two orthogonally polarized components. One component is rotated 90° by the half-wave retarder λ/2. Both components are incident upon a barium titanate crystal such that self-pumped phase conjugation occurs. When the two conjugates recombine at PBS, they form a conjugate wave that reproduces the polarization of the incident light.

polarization described by a complex vector amplitude $A = (a_1, a_2)$. This wave is decomposed into two orthogonally polarized components, $(a_1, 0)$ and $(0, a_2)$, by the polarizing beam splitter PBS. The component with polarization orthogonal to the plane of the figure $(0, a_2)$ has its polarization rotated by the half-wave retarder λ/2 such that its polarization state becomes $(a_2, 0)$. Both components are incident upon a barium titanate crystal at an angle such that self-pumped phase conjugation occurs.[7] Since both components have the same polarization and are reflected from the same phase-conjugate mirror, they experience the same complex phase-conjugate reflectivity r, becoming $r(a_1{}^*, 0)$ and $r(a_2{}^*, 0)$. The half-wave retarder restores the second of these components to its original polarization, $r(0, a_2{}^*)$. When the two components recombine at the polarizing beam splitter, they form the phase conjugate with the same polarization as the incident wave, $r(a_1{}^*, a_2{}^*) = rA^*$. Thus the configuration shown in Fig. 1 acts as a PPPC; henceforth we refer to it as "the PPPC."

Using the self-pumped configuration in the PPPC results in a frequency shift between the components incident upon the crystal and their conjugates.[8,9] However, since both components are incident upon the same region of the crystal, they see the same pumping waves, and therefore they experience the same frequency shift and phase-conjugate reflectivity. In fact, the two beams can be thought of as two components of a single probe beam. In the experiment, the two beams are made to overlap by aligning mirror M4 while observing the scattered light from the beams in the crystal. This procedure is sufficient to obtain the results presented here, and exact alignment is not required. The two beams interact by coherently pumping the oscillation of a resonator formed by internal reflections in the crystal.[10] The counterpropagating waves in the resonator then provide the pump waves for degenerate four-wave mixing (DFWM). Since the two beams entering the crystal see the same pump waves, they experience the same DFWM reflectivity. It should be noted that the two beams entering the crystal must be coherent to within the response time of

the crystal. In the experiment, the path lengths from the polarizing beam splitter to the crystal were made equal to within the coherence length of the laser. The excellent frequency locking[11] of the conjugates when both beams are present is indicated by the fact that no beating is detected in the return from the PPPC.

To show that the PPPC reproduces the ellipticity of polarized light, we use the experimental setup shown in Fig. 2(a). A highly reflective beam splitter BS1 isolates the laser from any retroreflections of its output. The polarizer P1 ensures that the light is linearly polarized in the plane of the figure. In all the experiments presented here, the power after P1 is ~1 mW at 514.5 nm. Either a half-wave retarder λ/2 or a quarter-wave retarder λ/4 is used to alter the polarization state of the light. This light is then reflected from


(a)

(b)

(c)
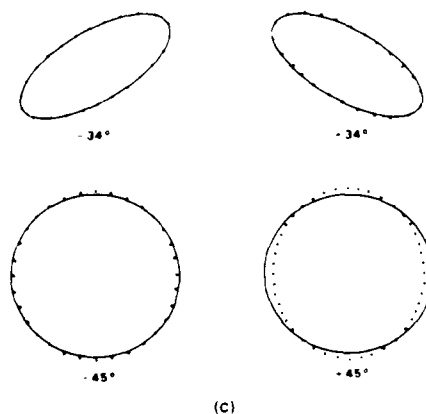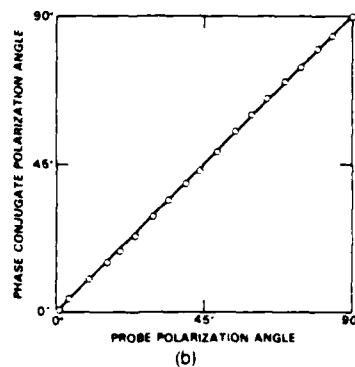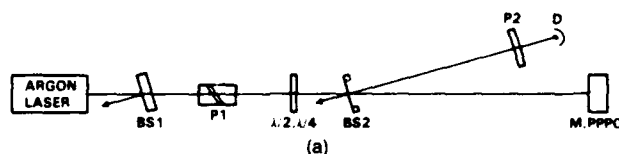
Fig. 2. Reproduction of the ellipticity of polarized light by the PPPC. (a) Experimental setup. A half- or quarter-wave retarder alters the polarization state of light incident on a normal mirror M or the PPPC. (b) Measured angle of polarization for the reflection from the PPPC versus that from M. (c) Measured polarization ellipse for the reflection from the PPPC (dotted line) compared with that from M (solid line).

(a)

(b)
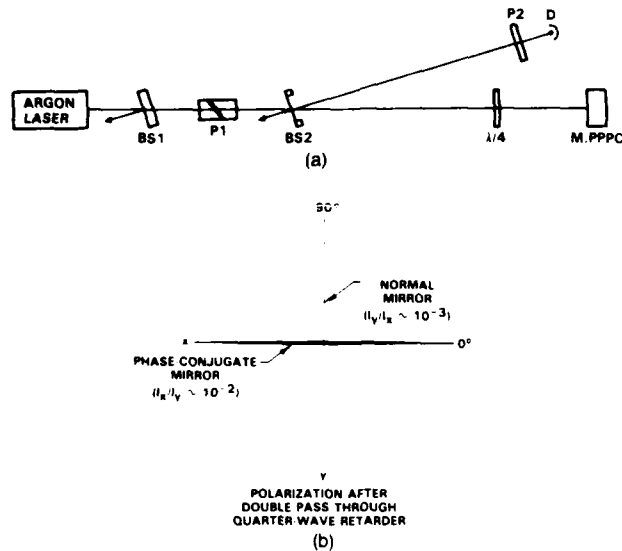
Fig. 3.   Reproduction of the helicity of polarized light by the PPPC. (a) Experimental setup. The quarter-wave retarder λ/4 is oriented such that the light incident upon M or the PPPC is converted from linearly polarized light to circularly polarized light. (b) Measured polarization ellipses for the reflections from M and the PPPC after retraversing λ/4.

either a normal mirror M (multilayer dielectric high reflector) or the PPPC. The reflected light is sampled by the beam splitter BS2, and it is analyzed by the combination of polarizer P2 and detector D. Since BS2 is an uncoated pellicle beam splitter used near normal incidence (the angle of incidence is exaggerated in the figure; the actual angle of incidence is 2°), the reflection coefficients for the s and p polarizations are nearly equal and the polarization measured by P2 and D is nearly the same as that reflected by M.

Figure 2(b) shows the measured angle of polarization for the reflection from the PPPC as a function of the measured angle of polarization for the reflection from the normal mirror M for various orientations of the half-wave retarder. Zero degrees corresponds to polarization in the plane of the previous figures. The open circles are the data (with diameters corresponding to the uncertainty), and the solid line indicates what is expected in the case of an ideal PPPC. The measured ellipticity of the polarization for the light reflected by the PPPC (defined as the ratio of the minor polarization axis to the major polarization axis) never exceeded 1%.

Figure 2(c) shows the measured polarization ellipse for the reflection from the PPPC (dotted line), and the measured polarization ellipse for the reflection from the normal mirror (solid line), for various orientations of the quarter-wave retarder. Zero degrees corresponds to orientation of the axis of the quarter-wave retarder in the plane of the previous figures. The ellipticity of the reflected light is measured by rotating polarizer P2 and noting the minimum and maximum intensities at detector D.

The results shown in Fig. 2 demonstrate that the reflection from the PPPC reproduces the ellipticity of

the polarization of the incident wave. To show that it reproduces the helicity of the polarization of the incident wave, we use the setup shown in Fig. 3(a). A quarter-wave retarder λ/4 is placed between the sampling beam splitter and the mirror and is oriented such that the light incident on the mirror is converted from linearly polarized light to circularly polarized light. Figure 3(b) shows the measured polarization ellipses for the normal mirror and the PPPC. Light reflected from the normal mirror changes helicity. After the reflected light passes back through the quarter-wave retarder, its polarization is orthogonal to the incident light. This is the principle by which quarter-wave isolation works. On the other hand, light reflected by the PPPC has the same helicity as the incident light and returns to its original polarization state after passing back through the quarter-wave retarder.

In order to quantify how well the technique works when there is an aberration in the beam, a multimode fiber is placed at the position of the quarter-wave retarder in Fig. 3(a). The multimode fiber scrambles the polarization of the input wave. With a normal mirror at the end of the fiber, approximately 50% of the power returns in each of the two linear-polarization states (parallel and orthogonal to the linear input polarization). With the PPPC at the end of the fiber, less than 1% of the light returns with the orthogonal polarization.

In conclusion, we have demonstrated a polarization-preserving phase conjugator that is capable of correcting for both the phase distortions and the changes in polarization induced by optically anisotropic phase-distorting media. Potential applications of this device include the phase-conjugate fiber-optic gyro[12,13] and interferometry with multimode fibers.[14]

References

1. R. Ulrich and M. Johnson, Opt. Lett. 4, 152 (1979).
2. J. Feinberg and R. W. Hellwarth, Opt. Lett. 5, 519 (1980).
3. P. Yeh, Opt. Commun. 51, 195 (1984).
4. See, for example, A. Yariv and P. Yeh, Optical Waves in Crystals (Wiley, New York, 1984).
5. N. G. Basov, V. F. Efimkov, I. G. Zuberev, A. V. Kotov, S. I. Mikhailov, and M. G. Smirnov, JETP Lett. 4, 197 (1978).
6. G. Martin, L. K. Lam, and R. W. Hellwarth, Opt. Lett. 5, 185 (1980).
7. J. Feinberg, Opt. Lett. 7, 486 (1982).
8. W. B. Whitten and J. M. Ramsey, Opt. Lett. 9, 44 (1984).
9. J. Feinberg and G. D. Bacher, Opt. Lett. 9, 420 (1984).
10. M. Ewbank and P. Yeh, Proc. Soc. Photo-Opt. Instrum. Eng. 613, 59 (1986).
11. M. D. Ewbank, P. Yeh, M. Khoshnevisan, and J. Feinberg, Opt. Lett. 10, 282 (1985).
12. C. J. Borde, in Experimental Gravitation and Measurement Theory, P. Meystre and M. O. Scully, eds. (Plenum, New York, 1983), pp. 269–291.
13. P. Yeh, I. McMichael, and M. Khoshnevisan, Appl. Opt. 25, 1029 (1986).
14. B. Fischer and S. Sternkler, Appl. Phys. Lett. 46, 113 (1985).

APPENDIX 4.14

ABSOLUTE PHASE SHIFT OF PHASE CONJUGATORS

Absolute Phase Shift of Phase Conjugators

Ian McMichael, Pochi Yeh and Monte Khoshnevisan

Rockwell International Science Center
1049 Camino Dos Rios, Thousand Oaks, CA   91360

Abstract

We present theoretical expressions and experimental measurements of the absolute phase shifts of phase conjugators. Photorefractive media, transparent media, saturable absorbers and saturable amplifiers are considered in the analysis. Experimental measurements of the absolute phase shifts are presented for barium titanate, strontium barium niobate and ruby.

Introduction

Although the reflectivity of phase conjugators has been of significant interest recently, the phase of the phase-conjugate wave has received little attention. This phase determines the operating point of some phase-conjugate interferometers. If this phase can be controlled, the interferometers can be biased at the operating point of highest sensitivity and linear response (quadrature). With this motivation, we have studied the absolute phase of phase conjugators theoretically and experimentally.

Theory

We consider the usual case of degenerate four-wave mixing of two countepropagating pump waves having amplitudes A_1 and A_2 with a probe wave having amplitude A_4 propagating in the $+z$ direction and a phase-conjugate wave A_3 propagating in the $-z$ direction. Let the phase of the phase-conjugate reflection ϕ_3, where $A_n = |A_n|e^{i\phi_n}$, be written as,

$$\phi_3 = \phi_0 + \phi_1 + \phi_2 - \phi_4 \tag{1}$$

We then refer to ϕ_0 as the absolute phase shift of the phase conjugator. The phase shift ϕ_0 can be obtained from the solution of the coupled-wave equations describing the degenerate four-wave mixing. In general, ϕ_0 depends on the type of grating (index, absorption, or gain) involved in the degenerate four-wave mixing, the phase shift of this grating with respect to the light intensity pattern that produces the grating, and the intensities of the interacting waves.

For a photorefractive medium, the complex amplitude of the phase-conjugate wave at the input to the medium ($z = 0$) is given by,[1]

$$A_3(0) = A_4{}^*(0)(A_1/A_2{}^*)(e^{-\gamma L} - 1)/(r^{-1}e^{-\gamma L} + 1) \tag{2}$$

where L is the length of the medium, r is the pump-beam intensity ratio,

$$r = |A_2/A_1|^2 \tag{3}$$

and γ is the complex coupling constant that depends on the physical process involved in the generation of the hologram. If ones makes the usual assumption that the phase grating in photorefractive media is shifted by $\pi/2$ radians with respect to the intensity pattern, then γ is real and the phase shift of a photorefractive phase conjugator is

$$\phi_0 = 0 \text{ for } \gamma < 0$$

$$= \pi \text{ for } \gamma > 0 \tag{4}$$

For degenerate four-wave mixing in a transparent medium with a local response (no phase shift of the index grating with respect to the intensity pattern), the amplitude of the phase-conjugate wave at the input of the medium is given by,[2]

$$A_3(0) = -iA_4{}^*(0)(|\kappa^*|/\kappa) \tan |\kappa|L \tag{5}$$

where κ is the complex coupling constant,

$$\kappa^* = (2\pi\omega/cn)\chi A_1 A_2 \tag{6}$$

From Equations (5) and (6), we obtain the phase of the phase conjugator for a transparent medium with a local response,

$$\phi_0 = -\pi/2 \text{ for } \chi > 0$$

$$= +\pi/2 \text{ for } \chi < 0 \tag{7}$$

Finally, for degenerate four-wave mixing in a saturable absorber or amplifier with a local response, the amplitude of the phase-conjugate wave at the input of the medium is given by,[3]

$$A_3(0) = -iK^*A_4{}^*(0) [\sin wL/(w \cos wL + \alpha_R \sin wL)] \tag{8}$$

$$K^* = i\alpha_0 [(1-i\delta)/(1 + \delta^2)] (2A_1 A_2/I_S)/(1 + 4I/I_S)^{3/2} \tag{9}$$

$$\alpha = \alpha_0 [(1 - i\delta)/(1 + \delta^2)] (1 + 2I/I_S)/(1 + 4I/I_S)^{3/2} = \alpha_R - i\alpha_I \tag{10}$$

$$w = (|K|^2 - \alpha_R{}^2)^{1/2} \tag{11}$$

α_0 is the line-center small-signal field attenuation or gain coefficient, I_S is the saturation intensity for the detuning from line center δ, and I is the intensity of the pump waves ($I_1 = I_2 = I$). If the frequency of the interacting waves is on resonance with the atomic transition of the medium, then $\delta = 0$ and w is imaginary. From Equation (8), we obtain the phase of the phase conjugator for degenerate four-wave mixing on resonance with a saturable absorber or gain medium,

$$\phi_0 = 0 \text{ for } \alpha_0 > 0$$

$$= \pi \text{ for } \alpha_0 < 0 \tag{12}$$

Experiment

To measure the phase of the phase-conjugate reflection ϕ_0, we use the experimental setup shown in Figure 1. Light from a laser is split by beamsplitter BS into two arms of an interferometer. In the reference arm of the interferometer, the light transmitted by BS passes through a photorefractive crystal XTL, and is retroreflected by mirror M1. This provides the counterpropagating pump waves for degenerate four-wave mixing in the crystal. In the signal arm of the interferometer, the light reflected by BS is then reflected by mirror M2 to provide the probe beam for degenerate four-wave mixing. The intensity measured by detector D is given by

$$I = I_1 + I_2 - 2\sqrt{I_1 I_2} \cos \phi_0 \tag{13}$$

where I_1 and I_2 are the intensities of the combining waves. This equation indicates that the operating point of this interferometer is completely determined by the absolute phase of the phase conjugator ϕ_0, and is independent of phases of the pumping and probe waves.
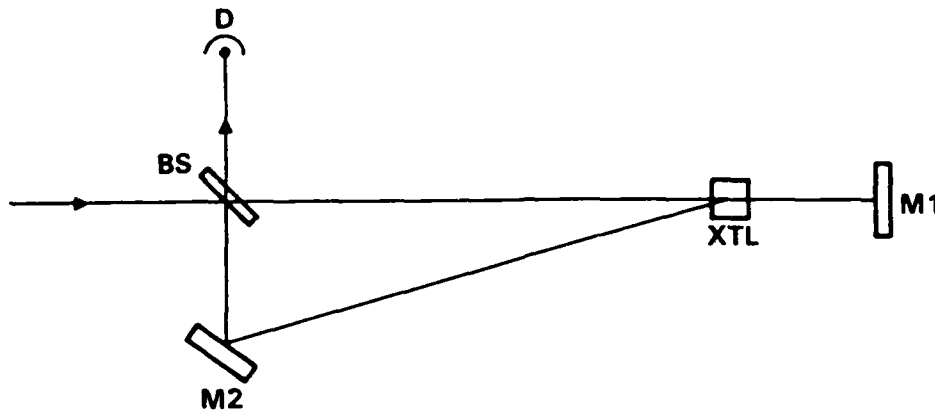
Figure 1. Experimental setup used to measure the absolute phase of phase conjugators.

To derive Equation (13), we consider a light wave of unit amplitude that is incident on the beamsplitter BS. The amplitudes of the transmitted and externally reflected waves are then t and r, respectively. The amplitudes of the pumping waves at the crystal are $te^{i\Phi_1}$ and $te^{i\Phi_2}$, and the amplitude of the probe wave is $re^{i\Phi_4}$, where the phase factors Φ describe the accumulated phase for propagation from the beamsplitter to the nonlinear medium. These three waves interact in the nonlinear medium to produce a phase-conjugate wave with an amplitude A_3,

$$A_3 = \rho t^2 r^* e^{i(\phi_0 + \Phi_1 + \Phi_2 - \Phi_4)} \tag{14}$$

where ρ is a real constant describing the reflectivity of the phase conjugator. When this wave returns to the beamsplitter, it combines with the wave retroreflected by mirror M1 to produce an intensity I at the detector D given by

$$I = \left| \rho t^2 r^* e^{i(\phi_0 + \Phi_1 + \Phi_2)} + tr'e^{i(\Phi_1 + \Phi_2)} \right|^2 \tag{15}$$

where r' is the amplitude reflection coefficient for internal reflection from the beamsplitter. Using the Stoke's relation $tr^* = -t^*r'$, we can obtain Equation (13) from Equation (15).

In principle, ϕ_0 can be determined from a measurement of the intensities. However, in practice, the uncertainties in measuring the intensities do not allow for an accurate determination of ϕ_0. A more accurate determination can be made by modulating the phase of the cosine term at a frequency ω and measuring the ration R of the fundamental power to the second harmonic power at the detector. In the experiment, a piezoelectric transducer is attached to the mirror M2 to produce a phase modulation $\phi_m \sin \omega t$. The phase modulation is faster than the response time of the nonlinear medium in which the degenerate four-wave mixing takes place so that it is not compensated by phase conjugation. The amplitude of the phase modulation is small ($\phi_m \ll \pi$) so that the gratings involved in the degenerate four-wave mixing are not washed out. The time varying intensity at the detector D is proportional to,

$$-\cos(\phi_0 + \phi_m \sin \omega t) \tag{16}$$

From this equation, we obtain the ratio R of the fundamental power to the second harmonic power

$$R = [J_1(\phi_m)/J_2(\phi_m)] \tan\phi_0 \tag{17}$$

where J_1 and J_2 are Bessel functions. For $\phi_m \ll \pi$, the absolute phase shift of the phase-conjugate reflection is given by

$$\phi_0 = \tan^{-1}(R\phi_m/4) \tag{18}$$

Results

Using the technique described above, we have measured the phase shift of the phase-conjugate reflections from barium titanate, strontium barium niobate and ruby. Our results are given in Table 1, where θ is the angle between the grating k vector and the crystal axis.

Table 1. Phase of Phase-Conjugate Reflections

Material	θ	ϕ_0
$BaTiO_3$	0°	$(19 \pm 3)°$
	45°	$(6 \pm 4)°$
	135°	$(176 \pm 3)°$
	180°	$(164 \pm 3)°$
SBN	0°	$(3 \pm 3)°$
	180°	$(175 \pm 5)°$
Ruby	—	$(80 \pm 5)°$

For the photorefractive materials $BaTiO_3$ and SBN, the measured values of ϕ_0 compare well with the expected values from Equation (4). The differences between the expected values $\phi_0 = 0°$ and 180°, and the measured values $\phi_0 = (19 \pm 3)°$ and $(164 \pm 3)°$ for $BaTiO_3$ at $\theta = 0°$ and 180° indicate that the index grating is not shifted by exactly $\pi/2$ radians, as is often assumed. We have verified this fact by an independent measurement of the two-wave mixing gain Γ as a function of the frequency detuning between the two waves. The fact that for ruby, ϕ_0 is close to 90°, indicates that the grating involved is predominantly an index grating rather than an absorption grating.

Summary

We have presented theoretical expressions and experimental measurements of the absolute phase shifts of phase conjugators. Photorefractive media, transparent media, saturable absorbers and saturable amplifiers were considered in the analysis. Experimental measurements of the absolute phase shifts for barium titanate, strontium barium niobate and ruby are in good agreement with the theory.

Acknowledgements

References

1. Fisher, B., Cronin-Golomb, M., White, J., and Yariv, A., "Amplified Reflection, Transmission, and Self-oscillation in Real-time Holography," Opt. Lett., Vol. 6, pp. 519-521. 1981.

2. Yariv, A. and Pepper, D, "Amplified Reflection, Phase Conjugation, and Oscillation in Degenerate Four-Wave Mixing," Opt. Lett., Vol. 1, pp. 16-18. 1977.

3. Abrams, R. and Lind, R., "Degenerate Four-Wave Mixing in an Absorbing Media," Opt. Lett., Vol. 2, pp. 94-96. 1978; "Errata," Opt. Lett., Vol. 3, p 205. 1978.

APPENDIX 4.15

PARALLEL IMAGE SUBTRACTION USING A PHASE-CONJUGATE
MICHELSON INTERFEROMETER

Parallel image subtraction using a phase-conjugate Michelson interferometer

Arthur E. Chiou and Pochi Yeh

Rockwell International Science Center, Thousand Oaks, California 91360

A phase-conjugate Michelson interferometer using an internally self-pumped barium titanate crystal as reflectors has been constructed to perform parallel image subtraction, intensity inversion, and exclusive OR logic operation. These operations are independent of the optical path differences and phase aberration.

We report parallel image subtraction, exclusive OR (XOR) logic operation, and intensity inversion using a phase-conjugate Michelson interferometer that consists of a beam splitter and a phase-conjugate reflector in place of the usual interferometer mirrors (see Fig. 1). Such an interferometer is equivalent to the double phase-conjugate interferometer and also exhibits time reversal.[1]

Image subtraction has been a subject of considerable interest in signal processing. Electronic digital processing of images is slow because of its serial nature. Optical techniques offer the capability of parallel processing over the entire images. The parallel processing is versatile and inherently faster. The technique of optical image synthesis by the addition and subtraction of the complex amplitude of light was first described by Gabor *et al.*[2] The basic principle consists of spatially modulating the two images by periodic waves that are mutually shifted by a phase of 180 deg.[3,4]

Although there are other techniques of image subtraction,[5-8] interferometers such as the Mach–Zehnder or Michelson offer convenient ways for the addition and subtraction of the complex amplitude of images.[9-11] In the interferometric methods the subtraction is obtained by introducing the two images symmetrically in the two arms of the interferometer where a path difference corresponding to π phase shift exists between them. It is known that the interferometers are extremely difficult to adjust and that they cannot easily maintain the fixed path difference. In addition, only the center fringe is useful for image subtraction or addition. In many cases the center fringe is not large enough to cover all the images. The new method of parallel image subtraction by phase-conjugate interferometry described in this Letter eliminates these two problems.

In our phase-conjugate Michelson interferometer, a plane wave with amplitude E is divided into two by the beam splitter BS$_2$. Each of these two beams passes through a transparency and is then reflected by a self-pumped BaTiO$_3$ phase conjugator.[12-15] When these two phase-conjugated beams recombine at the beam splitter, image subtraction is obtained at the usual interferometer output port A (see Fig. 1). Let the

reflection coefficient of the phase conjugator be ρ.[16] The image intensity at the output port A is given by

$$I_A(x, y) = |E|^2|\rho|^2|t^*r'T_1(x, y) + r^*tT_2(x, y)|^2, \quad (1)$$

where r and r' are the amplitude reflection coefficients of the beam splitter BS$_2$ for beam incidence from the left and right sides, respectively; t is the amplitude-transmission coefficient; * denotes complex conjugation; and $T_1(x, y)$ and $T_2(x, y)$ are the intensity-transmittance functions of transparencies 1 and 2, respectively. Using Stokes's relation[17]

$$r't^* + r^*t = 0, \quad (2)$$

Eq. (1) for the intensity at the output port becomes

$$I_A(x, y) = |E|^2|\rho|^2RT|T_1(x, y) - T_2(x, y)|^2, \quad (3)$$

where R and T are intensity reflectance and transmittance, respectively, of the beam splitter BS$_2$. Note that the output intensity is proportional to the square of the difference of the intensity-transmittance functions.

The 180-deg phase shift between the two images as dictated by the Stokes's relation plays a crucial role in this image-subtraction technique. The Stokes relation holds for any lossless dielectric mirror and results directly from the time reversal. Such a relation was first predicted by Stokes[18] in the nineteenth century and was not proved experimentally until recently by using phase-conjugate reflectors.[1] The phase-conju-
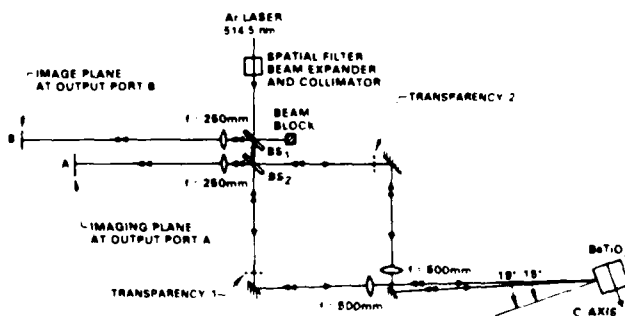

Fig. 1. Schematic diagram illustrating the basic idea of coherent image subtraction and addition by a phase-conjugate Michelson interferometer.

$I_1 \propto |T_1|^2$ $I_2 \propto |T_2|^2$ $I_A \propto |T_1 - T_2|^2$

$I_1 \propto |T_1|^2$ $I_2 \propto |T_2|^2$ $I_B \propto |T_1 + T_2|^2$
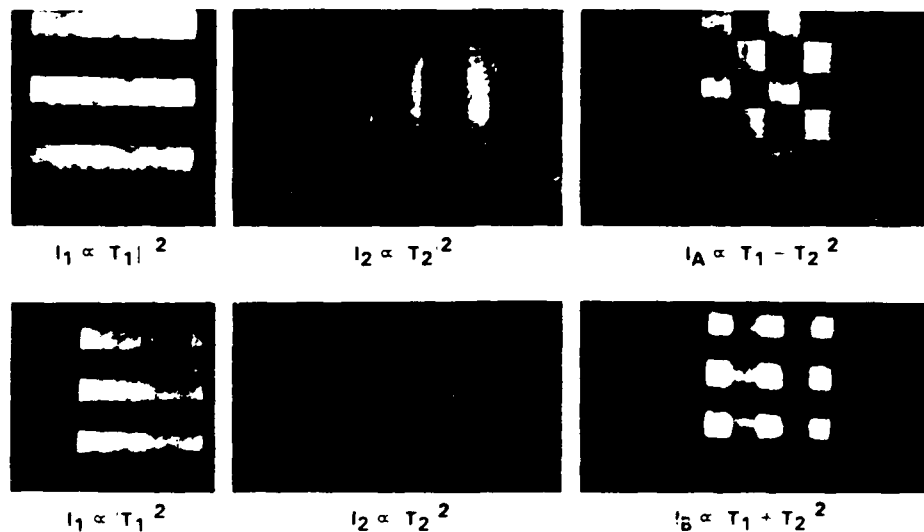
Fig. 2.   Experimental results for the image subtraction and addition by the phase-conjugate Michelson interferometer. The horizontal and the vertical bars are the images of transparencies 1 and 2, respectively, when the illuminating beam for the other arm is blocked. The checkerboard patterns at upper and lower right are the intensity distribution of the coherent subtraction and addition, respectively, of the two images.

gation process also eliminates the problems of phase distortion and the critical alignment requirement associated with conventional interferometry.

At the image plane B (see Fig. 1) the intensity distribution is given by

$$I_B(x, y) = |E|^2 |\rho|^2 |TT_1(x, y) + RT_2(x, y)|^2. \quad (4)$$

In our experiment, an argon-ion laser (514.5 nm) with output power of a few hundred milliwatts is used as the coherent light source. The laser output, after spatial filtering through a 5× microscope objective and a 25-μm-diameter aperture, is expanded and collimated to a 1-cm-diameter beam size. The collimated beam is split into two by beam splitters BS_2 (intensity transmittance, 64%) to illuminate the two transparencies (the horizontal and the vertical triplet bars from the U.S. Air Force Resolution Chart). They are then redirected and focused (f-number, f/50) onto the a face of a BaTiO$_3$ crystal with angles of incidence of approximately 15 and 19 deg. These beams are polarized in the xz plane (i.e., the plane of incidence) and excite only extraordinary wave in the crystal. Both beams self-pump the crystal and are phase conjugated with a reflectance of about 32%. Each of the phase-conjugated beams retraces its incoming path backward through the transparencies, and the two recombine at the beam splitter BS_2. Note that the beam splitter BS_1 simply serves physically to separate the output port B from the input. It is not part of the interferometer. At each of the interferometer output ports, a lens (f-number, f/25) is used to image both objects onto the image plane.

We have experimentally demonstrated that the two images are subtracted from each other in the image plane A and are added together in the image plane B. These operations are independent of the optical path lengths of the two arms of the interferometer. According to Eq. (4), the addition of the two images is

performed with weighing factors T and R, respectively. The subtraction, however, is independent of the ratio of R and T. Typical experimental results are shown in Fig. 2. The horizontal and the vertical bars in the upper photos are the images at output port A(see Fig. 1) of transparencies 1 and 2, respectively, when the illuminating beam for the other arm is blocked. The upper right checkerboard pattern represents the coherent subtraction of the two images due to destructive interference when both illuminating beams are present. Note that the intensity distribution where subtraction takes place is fairly uniform and is very close to that of the true dark background (four dark squares where the dark regions of the bars overlap). The lower photos are the corresponding results at output port B where image addition takes place.

The image subtracter can also perform logic operation. Consider the case when both transparencies are either 1 or 0. According to Eq. (3), a complete cancellation would require that these two transparencies be identical. An output intensity of 1 will appear at port A when only one of these two transparencies transmits. Thus such an image subtracter can act as an XOR gate. The truth table of such a logic operation is given in Table 1. In the case when the transparencies are encoded with a matrix of binary data, such an

Table 1.   The Logic Operations Represented by the Intensity I_A

T_1	T_2	$I_A \propto |T_1 - T_2|^2$
1	1	0
1	0	1
0	1	1
0	0	0

(a)   (b)   (c)
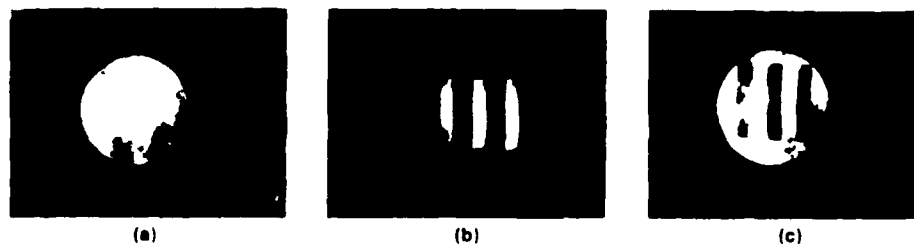
Fig. 3.   Experimental results for the intensity inversion: (a) intensity distribution of the phase-conjugate beam in the first
arm with the transparency removed. (b) image of the transparency in the second arm. and (c) the intensity inversion of (b). (a)
$I_1 \propto |T_1(x,y)|^2 = 1$, (b) $I_2 \propto |T_2(x,y)|^2$, (c) $I \propto |T_1(x,y) - T_2(x,y)|^2 = |1 - T_2(x,y)|^2$.
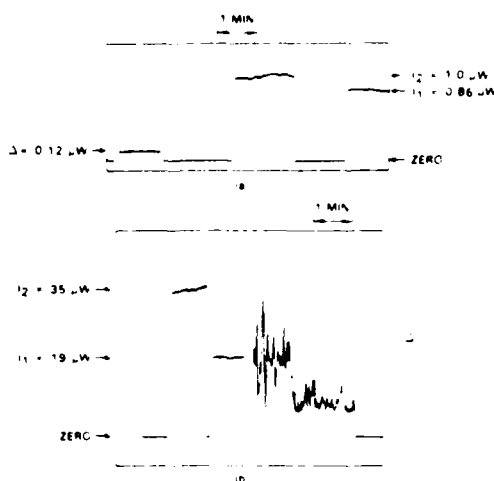

Fig. 4.   Temporal fluctuation of the intensity of each image
and their coherent subtraction for (a) a phase-conjugate
Michelson interferometer. (b) a Mach–Zehnder interferom-
eter with regular mirrors. Δ is the signal output at the sub-
traction port.

image subtracter acts as a two-dimensional array of
XOR gates.

A special case of image subtraction is intensity in-
version. which is obtained by removing one of the
transparencies so that the transmittance $T_i(x, y)$ be-
comes unity in one arm. The experimental result is
shown in Fig. 3.

The temporal stability of the subtracted image in-
tensities is compared in Fig. 4 for the case of an inter-
ferometer with a phase conjugator and that of one with
regular mirrors. For both cases, the centermost
square of the checkerboard pattern (the upper right in
Fig. 2) is imaged on the detector through a circular
aperture with diameter slightly smaller than the side
of the square. The temporal evolution of intensity I_1
and I_2 is recorded in turn when the illuminating beam
in the other arm is blocked. The intensity difference
Δ is then recorded when both beams are present. The
improvement in temporal stability of the subtracted
image intensity is dramatic.

In conclusion. we have demonstrated coherent im-
age subtraction. intensity inversion. and exclusive OR
logic operation using a phase-conjugate Michelson in-

terferometer. The experimental results can be ex-
plained theoretically by the principle of time reversal.

Similar work has been carried out independently by
Kwong et al.[19] and was reported recently.

References

1. M. D. Ewbank. P. Yeh. M. Khoshnevisan. and J. Fein-
berg. Opt. Lett. 10, 282 (1985).
2. D. Gabor. G. W. Stroke. R. Restrick. A. Funkhouser. and
D. Brumm. Phys. Lett. 18, 116 (1965).
3. See. for example. J. F. Ebersole. Opt. Eng. 14, 436 (1975).
4. See. for example. G. Idebetouw. L. Bernardo. and M.
Miller. Appl. Opt. 19, 1218 (1980).
5. Y. H. Ja. Opt. Commun. 42, 377 (1982).
6. C. P. Grover and R. Tremblay. Appl. Opt. 21, 2666
(1982).
7. C. Warde and J. I. Thackara. Opt. Lett. 7, 344 (1982).
8. G. G. Mu. C. K. Chiang. and H. K. Liu. Opt. Lett. 6, 389
(1981).
9. K. Matsuda. N. Takeya. T. Tsujiuchi. and M. Shimoda.
Opt. Commun. 2, 425 (1971).
10. K. Patroski. S. Yokozeki. and T. Suzuki. Nouv. Rev.
Opt. 6, 25 (1975).
11. W. T. Cathey. Jr.. and J. G. Doidge. J. Opt. Soc. Am. 56,
1139 (1966).
12. J. O. White. M. Cronin-Golomb. B. Fischer. and A.
Yariv. Appl. Phys. Lett. 40, 450 (1982).
13. M. Gronin-Golomb. B. Fischer. J. O. White. and A.
Yariv. Appl. Phys. Lett. 41, 689 (1982).
14. J. Feinberg. Opt. Lett. 7, 486 (1982).
15. K. R. McDonald and J. Feinberg. J. Opt. Soc. Am. 73,
458 (1983).
16. These two beams enter the BaTiO$_3$ phase conjugator at
the same spot with approximately the same angle of
incidence and are considered parts of a composite beam.
Thus the assumption of a unique phase-conjugate re-
flectivity is legitimate. This has also been proved ex-
perimentally.
17. Z. Knittl. Optics of Thin Films (Wiley. New York. 1976).
p. 242.
18. G. G. Stokes. Camb. Dubl. Math. J. 4, 1 (1849).
19. S. K. Kwong G. A. Rakuljuc. and A. Yariv. Appl. Phys.
Lett. 48, 201 (1985).

APPENDIX 4.16

PHASE-CONJUGATE FIBER OPTIC GYRO

Phase-conjugate fiber-optic gyro

Pochi Yeh, Ian McMichael, and Monte Khoshnevisan

Rockwell International Science Center, 1049 Camino Dos
Rios, Thousand Oaks, California 91360.
Received 23 December 1985.
0003-6935/86/071029-02$02.00/0.
© 1986 Optica Society of America.

Several types of phase-conjugate gyro are proposed in the literature.[1-4] In this Letter, we describe a new type of fiber-optic gyro that uses the phase-reversal property of polarization-preserving phase conjugation. Although the insensitivity of phase-conjugate gyros to reciprocal phase shifts and their sensitivity to nonreciprocal phase shifts such as the Faraday effect have been reported,[3,4] to date no one has demonstrated rotation sensing. In this Letter, we report the first demonstration of rotation sensing with a phase-conjugate gyro.

Polarization scrambling is a well-known source of signal fading and noise in fiber-optic gyros. Polarization-preserving fibers and couplers must be used to decouple the two states of polarization and hence improve the sensitivity.[5] In the phase-conjugate fiber-optic gyro, a polarization-preserving phase conjugator is used to restore the severely scrambled waves to their original state of polarization.[6-8] This eliminates the signal fading and noise due to polarization scrambling without the need for polarization-preserving fiber.

Referring to Fig. 1, we consider a phase-conjugate Michelson interferometer[9] in which a fiber loop is inserted in the arm that contains the phase-conjugate reflector ϕ^*. We now examine the phase shift of light as it propagates along the fiber. From point A to point B, the light experiences a phase shift of

$$\phi_1 = kL - \frac{2\pi RL\Omega}{\lambda c} ,\qquad (1)$$

where $k = (2\pi n)/\lambda$ is the wave number and L is the length of fiber, R is the radius of the fiber coil, Ω is the rotation rate, λ is the wavelength, and c is the velocity of light. The second term in Eq. (1) is due to rotation. In the return trip, the phase shift is

$$\phi_2 = kL + \frac{2\pi RL\Omega}{\lambda c} ,\qquad (2)$$

where we notice that the term due to rotation is reversed because of the change in propagation direction relative to the rotation. If there were no phase conjugation, the total round-trip phase shift due to regular mirror reflection would be $2kL$. However, because of the phase reversal on phase-conjugate reflection, the round-trip phase shift becomes
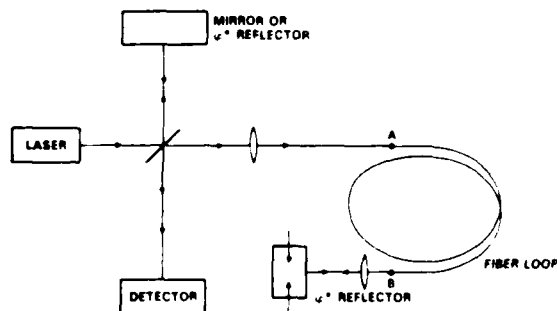
$$\phi = \frac{4\pi RL\Omega}{\lambda c} .\qquad (3)$$

This phase shift can be measured by using the interference with the reference beam from the other arm. Notice that as a result of the phase reversal on reflection, the reciprocal phase shift kL is canceled on completion of a round trip. The net phase shift left is due to anything nonreciprocal such as rotation.

This net phase shift is proportional to the rotation rate and can be used for rotation sensing. In addition, if the phase-conjugate reflector is polarization-preserving,[6-8] it will produce a true time-reversed version of the incident wave and will undo all the reciprocal changes (e.g., polarization scrambling, modal aberration, temperature fluctuation) when the light completes the round trip in the fiber. Since the polarization scrambling and modal aberration of multimode fibers can be corrected by polarization-preserving phase conjugation, multimode fibers can replace the polarization-preserving single-mode fiber in this new type of gyro.

Figure 2 shows a schematic diagram of the experimental setup used to demonstrate the phase-conjugate fiber-optic gyro. Since this experiment does not use a polarization-preserving phase-conjugate mirror, it does not demonstrate the correction of polarization scrambling. However, the experiment does measure the phase shift described by Eq. (3). A highly reflective beam splitter $BS1$ isolates the argon laser from retroreflections of its output. The light reflected by $BS2$ is focused by lens $L1$ (60-cm focal length) into a crystal of barium titanate to provide the pumping waves for degenerate four-wave mixing (DFWM). The light transmitted by $BS2$ is split into two arms of a Michelson interferometer by $BS5$. One arm of the interferometer contains a 10-cm radius coil of ~7 m of optical fiber. Since the phase-conjugate mirror in this experiment is not polarization-preserving, we use single-mode polarization-preserving optical fiber. Light exiting the fiber provides the probe wave for DFWM. The c-axis of the barium titanate crystal is parallel to the long faces of the crystal and points in the direction of beam splitter $BS3$. The pumping waves from mirrors $M2$ and $M3$ have powers of 18 and 3 mW, respectively, and their angle of incidence is ~45°. The probe wave, exiting from the end of the fiber loop, makes a small angle (<10°) with the pumping wave from mirror $M2$ and has a power of 0.7 mW. Under these conditions we obtain a phase-conjugate reflectivity of 50% and a response time of 0.1 s. The reference arm of the interferometer is terminated by a mirror $M4$ mounted on a piezoelectric transducer so that the operating point of the interferometer can be set at quadrature. Light from both arms combines to form complementary fringe patterns at detectors $D3$ and $D4$. Detectors $D1$ and $D2$ measure the powers in the recombining waves.

The fiber coil is rotated with the rest of the setup remaining fixed at various rotation rates [first clockwise (CW), then
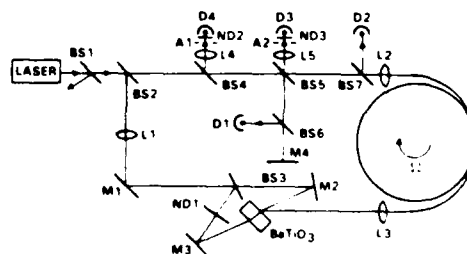
Fig. 1. Schematic drawing of the phase-conjugate fiber-optic gyro.

Fig. 2. Experimental setup of the phase-conjugate fiber-optic gyro.
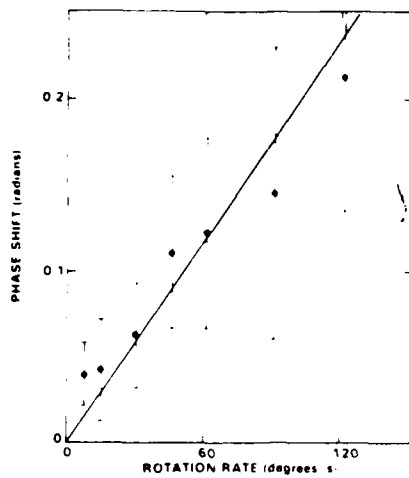
Fig. 3. Measured phase shift as a function of applied rotation rate.

counterclockwise (CCW), etc.] in a square wave fashion for 10 cycles with an amplitude of 120°. The measured powers from all detectors are used to calculate the average phase shift between rotation in the CW and CCW directions of rotation. Figure 3 shows a plot of the measured phase shift as a function of the rotation rate. The solid line indicates the expected rotation-induced Sagnac phase shift. The large uncertainty in the data is due to rapid (faster than the response time of the DFWM) phase changes that are produced by the twisting of the fiber when the fiber loop is rotated and that act as a source of noise.

In conclusion, we have proposed a new type of fiber-optic gyro that uses polarization-preserving optical phase conjugation, and we have presented the first demonstration of rotation sensing by a phase-conjugate gyro.

References

1. J.-C. Diels and I. C. McMichael. "Influence of Wave-Front-Conjugated Coupling on the Operation of a Laser Gyro." Opt. Lett. 6, 219 (1981).
2. P. Yeh. J. Tracy. and M. Khoshnevisan. "Phase-Conjugate Ring Gyroscopes." Proc. Soc. Photo-Opt. Instrum. Eng. 412, 240 (1983).
3. C. J. Bode. "Phase Conjugate Optics and Applications to Interferometry and to Laser Gyroscope." in *Experimental Gravitation and Measurement Theory.* P. Meystre and M. O. Scully. Eds (Plenum. New York. 1983), pp. 269–291.
4. B. Fischer and Shmuel Sternklar. "New Optical Gyroscope Based on the Ring Passive Phase Conjugator." Appl. Phys. Lett. 47, 1 (1985).
5. W. K. Burns. R. P. Moeller. C. A. Villarruel. and M. Abebe. "Fiber Optic Gyroscopes with Polarization Holding Fiber." Opt. Lett. 8, 540 (1983).
6. P. Yeh. "Scalar Phase Conjugation for Polarization Correction." Opt. Commun. 51, 195 (1984).
7. I. McMichael and M. Khoshnevisan. "Scalar Phase Conjugation Using a Barium Titanate Crystal." in *Technical Digest. Conference on Lasers and Electro-Optics* (Optical Society of America. Washington. D.C.. 1985). paper THN1.
8. I. McMichael. M. Khoshnevisan. and P Yeh. "Polarization-Preserving Phase Conjugator." submitted to Opt. Lett.
9. M. D. Ewbank. M. Khoshnevisan. and P. Yeh. "Phase-Conjugate Interferometry." Proc. Soc. Photo-Opt. Instrum. Eng. 464, 2 (1984).

APPENDIX 4.17

FREQUENCY SHIFT OF SELF-PUMP0ED PHASE CONJUGATOR

Frequency shifts of self-pumped phase conjugators

M. D. Ewbank and P. Yeh

Rockwell International Science Center
1049 Camino Dos Rios, Thousand Oaks, California 91360

Abstract

The reflection from most photorefractive, self-pumped phase conjugators differs in frequency from the incident beam by a small amount ($\Delta\omega/\omega \sim 10^{-15}$). A theory and the supporting experiments which explain such frequency shifts are presented. In our theory, four-wave mixing is responsible for the generation of the conjugated wave where a self-oscillation arising from photorefractive coupling provides the customary pumping beams. The frequency of these pumping beams is determined by a resonance cavity geometry and may be slightly different from that of the incident beam. Nondegenerate four-wave mixing using these self-oscillating pumping beams give rise to the frequency shift of the phase-conjugate reflection. Experimental results are in good agreement with theory.

Introduction

Self-pumped phase-conjugate reflectors[1-3] using photorefractive BaTiO$_3$ have recently received considerable attention because 30-50% reflectivities are relatively easy to achieve even with low-power lasers. In self-pumped (or passive) phase conjugators, the counter-propagating pumping beams needed in the four-wave mixing process are automatically generated by light photorefractively diffracted out of the incident beam. However, the phase-conjugate reflection is generally shifted slightly in frequency when compared to the incident beam (on the order of 1 Hz depending on intensity). This frequency shift has been attributed to moving photorefractive gratings which Doppler shift the diffracted light.[4] The physical mechanism, which is responsible for the moving gratings, is, however, not well understood.

The frequency shift first manifested itself as a frequency scanning when self-pumped BaTiO$_3$ was coupled to a dye laser.[4-6] Since those initial observations, numerous experiments and theories involving self-pumped phase conjugators and/or photorefractive resonators have addressed, either directly or indirectly, the frequency shift issue.[7-16] However, a general theory and the conclusive experiments are not available.

In this paper we present a theory and the supporting experiments which explain such frequency shifts of most self-pumped phase conjugators. In our theory, self-pumped phase conjugation results from an internal self-oscillation. The optical resonance cavity which supports such oscillation is formed by either external mirrors or crystal surfaces. The oscillating beams provide the counterpropagating pump beams which are required in the four-wave mixing process. The theory shows that despite the narrow gain bandwidth of the photorefractive two-wave coupling, internal oscillation can still occur over a large range of cavity length detuning. The frequency shift is proportional to the cavity length detuning. Such a dependence is explained by a photorefractive phase shift that is due to slightly nondegenerate two-wave mixing. The additional photorefractive phase shift compensates for cavity length detuning and satisfies the round-trip phase condition for steady-state oscillation.

When the self-pumping beams are spontaneously generated via photorefractive coupling in a linear resonance cavity with two external mirrors on opposite sides of a photorefractive crystal such as BaTiO$_3$, we observe that the frequency shift of the phase-conjugate reflection is directly proportional to cavity-length detuning. In the case where the self-pumping beams arise from internal reflections off the photorefractive crystal's surfaces, we experimentally prove that a previous description[2] of the self-pumping process is inadequate and we show that a closed-looped resonance cavity forming inside the crystal is a better description.

Theory

The theory is an extension of our earlier theory on unidirectional photorefractive ring oscillators.[16] In this theory, amplification owing to holographic two-wave mixing in the photorefractive crystal is responsible for the self-oscillation. When the configuration of the resonance cavity relative to the crystal supports bi-directional oscillation, a phase-conjugate beam is generated via the four-wave mixing process. The parametric two-wave mixing gain, defined as the output to input intensity ratio, is given by[16]

$$g = \frac{1 + m}{1 + me^{-\gamma\ell}} \; e^{-\alpha\ell} = g_o e^{-\alpha\ell} \quad , \tag{1}$$

where m is the ratio of the pump beam intensity to oscillating beam intensity, α is the bulk absorption coefficient, ℓ is the length of interaction γ is the intensity coupling constant, and g_o is the gain where there is no loss. For crystals such as $BaTiO_3$, this gain can be several thousand per pass. Thus oscillation can be sustained even in cavities with high scattering, diffraction, and/or mirror losses.

The phase shift in traversing through the photorefractive medium for the oscillating beam is

$$\frac{2\pi}{\lambda} n_o\ell + \Delta\psi \quad , \tag{2}$$

where $2\pi n_o\ell/\lambda$ is the phase shift in the absence of photorefractive coupling. The additional phase shift, $\Delta\psi$, is due to the photorefractive two-wave coupling and is given by[16]

$$\Delta\psi = -\frac{\beta}{\gamma} \log \left(\frac{1 + m}{1 + me^{-\gamma\ell}}\right) = \frac{-\beta}{\gamma} \log (g_o) \tag{3}$$

where β is the phase-coupling constant.[16] Note that this phase shift, $\Delta\psi$, is independent of absorption losses.

According to a nonlinear model of the photorefractive two-wave mixing, these coupling constants (i.e., β and γ) are given by

$$\gamma = \frac{2\pi n_1}{\lambda \cos\theta} \sin\phi \tag{4}$$

$$\beta = \frac{\pi n_1}{\lambda \cos\theta} \cos\phi \quad , \tag{5}$$

where θ is the half-angle between the pump beam and the oscillating beam. The parameters ϕ and n_1 can be written, respectively,

$$\phi = \phi_o + \tan^{-1} (\Omega\tau) \tag{6}$$

and

$$n_1 = \frac{2}{\sqrt{1 + \Omega^2\tau^2}} \Delta n_s \tag{7}$$

where τ is the decay time constant of the holograph grating, Δn_s is the saturation value of the photoinduced index change for degenerate two-wave mixing, ϕ_o is a constant phase shift related to the nonlocal response of the crystal under fringe illumination, and Ω is the frequency shift between the oscillating and pumping beams. According to Equation (1), amplification is possible (i.e., $g > 1$) only when $\gamma > \alpha$. Note that gain is significant only when $\Omega\tau < 1$. For materials such as $BaTiO_3$ and SBN, τ is typically between 0.1 s and 1.0 s for nominal laser intensities (1-10 W/cm^2). Thus, the gain bandwidth is only a few Hertz. In spite of such an extremely narrow bandwidth, self-oscillation can still be observed easily at "any" cavity length using $BaTiO_3$ crystals as the photorefractive medium. Such a phenomenon can be explained in terms of the additional phase shift (Equation (3)) introduced by the photorefractive coupling. This phase shift is a function of the oscillation frequency. For $BaTiO_3$ crystals with $\gamma\ell > 4\pi$, this phase shift can vary from $-\pi$ to $+\pi$ for a frequency drift of $\Delta\Omega\tau = \pm 1$. Such a phase shift contributes to the round-trip phase shift so that the latter can be an integer times 2π, a condition required for oscillation.

Concerning the initiation of the oscillation in the photorefractive resonator, like laser oscillators, the oscillation starts from noises that are due to physical processes such as scattering and quantum fluctuation. In photorefractive crystals, the scattering dominates the noise contribution. At the beginning, a slight amount of light may be scattered along the direction of the resonator. This slight amount of light will be amplified by the two-wave mixing process in the photorefractive crystal, provided that the frequencies are not appreciably different. As the intensity in the resonator builds up, the beam ratio parameter, m, decreases. The buildup of oscillation intensity leads to a saturation of the gain (see Equation (1) where the gain decreases as m decreases). At steady-state oscillation,

the electric field must reproduce itself, both in phase and intensity, after each round trip. In other words, the oscillation conditions can be written as

$$\Delta\psi + \int kds = 2N\pi \tag{8}$$

and

$$gR = 1 \quad , \tag{9}$$

where $\Delta\psi$ is the additional phase shift owing to photorefractive coupling, the integration is over a round-trip beam path, N is an integer, the parameter R represents the cavity losses (e.g., the product of the mirror reflectivities), and g is the parametric gain of Equation (1).

If we define a cavity-detuning parameter $\Delta\Gamma$ as

$$\Delta\Gamma = 2N'\pi - \int kds \quad , \tag{10}$$

where N' is an integer chosen in such a way that $\Delta\Gamma$ lies between $-\pi$ and $+\pi$, then the oscillation condition (Equation (8)) can be written as

$$\Delta\psi = \Delta\Gamma + 2M\pi \quad , \tag{11}$$

where M is an integer. In other words, oscillation can be achieved only when the cavity detuning can be compensated by the photorefractive phase shift.

Equations (8) and (9) may be used to solve for the two unknown quantities m and Ω. If we fix the pump intensity and the pump frequency, then Equations (8) and (9) can be solved for the oscillation frequency and the oscillation intensity. Substituting Equation (1) for g in Equation (9) and using Equation (3), we obtain

$$\Delta\psi = \frac{\beta}{\gamma} \log (Re^{-\alpha\ell}) \quad . \tag{12}$$

This equation can now be used to solve for the frequency shift Ω. For the case of pure diffusion, using Equation (6) for ϕ with $\phi_0 = \pi/2$ and Equations (4) and (5), we obtain from Equation (12)

$$\Omega\tau = \frac{-2\ \Delta\psi}{\alpha\ell - \log R} = \frac{-2(\Delta\Gamma + 2M\pi)}{\alpha\ell - \log R} \tag{13}$$

where $\Delta\Gamma$ is the cavity detuning and is given by Equation (10). Substituting Equation (1) for g in Equation (9), we can solve for m and obtain

$$m = \frac{1-Re^{-\alpha\ell}}{Re^{-\alpha\ell}-e^{-\gamma\ell}} \quad . \tag{14}$$

Since m must be positive, we obtain from Equation (14) the threshold condition for oscillation

$$\gamma\ell > \gamma_t\ell \equiv \alpha\ell - \log R \tag{15}$$

where γ_t is the threshold parametric gain constant. Since γ is a function of frequency Ω, Equation (15) dictates that the parametric gain is above threshold only in a finite spectral regime. Using Equation (1) for γ, Equation (15) becomes

$$|\Omega\tau| < [\frac{\gamma_0\ell}{\alpha\ell-\log R} -1]^{1/2} \tag{16}$$

where γ_0 is the parametric gain at $\Omega = 0$. Equation (16) defines the spectral regime where the parametric gain γ is above threshold (i.e., $\gamma > \gamma_t$).

We have obtained expressions for the oscillation frequency (Equation (13)) and the spectral regime where the gain is above threshold. The self-oscillation will be sustained only when the parametric gain is greater than the round-trip cavity loss and the oscillation frequency falls within this spectral region. The frequency shift is determined by Equation (13), with $\Delta\Gamma$ being the cavity detuning given by Equation (10). According to Equations

(15) and (16), the resonator can be made to fall below threshold by decreasing the reflectivity, R. When this happens, oscillations ceases.

The $\Delta\Gamma$ in Equation (10) is the cavity detuning and is defined between $-\pi$ and π. However, the photorefractive phase shift (3) can be greater than π. When this happens, the internal oscillation may occur at more than one frequency. These frequencies are given by Equation (13), with $M = 0, \pm 1, \pm 2, \ldots$ etc. In other words, for each cavity detuning $\Delta\Gamma$, the resonator can support multimode oscillation, provided the coupling constant γ_0 is large enough. Note that when $\gamma_0 l$ is large compared to the natural logarithm of the cavity losses, the resonator can oscillate at almost any cavity detuning $\Delta\Gamma$; whereas when $\gamma_0 l$ is small, oscillation occurs only when the cavity detuning is limited to some small region around $\Delta\Gamma = 0$.

The interdependence of the cavity length detuning and the frequency shift between the oscillating and pumping beams is a general property of photorefractive resonators. Such frequency shifts have been measured in unidirectional ring resonators and self-pumped phase conjugators using external mirrors.[15] In these two types of resonators, the cavity length, cavity losses and two-wave mixing gain (via crystal orientation) can be varied in a controlled fashion. The results, described below, show that the frequency shift of the self-oscillation is directly proportional to cavity length detuning for both of these resonators in excellent agreement with the above theory.

In self-pumped phase conjugator using internal reflections, bi-directional internal oscillations must simultaneously be present. These two counterpropagating beams act as the customary pumping beams of the four-wave mixing process. If each of these pumping beams is frequency shifted by Ω, then the generated phase conjugate beam has a frequency shift of 2Ω as required by conservation of energy.

Experiments

Unidirectional Ring Oscillator

Before describing the frequency shift experiments with self-pumped phase conjugators, let's first review similar experiments performed on a unidirectional ring oscillator[15] with only two-wave mixing photorefractive gain. The optical arrangement is shown in Figure 1 where two-wave mixing in BaTiO$_3$ couples light from an argon ion laser into the unidirectional ring cavity, formed by two planar mirrors (M$_1$ and M$_2$ with the former being piezoelectrically (PZT) driven) and a planar beamsplitter (BS$_3$). The unidirectional oscillation in the ring cavity (confined to a single mode by the pinhole aperture[17]) is sampled via the output coupler BS$_3$, its intensity being measured at detector D$_1$ and the frequency shift between the self-oscillating and pumping beams being determined interferometrically using complementary fringe patterns at detectors D$_2$ and D$_3$.
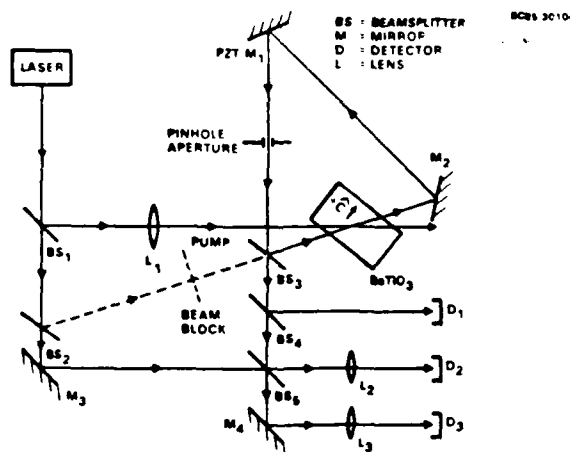
Figure 1 Optical setup for a photorefractive unidirectional ring resonator with variable cavity length. Two-wave mixing coupling in BaTiO$_3$ provides the gain for self-oscillation. The beat frequency between the pumping and self-oscillating beams is derived from the motion of the interferograms at D$_2$ and D$_3$.

Figure 2a shows the beat frequency, along with the ring cavity oscillation intensity, as a function of PZT mirror position or cavity detuning. A slow ramping rate of the PZT mirror is used to mimic steady-state for the two-wave mixing process in the slow photorefractive BaTiO$_3$ while, at the same time, permitting a controlled variation of the ring cavity
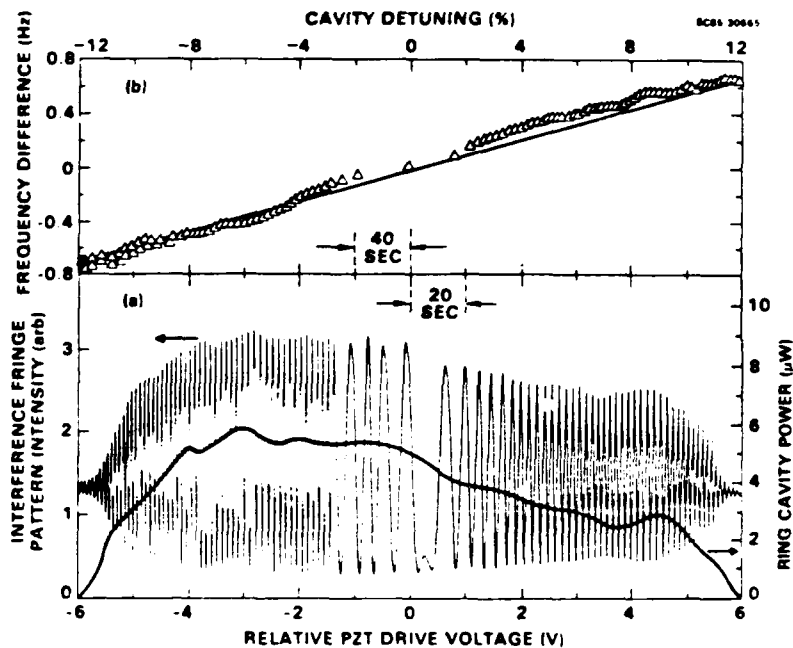
Figure 2 Characteristics of the unidirectional self-oscillation as a function of ring
         cavity length (i.e., PZT voltage or cavity detuning where 100% implies a
         detuning of one full optical wave): (a) ring cavity intensity (right) and
         beat-frequency signature (left); (b) frequency difference between the self-
         oscillation and pumping beam (solid line is a linear least squares fit to
         data).

length. The frequency difference between the pump beam and the unidirectional oscillation,
as observed in the time-variation of the fringe pattern intensity shown in Figure 2a, is
clearly related to position of the PZT mirror. When the mirror is exactly at the correct
position (here, arbitrarily assigned to be the "origin"), the fringe pattern is stationary,
i.e., no frequency shift. The farther the PZT moves away from this "origin," the faster
the fringe motion and, hence, the larger the frequency difference, until the self-
oscillation ceases (recall Equation 16 above). Figure 2b shows the linear dependence of
the frequency difference on cavity detuning, determined from the time intervals between the
maxima in the beat-frequency signature. This dependence agrees with Equation (13). Minor
deviations from the linear behavior could be due to air currents or the nonlinear response
in the PZT. Note that the observed beat-frequency signature vs cavity length also repro-
duces itself periodically as the PZT mirror moves every half optical wavelength (see
Equation (11)).

In the above experiment, unidirectional oscillation is observed only when the ring cavity
length is "tuned" to an appropriate length by the PZT mirror and the beat frequency between
the unidirectional oscillation and pumping beam is directly proportional to the cavity
length detuning. These observations are explained by the theory presented above. Specif-
ically , self-oscillation occurs only when the two-wave mixing gain, which is a function of
the frequency shift, is sufficient to overcome the cavity losses and when the ring cavity
roundtrip optical phase reproduces itself (to within an integer multiple of 2π).

Self-Pumped Phase Conjugator with External Linear Cavity

The frequency shifts in the self-pumped phase conjugator with two external mirrors form-
ing a linear cavity are observed to be very similar to those described above for the unidi-
rectional ring resonator. Specifically, both the sign and magnitude of the frequency shift
can be controlled by the linear cavity length detuning. The optical setup is shown in
Figure 3 where light from a single incident beam is photorefractively coupled by the $BaTiO_3$
crystal into the linear cavity formed between two highly reflecting beam splitters (BS$_8$ and
BS$_9$). This self-oscillation serves as the counterpropagating pumping beams in a tradi-
tional four-wave mixing geometry to phase conjugate the incident beam.[1]
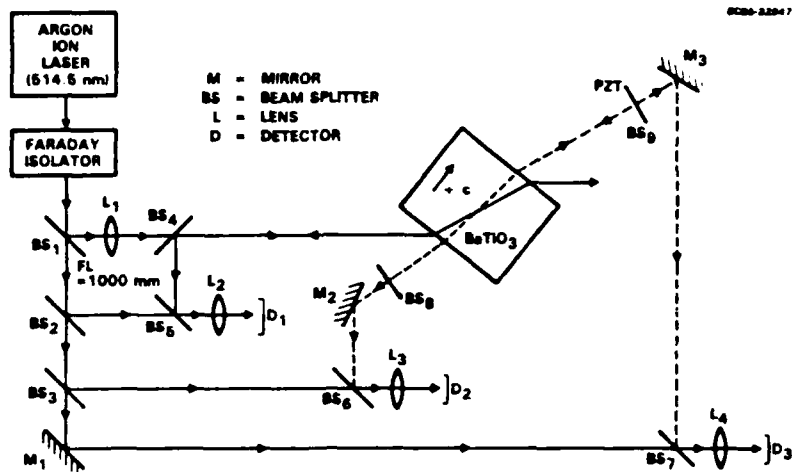
Figure 3 Optical setup for a self-pumped phase conjugator with external linear cavity. Photorefractive coupling in BaTiO$_3$ generates the self-oscillations in the resonant cavity (with variable length) formed by beam splitters BS$_8$ and BS$_9$. The beat frequencies for the phase-conjugate reflection and both of the two counter-propagating self-oscillations (relative to the incident beam) are derived from the motion of the interferograms at D$_1$, D$_2$ and D$_3$, respectively.

While only two-wave mixing occurs in the unidirectional ring oscillator previously described, both two- and four-wave mixing are occurring simultaneously in this self-pumped phase conjugator with external mirrors forming a linear cavity. The photorefractive coupling process is considerably more complicated in this latter situation.

As illustrated in Figure 3, the frequency shifts (relative to the incident beam) appearing on the phase-conjugate reflection and the two counterpropagating self-oscillations are simultaneously measured at detectors, D$_1$, D$_2$ and D$_3$, using the same interferometric techniques described in the unidirectional ring oscillator experiment. The resulting beat-frequency signatures, as a function of linear cavity length detuning, are shown in Figure 4 for the phase-conjugate reflection and one self-oscillating beam. Note that the other counter-propagating self-oscillation beat-frequency signature appears identical to the one shown.
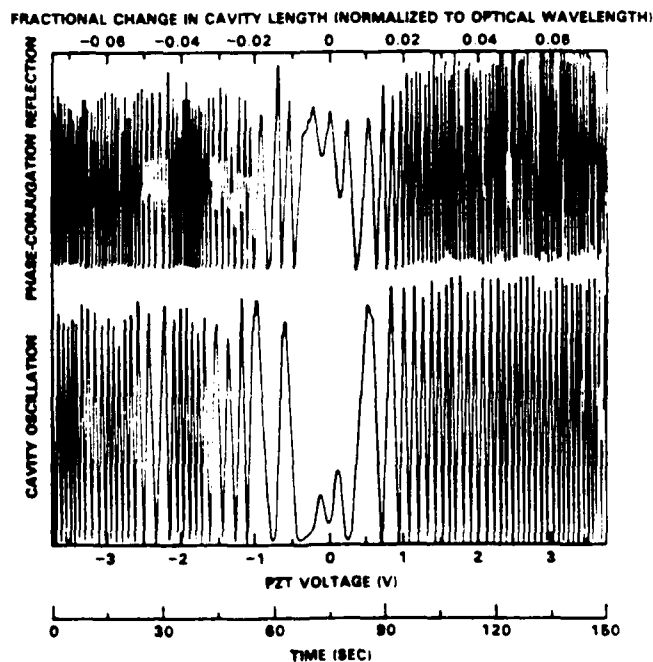
Figure 4 Self-pumped phase conjugator with external linear cavity: Dependence of the beat frequencies (relative to the incident beam) for the phase-conjugate reflection (top) and one self-oscillation (bottom) on cavity length detuning.

Regarding the beat-frequency signatures shown in Figure 4, two important features are evident. First, the frequency shift of the phase-conjugate reflection is exactly a factor of two larger than that of either self-oscillation. In fact, this is simply the conservation of energy constraint for slightly nondegenerate four-wave mixing when the two counterpropagating pump beams are the same frequency.[18] Second, the signs and magnitudes of the beat frequencies of the phase-conjugate reflection and the counterpropagating self-oscillations depend on the external linear cavity length detuning, similar to the unidirectional ring oscillator. That is, the beat frequencies are directly proportional to the detuning (see Equation (13)), becoming faster and faster as the cavity length detuning increases or decreases away from the length that gives no frequency shift.

Two additional observations concerning the beat-frequency signatures are not shown in Figure 4. First, if the cavity length detuning is increased or decreased far enough, the self-oscillation ceases because the frequency shift required by the phase oscillation condition could not be supported by the slow response time of the photorefractive $BaTiO_3$ (i.e., the threshold condition for oscillation as described by Equation (16)). Second, the beat-frequency signatures are periodic in cavity length detuning with the entire patterns repeating for every half wavelength change in PZT beam splitter position (see Equation (11)). Note that both of these effects are also present in the unidirectional ring resonator.

Self-Pumped Phase Conjugator with Internal Reflections

The self-pumped phase conjugator, where the "pumping beams" for the four-wave mixing process arise entirely from internal reflections at the crystal faces instead of external mirrors, is the simplest self-pumped phase conjugator configuration[2] since it does not require any additional optical components. This self-pumped phase conjugator also exhibits a frequency shift in its phase-conjugate reflection.[4]

We have speculated that the frequency shift observed in this self-pumped phase conjugator using internal reflections is due to the "oscillation conditions" (see Equations (8) and (9)) involving an optical resonance cavity,[15,16] just as in the unidirectional ring oscillator and in the self-pumped phase conjugator with an external linear cavity described above. A number of experiments investigating the self-pumped phase conjugator with internal reflections provide conclusive evidence that the aforementioned speculation is indeed the case.

In the first experiment where the optical setup is shown in Figure 5, the frequency shift of the phase-conjugate reflection is compared to frequency shifts on the internal self-pumping beams. The beat frequency of the phase-conjugate reflection is determined in the usual way (i.e., interferometrically) at detector, D_1. The frequency shifts on the internal self-pumping beams are inferred by observing the beat frequency for the scattered light that emanates from the primary self-pumping corner of the crystal. Upon interfering with a portion of the incident beam as shown in Figure 5, this scattered light forms a discernable fringe pattern at detector, D_2, only after it is spatially filtered to some degree by an aperture.

The results of this frequency shift comparison are shown in Figure 6. During the period where the frequency shift of the phase-conjugate reflection is constant, the beat-frequency signature of the scattered light is also reasonably consistent considering the poor quality of the fringe pattern used to make the determination. After taking the average of the time intervals between maxima in the beat-frequency signatures, we note that the frequency shift of the phase-conjugate reflection is approximately twice that of the scattered light. Just as with the self-pumped phase conjugator with an external linear cavity, this factor of two results from conservation of energy for slightly nondegenerate four-wave mixing (assuming, of course, that the frequency shift of the scattered light is the same as the frequency shift of the internal pumping beams). The deviation from two may be due to a multimode oscillation inside the crystal.

Unlike the unidirectional ring resonator and the self-pumped phase conjugator with an external linear cavity, any resonant cavity length in the self-pumped phase conjugator using internal reflections cannot be varied by simply moving a PZT mirror as was done previously. Any resonant cavity in the self-pumped phase conjugator with internal reflections is completely contained inside the photorefractive crystal. In a second experiment, attempts have been made to systematically vary the internal cavity length via thermal expansion by controlling the temperature.[19] The results of this investigation are currently inconclusive because small changes in temperature (< 1°C) induce instabilities in the frequency shift and intensity of the phase-conjugate reflection. We speculate that these instabilities are due to competition between the multiple spatial resonant cavity modes supported by a variety of internal reflections from the crystal surfaces. In the unidirectional ring oscillator and the self-pumped phase conjugator with an external linear cavity, the spatial modes of the resonance cavities were well-defined by the pinhole aperture. In this experiment with the self-pumped phase conjugator using internal reflections, it is impossible to place an aperture inside the crystal for mode selection.
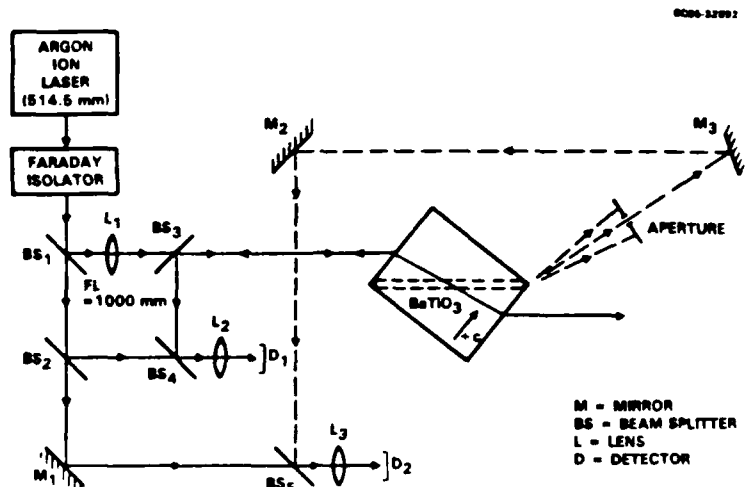
Figure 5   Optical setup for a self-pumped phase conjugator using internal reflections. Photorefractive coupling and internal reflections from the BaTiO₃ crystal surface automatically generate the self-pumping beams inside the crystal. The beat frequencies for the phase-conjugate reflection and the light scattered from the primary self-pumping corner (relative to the incident beam) are derived from the motion of the interferograms at D_1 and D_2, respectively.
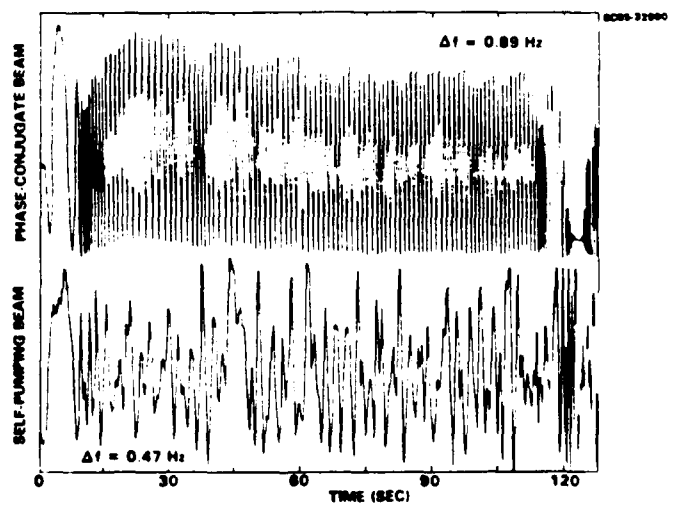

Figure 6   Self-pumped phase conjugator using internal reflections off crystal faces: correlation of the beat frequencies (relative to the incident beam) for the phase-conjugate reflection (top) and the light scattered from the primary self-pumping corner (bottom).

In a third experiment, we conclusively show that the old model[2,12,20] for the self-pumped phase conjugator using internal reflections in BaTiO₃ is incorrect and that the phase oscillation condition associated with a closed-loop resonance cavity is applicable to the self-pumped phase conjugator using internal reflections, as well as the previously described photorefractive resonators.[15] The picture of the old model[2,12,20] for the self-pumped phase conjugator using internal reflections in BaTiO₃ is schematically illustrated in Figure 7.   Simply stated, this model assumed a pair of four-wave mixing interaction regions where two counterpropagating (and mutually phase-conjugated) self-pumping beams

4-WAVE
MIXING

+C
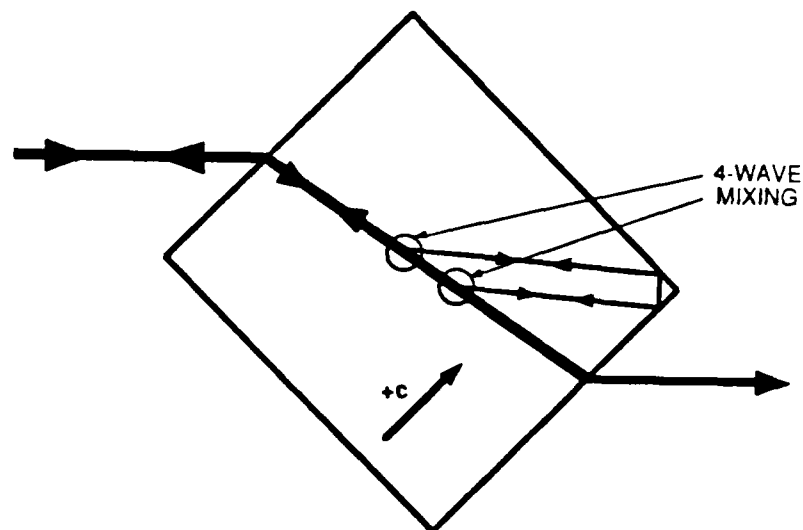
Figure 7   Schematic diagram for the self-pumped phase conjugator using internal
reflections off crystal faces, showing the pair of four-wave mixing
regions where the incident beams interact with the self-pumping beams
to generate the phase-conjugate reflection.

underwent total internal reflection in one corner (the primary self-pumping corner) of the
BaTiO₃ crystal. Using this model, the incident beam and its phase-conjugate reflection can
also serve as the four-wave mixing "pumping beams" to produce the double-phase-conjugate
oscillation[8,9] between the two interaction regions which make up the self-pumping beams.

The accuracy of this old model[2,12,20] can be ascertained by examining the pictures shown
in Figure 8.   An actual micrograph of the interacting beams in self-pumped BaTiO₃ is shown
in Figure 8a and tends to support the old model.   However, by increasing the exposure time
by a factor of ten in the same micrograph, it becomes evident that more than the two self-
pumping beams are present, as shown in Figure 8b.

(a)   (b)   (c)
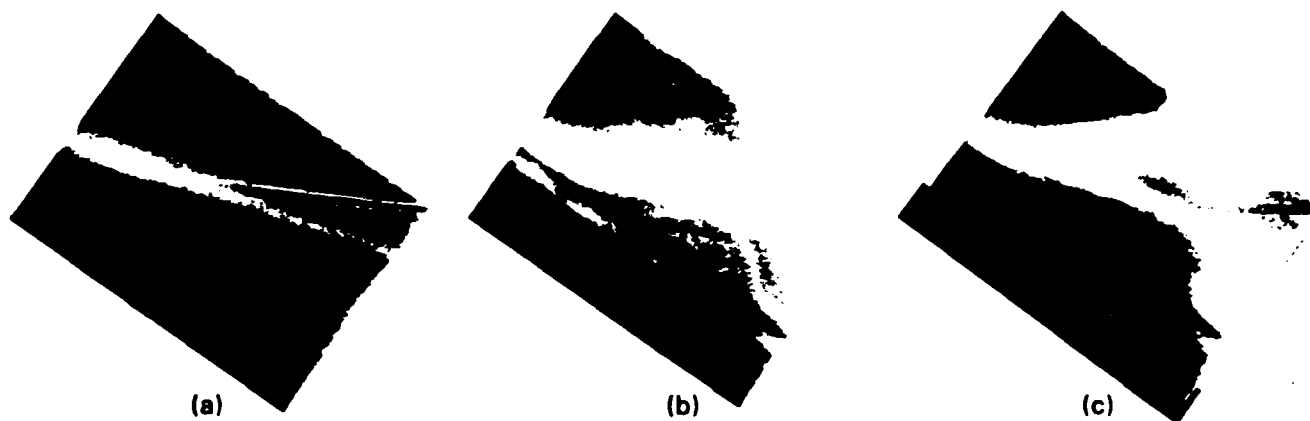
Figure 8   Microscope photographs of self-pumping process using internal reflections
in a crystal of BaTiO₃, (a) 12 s exposure showing only the primary self-
pumping beams along with the incident beam, (b) 120 s exposure showing
primary and secondary self-pumping beams along with the incident beam and
(c) 120 s exposure after painting lower-left crystal face black showing the
incident beam and the broad fan of photorefractively scattered light.   Note
that the phase-conjugate reflection and all self-pumping beams vanished
after painting even though primary self-pumping corner (right corner) was not
painted or changed in any way.

Finally, we have proven that these secondary beams which are apparent in Figure 8b are absolutely crucial to the operation of the self-pumped phase conjugator using internal reflections. It has been suggested that the surface reflectivity in photorefractive BaTiO$_3$ can be modified by painting the crystal faces.[11,21] We attempted to reduce the reflectivity of the lower-left surface of the crystal, as indicated in Figure 8c, by covering its entire width (all the way to the corners) with Krylon ultra-flat black paint, thereby attempting to eliminate the secondary beams shown in Figure 8b. When this painting was carried out "in-situ" (i.e., without disturbing the optical alignments used to obtain the self-pumping beam pictures shown in Figures 8a and 8b), not only did the secondary beams disappear, but the phase-conjugate reflections and primary self-pumping beams also vanish (as can be seen in Figure 8c) even though primary self-pumping corner of the BaTiO$_3$ crystal remained undisturbed. Only a broad fan of photorefractively scattered light, along with the incident beam, remains visible in Figure 8c. This observation agrees with our theory. According to Equation (16), the threshold oscillation condition depends on the roundtrip mirror reflectivity R. By decreasing the refectivity R, the internal cavity falls below threshold and thus oscillation dies. Furthermore, after painting, the crystal would not self-pump in any orientation (i.e., at any angle or position of the incident beam). This conclusively shows that self-pumping in BaTiO$_3$ involves more than the internal reflections from just one corner and that the old model[2,12,20] for the process is not correct. Also, the resonator model for the self-pumped phase conjugator using internal reflections which we proposed is consistent with the series of pictures shown in Figure 8.

Summary

In conclusion, we have presented a general theory and the supporting experiments which explain the frequency shifts of self-pumped phase conjugators. The cause of the slight frequency shifts (~ 1 Hz) observed in both the photorefractive unidirectional ring resonator and the self-pumped phase conjugator with an external linear cavity is unequivocally established[15] and is well understood. In addition, the previous description of the self-pumped phase conjugator using internal reflections[2,12,20] is proven inadequate. We view all photorefractive, self-pumped phase conjugators which exhibit a frequency shift in the phase-conjugate reflection as being almost equivalent. Note that only two known photorefractive, self-pumped phase conjugators do not show the ~ 1 Hz frequency shifts: the ring conjugator[22,23] and the stimulated-backscattering (2k-grating) conjugator.[24] The self-pumped phase conjugators which do exhibit a frequency shift all employ some sort of resonant cavity (using only internal reflections from crystal surfaces or using only external reflections from ordinary mirrors or using a combination of both) to automatically generate the self-pumping beams. Because a closed-loop resonance cavity forms, the frequency shift on the phase-conjugate reflection is dictated by the phase oscillation condition for this resonance cavity.

Acknowledgments

References

1. J.O. White, M. Cronin-Golomb, B. Fischer and A. Yariv, Appl. Phys. Lett. 40, 450 (1982).
2. J. Feinberg, Opt. Lett. 7, 486 (1982); J. Feinberg, Opt. Lett. 8, 480 (1983).
3. R.A. McFarlane and D.G. Steel, Opt. Lett. 8, 208 (1983).
4. J. Feinberg and G.D. Bacher, Opt. Lett. 9, 420 (1984).
5. W.B. Whitten abd J.M. Ramsey, Opt. Lett. 9, 44 (1984).
6. F.C. Jahoda, P.G. Weber and J. Feinberg, Opt. Lett. 9, 362 (1984).
7. H. Rajbenbach and J.P. Huignard, Opt. Lett. 10, 137 (1985).
8. M.D. Ewbank, P. Yeh, M. Khoshnevisan and J. Feinberg, Opt. Lett. 10, 282 (1985).
9. M. Cronin-Golomb, B. Fischer, S-K. Kwong, J.O. White and A. Yariv, Opt. Lett. 10, 353 (1985).
10. J.M. Ramsey and W.B. Whitten, Opt. Lett. 10, 362 (1985).
11. P. Gunter, E. Voit, M.Z. Zha and J. Albers, Opt. Comm. 55, 210 (1985).
12. K.R. MacDonald and J. Feinberg, Phys. Rev. Lett. 55, 821 (1985).
13. A. Yariv and S-K. Kwong, Opt. Lett. 10, 454 (1985).
14. S-K. Kwong, A. Yariv, M. Cronin-Golomb and I. Ury, Appl. Phys. Lett. 47, 460 (1985).
15. M.D. Ewbank and P. Yeh, Opt. Lett. 10, 496 (1985).
16. P. Yeh, J. Opt. Soc. Am. B2, 1924 (1985).
17. G.C. Valley and G.D. Dunning, Opt. Lett. 9, 513 (1984).
18. P. Yeh, M.D. Ewbank, M. Khoshnevisan and J.M. Tracy, Opt. Lett. 9, 41 (1984).
19. M. Khoshnevisan, Rockwell International Science Center, Thousand Oaks, CA, private communication.

20. K.R. MacDonald and J. Feinberg, J. Opt. Soc. Am. 73, 548 (1983).
21. S-K. Kwong, California Institute of Technology, Pasadena, CA, private communication.
22. M. Cronin-Golomb, B. Fischer, J.O. White and A. Yariv, Appl. Phys. Lett. 42, 919 (1983).
23. M. Cronin-Golomb, J. Paslaski and A. Yariv, Appl. Phys. Lett. 47, 1131 (1985).
24. T.Y. Chang and R.W. Hellwarth, Opt. Lett. 10, 408 (1985).

APPENDIX 4.18

THEORY OF UNIDIRECTONAL PHOTOREFRACTIVE
RING OSCILLATORS

Theory of unidirectional photorefractive ring oscillators

Pochi Yeh

Rockwell International Science Center. Thousand Oaks, California 91360

Amplification owing to holographic two-wave mixing in photorefractive crystals can be utilized to achieve unidirectional ring oscillation. Unlike for the conventional gain medium (e.g., He–Ne), the gain bandwidth of photorefractive two-wave coupling is very narrow (a few hertz for BaTiO₃). Despite this fact, the ring resonator can still oscillate over a large range of cavity detuning. A theory is presented that describes how the oscillating mode attains the round-trip phase condition.

INTRODUCTION

The photorefractive effect in electro-optic crystals (e.g., BaTiO₃, LiNbO₃) has been widely studied for many applications. These include real-time holography, optical data storage, and phase-conjugate wave-front generation. Recently, increasing attention has been focused on using coherent signal beam amplification in two-wave mixing. These new applications include image amplification,[1] vibrational analysis,[2] nonreciprocal transmission,[3,4] and laser-gyro biasing.[5] The coherent signal beam amplification in two-wave mixing can also be used to provide parametric gain for unidirectional oscillation in ring resonators. Although such an oscillation has been observed by using a BaTiO₃ crystal in a ring resonator,[6] a general theory is not available. The present state of the theory does not address such problems as the round-trip phase condition or even oscillation frequency.

In this paper we describe a theory of parametric ring oscillation using holographic two-wave mixing in photorefractive crystals. The theory shows that oscillation can occur at almost any cavity length despite the narrow-band nature of the coherent two-wave coupling gain, provided that the coupling is strong enough. A similar situation also occurs in phase-conjugate parametric oscillators.[7] The theory also provides explicit expressions for the oscillation frequency, intensity, and threshold conditions.

FORMULATION OF THE PROBLEM

Referring to Fig. 1, we consider an optical ring resonator consisting of three partially reflecting mirrors. A photorefractive medium, which is pumped by an external laser beam, is inserted into the cavity. To investigate the properties of such oscillators, we must first treat the problem of two-wave coupling in photorefractive media. This problem has been formulated and solved by many workers.[8–10] However, most work has been focused on the degenerate two-wave mixing. For the purpose of developing our theory, we need to address nearly degenerate two-wave mixing.

Let us focus our attention on the region occupied by the photorefractive crystal, so that the electric field of the two waves can be written as

$$E_j = A_j(z)\exp[i(\mathbf{k}_j \cdot \mathbf{r} - \omega_j t)] + \text{c.c.}, \quad j = 1, 2, \quad (1)$$

where z is measured along the bisector of the two beams, $\mathbf{k}_1$ and $\mathbf{k}_2$ are the wave vectors of the beams, and c.c. denotes a term that is the complex conjugate to the first term. In Eq. (1), we assume for simplicity that both waves have the same state of polarization and the photorefractive medium does not exhibit optical rotation. A_1 and A_2 are the wave amplitudes and are taken as functions of z only for steady-state situations.

In the photorefractive medium (from zero to $z = l$), these two waves generate an interference pattern (traveling if $\omega_1 \neq \omega_2$). This pattern may generate and redistribute photocarriers. As a result, a spatial charge field (also traveling if $\omega_1 \neq \omega_2$) is created in the medium. This field induces a volume index grating by means of the Pockels effect. In general, the index grating will have a finite spatial phase shift relative to the interference pattern,[9] so that, following the notation of Ref. 11, we can write the fundamental component of the intensity-induced grating as

$$n = n_0 + \frac{n_1}{2}\left\{e^{i\phi}\frac{A_1 A_2^{*}}{I_0}\exp[i(\mathbf{K}\cdot\mathbf{r} - \Omega t)] + \text{c.c.}\right\}, \quad (2)$$

where

$$I_0 = I_1 + I_2 \equiv |A_1|^2 + |A_2|^2. \quad (3)$$

ϕ is real and n_1 is a real and positive number, $\mathbf{K} = \mathbf{k}_1 - \mathbf{k}_2$, and $\Omega = \omega_1 - \omega_2$. Here again, for the sake of simplicity, we assume a scalar grating. The phase ϕ indicates the degree to which the index grating is shifted spatially with respect to the light interference pattern. According to Ref. 1, ϕ and n_1 can be written, respectively, as

$$\phi = \phi_0 + \tan^{-1}(\Omega\tau) \quad (4)$$

and

$$n_1 = \frac{2}{(1 + \Omega^2\tau^2)^{1/2}}\Delta n_s, \quad (5)$$

where τ is the decay time constant of the holograph grating. Δn_s is the saturation value of the photoinduced index change, and ϕ_0 is a constant phase shift related to the nonlocal response of the crystal under fringe illumination. Both parameters Δn_s and ϕ_0 depend on the grating spacing $(2\pi/K)$ and its direction as well as on the material properties of the crystal, e.g., the electro-optic coefficients. Expressions for
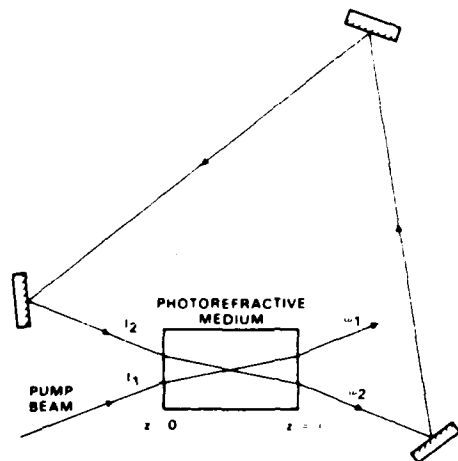
Fig. 1.   Schematic drawing of a unidirectional photorefractive ring resonator.

Δn_s and ϕ_0 can be found in Refs. 10 and 12.   In photorefractive media. e.g.. BaTiO$_3$, that operate by diffusion only (i.e., no external static field) the magnitude of ϕ_0 is $\pi/2$, with its sign depending on the direction of the c axis.

Now, by using expression (2) for n and the scalar-wave equation and by using the parabolic approximation (i.e., slowly varying amplitudes), we can derive the following coupled equations:

$$\frac{d}{dz} A_1 = i \frac{\pi n_1}{\lambda I_0 \cos \theta} e^{i\phi} |A_2|^2 A_1 - \frac{\alpha}{2} A_1.$$

$$\frac{d}{dz} A_2 = i \frac{\pi n_1}{\lambda I_0 \cos \theta} e^{-i\phi} |A_1|^2 A_2 - \frac{\alpha}{2} A_2, \qquad (6)$$

where θ is the half-angle between the beams and α is the absorption coefficient.

We now write

$$A_1 = \sqrt{I_1} \exp(i\psi_1).$$

$$A_2 = \sqrt{I_2} \exp(i\psi_2). \qquad (7)$$

where ψ_1 and ψ_2 are phases of the amplitudes A_1 and A_2, respectively. Using Eqs. (7) and (3), the coupled Eqs. (6) can be written as

$$\frac{d}{dz} I_1 = -\gamma \frac{I_1 I_2}{I_1 + I_2} - \alpha I_1.$$

$$\frac{d}{dz} I_2 = \gamma \frac{I_1 I_2}{I_1 + I_2} - \alpha I_2, \qquad (8)$$

and

$$\frac{d}{dz} \psi_1 = \beta \frac{I_2}{I_1 + I_2}.$$

$$\frac{d}{dz} \psi_2 = \beta \frac{I_2}{I_1 + I_2}. \qquad (9)$$

where

$$\gamma = \frac{2\pi n_1}{\lambda \cos \phi} \sin \phi. \qquad (10)$$

$$\beta = \frac{\pi n_1}{\lambda \cos \theta} \cos \phi. \qquad (11)$$

The solutions for the intensities $I_1(z)$ and $I_2(z)$ are

$$I_1(z) = I_1(0) \frac{1 + m^{-1}}{1 + m^{-1} e^{\gamma z}} e^{-\alpha z}, \qquad (12)$$

$$I_2(z) = I_2(0) \frac{1 + m}{1 + m e^{-\gamma z}} e^{-\alpha z}, \qquad (13)$$

where m is the input intensity ratio

$$m = \frac{I_1(0)}{I_2(0)}. \qquad (14)$$

Note that in the absence of absorption ($\alpha = 0$), $I_2(z)$ is an increasing function of z and $I_1(z)$ is a decreasing function of z, provided that γ is positive.   The sign of γ depends on the direction of the c axis.   As a result of the coupling for $\gamma > 0$ in Fig. 1, beam 2 gains energy from beam 1.   If this two-wave mixing gain is large enough to overcome the absorption loss, then beam 2 is amplified.   Such an amplification is responsible for the oscillation.

With $I_1(z)$ and $I_2(z)$ known, the phases ψ_1 and ψ_2 can be integrated directly from Eqs. (9).   The phase shift in traversing through the photorefractive medium for beam 2 is

$$\frac{2\pi}{\lambda} n_0 l + \psi_2(l) - \psi_2(0), \qquad (15)$$

where $2\pi n_0 l//\lambda$ is the phase shift in the absence of photorefractive coupling.   The additional phase shift

$$\Delta\psi \equiv \psi_2(l) - \psi_2(0), \qquad (16)$$

which is due to the photorefractive two-wave coupling, can be obtained by integrating Eqs. (9).   Substituting Eqs. (12) and (13) into Eqs. (9) for I_1 and I_2, respectively, we obtain

$$\Delta\psi = \psi_2(l) - \psi_2(0) = \int_0^l \frac{\beta dz}{1 + m^{-1} e^{\gamma z}}. \qquad (17)$$

Note that this photorefractive phase shift is independent of the absorption coefficient α.   Carrying out the integration in Eq. (17), we obtain

$$\Delta\psi = \psi_2(l) - \psi_2(0) = -\frac{\beta}{\gamma} \log \left(\frac{1 + m}{1 + m e^{-\gamma l}} \right). \qquad (18)$$

Equations (18) and (13) can now be used to investigate the properties of the unidirectional ring oscillation.

OSCILLATION FREQUENCY AND INTENSITY

In a conventional ring resonator, the oscillation occurs at those frequencies

$$f = N \frac{c}{L}. \qquad N = \text{integer} \qquad (19)$$

that lie within the gain curve of the laser medium (e.g., He–Ne).   Here, L is the effective length of a complete loop and N is a large integer.   For $L \leq 30$ cm, these frequencies [Eq. (19)] are separated by the mode spacing $c/L \geq 1$ GHz.   Since the width of the gain curve for the conventional gain medium is typically several gigahertz, principally because of Doppler broadening, oscillation can occur at almost any cavity length L.   On the contrary, if the bandwidth of the gain curve is
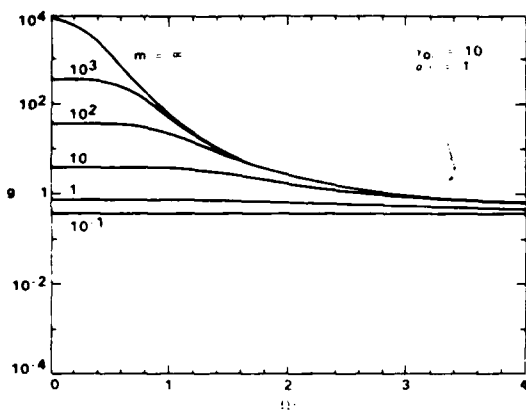
Fig. 2. Photorefractive gain g as a function of $\Omega\tau$ for various values of m.
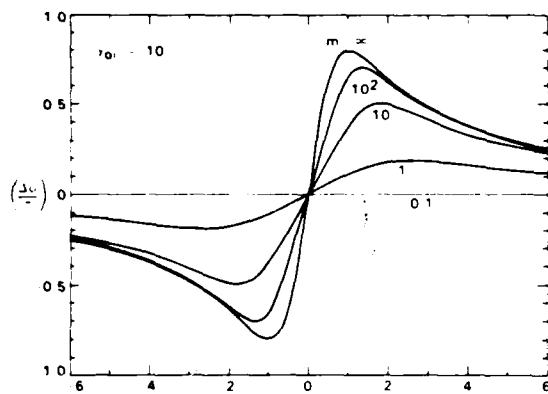

Fig. 3. Photorefractive phase shift $\Delta\psi$ as a function of $\Omega\tau$ for various values of m.

narrower than the mode spacing c/L, then oscillation can be sustained, provided that the cavity loop is kept at the appropriate length.

Unlike in the conventional gain medium, the bandwidth of the photorefractive two-wave mixing is very narrow. By using photorefractive crystals, e.g., BaTiO$_3$, that operate by diffusion only, the coupling constant can be written, according to Eqs. (4), (5), and (10), as

$$\gamma = \gamma_0/[1 + (\Omega\tau)^2]. \qquad (20)$$

where γ_0 is the coupling constant for the case of degenerate two-wave mixing (i.e., $\Omega = \omega_1 - \omega_2 = 0$) and is given by

$$\gamma_0 = \frac{4\pi\Delta n_s}{\lambda\cos\theta}. \qquad (21)$$

In deriving Eq. (20), we have used $\pi/2$ for ϕ_0 in Eq. (4).

The parametric two-wave mixing gain can be defined as

$$g \equiv \frac{I_2(l)}{I_2(0)} = \frac{1 + m}{1 + me^{-\gamma l}}e^{-\alpha l}, \qquad (22)$$

where we recall that m is the input beam ratio $m = I_1(0)/I_2(0)$ and l is the length of interaction. Note that amplification ($g > 1$) is possible only when $\gamma > \alpha$ and $m > (1 - e^{-\alpha l})/(e^{-\alpha l} - e^{-\gamma l})$. Also note that g is an increasing function of m (i.e., $\partial g/\partial m > 0$) and g is an increasing function of l, provided that $\gamma > \alpha$ and

$$l \leq \frac{1}{\gamma}\log\left[\frac{m(\gamma - \alpha)}{\alpha}\right]. \qquad (23)$$

The gain as a function of frequency ω_2 (or equivalently as a function of $\Omega = \omega_1 - \omega_2$) is plotted in Fig. 2 for various values of m. Note that gain is significant only when $|\omega_1 - \omega_2|\tau < 1$. For materials such as BaTiO$_3$ and SBN τ is between 1 and 0.1 sec. Thus the gain bandwidth is only a few hertz. In spite of such an extremely narrow bandwidth, unidirectional oscillation can still be observed easily at any cavity length in ring resonators by using BaTiO$_3$ crystals as the photorefractive medium.[13] Such a phenomenon can be explained in terms of the additional phase shift [Eq. (18)] introduced by the photorefractive coupling. This phase shift is a function of the oscillation frequency and is plotted in Fig. 3 as a function of $\Omega\tau$. For BaTiO$_3$ crystals with $\gamma_0 l > 4\pi$, this phase shift can vary from $-\pi$ to $+\pi$ for a frequency drift of $\Delta\Omega\tau = \pm 1$. Such a phase shift is responsible for the oscillation of the ring resonator, which requires a round-trip phase shift of an integer times 2π.

OSCILLATION CONDITIONS

It is interesting to note the initiation of the oscillation. Like laser oscillators, the oscillation of this ring resonator starts from noises that are due to physical processes such as scattering and quantum fluctuation. In photorefractive crystals the scattering dominates the noise contribution. At the beginning, there may be a slight amount of light scattered along the direction of the ring resonator. This slight amount of light will be amplified by the two-wave mixing process in the photorefractive crystal, provided that the frequencies are not appreciably different. As the intensity in the resonator builds up, the parameter m, defined by Eq. (14), decreases. The buildup of oscillation intensity leads to a saturation of the gain (see Fig. 2: the gain decreases as m decreases). At steady-state oscillation, the electric field must reproduce itself, both in phase and intensity, after each round trip. In other words, the oscillation conditions can be written as

$$\Delta\psi + \int k\,ds = 2N\pi \qquad (24)$$

and

$$gR = 1, \qquad (25)$$

where $\Delta\psi$ is the additional phase shift owing to photorefractive coupling, the integration is over a round-trip beam path, the parameter R is the product of the mirror reflectivities, and g is the parametric gain of Eq. (22).

If we define a cavity-detuning parameter $\Delta\Gamma$ as

$$\Delta\Gamma = 2N'\pi - \int k\,ds. \qquad (26)$$

where N' is an integer chosen in such a way that $\Delta\Gamma$ lies between $-\pi$ and $+\pi$, then the oscillation condition [Eq. (24)] can be written as

$$\Delta\psi = \Delta\Gamma + 2M\pi, \qquad (27)$$

where M is an integer. In other words, oscillation can be achieved only when the cavity detuning can be compensated for by the photorefractive phase shift.
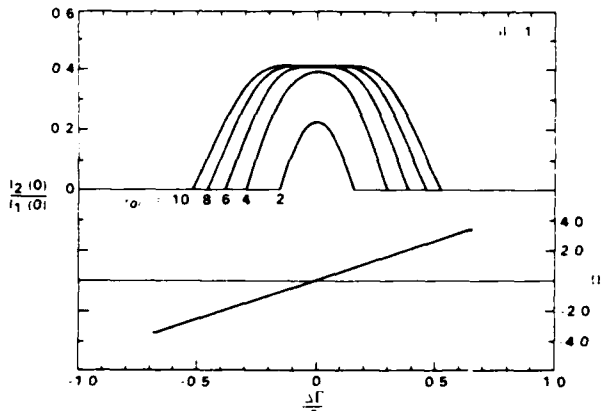
Fig. 4. Oscillation intensity and frequency as functions of cavity detuning $\Delta\Gamma$ for various values of $\gamma_0 l$.

Equations (24) and (25) may be used to solve for the two unknown quantities $m = I_1(0)/I_2(0)$ and $\Omega = \omega_1 - \omega_2$. If we fix the pump intensity $I_1(0)$ and the pump frequency ω_1, then Eqs. (24) and (25) can be solved for the oscillation frequency ω_2 and the oscillation intensity $I_2(0)$. Substituting Eq. (22) for g in Eq. (25) and using Eq. (18), we obtain

$$\Delta\psi = -\frac{\beta}{\gamma} \log(Re^{-\alpha l}). \tag{28}$$

This equation can now be used to solve for the oscillation frequency $\Omega\tau$. For the case of pure diffusion, using Eq. (4) for ϕ with $\phi_0 = \pi/2$ and Eqs. (10) and (11), we obtain from Eq. (28)

$$\Omega\tau = \frac{-2\Delta\psi}{\alpha l - \log R} = \frac{-2(\Delta\Gamma + 2M\pi)}{\alpha l - \log R}. \tag{29}$$

where $\Delta\Gamma$ is the cavity detuning and is given by Eq. (26). Substituting Eq. (22) for g in Eq. (25), we can solve for m and obtain

$$m = \frac{I_1(0)}{I_2(0)} = \frac{1 - Re^{-\alpha l}}{Re^{-\alpha l} - e^{-\gamma l}}. \tag{30}$$

Since m must be positive, we obtain from Eq. (30) the threshold condition for oscillation

$$\gamma l > \gamma_t l \equiv \alpha l - \log R, \tag{31}$$

where γ_t is the threshold parametric gain constant. Since γ is a function of frequency Ω, Eq. (31) dictates that the parametric gain is above threshold only in a finite spectral regime. When Eq. (20) is used for γ, Eq. (31) becomes

$$\Omega\tau < \left(\frac{\gamma_0 l}{\alpha l - \log R} - 1\right)^{1/2}. \tag{32}$$

where we recall that γ_0 is the parametric gain at $\Omega = \omega_1 - \omega_2 = 0$. Inequality (32) defines the spectral regime where the parametric gain γ is above threshold (i.e., $\gamma > \gamma_t$).

We have thus far obtained expressions for the oscillation frequency [Eq. (29)] and the spectral regime where the gain is above threshold. The ring resonator will oscillate only when the oscillation frequency falls within this spectral region. The oscillation frequency $\omega_2 = \omega_1 - \Omega$ is determined by Eq. (29), with $\Delta\Gamma$ being the cavity detuning [Eq. (26)].

The same oscillation frequency must also satisfy expression (32). Thus we obtain the following oscillation condition:

$$\frac{2|\Delta\psi|}{\alpha l - \log R} < \left[\frac{\gamma_0 l}{\alpha l - \log R} - 1\right]^{1/2}. \tag{33}$$

which can also be written as

$$\gamma_0 l > \gamma_t l + \frac{1}{\gamma_t l}(2\Delta\psi)^2 \equiv G_t l, \tag{34}$$

where γ_t is the threshold parametric gain of Eq. (31) for the case when $\Delta\psi = 0$ and G_t may be considered the threshold gain for the case when $\Delta\psi \neq 0$. According to Eq. (34), the threshold gain increases as a function of the cavity detuning $\Delta\Gamma$. The cavity detuning $\Delta\Gamma$ not only determines the oscillation frequency [Eq. (29)] but also determines the threshold gain G_t.

The $\Delta\Gamma$ in Eq. (26) is the cavity detuning and is defined between $-\pi$ and π. However, the photorefractive phase shift [Eq. (18)] can be greater than π. When this happens, the unidirectional ring resonator may oscillate at more than one frequency. These frequencies are given by Eq. (29), with $M = 0, \pm1, \pm2, \ldots$, etc., and with their corresponding threshold gain given by

$$G_t l = \gamma_t l + \frac{1}{\gamma_t l}[2(\Delta\psi + 2M\pi)]^2. \tag{35}$$

In other words, for each cavity detuning $\Delta\Gamma$, the ring resonator can support multimode oscillation, provided that the coupling constant γ_0 is large enough. Figure 4 shows the oscillation intensity as well as the oscillation frequency as functions of cavity detuning $\Delta\Gamma$. Note that for larger $\gamma_0 l$ the resonator can oscillate at almost any cavity detuning $\Delta\Gamma$, whereas for small $\gamma_0 l$ oscillation occurs only when the cavity detuning is limited to some small region around $\Delta\Gamma = 0$.

CONCLUSION AND DISCUSSION

In conclusion, we have derived a theory of unidirectional ring oscillators using parametric photorefractive two-wave mixing. By using the simple coupled-mode theory, we obtain an expression for the photorefractive phase shift. Such a photorefractive phase shift can compensate for cavity detuning and thus can allow the oscillation to occur. According to this theory, the oscillation frequency will be slightly detuned from the pump frequency. Such a frequency offset is necessary to produce the photorefractive phase shift to compensate for the cavity detuning. The photorefractive phase shift is proportional to the coupling constant. Thus, when materials with a large coupling constant (e.g., BaTiO₃) are used, oscillation can occur at almost any cavity detuning. Such a theory has been validated by the author and his co-worker.[14] The same theory can also be applied to linear oscillators and thus can be employed to explain the frequency shift of self-pumped phase conjugators.[6,13]

REFERENCES

1. J. P. Huignard and A. Marrackchi, "Coherent signal beam amplification in two-wave mixing experiments with photorefractive BSO crystals," Opt. Commun. 38, 249 (1981).
2. J. P. Huignard and A. Marrackchi, "Two-wave mixing and energy transfer in $B_{12}SiO_{20}$ crystals: amplification and vibration analysis," Opt. Let. 6, 622 (1981).
3. P. Yeh, "Contradirectional two-wave mixing in photorefractive media," Opt. Commun. 45, 323 (1983).
4. P. Yeh, "Electromagnetic propagation in a photorefractive layered medium," J. Opt. Soc. Am. 73, 1268 (1983).
5. P. Yeh, "Photorefractive coupling in ring resonators," Appl. Opt. 23, 2974 (1984).
6. J. O. White, M. Cronin-Golomb. B. Fischer, and A. Yariv, "Coherent oscillation by self-induced gratings, in photorefractive crystals," Appl. Phys. Lett. 40, 450 (1982).
7. P. Yeh, "Theory of phase-conjugate oscillators," J. Opt. Soc. Am. A 2, 727–730 (1985).
8. D. L. Staebler and J. J. Amodei, "Coupled wave analysis of holographic storage in $LiNbO_3$," J. Appl. Phys. 34, 1042 (1972).
9. V. L. Vinetskii, N. V. Kukhtarev, S. G. Odulov, and M. S. Soskin, "Dynamic self-diffraction of coherent light beams," Sov. Phys. Usp. 22, 742 (1979).
10. N. V. Kukhtarev, V. B. Markov, S. G. Odulov, M. S. Soskin, and V. L. Vinetskii, "Holographic storage in electro-optics crystals, beam coupling and light amplification," Ferroelectrics 22, 961 (1979).
11. B. Fischer, M. Cronin-Golomb, J. O. White, and A. Yariv, "Amplified reflection, transmission, and self-oscillation in real-time holography," Opt. Lett. 6, 519 (1981).
12. J. Feinberg, D. Heiman, A. R. Tanguay, and R. Hellwarth, J. Appl. Phys. 51, 1297 (1980).
13. J. Feinberg and G. D. Bacher, "Self-scanning of a continuous-wave dye laser having a phase-conjugating resonator cavity," Opt. Lett. 9, 420 (1984).
14. M. D. Ewbank and P. Yeh, "Frequency shift and cavity detuning in photorefractive resonators," Opt. Lett. 10, 496–498 (1985)

APPENDIX 4.19

FREQUENCY SHIFT AND CAVITY LENGTH IN
PHOTOREFRACTIVE RESONATORS

Frequency shift and cavity length in photorefractive resonators

M. D. Ewbank and P. Yeh

Rockwell International Science Center, Thousand Oaks, California 91360

Photorefractive resonators exhibit an extremely small frequency difference ($\Delta\omega/\omega \sim 10^{-15}$) between the oscillating and pumping beams. The observed frequency difference is proportional to cavity-length detuning. This dependence is explained by a photorefractive phase shift that is due to slightly nondegenerate two-wave mixing that compensates for cavity detuning and satisfies the round-trip phase condition for steady-state oscillation. The measured onset or threshold of oscillation as a function of photorefractive gain and intensity agrees with theory.

Despite the attention that self-pumped phase conjugators and optical resonators utilizing photorefractive BaTiO$_3$ have received recently,[1-3] two dilemmas remain unresolved. First, self-pumped phase conjugation in BaTiO$_3$ exhibits a slight frequency shift ($\sim$1-Hz),[4-7] attributed to a Doppler shift from moving photorefractive phase gratings.[4] Second, resonators using photorefractive gain media apparently oscillate at any optical cavity length.[4,8] In this Letter we show that these two dilemmas are interrelated and reveal the origin of the moving gratings and frequency shifts.

For simplicity, consider a unidirectional ring oscillator with photorefractive two-wave mixing providing the gain. The optical arrangement (Fig. 1) is chosen because only two-wave mixing occurs. The frequency difference between the unidirectional oscillation beam and the pump can be controlled by small changes ($<\lambda$) in ring-cavity length. In fact, both the *sign and the magnitude of the frequency shift exhibit a one-to-one correspondence to the cavity-length detuning.*

The above observations are predicted by a theory for unidirectional photorefractive ring resonators.[9] Oscillation occurs when the two-wave mixing gain dominates cavity losses and the round-trip optical phase reproduces itself (to within an integer multiple of 2π). The condition on phase is unique because of a significant *optical phase shift owing to nondegenerate two-wave mixing.* This condition is satisfied at any cavity length if the oscillation frequency is detuned from the pump frequency, since the photorefractive phase shift depends on the detuning. The frequency difference Ω between the pumping and oscillating beams is[9]

$$\Omega = - [2(\Delta\Gamma + 2m\pi)/\tau A], \qquad (1)$$

where $\Delta\Gamma$ is the cavity-length detuning with respect to an integer multiple of optical pump waves in the cavity, m is an integer, τ is the photorefractive time response, and A represents the total cavity loss. There are threshold conditions for oscillation involving cavity loss and gain (taking m to be zero):

$$|\Omega| \leq (1/\tau)(\gamma L/A - 1)^{1/2}, \qquad (2a)$$

$$|\Delta\Gamma| \leq (A/2)(\gamma L/A - 1)^{1/2}, \qquad (2b)$$

where γ is the degenerate two-wave mixing coupling coefficient, where L is the interaction length, and $A =$

$-\ln(RT_sT_p)$ [with R the product of the reflectivities of the cavity mirrors and output coupler; T_s the transmission through the BaTiO$_3$ sample accounting for the absorption, Fresnel reflections, and scattering (or beam fanning); and T_p the effective transmission through the pinhole aperture].

This theory predicts that the unidirectional ring resonator will oscillate at a frequency different from the pump frequency by an amount directly proportional to the cavity-length detuning. Furthermore, in a photorefractive material with moderate slow τ, the theory postulates a threshold where oscillation will cease if the cavity detuning (frequency difference) becomes too large.

The experiments performed to examine the above theory will now be discussed in detail. Referring to Fig. 1, a single-mode argon-ion laser (514.5 nm) serves multiple purposes: It pumps the BaTiO$_3$ crystal with the beam reflected from BS$_1$ and focused by lens L$_1$ ($F = 700$ mm) to a beam diameter of 0.5 mm at the crystal, it is a reference beam to determine interferometrically the relative frequency of the ring-cavity oscillation at BS$_5$, and it provides an accurate method to align the ring-cavity components (unblocking the beam reflected from BS$_2$) by monitoring the Fabry–Perot peaks when
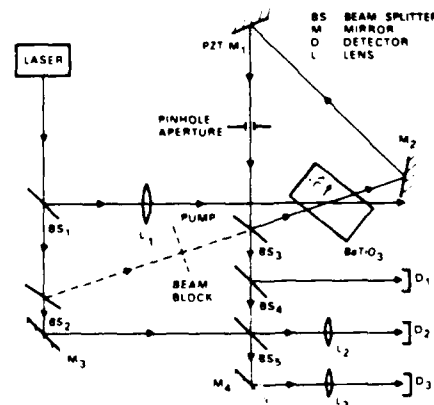

Fig. 1. Optical setup for the photorefractive unidirectional ring resonator with variable cavity length. The beat frequency between the self-oscillation and pump beams is derived from the motion of the interferograms at D$_2$ or D$_3$.
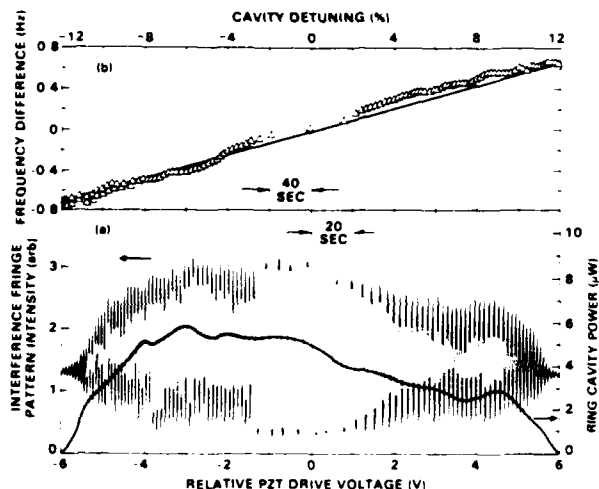
Fig. 2. Characteristics of the unidirectional self-oscillation as a function of ring-cavity length (i.e., PZT voltage or cavity detuning, where 100% implies a detuning of one full optical wave): (a) ring-cavity intensity (right) and beat-frequency signature (left); (b) frequency difference between the self-oscillation and the pumping beam.

rapidly scanning the piezo mirror PZT-M_1. Two-wave mixing in $BaTiO_3$ couples light into the unidirectional ring cavity, formed by two planar mirrors (M_1 and M_2) and a planar beam splitter (BS_3), even when the alignment beam is blocked. The ring-cavity beam is sampled through the output coupler BS_3, its intensity being detected at D_1 while the beat frequency between it and the pumping beam is determined using complementary fringe patterns formed at detectors D_2 and D_3. Without a ring-cavity pinhole aperture, unidirectional oscillation is observed at any cavity length. However, dynamically unstable multiple spatial modes are evident[4,10] in the fringe patterns at D_2 and D_3. To obtain a single mode (and clean fringe patterns), a 200-μm pinhole is placed in the ring cavity.

The basic premises of the theory[9] are verified by slowly ramping the PZT voltage and observing the beat frequency, along with the ring-cavity oscillation intensity. Typical results are shown in Fig. 2(a) for an 80-mW pump beam incident at 40° from the c axis of $BaTiO_3$ and at 20° from the oscillating beam (both angles are external in air). A triangle waveform (amplitude 250 V and period 10,000 sec) drives the PZT. The slow PZT scanning rate approximates steady-state two-wave mixing in $BaTiO_3$ while simultaneously permitting a controlled variation of the cavity length.

The unidirectional ring-cavity intensity versus cavity length [Fig. 2(a)] indicates threshold gain conditions [expressions (2a) and (2b)]. The beat frequency between oscillating and pumping beams, as observed in the time variation of the fringe-pattern intensity [Fig. 2(a)], clearly corresponds to the position of the PZT-M_1. This beat frequency is not simply due to the Doppler shift caused by the moving PZT-M_1 since this Doppler shift is 3 orders of magnitude smaller than the observed beat frequency. When M_1 is exactly at the correct position (chosen as the origin), the fringe pattern is stationary, i.e., there is no frequency shift. As M_1 moves

away from this origin, the fringe motion becomes faster and the frequency difference increases. Figure 2(b) shows the linear dependence of the frequency difference on cavity detuning with the ramping period equal to 20,000 sec for improved resolution. This frequency difference is estimated from the beat-frequency signature [similar to Fig. 2(a)] by measuring the time interval between intensity maxima.

The frequency difference changes sign as M_1 slowly moves through the origin. The frequency of oscillation is upshifted with respect to the frequency of the pumping beam when the position of M_1 is negative, corresponding to a decrease in ring-cavity length from that where no frequency shift occurs. The observed sign is consistent with the sign of the phase shift between the light intensity pattern and index modulation that determines the direction of energy exchange in two-wave mixing.

The beat-frequency signature [Fig. 2(a)] is also a periodic function of PZT mirror position. The Fabry–Perot peak spacing detected at D_1 during alignment of the passive ring cavity calibrates the PZT motion (~50-V/free-spectral range for 514.5 nm). The observed beat-frequency signature reproduces itself with a M_1 displacement of every ~ $\lambda/2$, as expected (i.e., a cavity length detuning periodicity of λ).

Experimentally, the frequency threshold for oscillation is approximately a linear function of the pumping-beam intensity, as shown in Fig. 3(a). According to Eq. 2(a), this frequency threshold is inversely proportional to τ, but τ can be approximately proportional to the inverse of the pump intensity (assuming that the cavity intensity is negligible by comparison) when the photoconductivities dominate.[11] Therefore, the observed dependence [Fig. 3(a)] agrees with theory.

The oscillation conditions for the unidirectional ring resonator are dependent on the two-wave mixing gain (γL) in the photorefractive medium. γL is varied by


(a)   (b)
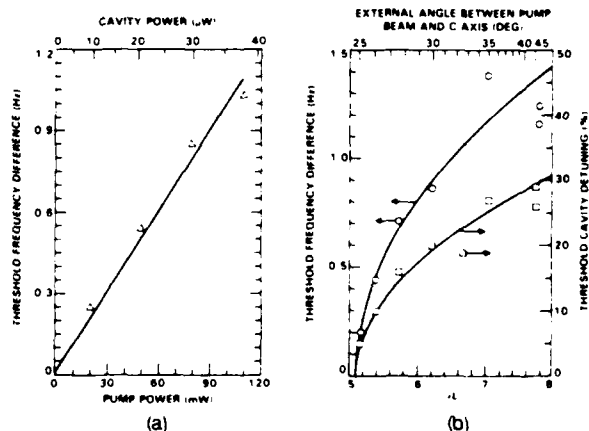
Fig. 3. Oscillation threshold behavior for the unidirectional ring resonator: (a) maximum beat frequency as a function of pumping-beam or ring-cavity power along with a linear fit (solid line); (b) maximum beat frequency (left) and cavity detuning (right) as a function of two-wave mixing gain, γL, where γL is related to the external angle that the pumping beam makes the crystal's c axis as shown (top scale). Note: the two solid curves in (b) correspond to the evaluation of expressions (2a) and (2b) as described in text.
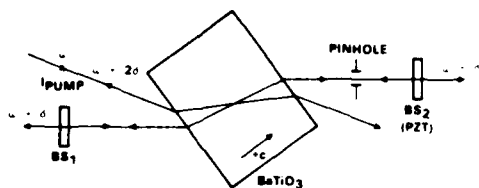
Fig. 4. Self-pumped phase conjugator using external reflectors to generate the self-oscillation with a frequency shift δ and the phase-conjugate reflection with a frequency shift 2δ, where δ is proportional to the linear cavity length.

rotating the $BaTiO_3$ crystal with respect to the pumping and oscillating beams.[12] When the gain is too small, no unidirectional oscillation is observed, regardless of ring-cavity length. For γL just above threshold, two pronounced differences are evident, contrasting with γL large. First, the amount of cavity detuning that is accommodated before oscillation ceases is greatly reduced. Second, the maximum frequency difference between the pumping and oscillating beams is much less. The quantitative trends of these two effects are given in Fig. 3(b) for a pump power of 80 mW.

The threshold oscillation conditions given in expressions (2a) and (2b) agree with the data [Fig. 3(b)]. The solid curve associated with the left-hand scale of Fig. 3(b) is generated from expression (2a) for $A = 5.1$ and $\tau = 0.53$ sec. This cavity-loss factor, A, is estimated independently from $R = 0.99 \times 0.91 \times 0.81$ (for M_1, M_2 and BS_3, respectively), $T_s = 0.52$ and $T_p = 0.016$ (for a cavity length of 50 cm). Accumulating these contributions gives $A = 5.2$, in excellent agreement with the observed 5.1. The right-hand scale of Fig. 3(b) shows the dependence of threshold cavity detuning (i.e., the maximum detuning that will still support self-oscillation) on γL, along with the prediction from Eq. 2(b), where $\Delta \Gamma$ is normalized by 2π. Remarkable agreement is obtained using $A = 5.1$ from Fig. 3(a) and no adjustable parameters.

The interdependence of the optical cavity length and the beat frequency between the oscillating and pumping beams is a general property of photorefractive resonators. These results are not unique to the optical setup shown in Fig. 1. Similar behavior is observed with other configurations. First, the orientation of the $BaTiO_3$ crystal in Fig. 1 can be altered so that the pumping and oscillating beams enter the a face but in such a way that no self-pumping occurs.[4] Second, the $BaTiO_3$ can be replaced by crystals of strontium barium niobate[13,14] (nominally undoped and cerium doped). Third, a linear resonator (Fig. 4) acts as a *self-pumped phase conjugator*.[1] The observed frequency shift of the phase-conjugate beam is exactly twice that of the self-oscillation, which is necessary to satisfy energy conservation for slightly nondegenerate four-wave mixing.[15] In all three variations, the measured frequency differences correlate with cavity length detuning; results equivalent to those shown in Fig. 2 are obtained.

Finally, consider another self-pumped phase conjugator, in which the four-wave mixing pumping beams arise from internal reflections at the crystal faces instead of external mirrors.[3-7] A resonance cavity containing the self-pumping beams is formed from the internal reflections off the crystal surfaces (but the cavity length cannot be systematically varied and the spatial modes cannot be restricted with an aperture). The frequencies of the beams can again be compared interferometrically. One self-pumping beam is monitored using the uncollimated light escaping the crystal's corner during reflection. Preliminary experiments indicate that the phase-conjugate beam sometimes exhibits a frequency shift exactly double that of a self-pumping beam, just as in Fig. 4. Even though four-wave mixing is occurring in all cases of self-pumped phase conjugators, two-wave mixing might be the dominating process in determining the oscillation conditions necessary for generating the self-pumping beams.

In conclusion, the frequency difference between the self-oscillating and pumping beams in the unidirectional ring resonator experimentally depends on the optical cavity length. This dependence supports a theory[9] that uses a photorefractive phase shift associated with slightly nondegenerate two-wave mixing to satisfy the round-trip phase-oscillation condition for the resonating beam. Similarly, the observed frequency shifts in other photorefractive resonators, including self-pumped phase conjugators, may also be explained by the same mechanism.

References

1. J. O. White, M. Cronin-Golomb, B. Fischer, and A. Yariv, Appl. Phys. Lett. **40**, 450 (1982).
2. R. McFarlane and D. Steel, Opt. Lett. **8**, 208 (1983).
3. J. Feinberg, Opt. Lett. **8**, 480 (1983).
4. J. Feinberg and G. D. Bacher, Opt. Lett. **9**, 420 (1984).
5. K. R. MacDonald and J. Feinberg, J. Opt. Soc. Am. A **1**, 1213 (A) 1984.
6. J. F. Lam, J. Opt. Soc. Am. A **1**, 1223 (A) 1984.
7. W. Whitten and J. Ramsey, Opt. Lett. **9**, 44 (1984).
8. H. Rajbenbach and J. P. Huignard, Opt. Lett. **10**, 137 (1985).
9. P. Yeh, J. Opt. Soc. Am. B **2** (to be published, November 1985).
10. G. Valley and G. Dunning, Opt. Lett. **9**, 513 (1984).
11. P. Gunter, Phys. Rep. **93**, 199 (1982).
12. As the orientation of the two-wave mixing fringe pattern with respect to the crystal axes changes, the effective electro-optic coefficient (and coupling efficiency of the index grating) is modified. γL is independently measured by removing ring-cavity mirror M_2 and using an attenuated probe beam from BS_2 with an external angle of 20° between probe and pump beams.
13. Provided by R. Neurganokar, Rockwell International, Thousand Oaks, Calif.
14. B. Fischer, M. Cronin-Goulomb, J. O. White, A. Yariv, and R. Neurgaonkar, Appl. Phys. Lett. **40**, 863 (1982).
15. P. Yeh, M. D. Ewbank, M. Khoshnevisan, and J. M. Tracy, Opt. Lett. **9**, 41 (1984).

APPENDIX 4.20

MULTIMODE FIBER GYRO USING A MUTUALLY
PUMPED CONJUGATOR

Multimode Fiber Gyro Using A Mutually Pumped Conjugator

Ian McMichael, Paul Beckwith, and Pochi Yeh

Rockwell International Science Center

ABSTRACT

The lack of a coherence requirement in mutually pumped phase conjugation is used to construct a multimode fiber gyro that uses the preferred technique of fast phase modulation for biasing.

SUMMARY

Phase-conjugate fiber-optic gyros (PCFOG) use phase conjugation to compensate for reciprocal phase changes due to thermal and mechanical effects on the fiber, while at the same time allowing for the measurement of the nonreciprocal phase shift produced by rotation. Where the best standard fiber-optic gyros require polarization-preserving fibers and couplers to avoid polarization scrambling that is a source of noise and signal fading, the PCFOG can avoid this problem by using polarization preserving phase-conjugation. This has the advantage of allowing for the use of inexpensive nonpolarization preserving, and even multimode fibers and components. We previously demonstrated rotation sensing with a PCFOG using multimode fiber and a self-pumped phase-conjugate mirror. However, to form a grating in the self-pumped conjugator, the two inputs to the conjugator (the two counterpropagating outputs from the fiber) must be coherent to within the response time of the conjugator. As a result, this configuration cannot use the preferred technique of fast phase modulation for biasing. We have solved this problem by constructing a PCFOG using a mutually pumped conjugator that does not require coherence between its two inputs. Demonstrations of rotation sensing will be presented.

MULTIMODE FIBER GYRO USING A MUTUALLY PUMPED CONJUGATOR

IAN McMICHAEL
PAUL BECKWITH
POCHI YEH

ONR CONTRACT N0014-85-C-0219
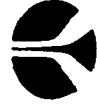
INTRODUCTION

-CONVENTIONAL FIBER-OPTIC GYROSCOPES

    -SINGLE-MODE POLARIZATION-PRESERVING FIBER

-PHASE-CONJUGATE FIBER-OPTIC GYROSCOPES (PCFOG)

    -SINGLE-MODE FIBER

      -MULTIMODE FIBER

-DEMONSTRATE A PCFOG THAT USES MULTIMODE FIBER
AND A MUTUALLY PUMPED PHASE CONJUGATOR

Rockwell International

Science Center

BACKGROUND

CONVENTIONAL FIBER OPTIC GYROSCOPES

W. Burns, R. Moeller, C. Villarruel, and M. Abebe, Opt. Lett. 8, 540(1983).

S.V. Bessonova et.al. Sov. J. Quantum Electon. 13, 1403 (1983).
R. Fredricks and D. Johnson, Proc. Soc. Photo-Opt. Instrum. Eng. Vol 83ε

PHASE CONJUGATE FIBER OPTIC GYROSCOPES

B. Fischer and S. Sternklar, Appl. Phys. Lett. 47, 1(1985).
P. Yeh, I. McMichael, and M. Khoshnevisan, Appl. Opt. 25, 1029(1986).

I. McMichael, P. Beckwith, and P. Yeh, Opt. Lett. 12, 1023 (1987).

Rockwell International
Science Center

CONCEPTUAL SCHEMATIC OF A PC FOG
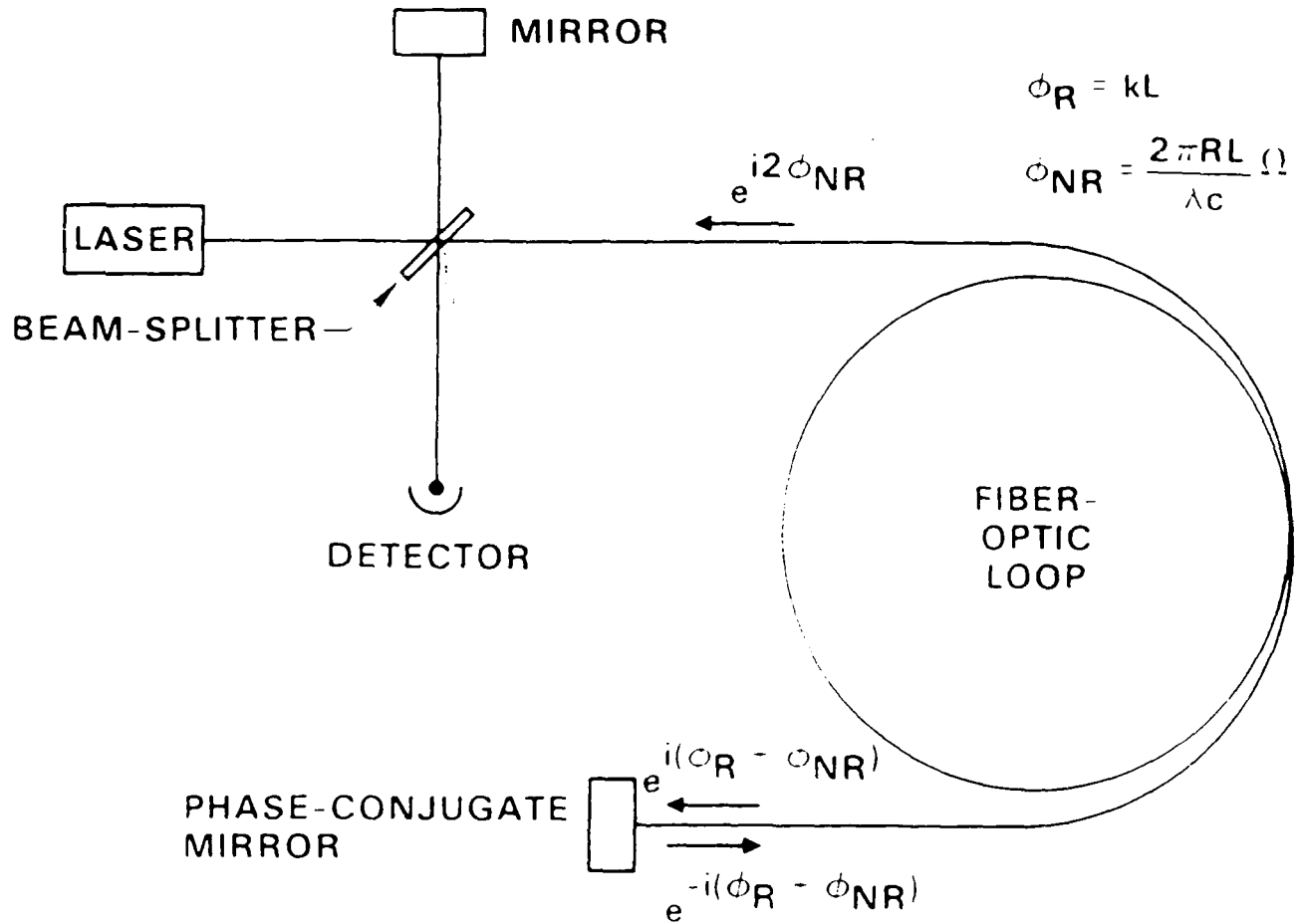
MIRROR

$\phi_R = kL$

$\phi_{NR} = \dfrac{2\pi RL}{\lambda c} \Omega$

$e^{i2\phi_{NR}}$

LASER

BEAM-SPLITTER —

FIBER-
OPTIC
LOOP

DETECTOR

PHASE-CONJUGATE
MIRROR

$e^{i(\phi_R - \phi_{NR})}$

$e^{-i(\phi_R - \phi_{NR})}$

Rockwell International

Science Center

CORRECTION OF MODAL SCRAMBLING IN MULTIMODE FIBERS BY A MUTUALLY PUMPED CONJUGATOR

INPUT POL
45° 10-4

OUTPUT POL

PPPC
45° 10-2

NPPPC
45° 10-1

Rockwell International
Science Center
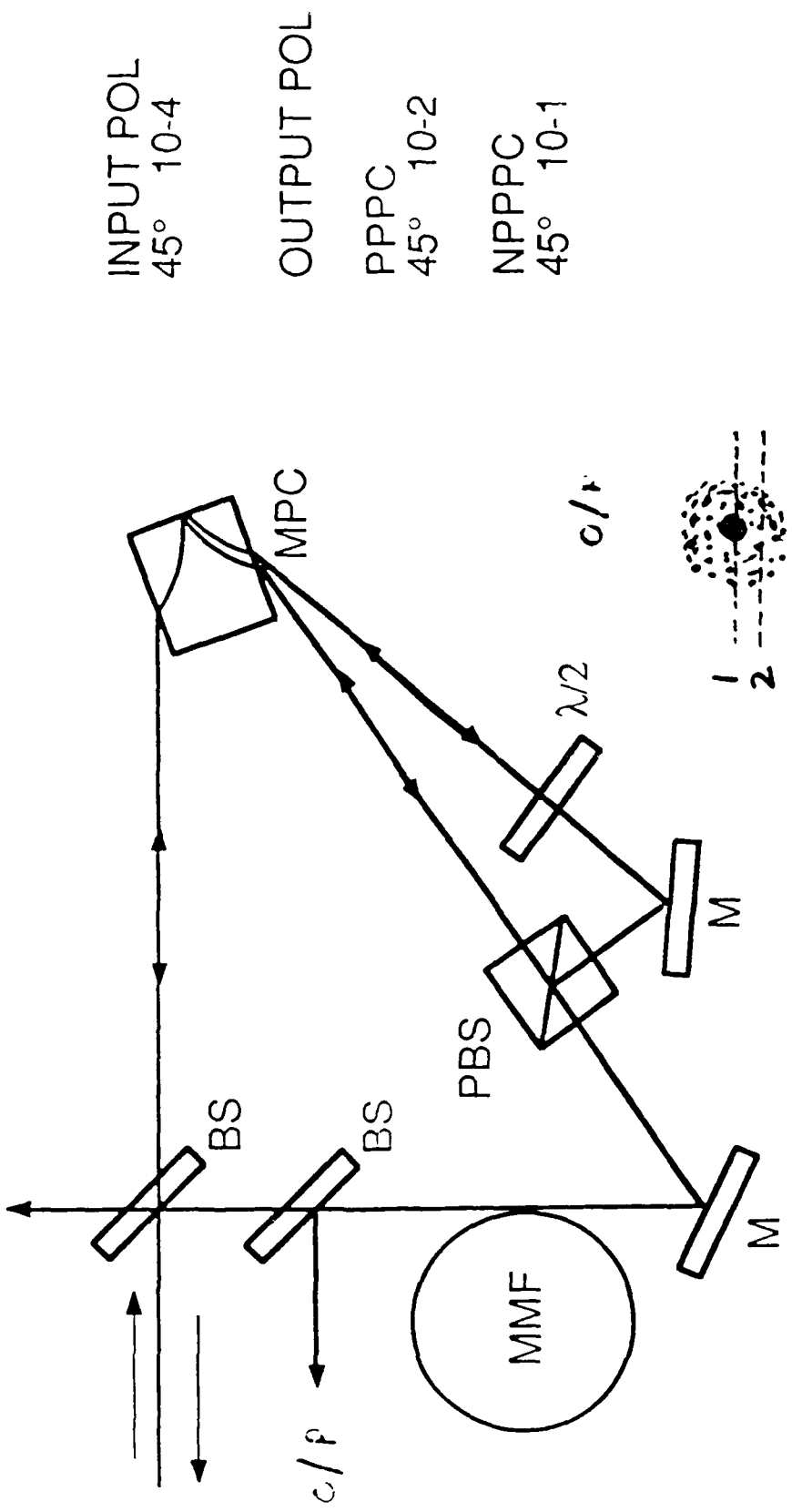
SPATIAL PROFILE OF MULTIMODE-FIBER DOUBLE-PASS OUTPUT

(WITH BIRD-WING PHASE-CONJUGATORS)
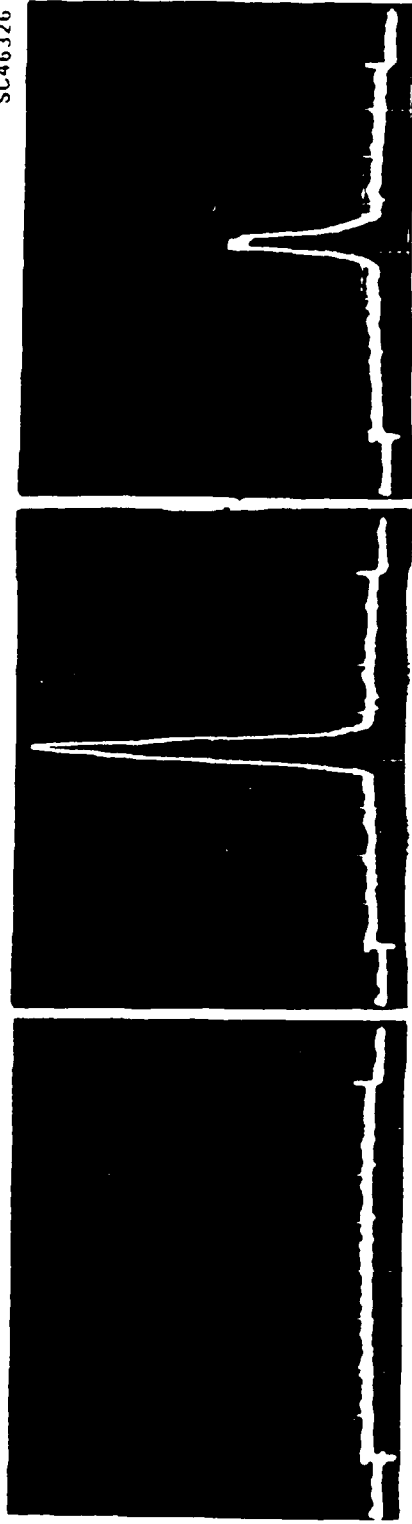
CENTRAL SPOT

BACKGROUND   PPPC   NPPPC
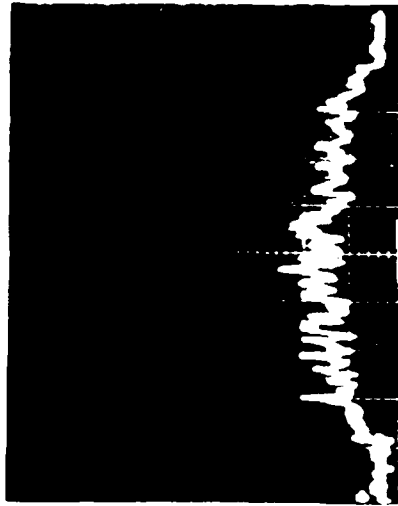
SPECKLE (EXPANDED SCALE)

SC46326
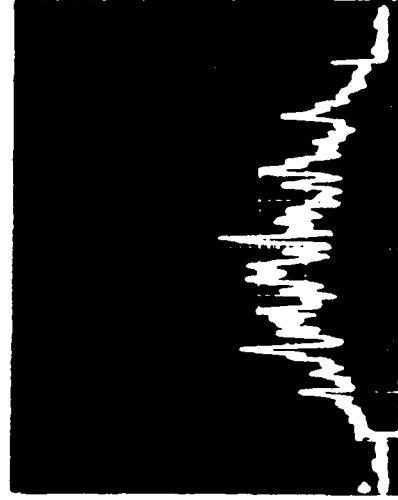
Rockwell International

Science Center

ALTERNATE CONFIGURATION FOR MODAL SCRAMBLING CORRECTION

SC46327

SCREEN

MMF

BS

PBS

λ/2

L

L

M

C

BaTiO₃
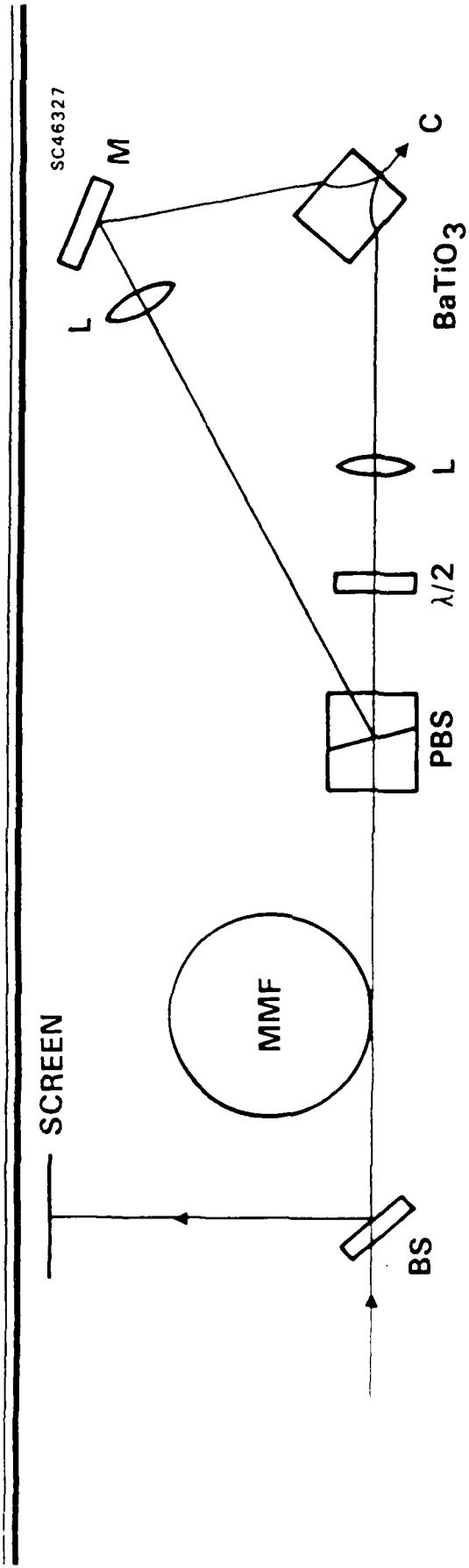
SPECKLE
PROFILES
ON SCREEN

BACKGROUND
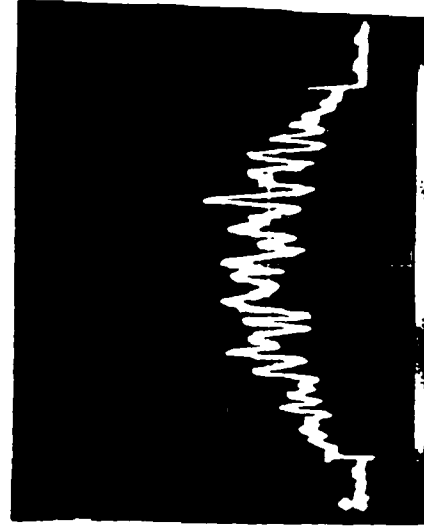
PPPC

Rockwell International
Science Center

MEASUREMENT OF NONRECIPROCAL PHASE SHIFT

INPUT

OUTPUT

PBS

λ/4

FM

λ/4

V

M

λ/2

MPC
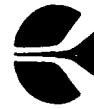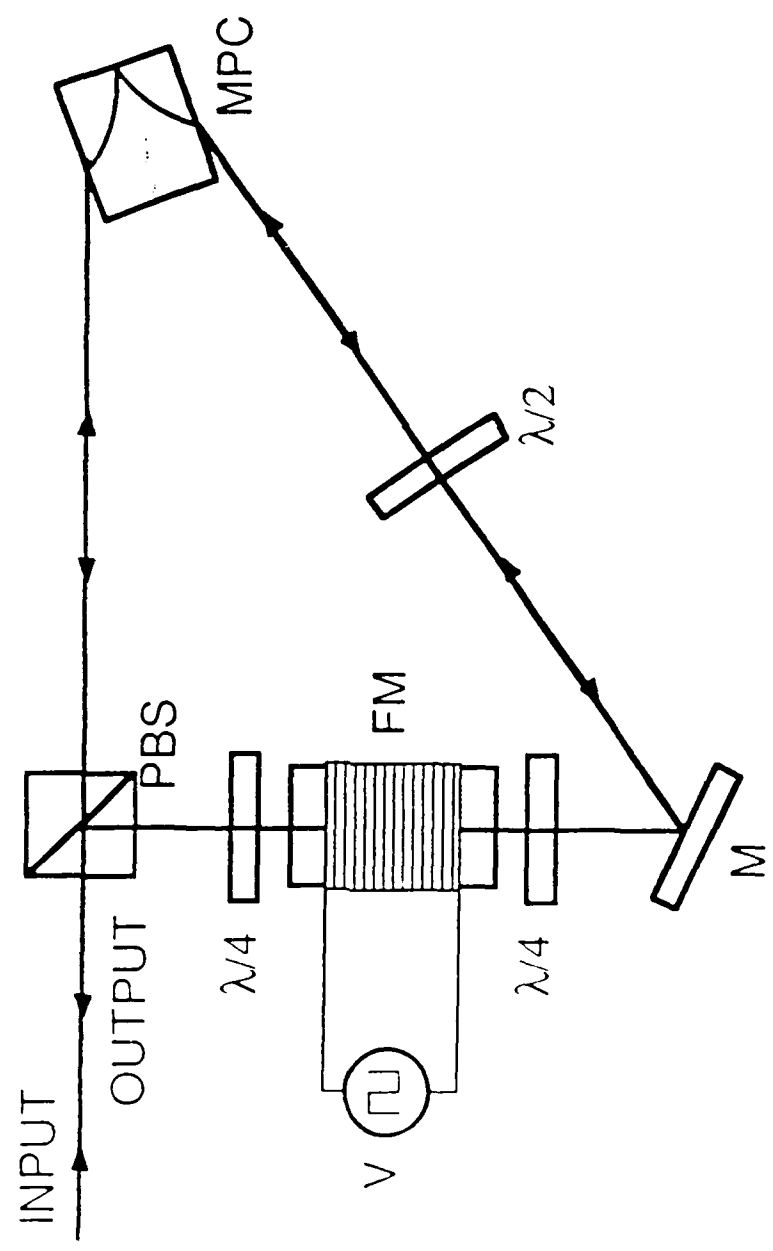
$V = \pm 0.4\,V$

ROTATION ANGLE
10 mrad

PHASE SHIFT
20 mrad

MULTIMODE FIBER-OPTIC GYRO USING A MUTUALLY-PUMPED PHASE CONJUGATOR

SC45476
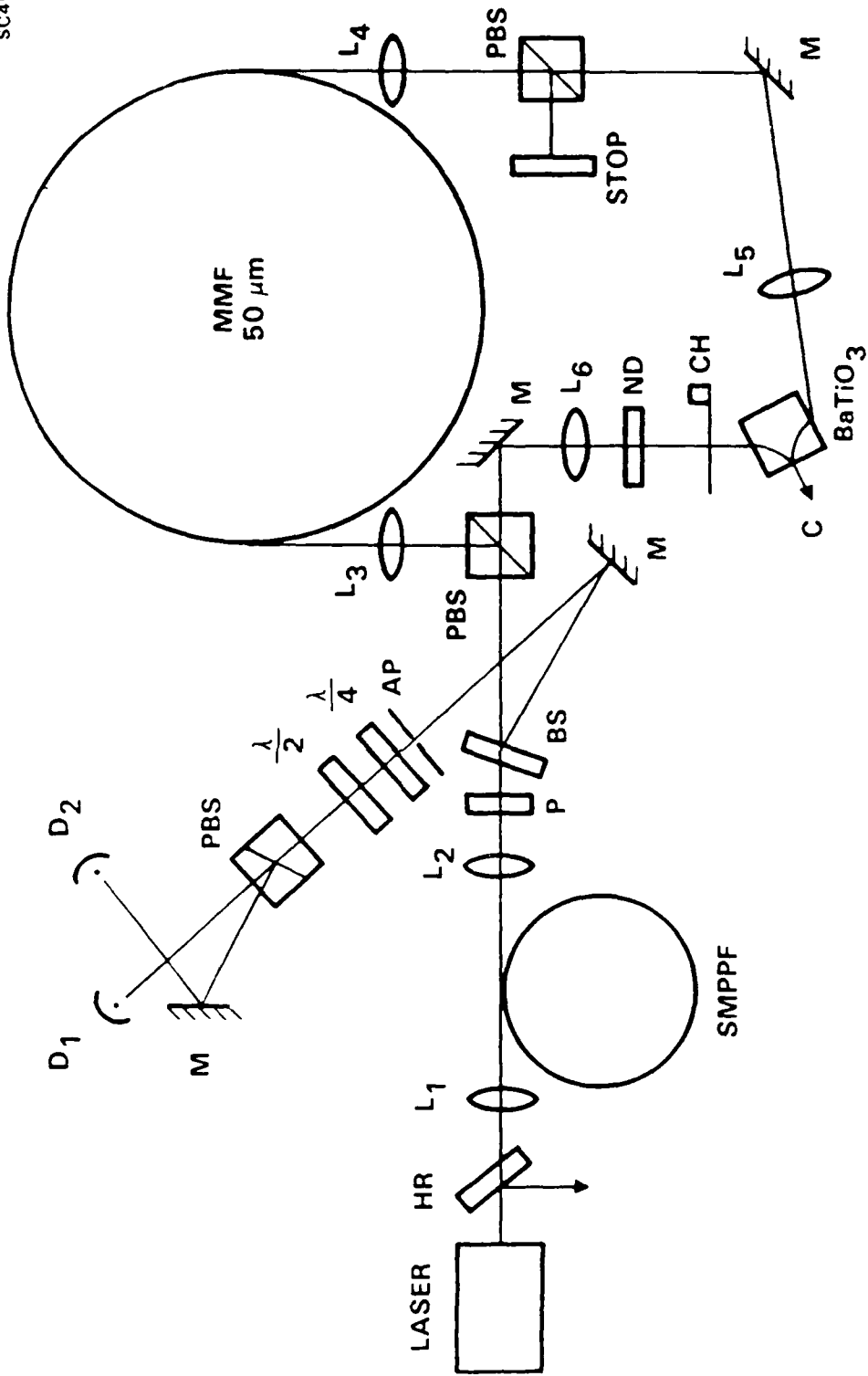
Rockwell International
Science Center

DEMONSTRATION OF ROTATION SENSING

SC45475

SIGNAL α $D_1 - D_2$

CHOPPER FREQUENCY 200 Hz
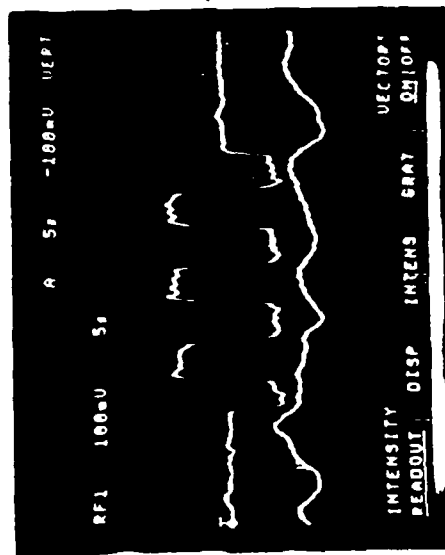
ROTATION SIGNAL
(6°/SECOND)
LOCK-IN T_c = 0.1 SEC

BACKGROUND NOISE
(VERTICAL SCALE $\div$ 10)
T_c = 1 SEC

Rockwell International
Science Center

PHASE MODULATION BIASING

PHASE MODULATION $\phi_m(t) = \phi_{mo} \sin(\omega_m t)$

PHASE DIFFERENCE BETWEEN CW, CCW WAVES

$\Delta\phi(t) = \Delta\phi_{NR} + \phi_m(t) - \phi_m(t - \tau)$

DETECTED POWER

$P_D(t) = 2 P_0 J_1(2 \phi_{mo} \sin(\omega_m \tau/2) \sin(\Delta\phi_{NR}) \sin(\omega_m t)$

OPTIMUM MODULATION FREQUENCY $\omega_m = \pi/\tau$

e.g. 1 km fiber loop, $\omega_m = 100$ kHz

Rockwell International

Science Center

MULTIMODE FIBER-OPTIC GYRO USING A MUTUALLY-PUMPED PHASE CONJUGATOR

Rockwell International
Science Center
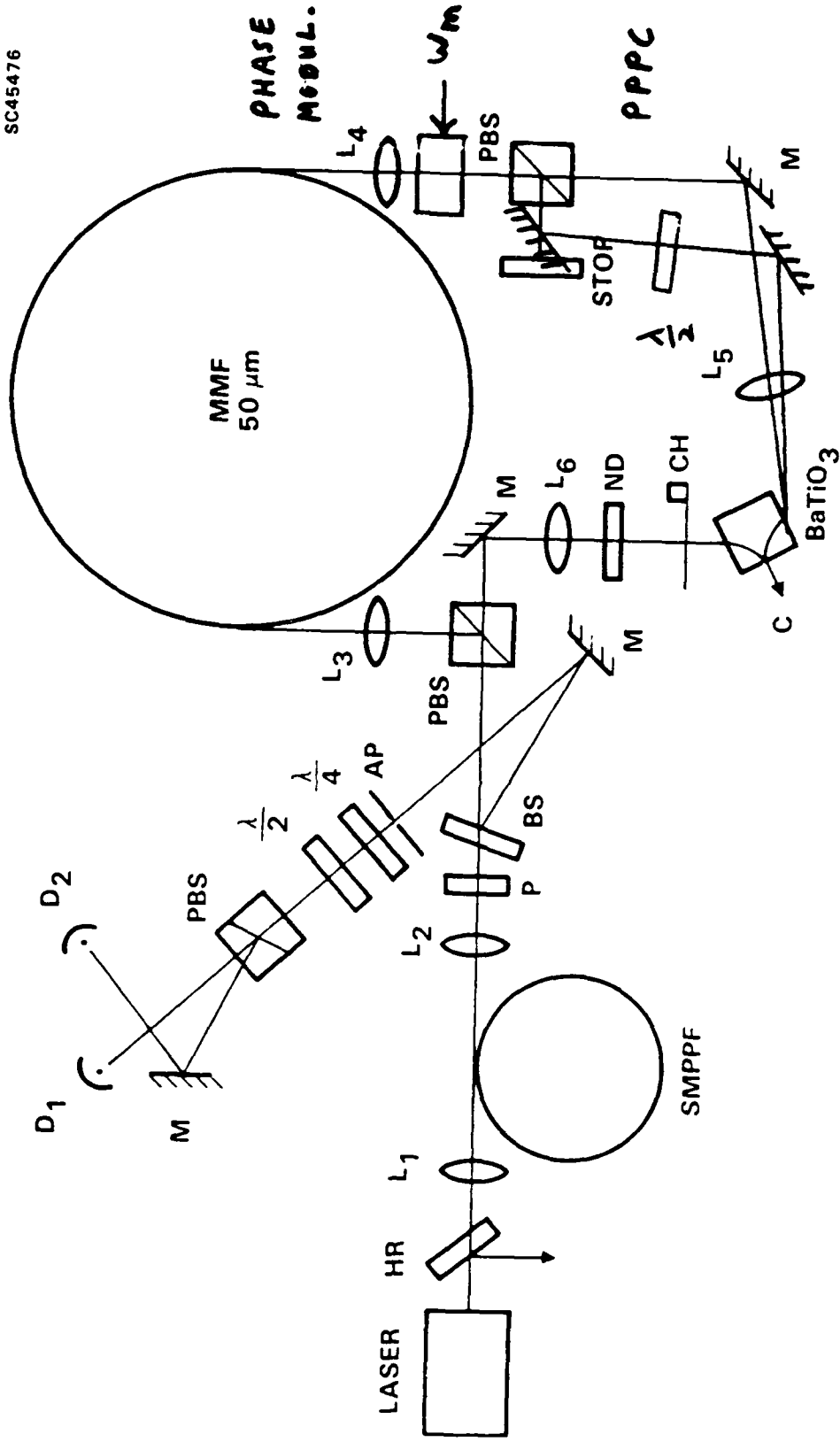
SUMMARY

-PERFORMED ROTATION SENSING WITH A PCFOG USING MULTIMODE FIBER AND A MUTUALLY PUMPED CONJUGATOR

-CONJUGATOR WILL ALLOW USE OF PHASE MODULATION BIASING WHICH CAN GREATLY INCREASE THE SENSITIVITY

Rockwell International
Science Center

APPENDIX 4.21

RECENT ADVANCES IN PHOTOREFRACTIVE
NONLINEAR OPTICS

RECENT ADVANCES IN PHOTOREFRACTIVE NONLINEAR OPTICS

(Invited Paper)

Pochi Yeh
Rockwell International Science Center
Thousand Oaks, California 91360

ABSTRACT

There have been several significant new developments in the area of photorefractive nonlinear optics during the past few years. This paper briefly describes some of the important and interesting phenomena and applications.

1.0 INTRODUCTION

The photorefractive effect is a phenomenon in which the local index of refraction is changed by the spatial variation of light intensity. This spatial index variation leads to a distortion of the wavefront and is referred to as "Optical Damage."[1] The photorefractive effect has since been observed in many electro-optic crystals, including $LiNbO_3$, $BaTiO_3$, SBN, BSO, BGO, GaAs, InP, and CdTe. This effect arises from optically generated charge carriers which migrate when the crystal is exposed to a spatially varying pattern of illumination with photons of sufficient energy.[2,3] Migration of charge carriers produces a space-charge separation, which then gives rise to a strong space-charge field. Such a field induces a change in index of refraction via the Pockels effect.[4] Photorefractive materials are, by far, the most efficient media for optical phase conjugation[5,6] and real-time holography using relatively low intensity levels (e.g., 1 W/cm^2).

2.0 TWO-WAVE MIXING

When two beams of coherent radiation intersect inside a photorefractive medium, an index grating is formed. This index grating is spatially shifted by $\pi/2$ relative to the intensity pattern. Such a phase shift leads to nonreciprocal energy transfer when these two beams propagate through the index grating. The hologram formed by the two-beam interference inside the photorefractive media can be erased by illuminating the hologram with light. Thus dynamic holography is possible using photorefractive materials.[7,8] Some of the most important and interesting applications are discussed as follows.

Laser Beam Cleanup

Two-wave mixing in photorefractive media exhibits energy transfer without any phase crosstalk.[9,10] This can be understood in terms of the diffraction from the self-induced index grating in the photorefractive crystal. Normally, if a beam that contains phase information $\psi(r,t)$ is diffracted from a fixed grating, the same phase information appears in the diffracted beam. In self-induced index gratings, the phase information $\psi(r,t)$ is impressed onto the grating in such a way that diffraction from this grating will be accompanied by a phase shift $-\psi(r,t)$. Such a self-cancellation of phase information is equivalent to the reconstruction of the reference beam when the hologram is read out by the object beam. Energy transfer without phase crosstalk can be employed to compress both

the spatial and the temporal spectra of a light beam.[10]   This has been demonstrated experimentally using $BaTiO_3$ and SBN crystals.[9-11]

Photorefractive Resonators

The beam amplification in two-wave mixing can be used to provide parametric gain for unidirectional oscillation in ring resonators. The oscillation has been observed using $BaTiO_3$ crystals.[12] Unlike the conventional gain medium (e.g., He-Ne), the gain bandwidth of photorefractive two-wave mixing is very narrow (a few hertz's for $BaTiO_3$). Despite this fact, the ring resonator can still oscillate over a large range of cavity detuning. This phenomenon was not well understood until a theory of photorefractive phase shift was developed.[13] This theory also predicts that the unidirectional ring resonator will oscillate at a frequency different from the pump frequency by an amount directly proportional to the cavity-length detuning. Furthermore, in a photorefractive material with moderately slow response time τ, the theory postulates a threshold where oscillation will cease if the cavity detuning becomes too large. The theory has been validated experimentally in a $BaTiO_3$ photorefractive ring resonator.[14]

Optical Nonreciprocity

It is known in linear optics that the transmittance as well as the phase shift experienced by a light beam transmitting through a dielectric layered medium is independent of the side of incidence.[15] This is no longer true when photorefractive coupling is present. Such nonreciprocal transmittance was first predicted by considering the coupling between the incident beam and the reflected beam inside a slab of photorefractive medium.[16] The energy exchange due to the coupling leads to an asymmetry in the transmittance. In the extreme case of strong coupling ($\gamma L \gg 1$), the slab acts as a "one-way" window. Nonreciprocal (optical) transmission has been observed in $BaTiO_3$ and $KNbO_3$:Mn crystals.[17,18] In addition, there exists a nonreciprocal phase shift in contra-directional two-wave mixing. Such nonreciprocity may be useful in applications such as the biasing of ring laser gyros.[18,19]

Conical Scattering

When a laser beam is incident on a photorefractive crystal, a cone of light (sometimes several cones) emerges from the crystal. This has been referred to as Photorefractive Conical Scattering. It is known that fanning of light occurs when a laser beam is incident on a photorefractive crystal.[20] Because of the strong two-beam coupling, any scattered light may get amplified and thus lead to fanning. In conical scattering, the noisy hologram formed by the incident light and the fanned light further scatters off the incident beam. The fanning hologram consists of a continuum of grating vectors, but only a selected portion of grating vectors satisfies the Bragg condition for scattering. This leads to a cone of scattered light. Photorefractive conical scattering has been observed in several different kinds of crystals.[21-23]

Cross-Polarization Two-Wave Mixing

Cubic crystals such as GaAs and InP exhibit significantly faster photorefractive response than many of the oxide crystals. In addition, the isotropy and the tensor nature of the electro-optic coefficients allow the possibility of cross-polarization two-wave mixing in which the s component of one beam is coupled to the p component of the other beam and vice versa. A coupled mode theory of

photorefractive two-wave mixing in cubic crystals was developed.[24] The theory predicts the existence of cross-polarization two-wave mixing in crystals possessing a point group symmetry of $\overline{4}3m$. Such a prediction was validated experimentally using photorefractive GaAs crystals.[25-27] Cross-polarization two-wave mixing provides extremely high signal-to-noise ratios in many of the applications which employ photorefractive two-wave mixing.

Photorefractive Optical Interconnection

A new method of reconfigurable optical interconnection using photorefractive dynamic holograms was conceived and demonstrated.[28] Reconfigurable optical interconnection using matrix-vector multiplication suffers a significant energy loss due to fanout and absorption at the spatial light modulators. In the new method, the nonreciprocal energy transfer in photorefractive media is employed to avoid the energy loss due to fanout. The result is a reconfigurable optical interconnection with a very high energy efficiency. The interconnection can be reconfigured by using a different SLM pattern. The reconfiguration time is limited by the formation of holograms inside the crystal. Once the hologram which contains the interconnection pattern is formed, such a scheme can provide optical interconnection between an array of lasers and an array of detectors for high data rate transmission.

3.0 OPTICAL PHASE CONJUGATION

Optical phase conjugation has been a subject of great interest because of its potential application in many areas of advanced optics.[4-6] For nonlinear materials with third-order susceptibilities, the operating intensity needed in four-wave mixing is often too high for many applications, especially for information processing. Photorefractive materials are known to be very efficient at low operating intensities. In fact, high phase conjugate reflectivities have been observed in $BaTiO_3$ crystals with very low operating power. In what follows, we will briefly describe some of the most important and interesting recent developments.

Self-Pumped Phase Conjugation

A class of phase conjugators which has received considerable attention recently are the self-pumped phase conjugators.[12,29] In these conjugators, there are no externally supplied counterpropagating pump beams. Thus, no alignment is needed. The reflectivity is relatively high at low laser power. These conjugators are, by far, the most convenient phase conjugate mirrors available. Although several models have been developed for self-pumped phase conjugation,[30-34] the phenomena can be easily understood by using the resonator model.[13,14,35] In this model, the crystal is viewed as an optical cavity which supports a multitude of modes. When a laser beam is incident into the crystal, some of the modes may be excited as a result of the parametric gain due to two-wave mixing. If the incident configuration supports bi-directional ring oscillation inside the crystal, then a phase conjugate beam is generated via the four-wave mixing. The model also explains the frequency shift of these conjugators.[35]

Mutually Pumped Phase Conjugators

Another class of phase conjugators consists of the mutually pumped phase conjugators (MPPC) in which two incident incoherent beams can pump each

other to produce a pair of phase conjugate beams inside a photorefractive crystal. The spatial wavefronts of the beams are conjugated and the temporal information is exchanged. The phase conjugation requires the simultaneous presence of both beams. Recently, conjugators were demonstrated experimentally using two incoherent laser beams in $BaTiO_3$.[36,38,39] These phenomena can be explained in terms of either hologram sharing[39,40] or self-oscillations[37] in a four-wave mixing process or resonator model.[41]

Phase Conjugate Michelson Interferometers

We will now consider a Michelson interferometer which is equipped with phase conjugate mirrors. Such an optical setup is known as a phase conjugate Michelson interferometer and has been studied by several workers.[42-44] By virtue of its names, this interferometer exhibits optical time reversal. Consequently, no interference is observed at the output port. The output port is, in fact, totally dark.[44] Such an interferometer is ideal for parallel subtraction of optical images because the two beams arriving at the output port are always out of phase by π. This has been demonstrated experimentally using a $BaTiO_3$ crystal as the phase conjugate mirrors.[45] Using a fiber loop as one of the arms, such an interferometer can be used to sense nonreciprocal phase shifts.[46] A phase conjugate fiber optic gyro has been built and demonstrated for rotation sensing using $BaTiO_3$ crystals.[47,48]

Phase Conjugate Sagnac Interferometers

Using the mutually pumped phase conjugators mentioned earlier, a new type of phase conjugate interferometer was conceived and demonstrated.[49] In the new interferometer, one of the mirrors of a conventional Sagnac ring interferometer is replaced with a MPPC. Such a new interferometer has a dual nature of Michelson and Sagnac interferometry. As far as wavefront information is concerned, the MPPC acts like a retro-reflector and the setup exhibits phase conjugate Michelson interferometry and optical time reversal.[44] As for the temporal information, the MPPC acts like a normal mirror and Sagnac interferometry is obtained. Such a new phase conjugate interferometer can be used to perform parallel image subtraction over a large aperture. With optical fiber loops inserted in the optical path, we have constructed fiber-optic gyros and demonstrated the rotation sensing.

Other Developments Related to Photorefractive Nonlinear Optics

In addition to those described above, there are other significant developments. These include polarization-preserving conjugators,[50] phase shifts of conjugators,[51] optical matrix algebra,[52] fundamental limit of photorefractive speed,[53] nondegenerate two-wave mixing in ruby crystal,[54] and nonlinear Bragg scattering in Kerr media.[55]

REFERENCES

1. Ashkin, A., et al, Appl. Phys. Lett. 9, 72 (1966).
2. Vinetskii, V.L., et al, Sov. Phys. Usp. 22, 742 (1979).
3. Kukhtarev, N.V., et al, Ferroelectrics 22, 961 (1979).
4. Yariv, A., and Yeh, P., "Optical Waves in Crystals," (Wiley, 1984).
5. See, for example, Pepper, D., Sci. Am. 254, 74 (1986).
6. Yariv, A., IEEE J. Quantum Electronics, QE-14, 650 (1978).

7. Staebler, D.L., and Amodei, J.J., J. Appl. Phys. 34, 1042 (1972).
8. Vahey, D.W., J. Appl. Phys. 46, 3510 (1975).
9. Chiou, A.E.T., and Yeh, P., Opt. Lett. 10, 621 (1985).
10. Yeh, P., CLEO Technical Digest (1985) p. 274.
11. Chiou, A.E.T., and Yeh, P., Opt. Lett. 11, 461 (1986).
12. White, J.O., et al, Appl. Phys. Lett. 40, 450 (1982).
13. Yeh, P., J. Opt. Soc. Am. B2, 1924 (1985).
14. Ewbank, M.D. and Yeh, P., Opt. Lett. 10, 496 (1985).
15. Knittl, Z., Optics of Thin Films (Wiley, New York, 1976), p. 240.
16. Yeh, P., J. Opt. Soc. Am. 73, 1268-1271 (1983).
17. Zha, M.Z., and Gunter, P., Opt. Lett. 10, 184-186 (1985).
18. Yeh, P., and Khoshnevisan, M., SPIE 487, 102-109 (1984).
19. Yeh, P., Appl. Opt. 23, 2974-2978 (1984).
20. Feinberg, J., J. Opt. Soc. Am. 72, 46 (1982).
21. Odoulov, S., Belabaev, K., and Kiseleva, I., Optics. Lett. 10, 31 (1985).
22. Temple, D.A., and Warde, C., J. Opt. Soc. Am. B3, 337 (1986).
23. Ewbank, M.D., Yeh, P., and Feinberg, J., Opt. Comm. 59, 423 (1986).
24. Yeh, P., J. Opt., Soc. Am. B4, 1382 (1987).
25. Cheng, L.-J. and Yeh, P., Opt. Lett. 13, 50 (1988).
26. Chang, T.Y., Chiou, A.E.T. and Yeh, P., OSA Tech. Digest 17, 55 (1987).
27. Chang, T.Y., Chiou, A.E.T. and Yeh, P., J. Opt. Soc. Am. B5, 1724 (1988).
28. Yeh, P., Chiou, A.E., and Hong, J., Appl. Opt. 27, 2093 (1988).
29. Feinberg, J., Opt. Lett. 7, 486 (1982); Opt. Lett. 8, 480 (1983).
30. Chang, T.Y. and Hellwarth, R.W., Opt. Lett. 10, 408 (1985).
31. Lam, J.F., Appl. Phys. Lett. 46, 909 (1985).
32. MacDonald, K.R., and Feinberg, J., J. Opt. Soc. Am. 73, 548 (1983).
33. Ganthica, D.J., et al, Phys. Rev. Lett. 58, 1644 (1987).
34. Gower, M.C., Opt. Lett. 11, 458 (1986).
35. Ewbank, M.D., and Yeh, P., Proc. SPIE Vol. 613, 59 (1986).
36. Ewbank, M.D., Opt. Lett. 13, 47 (1988).
37. Cronin-Golomb, M., et al, IEEE J. Quantum Electron. QE-20, 12 (1984).
38. Weiss, S., Sternklar, S. and Fischer, B. Opt. Lett. 12, 114 (1987).
39. Eason, R.W., Smout, A.M.C., Opt. Lett. 12, 51 (1987); 12, 498 (1987).
40. Yeh, P., submitted to Opt. Lett. (1988).
41. Yeh, P., Chang, T.Y., and Ewbank, M.D., J. Opt. Soc. Am. B5, 1743 (1988).
42. Ewbank, M., Yeh, P., and Khoshnevisan, M., SPIE Proc. Vol. 464, 2 (1984).
43. Chen, W.H., et al, SPIE Proc. Vol. 739, 105 (1987).
44. Ewbank, M.D., et al, J., Opt. Lett. 10, 282 (1985).
45. See, for example, Chiou, A.E.T., and Yeh, P., Opt. Lett. 11, 306 (1986).
46. Yeh, P., McMichael, I., and Khoshnevisan, M., Appl. Opt. 25, 1029 (1986).
47. McMichael, I., and Yeh, P., Opt. Lett. 11, 686 (1986).
48. McMichael, I., Beckwith, P., and Yeh, P., 12, 1023 (1987).
49. McMichael, I., et al, CLEO Tech. Digest Vol. 7, 134 (1988).
50. McMichael, I., Yeh, P., and Khoshnevisan, M., Opt. Lett. 11, 525 (1986).
51. McMichael, I., and Yeh, P., Opt. Lett. 12, 48 (1987).
52. Yeh, P., and Chiou, A.E.T., Opt. Lett. 12, 138 (1987).
53. Yeh, P., Appl. Opt. 26, 602 (1987).
54. McMichael, I., Yeh, P., and Beckwith, P., Opt. Lett. 13, 500 (1988).
55. Yeh, P., and Koshnevisan, M., J. Opt. Soc. Am. B4, 1954 (1987).

APPENDIX 4.22

PHASE-CONJUGATE RING INTERFEROMETER

Phase-Conjugate Ring Interferometer

Ian McMichael, M.D. Ewbank and Pochi Yeh

Rockwell International Science Center

1049 Camino Dos Rios

Thousand Oaks, CA 91360

(805) 373-4508

ABSTRACT

We describe a ring interferometer which incorporates a mutually-pumped phase conjugator as one of the mirrors. As expected, this interferometer acts like a Sagnac interferometer, but with a wide field-of-view and wavefront distortion correction. An unexpected nonreciprocal phase shift, introduced by the mutually-pumped phase conjugator, is also observed.

Phase-Conjugate Ring Interferometer

Ian McMichael, M.D. Ewbank and Pochi Yeh

Rockwell International Science Center

1049 Camino Dos Rios

Thousand Oaks, CA 91360

(805) 373-4508

SUMMARY

Referring to Fig. 1, we describe an interferometer that employs one of the recently discovered mutually-pumped phase conjugators[1,2,3] (MPPC's) as a mirror in a Sagnac ring configuration. Light incident on one side of the MPPC exits from the opposite side. In this sense, the MPPC acts like a reflector and, consequently, the phase-conjugate ring interferometer (PCRI) shown in Fig. 1 behaves like a Sagnac ring interferometer. However, the light exiting from each side the MPPC is the spatial phase conjugate of the light incident on that side. Therefore, unlike a Sagnac, the PCRI has a large field-of-view and can correct for wavefront distortions; thus, the PCRI resembles a phase-conjugate Michelson interferometer.

To demonstrate these features, we set up the PCRI shown in Fig. 1 using a "bird-wing" MPPC with photorefractive barium titanate.[3] We found that 15% of the total power exits from the output port of the interferometer. This contrasts what occurs when the MPPC is replaced by a self-pumped conjugator where less than 1% exits from the output.[4] For a typical Sagnac interferometer, with no nonreciprocal phase-shifts present, the percentage of power at the output is given by,

$$(T - R)^2 \times 100\% \tag{1}$$

where T and R are the intensity transmission and reflection coefficients of the beamsplitter. For our beamsplitter with T = 2/3, R = 1/3, Eq. 1 gives 11%. This was verified by replacing the MPPC with a normal mirror. There are two possibilities why the output of the PCRI is higher than that for the Sagnac interferometer: a nonreciprocal transmission and/or a nonreciprocal phase shift. Initially, neither of these two possibilities seems plausible since the configuration used for the "bird-wing" PCRI was very symmetric.

To investigate this nonreciprocal behavior, we set up the PCRI shown in Fig. 2. Light incident on the interferometer has linear polarization at 45° to the plane of incidence. With no nonreciprocal elements in the interferometer, the output should also be linear polarization at 45° to the plane of incidence. A nonreciprocal transmission will rotate the polarization of the output from 45°, and a nonreciprocal phase shift will change the polarization from linear to elliptical. For the bird-wing PCRI, the output is at 45° to the plane of incidence, indicating that the transmission is reciprocal. However, the output polarization is elliptical. The measured ratio of the intensity along the minor axis to that along the major axis is 6% and this indicates a nonreciprocal phase shift of 30°. Again, this contrasts what occurs when the MPPC is replaced by a self-pumped conjugator, where the polarization of the output is identical to the input to within 1%, both in angle, and in ellipticity.[5]

To compare the results of our second experiment with the first, we consider a Sagnac interferometer with no nonreciprocal transmission, but a nonreciprocal phase shift δ. In this case, the percentage of power at the output is given by,

$$[(T - R)^2 + 2 T R (1 - \cos \delta)] \times 100\% . \tag{2}$$

Using our values of T and R from the first experiment, and our value of δ from the second, Eq. 2 gives 17% which is reasonably close to the value of 15% measured in the first experiment. Consequently, these experiments indicate that the PCRI acts like a Sagnac interferometer with a

nonreciprocal phase shift.

The wide field-of-view of the PCRI is demonstrated by the fact that in the first experiment the two beams were lightly focussed into the bird-wing MPPC, and we were able to do image subtraction by placing transparencies in the two beams. We also demonstrated the ability of the bird-wing PCRI to sense nonreciprocal phase shifts by placing a Faraday modulator in the interferometer. Both of these applications (i.e., image subtraction and nonreciprocal phase-shift sensing) of the PCRI have been previously mentioned.[2]

REFERENCES

1. R.W. Eason and A.M.C. Smout, Opt. Lett. 12, 51 (1987); A.M.C. Smout and R.W. Eason, Opt. Lett. 12, 498 (1987).

2. S. Weiss, S. Sternklar and B. Fischer, Opt. Lett. 12, 114 (1987); S. Sternklar, S. Weiss, M. Segev and B. Fischer, Opt. Lett. 11, 528 (1986).

3. M.D. Ewbank, to be published, Opt. Lett. (Jan. 1988); M.D. Ewbank, OSA Topical Meeting on Photorefractive Materials, Effects, and Devices Technical Digest, Vol. 17, pp 179-182 (UCLA, Aug. 1987).

4. M.D. Ewbank, P. Yeh, M. Khoshnevisan, and J. Feinberg, Opt. Lett. 10, 282 (1985).

5. I. McMichael, M. Khoshnevisan, and P. Yeh, Opt. Lett. 11, 525 (1986).

FIGURE CAPTIONS

1. Phase-conjugate ring interferometer used in the first experiment. Light from a laser is split by beamsplitter BS into two beams, one is reflected by mirror M, and both are incident on a mutually-pumped phase conjugator MPPC.

2. Phase-conjugate ring interferometer used in the second experiment. Light from a laser with polarization at 45° to the plane of incidence is split by polarizing beamsplitter PBS into two beams, one is reflected by mirror M and has its polarization rotated by the half-wave retarder $\lambda/2$, and both are incident on a mutually pumped phase conjugator MPPC.

OUTPUT

INPUT

BS

MPPC

M

Fig. 1

INPUT

OUTPUT

PBS

MPPC

λ/2

M
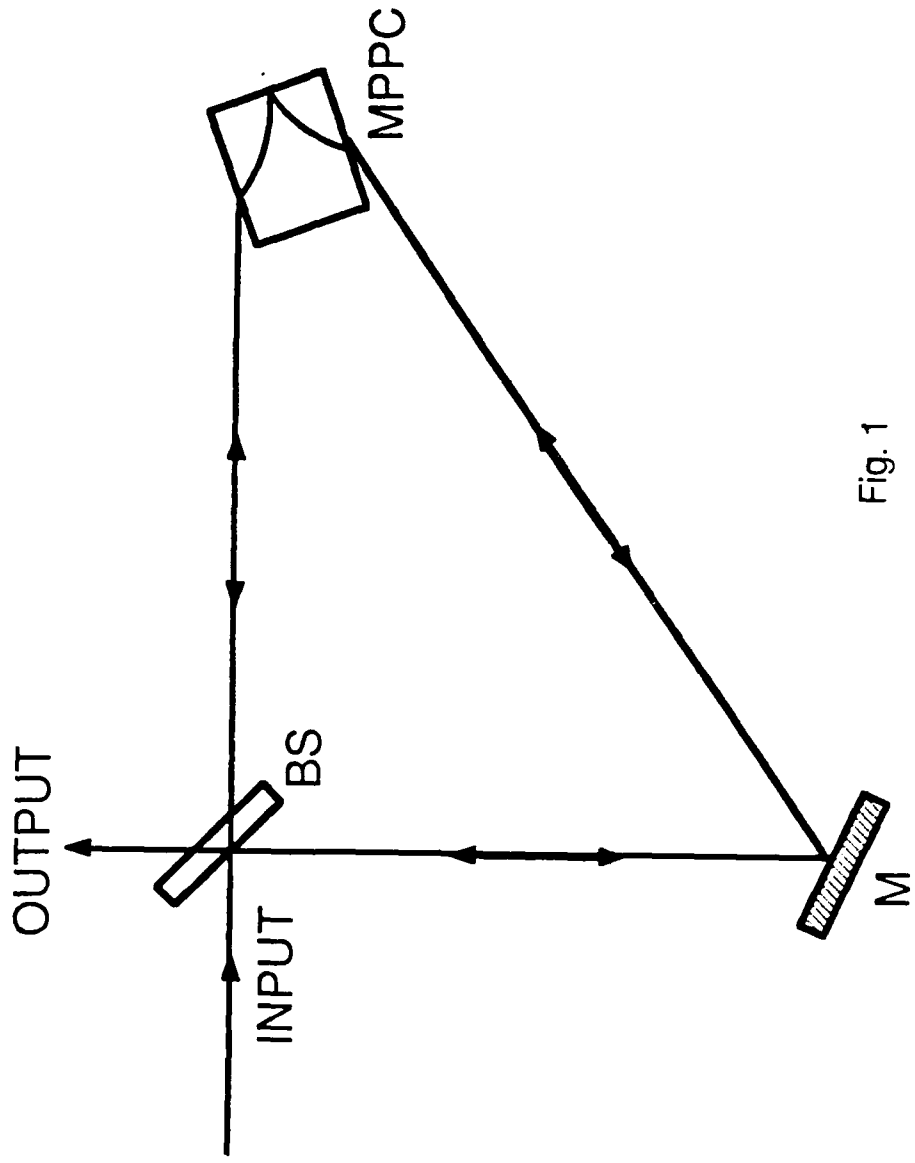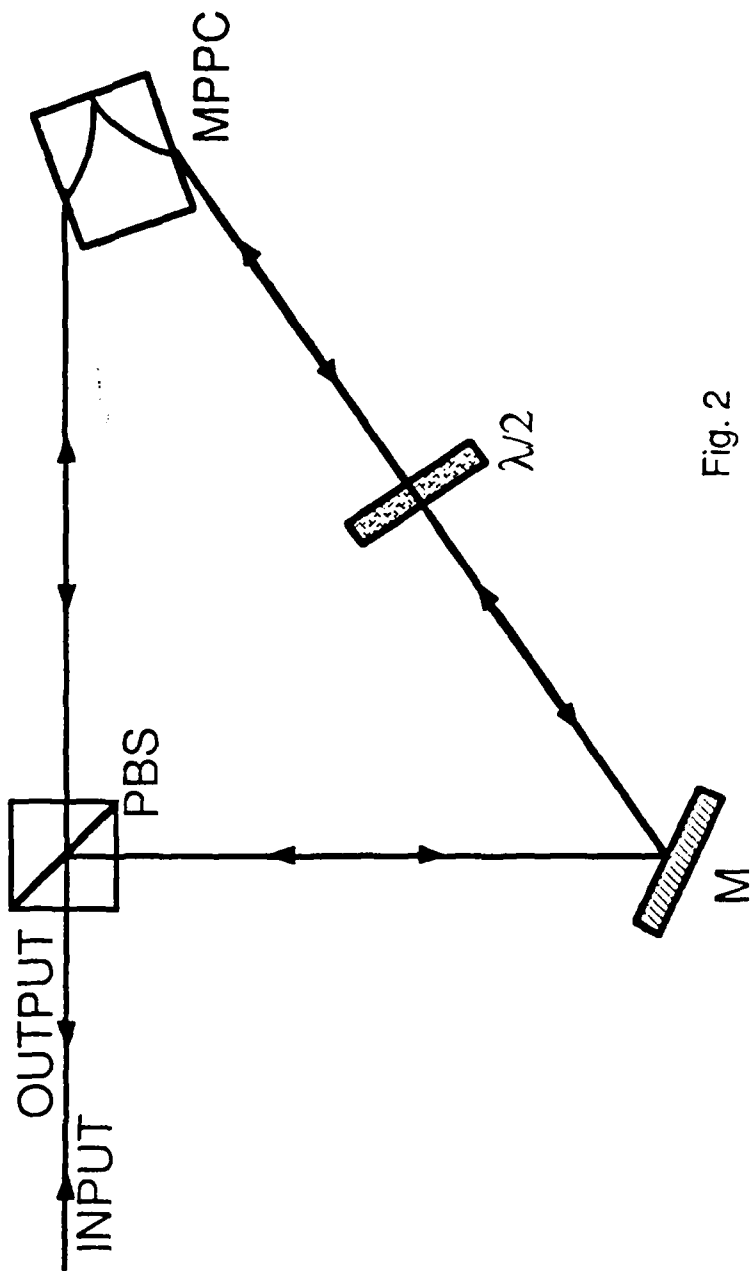
Fig. 2

PHASE-CONJUGATE RING INTERFEROMETER

IAN McMICHAEL, M.D. EWBANK AND POCHI YEH
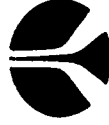
Rockwell International

Science Center

DISTORTION CORRECTION VS PHASE-CONJUGATE INTERFEROMETRY

PHASE-
CONJUGATE
MIRROR

BEAM
SPLITTER

DISTORTER

PHASE-
CONJUGATE
MIRROR
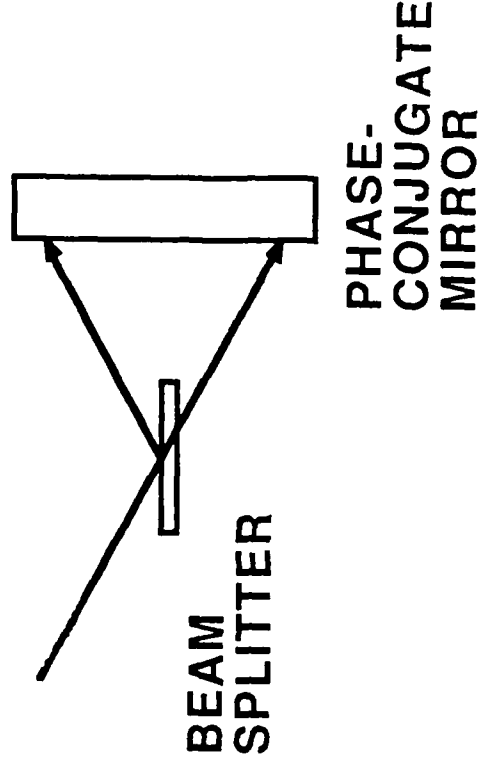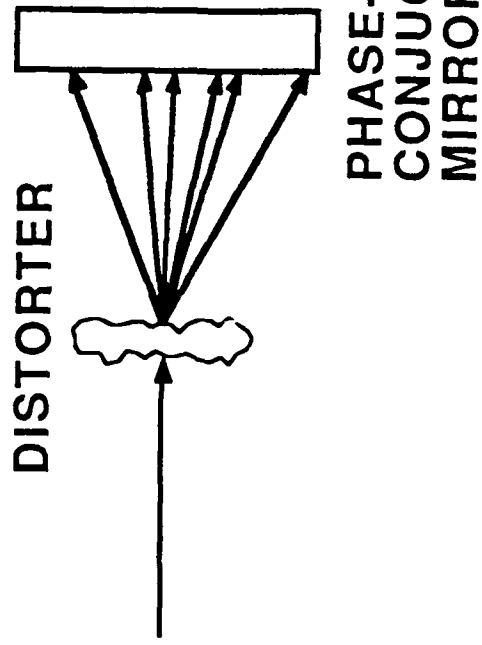
DEMONSTRATED APPLICATIONS OF PHASE-CONJUGATE INTERFEROMETRY

- POLARIZATION-PRESERVING PHASE CONJUGATION

- IMAGE SUBSTRACTION

- PARALLEL OPTICAL COMPUTATIONS

- NOVELTY FILTERS

- MEASUREMENT OF PHASE SHIFTS OF PHASE-CONJUGATE WAVES AND OF PHOTOREFRACTIVE GRATINGS

- GYROS

- HYDROPHONE

- INTERFEROMETRIC HOLOGRAPHY

Rockwell International
Science Center

PROPERTIES OF PHASE-CONJUGATE INTERFEROMETERS

- REAL TIME DISTORTION CORRECTION

- SELF-REFERENCING

- SELF-BIASING

- WIDE FIELD-OF-VIEW

- ALIGNMENT INSENSITIVE

Rockwell International
Science Center

PHASE-CONJUGATE MIRRORS
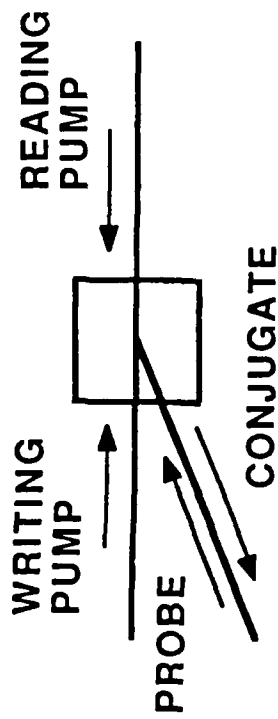
EXTERNALLY PUMPED

- REAL TIME HOLOGRAM
  CONTAINS PHASE INFORMATION
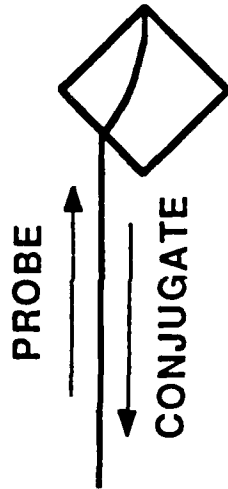
SELF PUMPED

- BIDIRECTIONAL OSCILLATION
  PROVIDES PUMPING WAVES
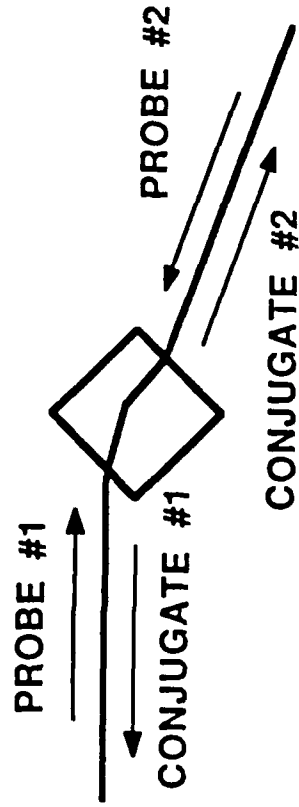
MUTUALLY PUMPED

- THERE IS ONE HOLOGRAM THAT
  IS SUPPORTED BY BOTH PROBES

PHASE-CONJUGATE INTERFEROMETERS
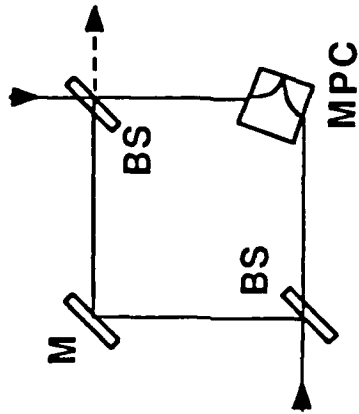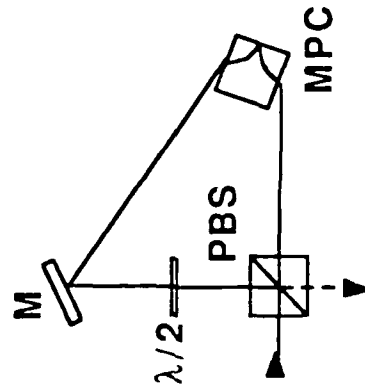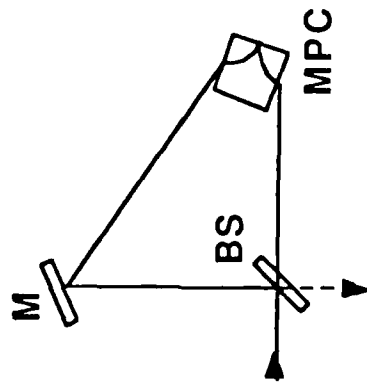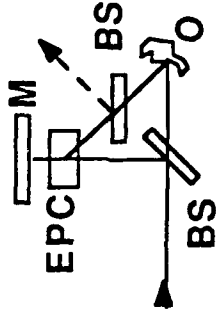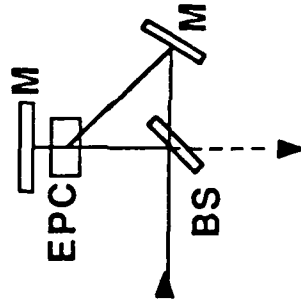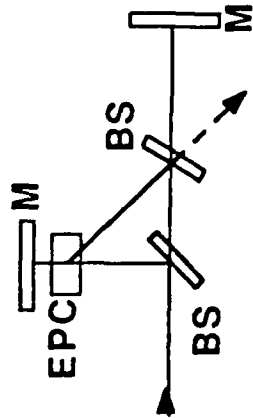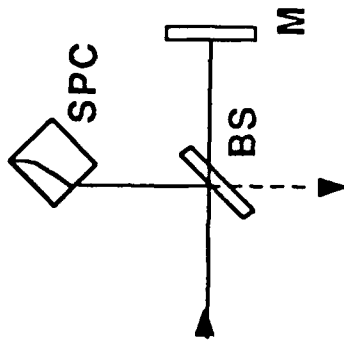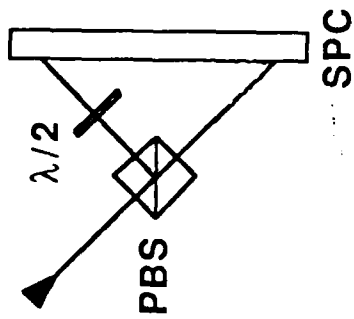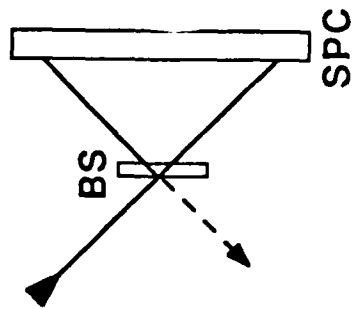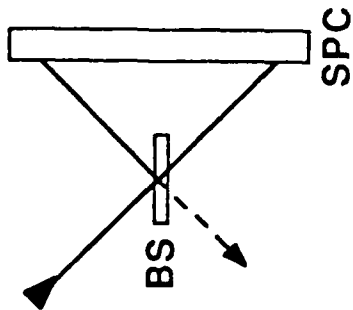
DEPENDENCE OF SUBTRACTION ON THE RATIO OF THE SPATIAL INTENSITY PROFILES

SIDE VIEW OF CRYSTAL

$I_1(x)$

GRATING REGION

$I_2(x)$

COMBINED OUTPUT

OUTPUTS

x

I
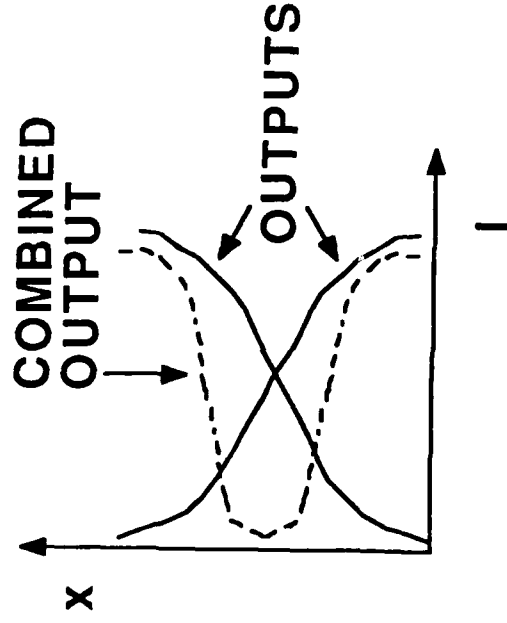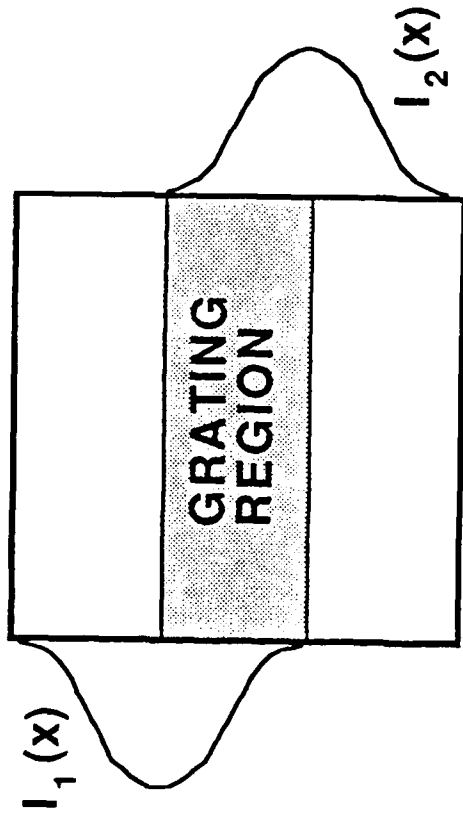
Rockwell International

Science Center

IMAGE INVERSION AND SUBTRACTION

IMAGE INVERSION
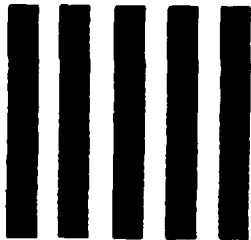
IMAGE

INVERSION
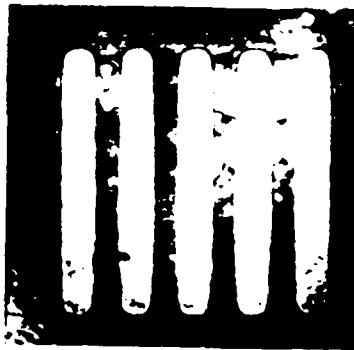
IMAGE SUBTRACTION
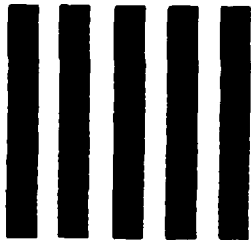
IMAGE #1   IMAGE #2

SUBTRACTION

SC44760
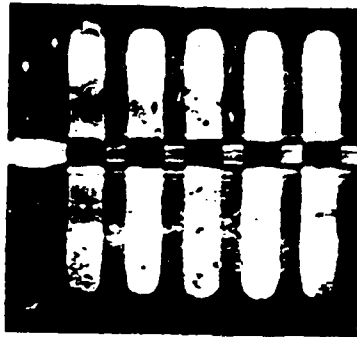
Rockwell International
Science Center

PHASE-CONJUGATE RING INTERFEROMETER #2
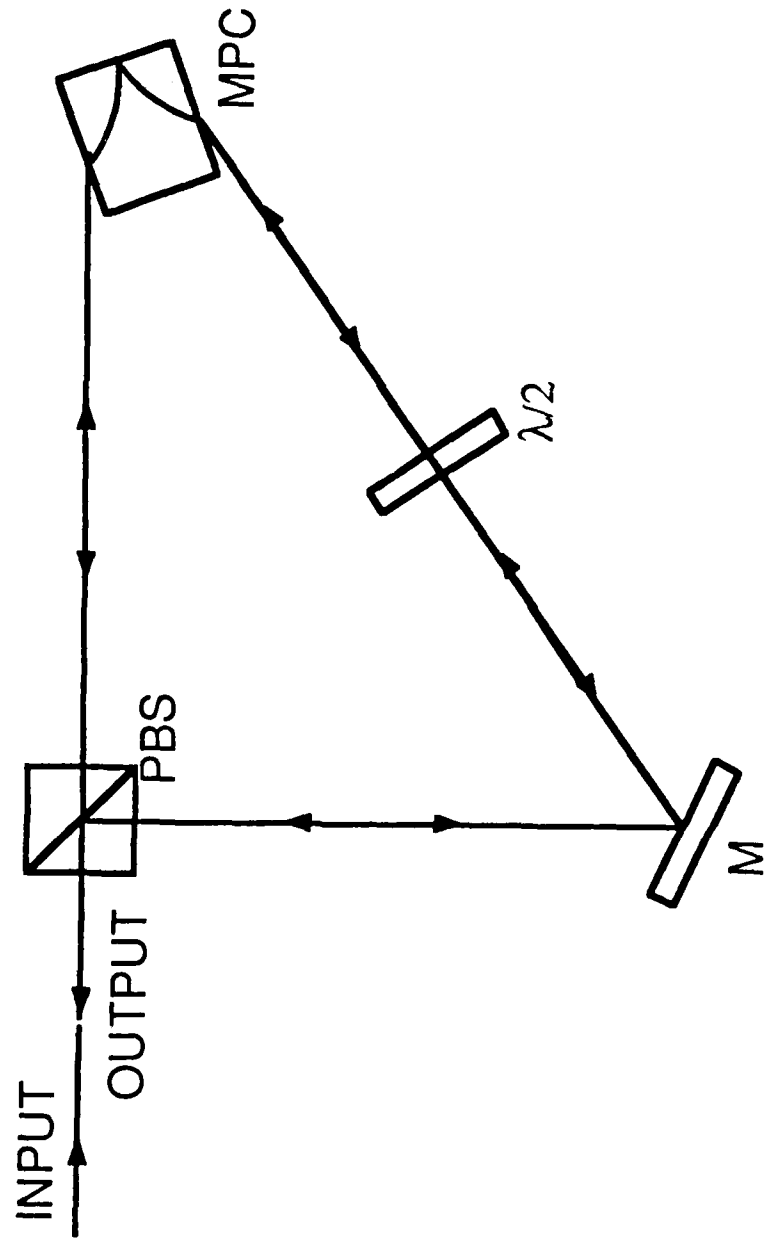
FOR LINEAR INPUT
POLARIZATION

NONRECIPROCAL
PHASE SHIFT
> ELLIPTICAL

NONRECIPROCAL
TRANSMISSION
> ROTATION

INPUT POL
45°   10-4

OUTPUT POL
45°   10-3

INPUT

OUTPUT

PBS

MPC

λ/2

M

Rockwell International
Science Center

OUTPUT VS CRYSTAL POSITION
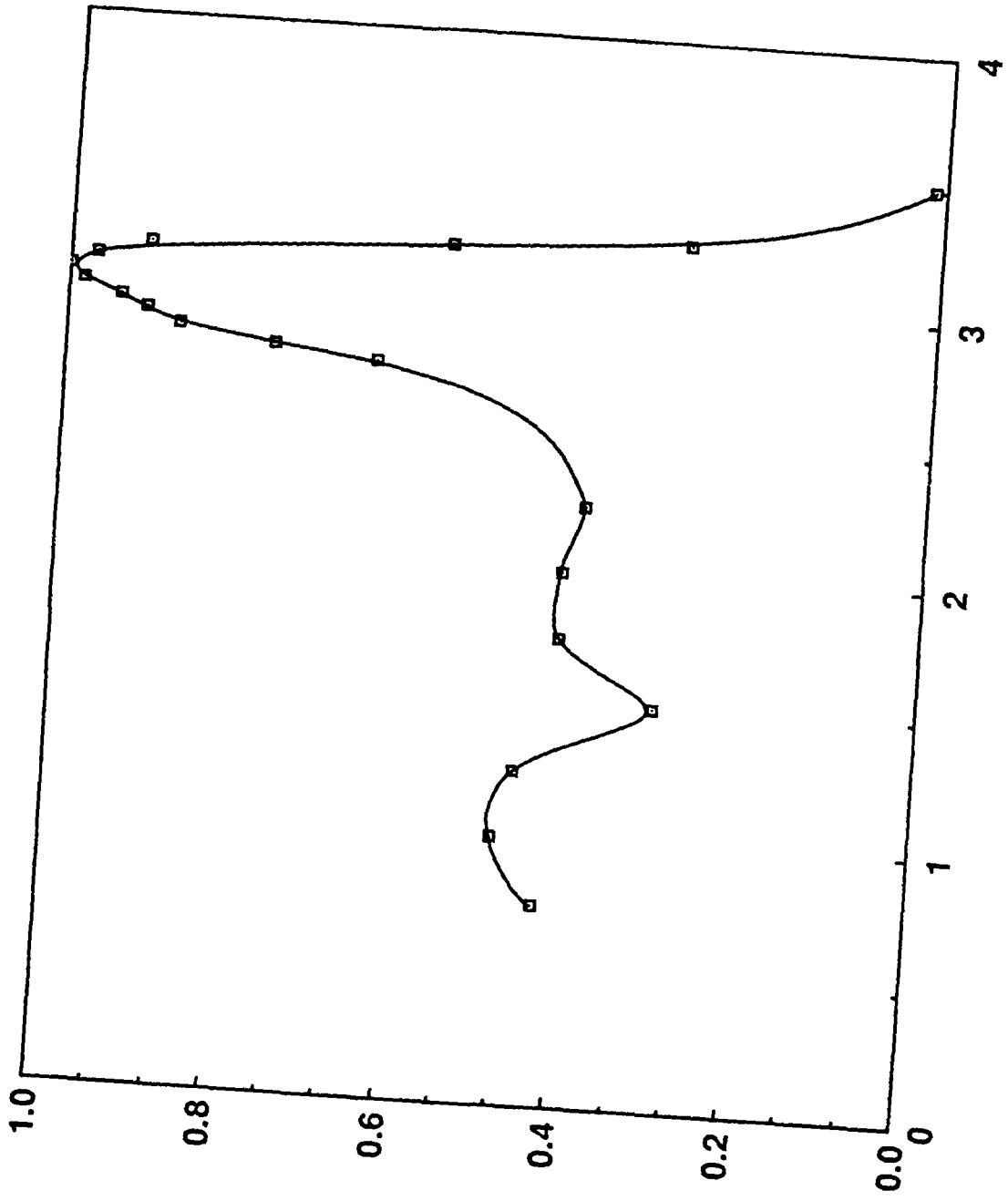
OUTPUT POWER (ARB.)

CRYSTAL POSITION (mm)

OUTPUT POWER (ARB.)

BEAM RATIO

INCIDENT POLARIZATION ANGLE (DEGREES)
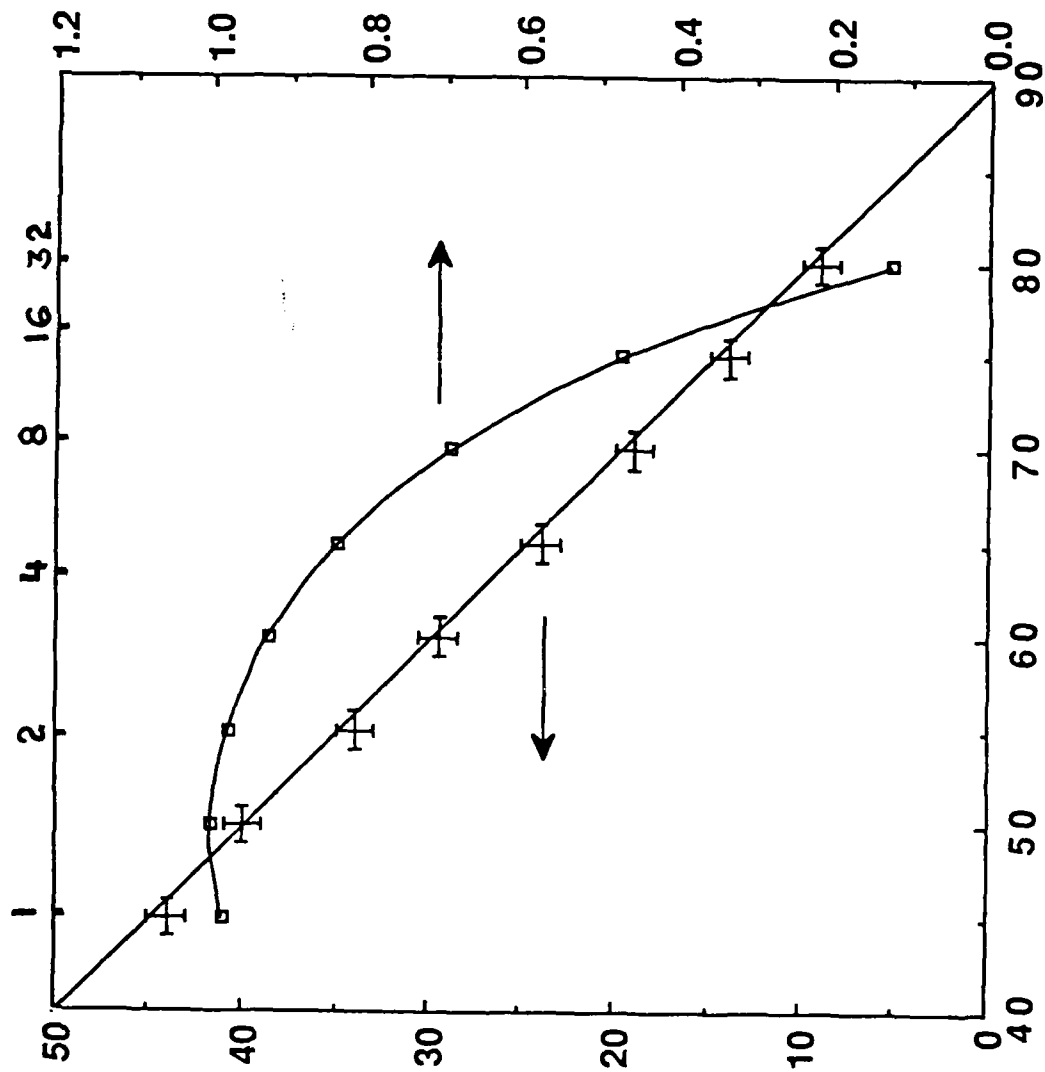
REFLECTED POLARIZATION ANGLE (DEGREES)

MEASUREMENT OF NONRECIPROCAL PHASE SHIFT

INPUT

OUTPUT

PBS

λ/4

FM

λ/4

M

λ/2

MPC

V
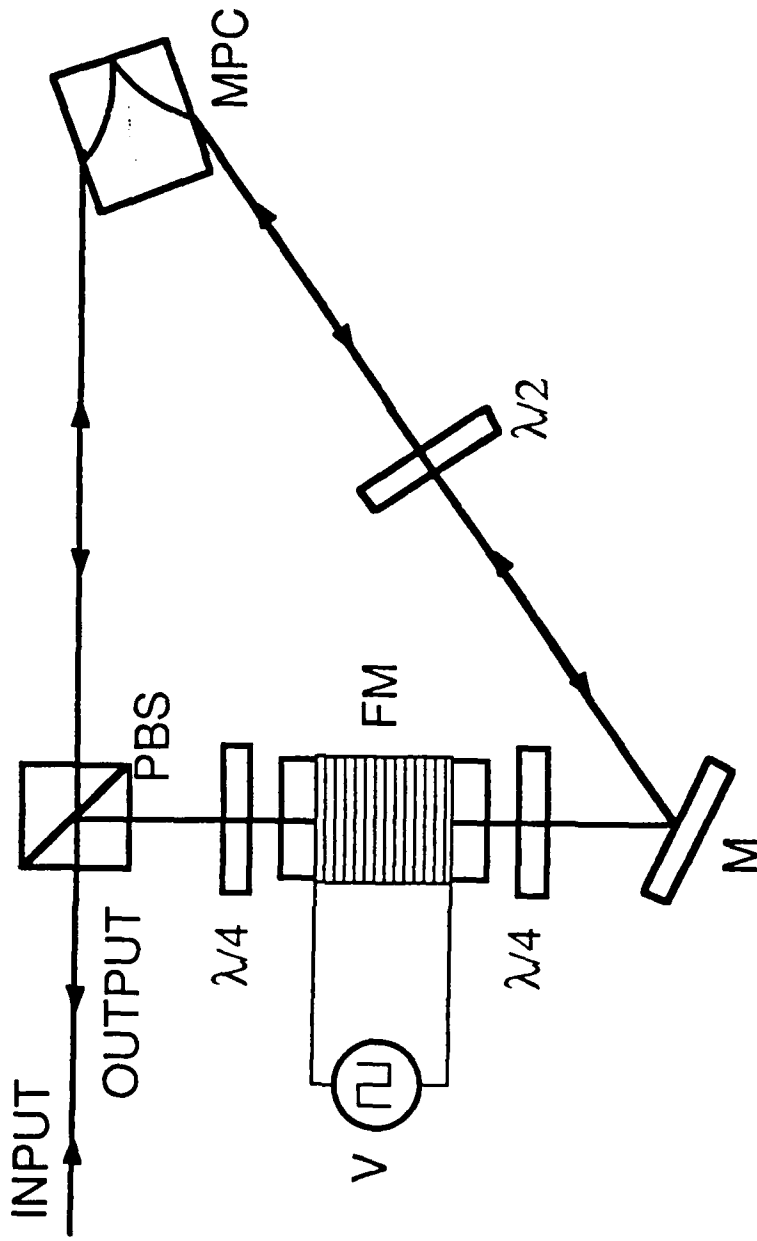
$V = \pm 0.4\,V$

ROTATION ANGLE
10 mrad

PHASE SHIFT
20 mrad

Rockwell International
Science Center

CORRECTION OF MODAL SCRAMBLING IN MULTIMODE FIBERS BY A MUTUALLY PUMPED CONJUGATOR

INPUT POL 45° 10-4

OUTPUT POL

PPPC 45° 10-2

NPPPC 45° 10-1

MPC

λ/2

M

PBS

M

BS

BS

MMF

Rockwell International
Science Center
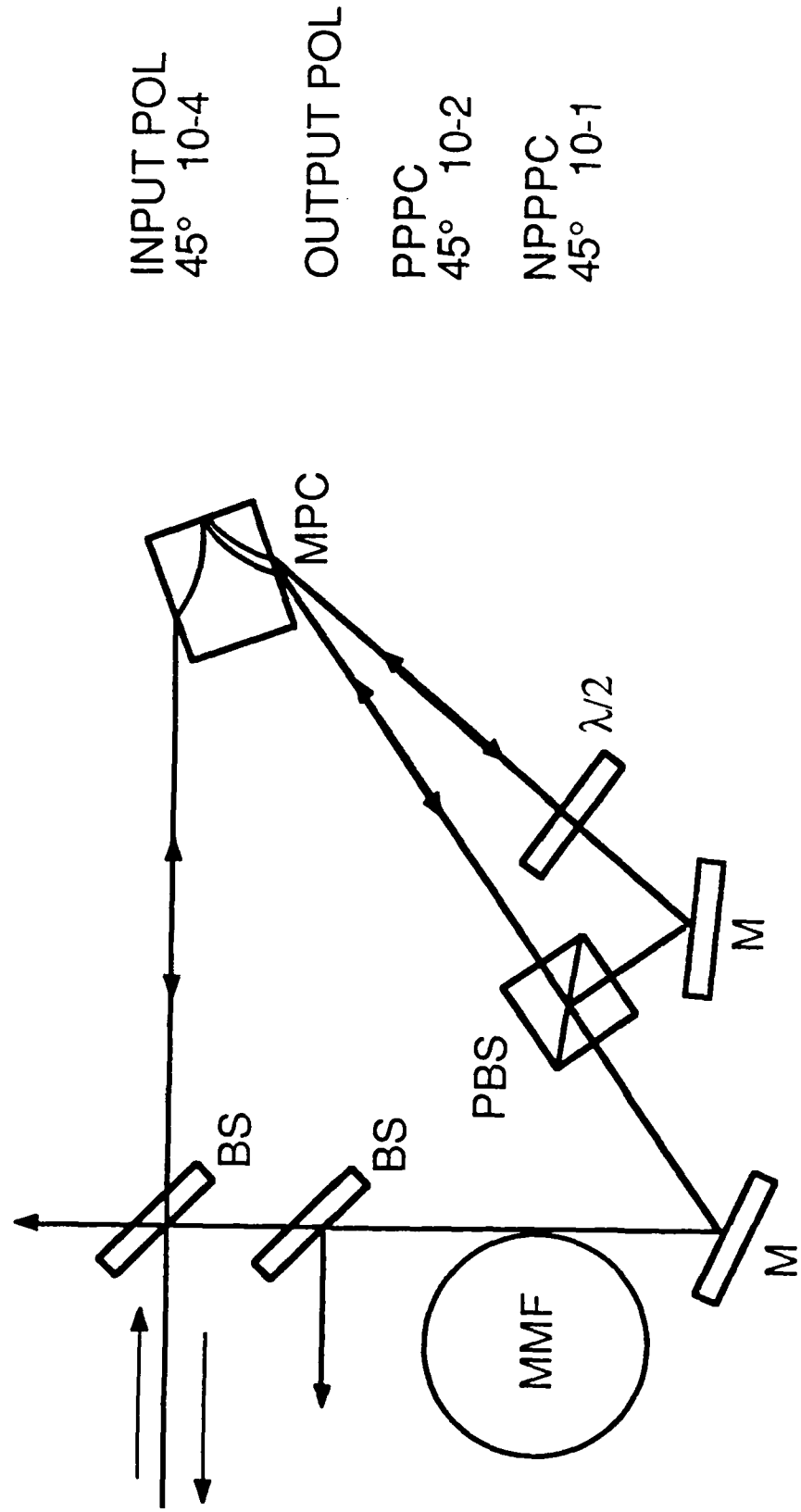
SUMMARY

- **PHASE CONJUGATORS**

- **PHASE-CONJUGATE INTERFEROMETERS**

- **PHASE-CONJUGATE RING INTERFEROMETERS**

  - SAGNAC NATURE

  - SUBTRACTION

  - OUTPUT VS CRYSTAL POSITION

  - POLARIZATION PROPERTIES

  - MEASUREMENT OF NONRECIPROCAL PHASE SHIFT

  - CORRECTION OF MODAL SCRAMBLING IN FIBERS

Rockwell International
Science Center